CANADIAN THESES ON MICROFICHE

I.S.B.N.

THESES CANADIENNES SUR MICROFICHE

National Library of Canada
Collections Development Branch

Canadian Theses on
Microfiche Service

Ottawa, Canada
K1A 0N4

Bibliothèque nationale du Canada
Direction du développement des collections

Service des thèses canadiennes
sur microfiche

NOTICE

The quality of this microfiche is heavily dependent upon the quality of the original thesis submitted for microfilming. Every effort has been made to ensure the highest quality of reproduction possible.

If pages are missing, contact the university which granted the degree.

Some pages may have indistinct print especially if the original pages were typed with a poor typewriter ribbon or if the university sent us a poor photocopy.

Previously copyrighted materials (journal articles, published tests, etc.) are not filmed.

Reproduction in full or in part of this film is governed by the Canadian Copyright Act, R.S.C. 1970, c. C-30. Please read the authorization forms which accompany this thesis.

THIS DISSERTATION
HAS BEEN MICROFILMED
EXACTLY AS RECEIVED

AVIS

La qualité de cette microfiche dépend grandement de la qualité de la thèse soumise au microfilmage. Nous avons tout fait pour assurer une qualité supérieure de reproduction.

S'il manque des pages, veuillez communiquer avec l'université qui a conféré le grade.

La qualité d'impression de certaines pages peut laisser à désirer, surtout si les pages originales ont été dactylographiées à l'aide d'un ruban usé ou si l'université nous a fait parvenir une photocopie de mauvaise qualité.

Les documents qui font déjà l'objet d'un droit d'auteur (articles de revue, examens publiés, etc.) ne sont pas microfilmés.

La reproduction, même partielle, de ce microfilm est soumise à la Loi canadienne sur le droit d'auteur, SRC 1970, c. C-30. Veuillez prendre connaissance des formules d'autorisation qui accompagnent cette thèse.

LA THÈSE A ÉTÉ
MICROFILMÉE TELLE QUE
NOUS L'AVONS REÇUE

NL-339 (r. 82/08)

Canada

National Library of Canada
Canadian Theses Division
Ottawa, Canada
K1A 0N4

Bibliothèque nationale du Canada
Division des thèses canadiennes

0-315-06036-0

53956

PERMISSION TO MICROFILM — AUTORISATION DE MICROFILMER

- Please print or type — Écrire en lettres moulées ou dactylographier

Full Name of Author — Nom complet de l'auteur
MINEO KIMURA

Date of Birth — Date de naissance
NOV 15 1946

Country of Birth — Lieu de naissance
JAPAN

Permanent Address — Résidence fixe
461-2-235, TERABUN, KAMAKURA, KANAGAWA, JAPAN

Title of Thesis — Titre de la thèse
A. MODIFIED-MOLECULAR-STATE STUDY OF CHARGE TRANSFER & DIRECT EXCITATION PROCESSES IN $H^+-H(1S)$, $He^{2+}-H(1S)$, AND $H^+-He^+(1S)$ COLLISIONS.

University — Université
UNIV. OF ALBERTA

Degree for which thesis was presented — Grade pour lequel cette thèse fut présentée
Ph.D.

Year this degree conferred — Année d'obtention de ce grade
1981

Name of Supervisor — Nom du directeur de thèse
DR. W. R. THORSON.

Permission is hereby granted to the NATIONAL LIBRARY OF CANADA to microfilm this thesis and to lend or sell copies of the film.

The author reserves other publication rights, and neither the thesis nor extensive extracts from it may be printed or otherwise reproduced without the author's written permission.

L'autorisation est, par la présente, accordée à la BIBLIOTHÈQUE NATIONALE DU CANADA de microfilmer cette thèse et de prêter ou de vendre des exemplaires du film.

L'auteur se réserve les autres droits de publication; ni la thèse ni de longs extraits de celle-ci ne doivent être imprimés ou autrement reproduits sans l'autorisation écrite de l'auteur.

Date
AUG 10, 1981

Signature

THE UNIVERSITY OF ALBERTA

A Modified-Molecular-State Study of Charge Transfer and Direct Excitation Processes in H^+-H(1s), He^{2+}-H(1s), and H^+-He^+(1s) Collisions

by

© M. Kimura

A THESIS
SUBMITTED TO THE FACULTY OF GRADUATE STUDIES AND RESEARCH
IN PARTIAL FULFILMENT OF THE REQUIREMENTS FOR THE DEGREE
OF DOCTOR OF PHILOSOPHY

Chemistry

EDMONTON, ALBERTA
FALL 1981

THE UNIVERSITY OF ALBERTA

RELEASE FORM

NAME OF AUTHOR M. Kimura

TITLE OF THESIS A Modified-Molecular-State Study of Charge Transfer and Direct Excitation Processes in H^+-H(1s), He^{2+}-H(1s), and H^+-He^+(1s) Collisions

DEGREE FOR WHICH THESIS WAS PRESENTED DOCTOR OF PHILOSOPHY

YEAR THIS DEGREE GRANTED .1981................................

Permission is hereby granted to THE UNIVERSITY OF ALBERTA LIBRARY to reproduce single copies of this thesis and to lend or sell such copies for private, scholarly or scientific research purposes only.

The author reserves other publication rights, and neither the thesis nor extensive extracts from it may be printed or otherwise reproduced without the author's written permission.

(SIGNED) M...Kimura......

PERMANENT ADDRESS:

C/o...Dept...of...Physics...
.Univ...of..Missouri.-Rolla
Rolla,..Mo...U.S.A....

DATED ..Aug 10.........1981

THE UNIVERSITY OF ALBERTA

FACULTY OF GRADUATE STUDIES AND RESEARCH

The undersigned certify that they have read, and recommend to the Faculty of Graduate Studies and Research, for acceptance, a thesis entitled A Modified-Molecular-State Study of Charge Transfer and Direct Excitation Processes in H^+-H(1s), He^{2+}-H(1s), and H^+-He^+(1s) Collisions submitted by M. Kimura in partial fulfilment of the requirements for the degree of DOCTOR OF PHILOSOPHY.

Walter R. Thorson

Supervisor

S. Huzinaga

R.S. Brown

R.E. McClung

M. Razavy

N.F. Lane

External Examiner

Date 5 August 1981

Abstract

The perturbed-stationary-states (PSS) method, modified to include electron translation factor (ETF) effects, has been used to calculate detailed cross sections for charge transfer and direct excitation in H^+-H(1s), He^{2+}-H(1s) and H^+-He^+(1s) collisions at low to intermediate energies ($E \leq 10$ KeV/amu). The close-coupled equations are solved using a classical trajectory description of nuclear motion, and electron translation factors appropriate to molecular states have been constructed using the method of switching functions, after the formulation of Delos and Thorson(12). Switching functions for molecular states of H_2^+ and HeH^{2+} systems have been determined by the "optimization" method developed in earlier work from this laboratory (29).

Our cross sections and other calculated results are compared with other theoretical studies and with recent experimental findings. A brief summary of the relevant conclusions is as follows:

1) H^+-H(1s) collisions

(a) Our differential and total charge transfer cross sections are in good agreement with earlier calculations and with experimental values.

(b) The H(2p) charge transfer cross section is in good agreement with the molecular state calculations of Crothers and Hughes (48) and with recent experimental values. Discrepancies

between our results and those of Refs.(48) may be traced directly to differences between the ETF descriptions used here and in Refs.(48). Our results appear to be in somewhat closer agreement with the experimental measurements.

(c) Our H(2s) charge transfer and direct excitation cross sections differ substantially from those found by Crothers and Hughes(48) and our results are in excellent agreement with the most recent experimental data.

(d) We have studied the convergence of cross sections as a function of increasing basis size and the excitations to higher (Rydberg) levels. We find that a small but non-negligible portion of the flux always escapes to the highest levels available in the basis set and conclude that the most important ionization mechanism in these collisions involves a "ladder-climbing" process of sequential excitations involving such states.

2) He^{2+}-H(1s) collisions

(a) Our total charge transfer cross sections are in good agreement with those calculated by Winter and Hatton(73) (see also Hatton, Lane and Winter(74)) and with recent experimental measurements, but disagree strongly with the values reported by Vaaben and Taulbjerg(72). As in Refs.(73) we find that inclusion of ETF corrections greatly improves convergence of the results as function of basis size, and also that the results seem to converge on slightly different limits.

(b) Our detailed excitation/charge transfer cross sections for individual states differ slightly from those of Winter *et al*(73), though both are in good agreement with experimental values.

3) H^+-He^+(1s) collisions

(a)Our total charge transfer cross sections are 14%-32% smaller than those of Winter, Hatton and Lane(75); the differences appear to result from differences in ETF descriptions used.

(b) Even larger discrepancies (as much as a factor of two in one case) are found between our (smaller) cross sections for individual state excitations, and those given by Winter *et al*; these differences persist as basis size is increased and are traceable to the ETF descriptions used.

Table of Contents

Chapter Page

PREFACE 1

I. INTRODUCTION 4

A. PURPOSE 4

B. THEORETICAL BACKGROUND 6

C. HISTORICAL SURVEY 12

1. Proton-Hydrogen Atom Collisions 13

2. He^{2+}-H(1s) and H^{+}-He^{+}(1s) Collisions 16

II. GENERAL THEORY 21

A. THE PSS THEORY 21

1. Quantum Mechanical Form 22

2. Classical Trajectory Form 23

3. The Validity of the Classical Trajectory Version of the Theory 25

B. DEFECTS OF PSS THEORY AND ORIGIN OF ELECTRON TRANSLATION FACTORS 27

C. THE CORRECTED PSS THEORY (MODIFIED BY ELECTRON TRANSLATION FACTORS (ETF)) 35

1. Coupled Equations for Slow Collsions 36

2. Unitarity 43

3. Components of P- and A-Matrices in the Rotating Molecular Frame 46

4. Choice of Trajectory 49

D. CROSS SECTION FORMULAS 52

1. Total and Detailed Cross Section Formulas 52

2. Differential Cross Section Formula 55

III. SWITCHING FUNCTION AND THE COUPLING MATRIX 57

A. INTRODUCTION AND SUMMARY OF OTHER WORK 57

B. GENERAL METHOD 65

1. Coupling "Optimization" Method 65

2. Analytical Decomposition Method 67

C. OPTIMIZATION CALCULATIONS 69

1. Overview 69

2. β_m -Determination in H_2^+ Couplings 72

3. Determination of Parameters for HeH^{2+} ...76

4. Behavior of Optimum Parameters (H_2^+ and HeH^{2+}) 83

D. COUPLING MATRIX ELEMENTS 89

IV. METHODS OF COMPUTATION 111

A. CALCULATION OF ELECTRONIC WAVEFUNCTIONS 111

B. CALCULATION OF COUPLING MATRIX ELEMENTS 114

1. Computation of First-Order Coupling Matrix Elements 114

2. Computation of Second-Order Coupling Matrix Elements 117

C. NUMERICAL INTEGRATION OF COUPLED EQUATIONS ...119

D. ANALYTICAL FORMULATION OF COUPLED EQUATIONS FOR ASYMPTOTIC LONG RANGE COUPLINGS 121

V. H^+-H(1s) COLLISIONS 128

A. COUPLINGS AND EXCITATION PATHS 131

1. Basis States 131

2. Couplings and Excitation Paths 131

3. Asymptotic Couplings within the H(n=2) manifold 140

4. ETF Effects on the Couplings 143

B. EXCITATION PROBABILITIES 148

1. Collision Histories 148

    2. Excitation Probabilities vs. Impact Parameter 148

  C. CROSS SECTIONS 154

    1. Total and Differential Charge Exchange Cross Sections 154

    2. H(2p) Cross Sections 161

    3. Polarization 164

    4. H(2s) Cross Section 167

  D. VELOCITY AND TRAJECTORY EFFECTS 173

  E. CONVERGENCE STUDIES 177

    1. Convergence of n=2 Levels 177

    2. Convergence and Flux Loss to Ionization 177

VI. He^{2+}-H(1s) AND H^+-He^+(1s) COLLISIONS 185

  A. BASIS SETS AND COUPLING MATRIX ELEMENTS 188

    1. Basis Set 188

    2. Dominant Couplings and Excitation Paths 191

    3. Asymptotic Coupling 195

    4. ETF Effects on Couplings 195

  B. α - PARTICLE - H(1s) COLLISIONS (PROCESS(a)) 203

    1. Excitation Paths 203

    2. Probabilities vs. Impact Parameter 203

    3. Cross Sections 214

    (a)Total Cross Section 214

    (b)Detailed Cross Sections 221

    (c)He(n=2) Manifold Cross sections 224

    (d)Effect of Higher Order Terms in Collision Velocity 226

  C. He^+(1s)-PROTON COLLISIONS (PROCESS(b)) 231

1. Excitation Paths 232

2. Cross Sections 237

BIBLIOGRAPHY 246

List of Tables

Table Page

III.1 H_3^+ Switching Function Parameters 77

III.2 H_3^+ Switching Function Parameters 78

III.3 H_3^+ Switching Function Parameters 79

III.4 HeH^{2+} Switching Function Parameters 84

III.5 HeH^{2+} Switching Function Parameters 85

V.1 4,8,10 Molecular basis sets 132

V.2 16 u-state basis sets 133

V.3 Charge exchange cross sections 158

V.4 Direct excitation cross sections 159

V.5 ETF effects on cross sections 171

V.6 Effects of second-order terms in velocity 174

V.7 Trajectory effects on cross sections 176

V.8 Convergence of cross sections 178

V.9 Convergence of cross sections 179

V.10 Excitation probabilities for higher n levels 181

VI.1 Molecular state basis sets 186

VI.2 Total charge transfer cross section 216

VI.3 Convergence of excitation probabilities 217

VI.4 Atomic level excitation cross sections 222

VI.5 $He^+(n=2)$ atomic state cross sections 225

VI.6 Effects of second-order terms in velocity 230

VI.7 Atomic level excitation cross sections 238

List of Figures

Figure Page

II.1 Nonadiabatic and corrected coupling matrix 31

II.2 Nonadiabatic and corrected coupling matrix 32

III.1 A-values vs. beta 74

III.2 Beta vs. R for H_2^+ 87

III.3 Beta vs. R for He^{2+} 90

III.4 Eta vs. R for He^{2+} 91

III.5 ETF-corrected nonadiabatic coupling matrix for H_2^+ 97

III.6 ETF-corrected nonadiabatic coupling matrix for H_2^+ 98

III.7 ETF-corrected nonadiabatic coupling matrix for H_2^+ 99

III.8 ETF-corrected nonadiabatic coupling matrix for H_2^+ 100

III.9 ETF-corrected nonadiabatic coupling matrix for H_2^+ 101

III.10 ETF-corrected nonadiabatic coupling matrix for He^{2+} 103

III.11 ETF-corrected nonadiabatic coupling matrix for He^{2+} 104

III.12 ETF-corrected nonadiabatic coupling matrix for He^{2+} 105

III.13 ETF-corrected nonadiabatic coupling matrix for He^{2+} 106

III.14 ETF-corrected nonadiabatic coupling matrix for He^{2+} 107

III.15 ETF-corrected nonadiabatic coupling matrix for He^{2+} 108

III.16 Long-range coupling matrix 110

V.1 Electronic potential energy vs. R 134

Figure Page

V.2 Electronic potential energy vs. R 135

V.3 Couplings and energy separations vs. R for u-manifold 137

V.4 Couplings and energy separations vs. R for g-manifold 138

V.5 Effective couplings and excitation paths 139

V.6 Flux pathways 141

V.7 Coupling matrix 145

V.8 Coupling matrix 146

V.9 Coupling matrix 147

V.10 Collision history 149

V.11 Collision history 150

V.12 Probabilities for excitation 151

V.13 Probabilities for excitation 152

V.14 Atomic state excitation probabilities 155

V.15 Charge exchange cross sections 156

V.16 Charge exchange differential cross section 160

V.17 Charge exchange cross section for H(2p) 162

V.18 Polarization 166

V.19 Direct excitation cross section for H(2s) 168

V.20 Charge exchange cross section for H(2s) 169

V.21 Collision history for Rydberg states 182

VI.1 Electronic energy vs. R 189

VI.2 Coupling matrix elements and energy separations vs. R 192

Figure Page

VI.3 Effective couplings and excitation paths 194
VI.4 Coupling matrix elements 197
VI.5 Coupling matrix elements 198
VI.6 Coupling matrix elements 200
VI.7 Coupling matrix elements 201
VI.8 Collision history 204
VI.9 Collision history 205
VI.10 Collision history 206
VI.11 Collision history 207
VI.12 Excitation probabilities vs. impact parameter 209
VI.13 Probability X impact parameter vs. impact parameter 210
VI.14 Probability X impact parameter vs. impact parameter 211
VI.15 Probability X impact parameter vs. impact parameter 212
VI.16 Total charge transfer cross section for He^{2+}-H(1s) collisions 219
VI.17 Detailed level cross sections 223
VI.18 He^{+}(2s) capture cross section 227
VI.19 Detailed He^{+}(n=2) capture cross sections 228
VI.20 Collision history 233
VI.21 Collision history 234
VI.22 Probability X impact parameter vs. impact parameter 236
VI.23 Total charge transfer cross section for H^{+}-He^{+}(1s) collisions 243

Figure Page

VI.24 Total charge transfer cross section for H^+-$He^+(1s)$ collisions 244

PREFACE

When I handed the manuscript of my thesis to Prof. Thorson, he corrected and extensively revised my Japanese English. Therefore not a single Japanese phrase in my original manuscript survived in the revised thesis. This preface is supposed to be my last territory where no one is allowed to trespass, so that at least a part of my thesis contains my original word.

In July 1975, I received a letter from Prof. Thorson after I asked him about the possibility of my study with him at the Univ. of Alberta. He kindly provided me with a lot of information about graduate study in Chemistry in this University and I was so excited after I read the letter. A few days later, I received a telegram from Dr. S. Davis confirming my acceptance as graduate student at the Univ. of Alberta. When I received it, the telegram man said to me "a couple of words in the telegram were lost somewhere between Vancouver and Tokyo. We are now trying to find out what they are". I was worried that the missing word was "not" in the sentence "for not accepting you". But fortunately, it was not "not". Then I rushed into the bookstore and looked at the map of Canada to find out exactly where Edmonton is. When I told my father about my plan to study in Canada, he said "It must take a long time to finish it and maybe I won't see you in this world, but good luck". I am pleased to say that he is doing fine now.

On Christmas Eve, 1975, I flew from Tokyo to Edmonton with more than a hundred of Vietnamese orphans who seemed to me to be one or two years of age. It was my first shock of seeing what is happening in the world. I arrived in Edmonton at 5:30 PM and the temperature was -7 C, which was not so bad. But I soon realized it was just a short break. I stayed on a huge "queen"-size bed at the MacDonald Hotel during the first night in Edmonton without any blink of sleep, thinking of my study, life, etc. (I thought the MacDonald Hotel must be a cheap place for a poor graduate student, since it was suggested I stay there by the Chem. Dept. officer. Actually, it was not a cheap place.) Next morning, on Christmas day, I met Prof. and Mrs. Thorson for the first time at his office and thought, "Gee!, it is not fair to work with him as a graduate student, because of such a huge difference in physical size and mass". But it was just too pessimistic, because I am still surviving. As a matter of fact, I really enjoyed working with him, and learned not only his attitude towards science, but also his attitude towards life which I had never experienced before. In the last five years, I have met many nice friends inside and outside the university community, and they are among the most valuable benefits that I obtained in Canada.

I would like to dedicate this thesis to my teacher, colleagues, friends and parents. The work in this thesis was not done by myself alone, but in collaboration with many people.

Prof. Thorson guided me in the proper direction from kindergarden to the PhD as a Chemistry professor and an English teacher, and from Lake Louise to Sentinel pass as a mountain guide.

Drs. S. Knudson and J. Delos taught me a lot about physics. J. Choi, J. Davis, J. Rankin and S. Barton created an enjoyable atmosphere in this laboratory. The members in the Theoretical Div. (Drs. Birss, Huzinaga, Fraga, Clarke, Mrs. J. Charter and colleagues) supported me in many ways. And my friends, Oh! what nice people.

Without those people, I could not have completed my work. I cannot thank them enough.

Following the North American tradition, I also would like to thank my wife, Keiko, and my daughter, Kana for substantial moral support and sharing life with me, and of course, would like to thank to our parents for giving me many kinds of support.

I should mention special thanks to Mrs. Thorson who has considered us so warm-heartedly that Kana feels as if she were her "auntie" in Edmonton. We really appreciate her.

I. INTRODUCTION

A. PURPOSE

We have investigated fundamental processes occurring in slow ion-atom collisions. The systems we have studied are of the simplest 3-body type (one electron and two nuclei), but serve as adequate prototypes for studies on the basic aspects of the general ion-atom scattering problem with which we are concerned in this thesis. Although these primitive systems are not always convenient from an experimental standpoint, they are most useful for theoretical purposes because

(1). The electronic wavefunction for the one-electron, two-nucleus system is known exactly so that we can avoid uncertainties about the accuracy of the electronic basis functions;

(2). The fundamental dynamical effects which cause physical changes to the system can be clearly represented without any interference of effects arising from multi-electron system phenomena (e.g., autoionization, configuration mixing effects at curve crossings,etc.)

A major objective of this thesis is to determine the degree and importance of the electron translation factor effects on calculated cross sections for charge exchange and direct excitation processes in one-electron systems, in particular, the H_2^+ and HeH^{2+} systems. Only recently has it been recognized that these effects are of importance, and that their adequate treatment may require quite elaborate descriptions of electron translation factors. A second objective of this work is to examine the overall validity of the close-coupling method as it is normally employed, which neglects loss of flux due to ionization. We present some evidence that a small but not negligible portion of the scattering flux in these collisions would correspond in reality to ionizing events, and we can make some estimate of its magnitude.

To study these collisions, we used the impact parameter or classical trajectory multistate perturbed stationary state (PSS) method, corrected for electron translation effects by following the recent formulation of Delos and Thorson(11,12). This method treats the nuclear motion classically, and the electronic problem is solved by the close-coupling method , quantum mechanically, using molecular states as basis states.

We have mainly applied the theory to investigate charge exchange and direct excitation for the symmetric H^+-H(1s) system and the asymmetric He^{2+}-H(1s) and He^+(1s)-H^+ collision systems. Reliable experimental measurements have been performed recently and extensive molecular state calculations have also been reported. These serve as useful comparisons with the present theory.

B. THEORETICAL BACKGROUND

In a low to intermediate energy collision, where the relative velocity of the nuclei is smaller than the orbital electron speed, the colliding system may be regarded as forming a quasi-molecule. If this is the case, we might suppose , as Born and Oppenheimer did for their treatment of molecules(1), that the electron system can adjust smoothly to the slowly changing nuclear position. It would appear that the best basis in which to expand the scattering wave function would be the set of Born-Oppenheimer(1) (BO) (fixed nuclei) adiabatic molecular electronic states, i.e., the expansion

$$\Psi(\vec{r},\vec{R}) = \sum_n \phi_n(\vec{r};\vec{R})\chi_n(R) \qquad \text{I-1}$$

where the BO states $\phi_n(\vec{r};\vec{R})$ are the eigenfunctions of the electronic Hamiltonian at each (fixed) nuclear position R,

$$H_{el}(\vec{r};\vec{R})\phi_n(\vec{r};\vec{R}) = \epsilon_n(R)\phi_n(\vec{r};\vec{R}) \qquad \text{I-2}$$

and depend parametrically upon R.

Substitution of this expansion into the complete (time-independent) Schroedinger equation leads to coupled equations for the components $\chi_n(\vec{R})$ of a vector $\underline{\chi}$,

$$(2\mu)^{-1}[-i\hbar\underline{1}\vec{\nabla}_R + \underline{\vec{P}}(\vec{R})]^2\underline{\chi}(\vec{R}) + \underline{\varepsilon}(R)\underline{\chi}(\vec{R}) = E\underline{\chi}(\vec{R}) \qquad \text{I-3}$$

where $\underline{\varepsilon}$ is the diagonal matrix with elements $\epsilon_m(R)$. In this formulation, all couplings (and electronic transitions) result from the nonadiabatic coupling matrix $\vec{P}(\vec{R})$. This matrix has both angular and radial coupling components; the radial component, for example, is defined as

$$\vec{P}_{kn}(\vec{R}) = \langle k|-i\hbar\vec{\nabla}_R|n\rangle \qquad \text{I-4}$$

and is supposed to represent the effects of deformation of the electronic wavefunctions due to changes in the internuclear distance R. This formulation of scattering problems for slow collisions is called the perturbed-stationary-states (P.S.S.) method, and investigations using it go back to 1953, with work by Bates, Massey and Stewart(3). The method has been widely used in studies of elastic and inelastic collisions at thermal energies. However, it has been known for a long time that it suffers from some fundamental difficulties, which become quite evident when the method is applied to practical problems involving charge transfer or direct electronic excitations. Firstly, it can be shown generally that the asymptotic boundary conditions appropriate to a scattering problem are not properly satisfied by the molecular state expansion given in Eq.(I-1). Secondly, the coupling matrix elements $\underline{P}_{mn}(\vec{R})$ (both radial and angular components) entering into the coupled equations(I-3) are found to depend markedly on the reference origin chosen for electron coordinates (i.e., they do not exhibit proper translational invariance), and furthermore they show a quite unphysical behavior; for example, some matrix elements do not tend correctly to zero, but to constant asymptotic values, as $R \to \infty$. Also, some matrix elements have unreasonably large magnitudes at intermediate nuclear separations, and may be expected to give cross sections which are much too large.

All the above defects in the PSS method originate in the fact that the Born-Oppenheimer expansion(I-1) entirely ignores the translational motion of an electron due to motion of a nucleus to which it is attached. Suppose we consider any reference origin (for example, the centre of mass), with respect to which a nucleus is moving: an electron bound to that nucleus is carried along with it, and a factor describing that translation for the *electron* is a necessary part of the *electronic* wavefunction. But no such factor appears in the Born-Oppenheimer expansion.

Numerous attempts have been made to reformulate PSS theory correctly by including such *electron translation* factors (ETF). In the pioneering work of Bates and McCarroll(4), this is achieved in a manner appropriate to an atomic state (i.e., a single-centre orbital): for atomic orbitals associated with nucleus A, a factor describing translation with A is attached, and correspondingly a factor describing translation with B for orbitals centred on nucleus B. If a molecular state is asymptotically correlated to an atomic state on nucleus A (or on B), Bates and McCarroll assign to it the corresponding atomic translation factor. (Some additional complications are involved for molecular states of symmetric systems like H_2^+ which have g or u symmetry and do not correlate in a one-to-one fashion with unique atomic states). Most attempts to correct the defects of PSS theory have been based on the Bates-McCarroll scheme or minor formal modifications of it.

The Bates-McCarroll(4) description of ETF's ensures that asymptotic scattering boundary conditions and translational invariance requirements are satisfied; a formally correct theory is then obtained and defects such as the incorrect asymptotic behavior of coupling matrix elements are removed. However, physically, in the region of small to intermediate internuclear distances where the system forms a quasimolecule, the electron moves under the influence of the molecular field: it belongs completely to neither nucleus but is partially attached to both. Therefore a proper ETF for molecular states should have molecular or two-centre character.

Thorson and Delos (11,12) have shown that ETF's appropriate for molecular states can be constructed using the idea of switching functions introduced originally by Schneiderman and Russek(9); the resulting formulation meets all requirements of translational invariance and scattering boundary conditions, and leads to coupled equations identical in form to those of PSS theory (Eq.(I-3)), except that the coupling matrix P is corrected for the effects of inclusion of electron translation factors. This scheme effectively recovers the same asymptotic description of ETF's as the method of Bates and McCarroll does for single-centre states, but the flexibility of the switching function also permits ETF's to describe the two-centre character of a molecular state at finite internuclear distances. Initially, Thorson and Delos assumed that a common switching function may be used for all electronic states of a given system, but more generally it may be expected that the most appropriate switching function will be different for each distinct molecular bound state. More recently, Delos and Thorson(12) have given a formulation of slow collision theory, based on this more general assumption, within the framework of a classical trajectory theory.

However, these formulations do not fully specify the choice of molecular state switching functions to be used, and as a matter of fact their selection is an important practical problem since the nonadiabatic coupling matrix elements for many electronic transitions are very sensitive to the switching functions used.

As a first part of this thesis, it is shown that several independent lines of thought can be used to make a consistent and definite choice of the proper molecular state switching functions for the systems considered.

The remaining part of the thesis then proceeds to a test of the corrected PSS method by applying it to calculations of cross sections for the following collision processes:

a. Symmetric System

$H^+ + H(1s) \longrightarrow H^+ + H(nl)$ (Direct excitation)

$H^+ + H(1s) \longrightarrow H(nl) + H^+$ (Charge exchange)

b. Asymmetric System

$He^{2+} + H(1s) \longrightarrow He^{2+} + H(nl)$ (Direct excitation)

$He^{2+} + H(1s) \longrightarrow He^+(nl) + H^+$ (Charge exchange)

c. Asymmetric System

$He^+(1s) + H^+ \longrightarrow He^+(nl) + H^+$ (Direct excitation)

$He^+(1s) + H^+ \longrightarrow He^{2+} + H(nl)$ (Charge exchange)

Our results are compared with other recent molecular state calculations and with experimental measurements.

In the symmetric H^+-$H(1s)$ collision system, I have made some studies with basis sets involving a large number of molecular states (up to 16 ungerade states), in an effort to test the limits of the close-coupling method in this context. Close-coupling methods at present use only bound state basis functions and give no account of flux loss due to ionizing events. The results of these studies suggest that a small but not completely negligible portion of the collision probability, even at the lower collision energies, will in reality appear as ionization by a sequence of "ladder-climbing" excitations, and we can form a rough estimate of the magnitudes involved.

C. HISTORICAL SURVEY

Unresolved problems still remain for the study of ion-atom collisions in the one-electron prototype systems despite their simplicity. In all energy regions there are some major discrepancies among theories, among different experimental measurements, and between theory and experiment. These systems have been extensively studied; specifically more than fifty theoretical and more than ten experimental investigations have been reported for the H^+-H(1s) collision system and only slightly fewer for the He^{2+}-H(1s) system. Here we will not attempt a survey of all the work reported, but will concentrate most attention on studies of low to intermediate energy collisions.

1. Proton-Hydrogen Atom Collisions

Numerous theoretical studies have been reported which are most likely to be valid at energies above the intermediate region(E≥10 KeV), and these have obtained reasonably accurate cross sections for higher energies. Methods used include Born and distorted-wave approximations(50),Glauber's method(51,52), the eikonal approximation(54), impulse approximation(53), Faddeev's method(55), and close-coupling treatments involving pseudo-states(56,57,58), as well as a variety of hybrids of these(59). However, all these methods fail increasingly at lower collision energies, giving wrong positions for cross section maxima and in many cases qualitatively quite incorrect behavior. The remedy for these difficulties is the use of molecular state descriptions which should be more appropriate below 10 KeV.

A pioneering study was done by Bates and Williams(40) using the straight-line impact parameter approximation and a three-state PSS close-coupling theory (corrected by Bates-McCarroll ETF's). Their calculations showed that at low collision velocities the most important inelastic process is the population of H(2p) via $2p\sigma_u$ -$2p\pi_u$ rotational coupling. (Their work has been of major importance in understanding primary excitation events in more complex ion-atom systems--especially in respect to inner-shell vacancy production processes).

Later, impact parameter multichannel PSS-type calculations were done by Rosenthal(45), Chidichimo-Frank and Piacentini(46), and Schinke and Krüger(47-a). All these studies neglected ETF effects as the uncorrected PSS method does and therefore the results lack the required Galilean invariance with respect to the choice of reference origin for electron coordinates; in addition, radial couplings were entirely neglected in these studies.

A more sophisticated molecular state calculation has been reported recently by Crothers and Hughes(48). Their treatment of ETF effects is based on a modification of the Bates-McCarroll scheme: they construct linear combination fragments of g and u molecular states which correspond asymptotically to one-centre atomic states, and with each of these fragments they associate the corresponding Bates-McCarroll ETF; finally they recombine the modified fragments to form g and u molecular basis states. However, this approach has the same general defects as the Bates-McCarroll scheme because the "atomic fragments" are not really one-centre atomic functions at finite internuclear separations but also have a two-centre molecular character. To offset the resulting deficiencies, Crothers and Hughes introduce a variable parameter $\lambda(R)$ in the ETF, and determine its optimal value at each R by the Euler-Lagrange variational principle(21). [It can be shown that their procedure is equivalent (in low-velocity limit) to the use of a crude switching function(33).]

The results obtained by Crothers and Hughes show much closer agreement with experiment than do the earlier studies, which completely ignore ETF effects. However, the defects in their somewhat ad hoc description of ETF effects do have significant effects on their calculated cross sections in certain cases (as I show in this thesis); in addition, they incorrectly used Hermitian averages of non-Hermitian couplings which appear in the theory, although it can be shown that the non-Hermitian character is necessary to preserve unitarity, and in some cases this may lead to incorrect values for individual state cross sections.

One of the purposes in my thesis investigation was to clear up ambiguities in the 1 KeV-10 KeV region resulting from these defects, by using a rigorous theory with more detailed molecular state switching functions to describe ETF effects, including an attempt to demonstrate convergence of the molecular state close-coupling results as a function of basis size.

(Some studies have been carried out for energies below 1 KeV, but these have been primarily concerned with the differential cross sections for charge exchange and Lyman-α excitation and its relation to the classical trajectories used; below 1 KeV it can be shown that effects of deviation from a straight-line (impact parameter) path are important (see, for example, papers by Knudson and Thorson(42), Bates and Sprevak(43), and Schinke(47-b)).

Until recently, experimental data on H^+- H(1s) excitation cross sections at low to intermediate energies have not been available; early measurements concentrated on the resonant charge exchange cross section (Fite, Smith and Stebbings(80) and McClure(63)). Lately, however, Morgan, Geddes and Gilbody(66) measured direct and charge-exchange excitation to H(2p) and H(2s) atomic levels in the range 2-30 KeV. In addition to the above, H(2s) production cross sections have been measured by Bayfield(64) (from 3 KeV), Hill, Geddes and Gilbody(67) (from 1.9 KeV), and most recently, Morgan, Stone and Mayo(68) (from 2 KeV). Hill et al give somewhat larger values than those of Morgan et al below 3 KeV, but above this energy are in excellent agreement with them. On the other hand, Bayfield's much older H(2s) measurements disagree with these, showing a pronounced minimum near 3-5 KeV, though above 10 KeV his data agree with those of other authors.

This major disagreement among the experiments is resolved by the rigorous theoretical study given here; our results are in excellent agreement with the more recent measurements by Morgan et al .

2. He^{2+}-H(1s) and H^+-He^+(1s) Collisions

Again most theoretical studies have been done for the high energy region ($E \geq 100$KeV) where atomic state methods are more appropriate; among the methods widely used are the close-coupling method(76,77,78) and unitarized distorted wave approximation (UDWA)(79). As expected, close agreement between experiments and the theoretical results is found at these high energies.

Below 100 KeV ,however, the situation becomes quite different. Attempts to reproduce the experimental behavior using atomic state basis schemes fail miserably and different theories give widely divergent predictions. It therefore seems clear that a molecular state approach is essential for this energy region.

The earliest molecular state treatment for He^{2+}-H(1s) collisions was reported by Piacentini and Salin(70). Their 3-state work was much more fully extended in a very thorough study by Winter and Lane(71) using up to 22 basis states. Both these studies took the reference origin for electron coordinates on the proton but did not take ETF effects into account (hence they lack proper translational invariance). Since asymptotic boundary conditions for all states H(nl)-He^{2+} are satisfied by this choice of reference origin, the total charge exchange cross section may in principle be calculated from the direct cross sections by using probability conservation; but individual state cross sections will not be correctly predicted, especially for charge exchange excitations. Even for the total cross sections, relatively poor agreement with experimental results is found when only a few basis states are used; agreement is improved if the basis set is extended greatly, but convergence as function of basis size is slow.

Recently, thorough calculations using PSS theory corrected with Bates-McCarroll (one-centre) ETF's have been done by Winter and Hatton(73) and Hatton,Winter and Lane(74). They examined convergence of cross sections with respect to basis size and calculated some individual He^{+}(n=2) state cross sections, as well as the total charge exchange. Their results show very markedly improved convergence as function of basis size and are in generally good agreement with measurements on total and He^{+}(2s) transfer cross sections. However, as pointed out previously, while some molecular states of HeH^{2+} are nearly "atomic He^{+}" states at most internuclear distances (e.g.,$1s\sigma$,$2p\pi$), others, such as $2p\sigma$, which correlates to H(1s), are truly molecular states with substantial two-centre character at the small R-values where coupling occurs, and Bates-McCarroll ETF's may not be adequate for these cases; molecular-state ETF's should be more appropriate.

[Vaaben and Taulbjerg(72) have reported a molecular state calculation of total charge exchange cross sections in He^{2+}-H(1s) collisions using a molecular state ETF based on a common switching function for all states. Their results are in very substantial disagreement with all the results cited above, particularly at the lower energies studied (their cross section at 1 KeV is only 50 % of the value reported by Winter et al); this is very surprising, in view of the fact that at lower energies the cross section is dominated by the

$2p\sigma$ -$2p\pi$ and $2p\sigma$ -$3d\sigma$ couplings and is relatively unaffected by ETF effects. In this thesis, I have done calculations using the switching function of Vaaben and Taulbjerg and find, contrary to their reported values, values in good agreement with Winter et al at 1 KeV (see SectionVI.B.2)].

Winter, Hatton and Lane(75) have carried out calculations of direct excitation and charge exchange in H^+-He^+(1s) collisions, again using Bates-McCarroll ETF's; only charge exchange into H(1s) is included. (They also checked the probability for capture to H(n=2) levels in a 22-state PSS calculation by the method used by Winter and Lane(71). The same questions may be raised as before regarding the validity of Bates-McCarroll ETF's (versus a molecular ETF description based on switching functions)).

In this thesis I have performed calculations for the HeH^{2+} collision systems using molecular states, with molecular state ETF's based on different switching functions for each molecular state. Convergence of the results as function of basis size, as well as behavior of both individual state and total cross sections, is studied. It is shown that individual state cross sections especially are sensitive to molecular effects on ETF's. Surprisingly, even for the qualitatively "He^+-like" $1s\sigma$ state, molecular character has a big influence on coupling matrix elements and this effect is particularly large for cross sections in H^+-He^+(1s) collisions ($1s\sigma$ initial state).

Experimental measurements for He^{2+}-H(1s) collisions have been done by Fite, Smith, and Stebbings(80) and Shah, and Gilbody(83), Nutt, McCullough, Brady, Shah, and Gilbody(84) and Bayfield and Khayrallah(82). All the measurements except those of Bayfield and Khayrallah are in reasonably good agreement above 10 KeV. (Bayfield et al give somewhat larger values in this energy region). Below 8 KeV, only two experimental measurements are available (Fite et al(80) & Gilbody et al(83,84)); however, data of Fite et al lie about an order of magnitude above the more recent values of Gilbody et al. For H^{+}-He^{+}(1s) collisions, the experimental values have been determined from the measured He^{2+} formation by Peart, Grey and Dolder(85) and Angel, Sewell, Dunn, and Gilbody(86,87). Dolder et al measured the He^{2+} formation cross section from c.m. energy 3 KeV and higher and their values tie in well to those of Gilbody et al (who measured only at higher energies ≥60 KeV.). These values for the He^{2+} formation cross section include both ionization and charge exchange to both ground state H(1s) and excited states H(nl) and this fact should be taken into account when one compares the theoretical results with the measured values.

II. GENERAL THEORY

The original perturbed stationary state(PSS) method and its serious deficiencies are described. The corrected PSS theory incorporating electron translation factors (ETF's), following Delos and Thorson(12) (see also Thorson and Delos 11), is summarized. The resulting coupled equations (in the classical trajectory formulation) are presented in a form adequate for low energy collisions. Both differential and total cross section formulae are shown and a brief discussion of the coherent effects is given.

A. THE PSS THEORY

In an atomic collision, if the relative velocity ,V_r , of the collision is smaller than the orbital velocity of a bound electron, V_e , i.e. $V_r << V_e$, the electron might be supposed to adjust smoothly to changes in the nuclear position. In such a case, the molecular adiabatic states should form the best expansion basis to represent the electronic state of the colliding system: fixed nuclei Born-Oppenheimer (B-O) adiabatic states are chosen as the basis set and the nuclear motion itself may be regarded as the perturbation which causes electronic transition between states. This formulation was named the perturbed stationary state (PSS) theory by Mott and Massey(2), who originally developed it.

The conventional form of the PSS method can be developed either in a classical trajectory form or in a fully quantum mechanical form.

1. Quantum Mechanical Form

In a quantum mechanical version, the total scattering wave function can be expanded in B-O wavefunctions , $|n\rangle$,

$$\Psi = \sum_n \chi_n(\vec{R})\,|n\rangle \qquad \text{II-1}$$

where $\chi_n(\vec{R})$ describes the nuclear motion associated with internal state n. The electronic state $|n\rangle$ is the eigenfunction of the electronic Hamiltonian, at fixed nuclear configuration R,

$$H_{el}(\vec{r};\vec{R})\,|n\rangle = \varepsilon_n(R)\,|n\rangle \qquad \text{II-2}$$

where H_{el} is the sum of potential energy $V(\vec{r},\vec{R})$ and electronic kinetic energy T_e .

Both the eigenvector $|n\rangle$ and its eigenvalue depend parametrically on R.

The total wavefunction satisfies the time-independent Schroedinger equation for the entire system,

$$[-\hbar^2/2\mu\vec{\nabla}_R^2 + H_{el}]\Psi = E\Psi \qquad \text{II-3}$$

Coupled equations for the components $\chi_n(R)$ of an abstract vector $\underline{\chi}(R)$ are obtained by multiplying Eq.(II-3) from the left by bra $\langle m|$ and have the form (see Ref.(11))

$$(2\mu)^{-1}[-i\hbar\vec{\nabla}_R + \vec{\underline{P}}(R)]^2\underline{\chi}(\vec{R}) + \underline{\varepsilon}(R)\underline{\chi}(\vec{R}) = E\underline{\chi}(\vec{R}) \qquad \text{II-4}$$

Since $\underline{\varepsilon}(R)$ is a diagonal matrix in this adiabatic representation, all the couplings between different states are caused by the matrix $\underline{P}$. $\underline{P}(\vec{R})$ is called the nonadiabatic coupling matrix; it is responsible for all the electronic transitions and is defined as

$$\vec{P}_{mn}(R) = -i\hbar\langle m|\vec{\nabla}_R|n\rangle \qquad \text{II-5}$$

2. Classical Trajectory Form

Alternatively, in the classical trajectory version, one can assume that the nuclei A and B move along a classical path, specified by the internuclear vector $\vec{R}(t)$, and that the wavefunction for the electron satisfies a time-dependent

Schroedinger equation,

$$H_{el}(\vec{r};\vec{R}(t))T(\vec{r};t) = i\hbar\partial/\partial t T(\vec{r};t) \qquad \text{II-6}$$

If the total wavefunction T is expanded in the set of B-O basis kets $|n\rangle$,

$$T = \sum_n a_n(t)\,|n\rangle \qquad \text{II-7}$$

coupled equations for the components $a_m(t)$ of an abstract vector $\underline{a}$, which result from substitution of Eq.(II-7) into Eq.(II-6) and multiplying again by $\langle m|$ from the left, are

$$i\hbar\dot{\underline{a}} = [\underline{\epsilon} + \vec{V}\cdot\underline{\vec{P}}]\underline{a} \qquad \text{II-8}$$

where

$$\vec{V} = d\vec{R}/dt$$

The classical trajectory version of the theory may be derived as an approximation from the more rigorous quantum mechanical version, under certain conditions, which will be discussed in the following section.

3. The Validity of the Classical Trajectory Version of the Theory

The problem of the derivation of the classical trajectory version of scattering theory from the more rigorous quantum-mechanical version, and the corresponding reduction of the coupled second-order equations (II-4) to first-order time-dependent classical trajectory equations in Eq.(II-8), has been widely discussed in the literature(17,18,19) . The reduction depends on the use of a semiclassical approximation to describe the nuclear motion. A simple illustration of the methods involved is provided if we set

$$\underline{\chi}(R) = \exp[i\mu\vec{V}\cdot\vec{R}/\hbar]\underline{a}(R) \qquad \text{II-9}$$

where $\vec{V}$ is a constant velocity of magnitude $(2E/\mu)^{1/2}$ (impact parameter approximation.). Applying Eq.(II-9) to Eq.(II-4) and sorting according to powers of μ^{-1}, we immediately obtain,

$$[-i\hbar\vec{V}\cdot\vec{\nabla}_R + \underline{\varepsilon} + \vec{V}\cdot\underline{\vec{P}}]\underline{a}(\vec{R}) = O(\mu^{-1}) \qquad \text{II-10}$$

Eq.(II-8) is recovered if the RHS of Eq.(II-10) is neglected and $\underline{a}(R)$ is interpreted as $\underline{a}(t)$ according to the classical connection $\vec{R}(t)$. More generally, the plane-wave factor in

Eq.(II-9) may be replaced by a suitable semiclassical approximation describing nuclear motion, in which $\vec{V}=d\vec{R}/dt$ need not be constant(18). Conditions under which a semiclassical reduction to the classical trajectory version of the theory is valid vary somewhat according to the methods used, but always require that(18):

(1). The momentum $\hbar k_m = [2\mu(E-\epsilon_m(R))]^{1/2}$ must be large, i.e. de Broglie wavelength for the state $|n\rangle$ must be small compared to distances over which $\epsilon_m(R)$ changes appreciably (this is the usual JWKB condition)

(2). Differences $|k_n-k_m| << k$, i.e., momentum and energy transfer in a transition must be a small fraction of the total momentum and energy in collision.

In most collisions of atoms at KeV or higher impact energies (and even lower for heavier atoms), such semiclassical approximation to the nuclear motion is certainly adequate, and in this study the classical trajectory form of the coupled equations is adopted for actual calculations. A separate question arises, whether a straight-line (impact parameter) approximation is valid or other more sophisticated trajectories (Coulomb trajectory or other trajectories) are needed, and this point will be discussed in a later section(II.C.4). However, even for such high energies that the semiclassical approximation is valid and even that a straight-line trajectory assumption is valid, a collision can still be slow in the sense that the collision speed is less than the orbital velocity of bound electrons, so that a molecular state description of the electron system is appropriate.

B. DEFECTS OF PSS THEORY AND ORIGIN OF ELECTRON TRANSLATION FACTORS

In both quantum mechanical and classical trajectory formulations of the PSS theory, transitions arise from the same non-adiabatic coupling matrix, $\underline{P}$, which is supposed to describe changes in the adiabatic state as the nuclear position alters. However, closer investigation reveals a fundamental ambiguity in the meaning of $\underline{P}$: the derivative in Eq.(II-6) is taken while keeping the electron coordinate fixed with respect to its reference origin, but this means that $\underline{P}$ depends upon the reference coordinates chosen to represent the system. Major defects of the PSS approximation arise from this situation. We can explain the problem as follows(11,12):

(1). In the usual treatment of molecular systems, the centre-of-mass of the nuclei (CMN) is taken as reference origin for the electron system. At large internuclear separations, however, the physically appropriate origin for an electron coordinate is not the CMN but the atomic centre to which the electron is bound: the electron moves with the nucleus to which it is attached.

(2). $\underline{P}$ is assumed to represent effects of polarization, distortion, change-of-character, etc., in the molecular wavefunctions as they adjust to the changing molecular fields, but if the reference origin for the electron is taken (for example) as the CMN, then a contribution to $\underline{P}$ also arises from simple displacement of the basis functions with the moving nuclei to which they are attached. This introduces spurious couplings into the $\underline{P}$-matrix, since it is obvious that the part of $\underline{P}$ which merely represents displacement of basis functions with respect to electronic reference origin is not a real coupling which could lead to electronic transitions; the "displacement part" must somehow be removed from $\underline{P}$, to remove these fictitious couplings.

(3). Since $\underline{P}$ is origin-dependent, the PSS theory as it stands does not meet physical invariance requirements. An electron bound to a particular nucleus has translational motion, with respect to some reference origin such as CMN, due to the nuclear motion with respect to that origin. Transformation theory requires that when a state which is at rest in one reference frame is described in a new frame, with respect to which it is uniformly moving with velocity $\vec{V}$, then the wavefunction (as seen in the new frame) must be subjected to a unitary transformation to maintain Galilean invariance:

$$\psi(\vec{r},\vec{R}) = \hat{U}\phi(\vec{r},\vec{R}) \qquad \text{II-11}$$

where U is a unitary transformation operator with the form

$$U = \exp[(im/\hbar)(\vec{V}\cdot\vec{r} - \tfrac{1}{2}V^2t)] \qquad \text{II-12}$$

This operator is here conventionally referred to as an electron translation factor (ETF); it describes the momentum and kinetic energy of the electron, associated with its translation along with a moving nucleus to which it is bound. Because PSS theory ignores such factors, it does not meet Galilean invariance requirements, and in particular the individual molecular states which make up the PSS expansion cannot meet asymptotic boundary conditions for scattering and are not in one-to-one correspondence with correct initial and final scattering states.

The defects of PSS theory which result from ignoring these considerations are not purely formal ones, but may lead to grossly incorrect physical predictions in some cases. The nonadiabatic coupling matrix, P, has the following unphysical properties:

(1). For certain discrete-discrete transitions, P tends to a finite value as $R \to \infty$ (e.g., H_2^+ $1s\sigma_g$ — $2s\sigma_g$ coupling Figure(II-1)), and the magnitude in the small R region is unreasonably large (e.g., H_2^+ $1s\sigma_g$ — $3d\sigma_g$ coupling Figure(II-2))(see also Ref.(38)).

(2). For ionizing transitions, the P-matrix elements are physically unrealistic: each initial bound electronic state is coupled to 30-40 partial waves in the electronic continuum and the couplings extend out to extremely large distances (~50 a.u.)(see Rankin(29b), Rankin and Thorson (29a)).

It might be argued formally that, in spite of these defects, since the molecular states $\{|n\rangle\}$ (including the continuum) form a complete set, the resulting coupled equations and hence PSS theory are still completely rigorous as a scheme for solving scattering problems. This would be true, provided that:

(1). a complete expansion basis were actually used (including continuum states); and

(2). the resulting wave function were projected onto a rigorously correct set of final scattering states.

However, such a procedure is completely impractical, and

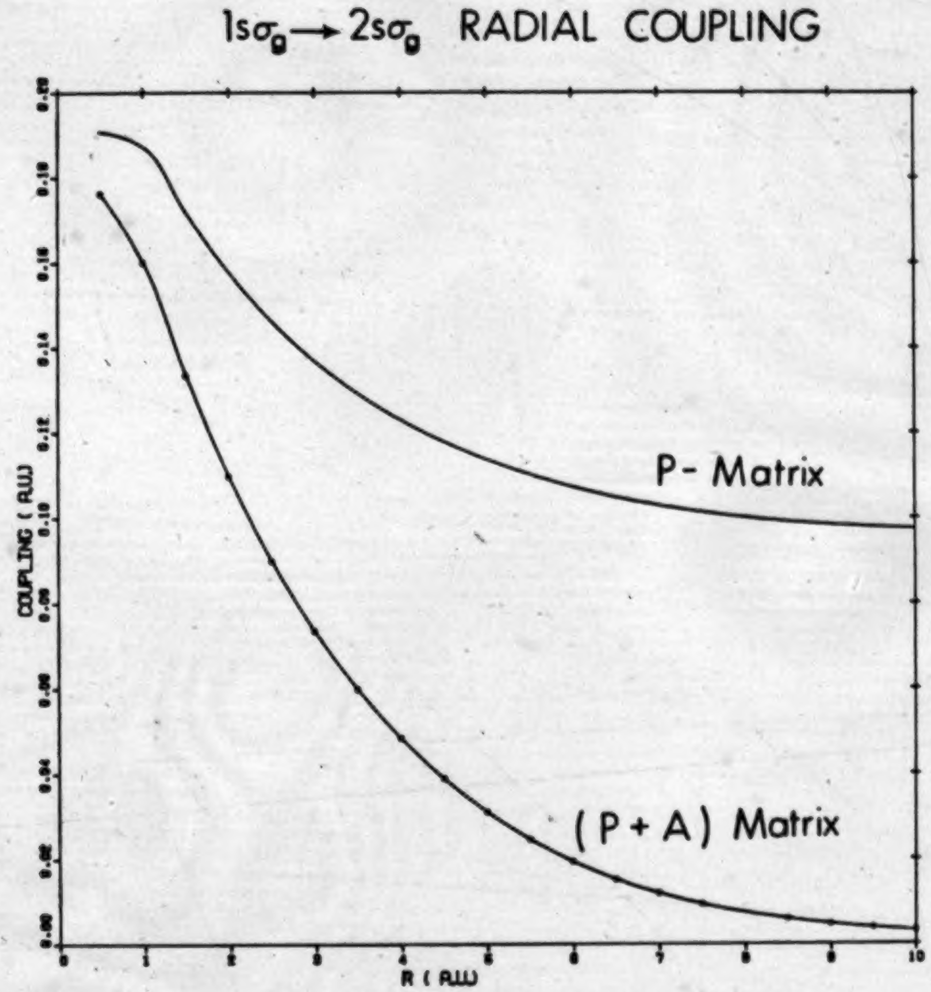
$1s\sigma_g \rightarrow 2s\sigma_g$ RADIAL COUPLING

Figure(II-1) Nonadiabatic coupling matrix, $\underline{P}$ (PSS matrix) and ETF (see text) corrected matrix, ($\underline{P}$ + $\underline{A}$) for $1s\sigma_g$ -$2s\sigma_g$ coupling matrix element.

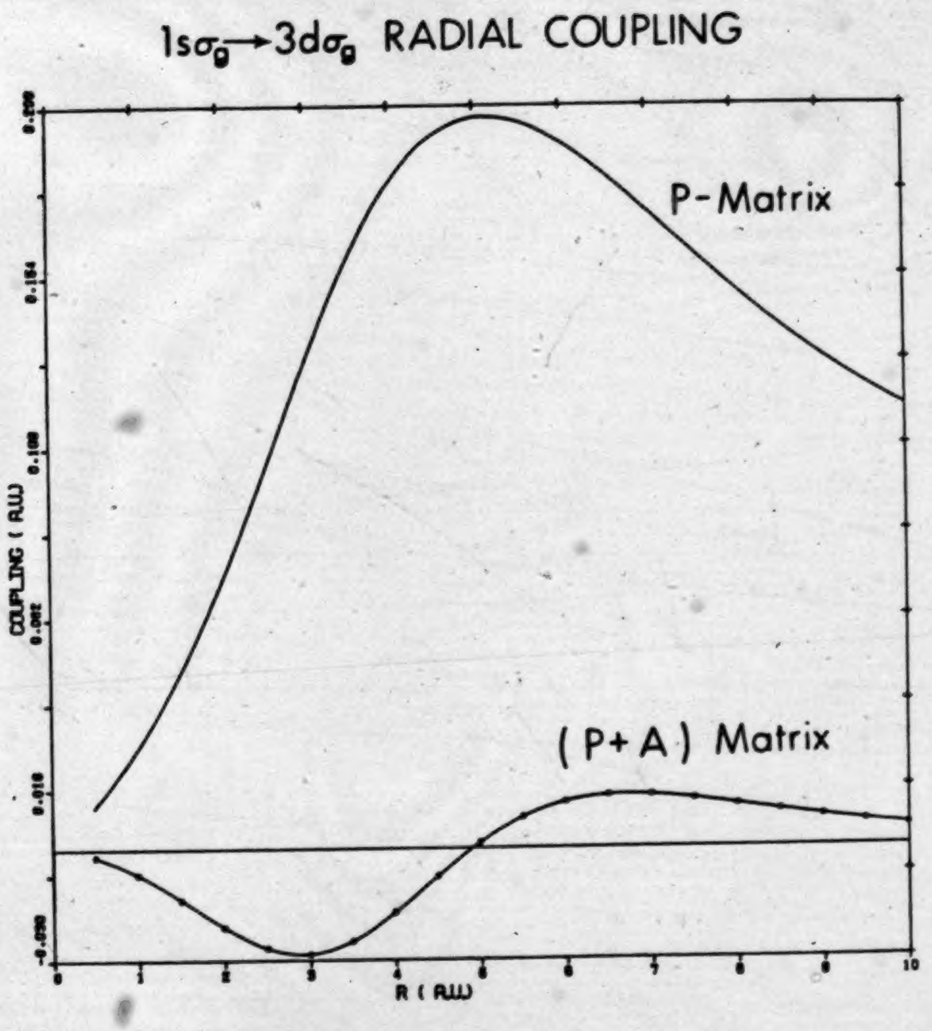

Figure(II-2) Nonadiabatic coupling matrix, P̲ (PSS matrix) and ETF (see text) corrected matrix, (P̲ + A̲) for $1s\sigma_g$ -$3d\sigma_g$ coupling matrix element.

when the expansion basis used is truncated to a finite set, the defects of PSS theory can lead to serious errors.

Defects of the P matrix all result from the spurious "displacement" terms described earlier. To obtain a physically correct theory, it will be necessary to correct the nonadiabatic coupling matrix by removing such terms. In the next section, we shall see that when a description of electron translation factors is properly included in the theory, the most important result is that the matrix P appearing in the coupled equations is in fact replaced by a corrected coupling matrix, P+A.

Bates and McCarroll(4) were the first to recognize the serious defects of the PSS method due to its neglect of electron translation effects, and they developed a modification of the theory which at least removes the asymptotic defects. In their formulation, a plane-wave ETF of the form (II-12) is associated with each molecular state. Assuming that the molecular state $|n\rangle$ is asymptotically correlated in unique fashion to a particular atomic state on nucleus J, they associate with state n a factor (II-12), in which the velocity V_J which appears is the velocity of nucleus J with respect to (say) the CMN. This guarantees that the basis states in the expansion are in one-to-one correspondence with the correct atomic scattering states, and removes such defects as the spurious finite values as R $\rightarrow \infty$ for some P matrix elements, and much of the very long-range behaviour of the ionizing-transition matrix elements. (In the special case of the symmetric molecular systems (for example,H_2^+), where molecular states have *gerade* (*g*) or *ungerade* (*u*) symmetry and do not correspond uniquely to atomic states on a single atom, a more complicated procedure is used by Bates and McCarroll(4): they combine pairs of *g* and *u* molecular states to form fragments which do correspond asymptotically to states on unique atoms ,J, and then associate an ETF of form (II-12) to each such fragment.)

In spite of these major improvements, the formulation of Bates and McCarroll(4) still contains assumptions which are physically incorrect, because they assign to an electron in a *molecular* state an ETF which describes transport associated with a particular atomic centre. At the finite internuclear distances where real couplings occur, a molecular electron may be partially attached to both centres (i.e., a molecular state may have *two-centre* character). For such situations, a proper ETF for a molecular state must itself have molecular, two-centre character. As we will see in the next section, this can be done using the device of switching functions.

C. THE CORRECTED PSS THEORY (MODIFIED BY ELECTRON TRANSLATION FACTORS (ETF))

We now present an account of a modified PSS theory which is corrected to include electron translation factors (ETF's) and their effects. The formulation meets all requirements of Galilean invariance and asymptotic boundary conditions. The method used is that first presented rigorously by Thorson and Delos(11), who showed that ETF's appropriate for molecular states can be constructed using switching functions. In effect, these describe an "electron translation" which is a function of the electron's local behavior: alternatively they can be viewed as defining a local reference origin for an electron adapted to its "degree of attachment" to one or the other of the nuclei. Asymptotically, provided the switching function meets certain boundary conditions, a description effectively identical to that of Bates & McCarroll is recovered as a limiting form.

The original formulation of Thorson and Delos(11) was based on the assumption that a single switching function may be used for all electronic states of a given system. However, study of the shapes of electronic wavefunctions reveals clearly that some states show substantial two-centre character at finite internuclear separations, while other groups of states have almost entirely one-centre character over nearly the whole range of internuclear separations. This as well as other evidence strongly supports the assumption that different switching functions for each molecular state are more appropriate. A formulation based on this more general assumption has been given by Delos and Thorson(12) in the framework of classical trajectory collision theory.

This theory is reviewed in slightly modified form for practical use bearing on the processes occurring in (symmetric) H^+-H(1s) and (asymmetric) He^{2+}-H(1s) and H^+-He^+(1s) collisions.

1. Coupled Equations for Slow Collsions

It is assumed that the nuclei A and B move along a classical path, specified by the internuclear vector $\vec{R}(t)$, and that the wavefunction for the electron satisfies a time-dependent Schroedinger equation

$$i\hbar\partial/\partial t T(\vec{r};t) = H_{el}(\vec{r};\vec{R}(t))T(\vec{r};t) \qquad \text{II-13}$$

The total electronic wavefunction Υ is expanded in the ETF modified set in the form

$$T = \sum_n a_n(t)F_n\phi_n \qquad \text{II-14}$$

where Φ_n are the basis states describing internal motion of the electron and F_m are associated electron translation factors (ETF) describing the electron's transport momentum and kinetic energy as it is carried along in state ϕ_m with one nucleus or the other. If the basis ϕ_m were a set of atomic states, then the appropriate F_m 's would be Bates-McCarroll factors of the form (II-12), but since ϕ_m are molecular states (for a PSS expansion) we shall define the ETF's F_n in a somewhat different way.

For convenience, we take the geometric centre of the system (GC), rather than CMN, as the reference origin for electron coordinate r. As Delos and Thorson(12) point out, the physical description is in any case invariant to choice of reference origin, if Galilean invariance requirements are met correctly for that choice; furthermore, since the velocity of the CMN with respect to the geometric centre is simply $-\frac{1}{2}\lambda\dot{R}$,where $\lambda = (M_A - M_B)/(M_A + M_B)$, it is easy to construct ETF's with respect to CMN as reference origin, if these were needed, by the rules of transformation theory (Schmid (27)).

With GC as reference origin, we define the ETF's as

$$F_n = \exp[(im/\hbar)(\vec{w}_n \cdot \vec{r} - \frac{1}{8}\int v^2\,dt')] \qquad \text{II-15}$$

where $\vec{w}_n$ is defined as

$$\vec{w}_n(\vec{r},\vec{R}) = \frac{1}{2}f_n(\vec{r},\vec{R})\vec{V} \qquad \text{II-16}$$

and

$$\vec{V} = \vec{\dot{R}} = d\vec{R}/dt$$

$\vec{v}_n$ is effectively a local transport velocity for an electron in molecular state n, and it is specified by the switching function $f_n(\vec{r},R)$. Since the electron in a bound state is attached asymptotically to one of the nuclei, we have the asymptotic constraints

$$\lim_{R\to\infty} f_n(\vec{r};\vec{R}) = +1 \quad , \text{ if } \vec{r}_B = |\vec{r} - \tfrac{1}{2}\vec{R}| \text{ finite} \qquad \text{II-17}$$

$$= -1 \quad , \text{ if } \vec{r}_A = |\vec{r} + \tfrac{1}{2}\vec{R}| \text{ finite}$$

The atomic-type ETF's of Bates & McCarroll,(II-12), are then effectively recovered as $R \to \infty$, since a "B-atom" state projects out a velocity $\vec{v} = +\ \frac{1}{2}\vec{V}$, and an "A-atom" state a velocity $\vec{v} = -\ \frac{1}{2}\vec{V}$, in Eq.(II-16).

The idea of using a switching function to achieve such a molecular ETF description was first introduced by Schneiderman and Russek(9), who also considered the constraints which must be met by such a function. Thorson and Delos(11) carried out the first rigorous formulation of a scattering theory using the device.

Apart from the asymptotic constraints given above, the form of the switching function $f_m(\vec{r},R)$ is not fully specified. The determination of appropriate switching functions for molecular states is an important practical problem, because the corrected nonadiabatic coupling matrix elements which result are in some cases extremely sensitive to the choice used for f_m. Detailed methods for determining switching functions are discussed in Chapter III.

In this formulation, the expansion basis states ϕ_m are again just the Born-Oppenheimer adiabatic eigenfunctions for the electronic Hamiltonian, which obey Eq.(II-2). To obtain the coupled equations, we substitute Eq.(II-14) into Schroedinger equation Eq.(II-13), multiply on the left by F_k^*, and close with the bra $\langle k|$, with the result

$$\sum_n \langle m|F_m^* F_n|n\rangle i\hbar d/dt\, a_n = \sum_n \Big[\langle m|F_m^* F_n (H_{el} - i\hbar\vec{V}\cdot\vec{\nabla}_R)|n\rangle + \langle m|F_m^*\{[H_{el},F_n] - i\hbar\partial/\partial t\, F_n\}|n\rangle\Big] a_n \qquad \text{II-18}$$

These equations are equivalent to the Schroedinger equation(II-13) and, within the approximations in the classical trajectory theory, they are exact. After simplifying by neglecting small terms related to $d\vec{V}/dt$ and

$\vec{V}\cdot\vec{\nabla}_R f_n$, the coupled equations have the form (in the abstract vector notation)

$$\underline{S}(V) i\hbar d/dt\underline{a} = [\underline{h}(V) + \vec{V}\cdot(\vec{\underline{P}}(V) + \vec{\underline{A}}(V))]\underline{a} \qquad \text{II-19}$$

where

$$S(V)_{mn} = \langle m|F_m^* F_n|n\rangle \qquad \text{II-20a}$$

$$h(V)_{mn} = \langle m|F_m^* F_n h|n\rangle \qquad \text{II-20b}$$

$$P(V)_{mn} = \langle m|F_m^* F_n(-i\hbar\vec{\nabla}_R)|n\rangle \qquad \text{II-20c}$$

$$A(V)_{mn} = (im/\hbar)\langle m|F_m^* F_n[h,\vec{s}_n]|n\rangle \qquad \text{II-20d}$$

$$\vec{s}_n = \frac{1}{2} f_n(\vec{r};R)\vec{r} \qquad \text{II-20e}$$

For low and intermediate energy collisions, which are of particular interest in our present studies, we can apply a substantial simplification to the above coupled equations . Expanding the ETF's in power series of velocity, $\vec{V}$, and neglecting all terms of order V^3 and higher, we can obtain simpler coupled equations by retaining terms to first-order in V; and to second-order in V, as required.

a. Coupled equations to first-order in velocity

When terms of order (V^2) are also neglected, the coupled equations have the simple form

$$i\hbar\, d/dt\, \underline{a} = (\underline{\varepsilon} + \vec{V}\cdot(\underline{\vec{P}} + \underline{\vec{A}}))\underline{a} \qquad \text{II-21}$$

where

$$\underline{\varepsilon}_n = \langle m|h|n\rangle \delta_{mn} \qquad \text{II-22a}$$

$$\underline{P}_{mn} = \langle m|(-i\hbar\vec{\nabla}_R)|n\rangle \qquad \text{II-22b}$$

$$\underline{A}_{mn} = (ih/m)\langle m|[h,\vec{s}_n]|n\rangle \qquad \text{II-22c}$$

In these equations $\underline{\varepsilon}$ and $\underline{P}$ are familiar terms which arise in the PSS theory in which ETF's are neglected. P is the nonadiabatic PSS coupling term. The new coupling matrix $\underline{A}$ arises from the presence of the ETF in expansion(II-14); it is the correction matrix which identifies and removes from $\underline{P}$ that portion which represents just simple "displacement" of basis states with nuclei to which they are attached. Eqs.(II-21) have just the same form as the original equations (II-8) of PSS theory, but the nonadiabatic coupling matrix has been corrected to remove the fictitious couplings due to displacement.

b. Inclusion of second-order terms in velocity

When second-order terms are also included, the coupled equations are

$$
\begin{aligned}
i\hbar d/dt\ a_k = {} & \varepsilon_k a_k + \textstyle\sum_n \vec{V}\cdot(\vec{P}+\vec{A})a_n \\
& + \textstyle\sum_n \Big[(im/\hbar)\Big\{\langle k|[\vec{V}\cdot(\vec{s}_n-\vec{s}_k)][\vec{V}\cdot(-i\hbar\vec{\nabla}_R + (im/\hbar)[H_{el},\vec{s}_n])]|n\rangle \\
& - \textstyle\sum_j \langle k|[\vec{V}\cdot(\vec{s}_j-\vec{s}_k)]|j\rangle\langle j|\vec{V}\cdot(-i\hbar\vec{\nabla}_R + (im/\hbar)[H_{el},\vec{s}_n])|n\rangle\Big\} \\
& + \langle k|(m/8)[(f_n^2-1)\vec{V}^2 + (\vec{V}\cdot\vec{r})^2(\vec{\nabla}_r\cdot f_n\vec{r})^2 \\
& \quad + 2(\vec{V}\cdot\vec{r})(f_n\vec{V}\cdot\vec{\nabla}_r f_n + 2\vec{V}\cdot\vec{\nabla}_R f_n)]|n\rangle\Big]a_n \qquad \text{II-23}
\end{aligned}
$$

These equations contain the same first-order terms as (II-21), but also include the very messy and complicated second-order terms shown. These terms become increasingly important as the collision velocity becomes comparable with the orbital speed of a bound electron, but as a rule we have found that for energies below about 5 KeV/amu their effects in the systems studied are negligibly small. Their importance, however, also varies somewhat from system to system; if one considers couplings involving states which have strongly "molecular" character out to relatively large internuclear separation, differences between switching functions for different states have a relatively much larger effect; for example, in the symmetric H^+-H(1s) collision system, this effect is much more pronounced than for He^{2+}-H(1s) or H^+-He^+(1s), where many of the states are effectively He^+(nl) atomic states at relatively small internuclear separations. As a result, in H^+-H(1s) collisions , second-order terms have a noticeable effect already at collision energies 4-5 KeV, while for the HeH^{2+} system they remain quite small even up to 20 KeV.

These are the required forms for the coupled equations for practical applications to slow and intermediate energy collisions. They can be solved numerically. Because of the neglected terms in $(d\vec{V}/dt)$ and the higher order terms in $\vec{V}$, Eq.(II-21) and Eq.(II-23) may not exactly conserve probability in general, but this failure of unitarity is small, of the order of the neglected terms, and we will prove this in the next section.

2. Unitarity

As pointed out earlier, the coupled equations (II-19) are equivalent to the time-dependent Schroedinger equation (II-13) from which they were obtained, and, within the classical trajectory description they are exact. Since the Schroedinger equation conserves probability, it follows that the quantity

$$\langle T|T\rangle = \sum_{m,n} a_m^*(t)a_n(t)\ \langle m|F_m^*F_n|n\rangle \qquad \text{II-24a}$$

is conserved, i.e.,

$$i\hbar d/dt\langle T|T\rangle = \sum_{m,n} \{a_m^* S_{mn}[i\hbar\dot{a}_n] - [-i\hbar\dot{a}_m^*]S_{mn}a_n + a_m^*[i\hbar\partial/\partial t\ S_{mn}]a_n\} = 0 \qquad \text{II-24b}$$

If (as we have done) the exact equations (II-19) are approximated by neglecting certain terms, then there will be a corresponding failure of the conservation of probability in Eq.(II-24b).

To derive Eqs.(II-21) or (II-23), we have (1) neglected terms in $(d\vec{V}/dt)$ and $\vec{v}\cdot\vec{\nabla}_R f_n$ and (2) after expanding ETF's in powers of the velocity, we have kept terms in the coupled equations only up through first-order in velocity (Eq.(II-21)) or second-order in velocity (Eq.(II-23)) and have discarded higher terms. Correspondingly, it can be shown that errors in the conservation of probability are of the order of the discarded terms. Thus, for the first-order equations (II-21) it can be shown explicitly that Eq.(II-24b) is satisfied to within errors of order V^2(and, of course, $d\vec{V}/dt$ and $\vec{v}\cdot\vec{\nabla}_R f_n$). It is illuminating to give this proof explicitly (Green(14)). Using Eqs.(II-21) in eqs.(II-24b), we obtain

$$
\begin{aligned}
i\hbar d/dt\langle T|T\rangle = {} & \underline{a}^{*}[\vec{V}\cdot(P-P^{*}) + \vec{V}\cdot(A-A^{*})]\underline{a} \\
& + \vec{V}\,\underline{a}^{*}(\underline{\sigma s}^{-1}\underline{h} - \underline{hs}^{-1}\underline{\sigma})\underline{a}] \\
& + \underline{a}^{*}[i\hbar\vec{V}\cdot\vec{\nabla}_{R}\vec{S} + O(v^{2})]\underline{a}
\end{aligned}
\qquad \text{II-25}
$$

Using the relations

$$A - A^{*} = -(im/\hbar)[\underline{\sigma s}^{-1}\underline{h} - \underline{hs}^{-1}\underline{\sigma}] \qquad \text{II-26}$$

we find

$$i\hbar d/dt\langle T|T\rangle = \underline{a}^{*}[\vec{V}\cdot(P-P^{*}) + i\hbar\vec{V}\cdot\vec{\nabla}_{R}\vec{S} + O(v^{2})]\underline{a} \qquad \text{II-27}$$

and since it is easily shown that

$$-i\hbar\vec{\nabla}_{R}S = \underline{P} - \underline{P}^{*} \qquad \text{II-28}$$

it follows that Eq.(II-24b) is satisfied to within errors of order V^2. This proof is relevant to a particular point in the practical calculations. Since the switching functions are different for different molecular states, it follows that $\underline{A}^*_{nm}$ is not equal to $\underline{A}_{mn}$, and hence the coupling matrices are not Hermitian. Some workers who have included treatment of ETF effects in calculations have incorrectly assumed that these distinct forward and reverse couplings should be replaced by their Hermitian averages (e.g.,Crothers and Hughes(30)). However, as Eq.(II-24) shows, what is to be conserved is not ($(\sum_n a^*_n a_n)$), but ($\langle T|T\rangle$) given by (II-24a) (to errors $O(V^2)$), and as we have just shown using Eqs.(II-27), the non-Hermitian character of the matrix elements is just what is needed to achieve this. Similarly, one can show that if terms up to order V^2 are included as in Eqs.(II-24), then errors in probability conservation in Eq.(II-24b) will be of order V^3 (as before, there are also errors of order $(d\vec{V}/dt)$ and $\vec{V}\cdot\vec{\nabla}_R f_n$).

3. Components of P- and A-Matrices in the Rotating Molecular Frame

In the foregoing developments we have shown the nonadiabatic coupling matrices (P+A) as vectors in three-dimensional space:

$$\vec{P}_{kn}(R) = \langle k|-i\hbar\vec{\nabla}_R|n\rangle \qquad \text{II-29}$$

$$\vec{A}_{kn}(R) = (im/2\hbar)(\varepsilon_k - \varepsilon_n)\langle k|f_n\vec{r}|n\rangle \qquad \text{II-30}$$

Now, it is well known that the Born-Oppenheimer eigenstates $|n\rangle$ depend parametrically only upon the magnitude of R, and not upon its direction, and it might therefore appear that the only non-vanishing component of $\underline{P}$ would be the radial one. This is not correct, because the gradient in Eq.(II-29) is to be taken keeping the electron coordinate $\vec{r}$ fixed in a non-rotating reference frame; but the Born-Oppenheimer eigenstates depend only upon R, provided that the electron coordinates are described in the rotating molecular reference frame. Let $\vec{r}=(x,y,z)$ be the coordinates of the electron in the lab. frame, while $\vec{r}\,'=(x',y',z')$ denotes the same point in the molecular frame. These are related by(7,15,16)

$$\begin{bmatrix} x' \\ y' \\ z' \end{bmatrix} = \begin{bmatrix} \cos\Theta\cos\Phi & \cos\Theta\sin\Phi & -\sin\Theta \\ -\sin\Phi & \cos\Phi & 0 \\ \sin\Theta\cos\Phi & \sin\Theta\sin\Phi & \cos\Theta \end{bmatrix} \begin{bmatrix} x \\ y \\ z \end{bmatrix} \qquad \text{II-31}$$

where Θ, Φ are the polar coordinates of the vector $\vec{R}$. From this it can be shown that

$$-i\hbar(\partial/\partial R)_{xyz} = -i\hbar(\partial/\partial R)_{x'y'z'} \qquad \text{II-32a}$$

$$-i\hbar(\partial/\partial\Theta)_{xyz} = -i\hbar(\partial/\partial\Theta)_{x'y'z'} - \hat{L}_{y'} \qquad \text{II-32b}$$

$$-i\hbar(\partial/\partial\Phi)_{xyz} = -i\hbar(\partial/\partial\Phi)_{x'y'z'} + [\sin\Theta\hat{L}_{x'} - \cos\Theta\hat{L}_{z'}] \qquad \text{II-32c}$$

where $\hat{L}_x$, $\hat{L}_y$, $\hat{L}_z$, are the components of the electronic orbital angular momentum operator in the molecular frame (with respect to GC as origin). It follows that $\underline{P}$ has angular as well as radial components.

In a classical trajectory description of a collision, the vector $\vec{R}(t)$ moves in a plane, which we may take to be $\Phi = 0$. The velocity $\vec{V} = d\vec{R}/dt$ has components: $\vec{V}_R = \dot{R}$, $\vec{V}_\Theta = \dot{R}\Theta$. Corresponding to these components the vector $\underline{P}$ has components

$$P^R_{kn} = -i\hbar \langle k|(\partial/\partial R)_{x'y'z'}|n\rangle \qquad \text{II-33a}$$

and

$$P^\Theta_{kn} = -R^{-1}\langle k|\hat{L}_{y'}|n\rangle \qquad \text{II-33b}$$

The corresponding components of the ETF correction matrix $\underline{A}$ are:

$$A^R_{kn} = (im/2\hbar)(\varepsilon_k - \varepsilon_n)\langle k|f_n z'|n\rangle \qquad \text{II-34a}$$

$$A_{kn} = (im/2\hbar)(\varepsilon_k - \varepsilon_n)\langle k|f_n x'|n\rangle \qquad \text{II-34b}$$

In the developments which follow, we shall understand $\vec{r}(x,y,z)$ to refer to rotating molecular frame electron coordinates, i.e., we shall drop the prime superscript in the above equations. In the molecular frame coordinates, not only the eigenstates $|n\rangle$,but also the switching functions $f_n(\vec{r};R)$ depend parametrically only upon R; therefore it follows from the above equations that both radial and angular coupling matrix elements (II-33),(II-34) are functions only of R. The Born-Oppenheimer eigenstates are also eigenfunctions of $\hat{L}_z$, the component of orbital angular momentum on the molecular axis:

$$\hat{L}_z|n\rangle = m_n\hbar|n\rangle \qquad \text{II-35}$$

It follows that radial couplings $(\underline{P}^R + \underline{A}^R)_{km}$ may connect only states with the same m, while angular couplings connect only states for which $m'_k = m_m \pm 1$.

4. Choice of Trajectory

In the derivation of a classical trajectory formulation of a collision problem from the fully quantum-mechanical description, the definition of the classical trajectory $\vec{R}(t)$ to be used is not completely arbitrary; it must be determined in some way which is self-consistent with the assumptions used in the derivation. In most cases---particularly where the JWKB approximation is the basis for the reduction---the trajectory $\vec{R}(t)$ is defined by defining some suitable average momentum (in terms of the classical momenta associated with different states, $|n\rangle$).

A great deal of discussion in connection with semiclassical reductions has concentrated on the problem of determining the best average trajectory. While it can be shown in many cases that some choices appear to give somewhat more accurate results than others, this question remains still open. Delos and Thorson(18) state that if it makes very much difference which average trajectory must be used, then the validity of the semiclassical reduction itself may be questionable.

For the collision energies considered in this study, the validity of the semiclassical reduction and therefore of the classical trajectory approach is not in question. For example, studies in the H^+-H(1s) collision problem by Knudson and Thorson(42) show that the classical trajectory equations are able to reproduce fully quantum-mechanical calculations for c.m. collision energies as low as 30-50 eV, which is more than an order of magnitude below the lowest energies considered in the present studies.

However, Knudson and Thorson(42) also showed that the classical trajectory equations must be solved using a classical trajectory which is appropriate to the actual behavior of the system. In particular, for the case of strong rotational coupling in the united atom limit ($R \rightarrow 0$) between $2p\sigma_u$ and $2p\pi_u$ molecular states of the H^+-H(1s) system, it is important to use a classical trajectory which correctly describes how the system passes through the strong coupling region near $R \rightarrow 0$. In earlier studies of atomic collision processes, it was a common practice to use the classical trajectory equations with the arbitrary assumption of a straight-line, constant-velocity trajectory:

$$\vec{R}(t) = \vec{\rho} + \vec{V}t \tag{II-36}$$

(this is often called the impact-parameter approximation). If the collision energy is high enough, this assumption can always be justified in the limiting case. However, Knudson and Thorson(42) found that as R ⟶ 0 the distortion of trajectory from a straight line due to Coulomb repulsion of the nuclei leads to major differences between the impact parameter results and the correct behavior at lower energies. Correct results are obtained for $E \geq 100$ eV, if Coulomb trajectories are used instead. Additional modifications of trajectory due to electronic potential curve details were found to be much less important. Since the united-atom rotational coupling is known to be a main excitation mechanism in many types of atomic collision problems (including cases we study here), the question of accuracy of impact parameter (straight-line) trajectories, versus Coulombic trajectories, is perhaps important at the lower energies considered (≤ 1 KeV).

We have tested the validity of the straight-line trajectory by comparing results with those found for Coulombic trajectories in H^{+}-H(1s) collisions at 1 KeV (projectile energy). As shown by Knudson and Thorson, the main effect of the Coulombic trajectory is to shift the position of the peak of maximum probability to smaller impact parameters and create a new peak at very small impact parameter, which contributes a very small effect to the cross sections at higher energies. In our studies at 1 KeV we found that the total deviation between excitation and charge exchange cross sections computed with straight-line and with Coulombic trajectories is at most 5 %. Needless to say, as the collision energy increases, the results will coincide still more closely.

For the HeH^{2+} collision system, Winter and Lane(71) made a careful study of differences between straight-line and Coulombic trajectory cross sections at 1 KeV, and found they were at most 8 %.

Therefore we concluded that the straight-line trajectory could be used safely in these studies and we have carried out our calculations on this assumption because of its simplicity. For this case, the radial and angular velocities can be written,

$$\dot{R} = \pm V(1 - \rho^2/R^2)^{1/2} \qquad \text{II-37a}$$

$$\dot{\theta} = V\rho/R \qquad \text{II-37b}$$

where ρ is the impact parameter and V is the (constant) relative velocity.

D. CROSS SECTION FORMULAS

1. Total and Detailed Cross Section Formulas

The coupled equations, Eqs.(II-21) and (II-23) should be solved to obtain the amplitude and probability as $t \rightarrow +\infty$

. These equations are solved numerically with the following initial condition: if the index "1" designates the initial state ($1s\sigma_g$ and $2p\sigma_u$ for H_2^+ system, and $2p\sigma_u$ for the He^{2+}-H(1s), $1s\sigma$ for $He^+(1s)$-H^+ system), the initial conditions for the coupled equation are

$$a_1(-\infty;\rho) = 1/\sqrt{2}\,\delta_{1k} \quad \text{for } H_2^+ \qquad \text{II-38a}$$

$$a_1(-\infty;\rho) = \delta_{1k} \quad \text{for } HeH^{2+} \qquad \text{II-38b}$$

and the final state amplitudes $a_k(+\infty;\rho)$ for given energy and impact parameter are computed. The probability of excitation to molecular state k is defined as

$$P_k(E,\rho) = |a_k(+\infty;\rho)|^2 \qquad \text{II-39}$$

The corresponding integrated cross section for molecular state k is conventionally given

$$Q_k = 2\pi\int_0^\infty \rho d\rho \; P_k(E,\rho) \qquad \text{II-40}$$

However, to compute probabilities and cross sections for excitation to specific atomic states(j), atomic state amplitudes $b_j(+\infty;\rho)$ must first be formed by an appropriate coherent addition of molecular state amplitudes before using Eq.(II-40),i.e.,

$$b_j(+\infty;\rho) = e^{i\gamma}\sum_k c_{jk}a_k(+\infty;\rho)\exp[-(i/\hbar)\ (\varepsilon_k(t')-\varepsilon_j^{\circ})dt'] \qquad \text{II-41}$$

where γ is an arbitrary phase, and ε_j° is the atomic state energy.

The coherences considered in Eq.(II-41) are of two types(a,b) for the H_2^+ case and one type(b) for the HeH^{2+} case. (In the asymmetric system, the MO correlates in one-to-one fashion to a corresponding AO.)

a. g and u Coherences

The direct and charge exchange amplitudes for H_2^+ system are formed by addition and/or subtraction of the amplitude for matching pairs of g and u molecular states. For the incident channel where final amplitudes are significant for both g and u components, the well known resonant charge exchange oscillations result(e.g. resonant H(1s) charge exchange involves both the initial states $1s\sigma_g$ and $2p\sigma_u$ states). For the excited channels , on the other hand, amplitudes for excitation of g molecular states are smaller below 5 KeV, with the result that the direct and charge exchange cross sections are nearly the same($3p\sigma_u$ and $4f\sigma_u$ for u-state and $2s\sigma_g$ and $3d\sigma_g$ for g-state).

b. Hybridization Coherences

In a hydrogenic ion or atom where atomic levels like 2s and 2p are essentially degenerate, the molecular states are asymptotically correlated not to atomic eigenstates but to the hybrid (Stark field) states. For H_2^+, the pairs of molecular states ($2s\sigma_g$, $3d\sigma_g$) and ($3p\sigma_u$, $4f\sigma_u$) correlate to g and u "sp hybrids" of H(n=2), respectively. For n=2 level in HeH^{2+}, the molecular states ($2s\sigma$, $3d\sigma$) correlate to the sp-hybrid of $He^+(n=2)$ atomic states. These mixings must be unscrambled to obtain 2s and 2p atomic amplitudes, and cross sections for H(2s),H(2p) and $He^+(2s)$,$He^+(2p)$ individual atomic states.

2. Differential Cross Section Formula

A formula for the differential cross section is given by McCarroll and Salin(20) within the frame of the Eikonal approximation,

$$\sigma_k^{d,c}(\theta) = 2\pi\mu^2 V^2 \left| \int_0^\infty \rho\, d\rho \; a_k^{d,c}(+\infty;\rho) J_m(2\mu V \rho \sin\tfrac{1}{2}\theta) \right|^2 \qquad \text{II-42}$$

where μ is the reduced mass, $\vec{V}$ is the collision velocity, θ is the scattering angle ; $J_m(x)$ is the Bessel function of order m, and m is the difference between the magnetic quantum numbers in the initial and final molecular states. The total exchange probability may be therefore calculated from the expression

$$P_{ex}(\theta) = \frac{\sum_i \sigma_i^c(\theta)}{\sum_i (\sigma_i^d(\theta) + \sigma_i^c(\theta))} \qquad \text{II-43}$$

which describes the ratio of differential cross sections, and d,c denote direct excitation and charge-exchange excitation, respectively. Eq.(II-42) has been derived under the assumption that the forward scattering which occurs at the angle $\theta \sim 0$ is the dominant process in the scattering. [McCarroll et al used this assumption and expanded the terms which involved the angle, θ, and then retained the first term of the expansion only.] Therefore this formula is valid only for small angle scattering.

III. SWITCHING FUNCTION AND THE COUPLING MATRIX

A. INTRODUCTION AND SUMMARY OF OTHER WORK

In this work, we have used the switching function, $f(\vec{r};R)$, as a device to represent the translational motion of an electron in a molecular electronic state, as a local function of its position. In a molecular state, it is not possible to say that the electron is attached to a particular nucleus (as would be true for an atomic state); in effect, the switching function shows the local degree of attachment to either nucleus. Asymptotically $(R \longrightarrow \infty)$, we can say that a bound state electron must be attached to a definite nucleus, and therefore it follows that there are asymptotic constraints

$$\lim_{R\to\infty} [f(\vec{r};R)] = +1 \qquad \vec{r}_B = |\vec{r}-\vec{R}/2| \text{ finite} \qquad \text{III-1a}$$

$$\lim_{R\to\infty} [f(\vec{r};R)] = -1 \qquad \vec{r}_A = |\vec{r}+\vec{R}/2| \text{ finite} \qquad \text{III-1b}$$

In the united atom limit $R \longrightarrow 0$, it can be shown that the bound electron should translate with the centre of charge of the system (rather than the geometric centre). For an asymmetric system, the switching function (which describes translation with respect to the geometric centre) must therefore tend to a finite mean value, not to zero (as has sometimes been assumed in earlier work). This has been pointed out earlier by T. A. Green(32-a) and more recently has been emphasized by Taulbjerg and Vaaben(28) in a recent paper on switching functions.

Apart from these two types of limiting constraints, however, the specific form of the switching function is not defined.

The formal requirements of a scattering theory are met using ETF's based on an arbitrary choice of switching function, provided it meets the asymptotic constraints (III-1a,b). The results of a scattering calculation should thus be invariant to the choice actually made for f, assuming a complete basis set is used. However, practically, the basis sets used for close-coupling calculations are far from complete, and one then finds that the choice made for the switching function directly affects the coupling matrix elements and through them the resulting cross sections.

This problem has great theoretical importance because the corrected nonadiabatic couplings for many transitions are in fact extremely sensitive to the form and parameters used for the switching function, and a precise determination of switching functions for molecular states of H_2^+ and HeH^{2+} was an important investigation topic for this research.

Various authors(21-33) have proposed methods for treating ETF descriptions and, in particular, for constructing switching functions. A good discussion of earlier aspects of the ETF description problem has been given by Riera and Salin(34).

Apart from the methods we have used in this work, which are described more fully below, most attempts to find criteria for determining switching functions have taken the Euler-Lagrange variation method(21a) as the formal starting-point for obtaining such criteria.

A first application of the Euler-Lagrange method to the determination of ETF's was given by Riley and Green(21b). However, in that paper they considered only single-centre-type ETF's, i.e., they considered only ETF's based on R-dependent parameters and did not treat the more general problem of ETF's based on switching functions. Recently, a much more elaborate formulation, including switching functions as a possible device, has been presented by T. A. Green(13) ' In this formulation, "optimum" switching functions may be determined variationally by solving a set of coupled differential equations. However, these equations are extremely complicated and their solution seemed to us to be quite impractical for purposes of our present work.

More limited application of the Euler-Lagrange method to ETF description in the case of a single molecular state leads to equations closely resembling the equation of continuity for the probability density. Some authors have attempted to use such equations, or equations closely

---

'We thank Dr. Green for showing us these equations in advance of publication.

related to them and based on physical arguments, to derive switching functions. One such attempt was made formally by Schmid(27); it can be shown, however, that his "definition" is not unique, since it requires the evaluation of a line integral whose value depends on the path used to compute it, i.e., the quantity integrated is not an exact differential. Also, zeroes in the molecular state wave function appear to introduce poles and essential singularities into Schmid's definition.

A more successful attempt has been made by Ponce(31), who also applied his definition in a very approximate fashion to calculations on the $1s\sigma_g$, $2p\sigma_u$ and $2p\pi_u$ states of H_2^+. He obtains "velocity field" functions which may be roughly compared with our switching functions, and in fact they do resemble our functions in a qualitative (but not quantitative) way. Difficulties with Ponce's method are that it uses Cartesian separations of electron coordinates (the molecular states are separable only in prolate spheroidal coordinates).

Crothers and Hughes(30) have used the Euler-Lagrange scheme in a still more limited context, to define ETF's which are equivalent, to lowest order in the collision velocity, to the use of a particular type of switching function, for the special case of a symmetric system (e.g., H_2^+).

We can illustrate their method by its application to the $1s\sigma_g$ and $2p\sigma_u$ states of H_2^+ : They define "atomic" fragments $\phi_\pm$, given by

$$\phi_{\pm} = 2^{-1/2}[\psi_{1s\sigma_g} \pm \psi_{2p\sigma_u}] \qquad \text{III-2}$$

which correspond, asymptotically, to 1s atomic orbitals on nucleus B and A, respectively. With each such $\phi_\pm$ they associate a Bates-McCarroll type (single-centre) ETF,

$$\Phi = \phi_{\pm}\exp[\pm(im/2\hbar)\lambda(R)\vec{V}\cdot\vec{r} - (im/8\hbar)V^2t] \qquad \text{III-3}$$

where λ (R) is a variable parameter. Finally, they reconstruct molecular basis states of g and u symmetry by

$$\Psi_{g,u} = 2^{-1/2}[\Phi_{+} \pm \Phi_{-}]$$

and determine the parameter λ (R) using the Euler-Lagrange method along the lines proposed by Riley and Green(21). It can be shown(33) that (to first-order in velocity) this procedure is equivalent to the use of the switching functions

$$f_{1s\sigma_g}(\vec{r};\vec{R}) = \lambda(R)[\psi_{2p\sigma_u}(\vec{r};\vec{R})/\psi_{1s\sigma_g}(\vec{r};\vec{R})] \qquad \text{III-4}$$

and

$$f_{2p\sigma_u}(\vec{r};\vec{R}) = \lambda(R)[\psi_{1s\sigma_g}(\vec{r};\vec{R})/\psi_{2p\sigma_u}(\vec{r};\vec{R})] \qquad \text{III-5}$$

For the $1s\sigma_g$ state, this switching function is in quite surprisingly good agreement with the one we use (see the paper by Thorson, Kimura, Choi and Knudson(33), Fig.(7)) (for $R \geq 4.0$ a.u.), but for the $2p\sigma_u$ state, it is very different, and leads to some very different coupling matrix elements. We will discuss this point further when comparing our results for cross sections with those found by Crothers and Hughes(48) (Chapter V).

Independently there is also a recent paper by Taulbjerg and Vaaben(28) which attempts to derive a common switching function for all states of a molecular electronic system by general arguments based on the electronic Hamiltonian. One topic to which these authors pay much attention is the united-atom limit $R \longrightarrow 0$; they especially emphasize the idea that as $R \longrightarrow 0$ the electronic density must be moving with the centre-of-charge, rather than with either individual nucleus, or with the geometric centre. As a matter of fact, we find that the switching functions we have obtained for HeH^{2+} by the methods used here do seem to have this limiting property; however, we find it does not become important until very small internuclear distances, and we have found no evidence that such limiting behaviour has a significant effect on the cross sections calculated for the systems we study here.

Much more important to our present work is the fact that different switching functions are required for each electronic state, and this possibility has not been allowed by Taulbjerg and Vaaben. These authors do not seem to have done any extensive cross section calculations testing their proposed switching functions (see Section VI.A).

In this work, I have followed the methods and ideas employed by Thorson and his coworkers (Levy & Thorson(8b) and Rankin & Thorson(29)) in this laboratory to determine switching functions. I have used the form:

$$f_n(\vec{r};R) = \tanh[R\beta_n(R)(\eta - \eta_n^0(R))] \qquad \text{III-6}$$

where $\beta_n(R)$ and $\eta^{\circ}_m(R)$ are variable parameters depending upon the state n and internuclear distance R, and $\eta = \frac{r_A - r_B}{R}$ is the "angle" variable of prolate spheroidal electron coordinates $(-1 \leq \eta \leq +1)$. This form is closely related to that first proposed by Thorson et al(8) in conjunction with the calculation of coupling matrix elements for direct impact ionization in H^+-$H(1s)$ collisions, and was extensively studied by Rankin for ionization couplings in both H_2^+ and HeH^{2+} systems. Advantages of this form are that:

(1). Theoretically, as we will show below (and is shown in detail in recent work by Thorson, Kimura, Choi, and Knudson (hereafter TKCK)(33)) this form can be justified by its derivation for H_2^+ using analytical methods, and is not therefore a purely arbitrary choice, and

(2). From a practical viewpoint, it is easy to compute the nonadiabatic coupling matrix elements for this form, compared with other proposed forms discussed earlier.

In this Chapter, I will describe in detail the studies I have made of "optimization" calculations to obtain "best" switching functions of the form (III-6), similar to the studies made by Rankin(29), but in the present case looking also at discrete-state couplings in addition to ionization couplings. These calculations give results qualitatively similar to those found by Rankin(29), but slightly changed quantitatively, when couplings between discrete states are considered. The work described here was done before the analytical derivations done by Professor Thorson were obtained, and they served as an important confirmation of the correctness of the analysis he obtained because they are in excellent agreement with his analytical results for H_2^+ . In Section B. we discuss the methods and ideas to be used and also describe the ideas of the analytical method of TKCK briefly. The rest of the chapter is devoted to the detailed optimization procedures used and their results.

B. GENERAL METHOD

In this laboratory, two entirely distinct approaches have been developed for the determination of switching functions for molecular bound states. The first approach is the so-called coupling "optimization" scheme used previously by Thorson and coworkers. The second approach is suggested by a result obtained by Delos and Thorson(12) in their discussion of diabatic and adiabatic state descriptions of atomic collisions, and is based on an analytical decomposition of two-centre wavefunctions into "one-centre components". In my thesis work, I have concentrated mainly on the former method.

1. Coupling "Optimization" Method

Some time ago, it was found by Thorson and coworkers(8) that the corrected non-adiabatic coupling matrix elements connecting bound molecular states to the two-centre continuum states in H_2^+ are hypersensitive to the choice of switching function used. The problem has practical importance because the PSS couplings if not corrected are very large (~0.1 to ~1.0 a.u.), very numerous (30-40 continuum partial waves are importantly coupled), and have very long range (30-50 a.u.).

Since it is believed that most of these couplings are a result of the fictitious "displacement" terms, an argument appealing to variational ideas suggests that a "good" choice for a switching function should have the result of greatly reducing or even minimizing the corrected couplings(Levy and Thorson(8b)). After empirical studies, it was found that when form (III-6) is used there are quite well-defined choices of the parameters $\beta_n(R)$ (for H_2^+, $\eta_n^{\circ}=0$ by symmetry) for each bound state, which produce very great reductions in magnitude of all continuum couplings simultaneously, except those for the first few partial waves (see Rankin(29)). The "optimum parameters" obtained are independent of the continuum states, energies or quantum numbers, and also independent of the type of coupling studied (radial or angular). However they depend sensitively on each discrete state in which the electron is initially bound. This suggests they are actually properties of the bound states, ψ_n. In his doctoral thesis, J. Rankin(29) formalized the optimization procedure more systematically, and also extended it to asymmetric one-electron systems, particularly HeH^{2+}. He was able to determine parameters for $\beta_n(R)$, $\eta_n^{\circ}(R)$ for six or seven states of H_2^+ and HeH^{2+} for $0 \le R \le 12$ a.u., and his coupling matrix elements for ionization show very great reductions of magnitude relative to the uncorrected PSS values and in some cases are also much smaller (at finite internuclear separations) than those obtained using Bates-McCarroll ETF's.

2. Analytical Decomposition Method

Using a classical trajectory formulation, Delos and Thorson presented a unified description of low-velocity collisions, in which either one-centre (atomic) or two-centre (molecular) states, including the appropriate ETF's, could be used as basis states, and considered the effects of transformations between such basis descriptions. In particular, suppose a basis transformation is defined uniquely,

$$\psi_\mu = \sum_k U_{k\mu}\phi_k \qquad \text{III-7}$$

which links atomic states ϕ_k to molecular states ψ_μ. Since an atomic state ϕ_k has a uniquely defined Bates-McCarroll ETF whose "switching function" is just $f_J = \pm 1$, J=B,A, then, to maintain physical invariance of the description under transformation, the switching function f_μ associated with ψ_μ is uniquely defined by the relation

$$f_\mu\psi_\mu = \sum_k \phi_k f_{J_k} \qquad \text{III-8}$$

where J_ℓ=B or A, respectively, if ϕ_ℓ is attached to nucleus B or A. This decomposition formula shows how a switching function represents, in a local way, the degree of attachment to each nucleus. Therefore, if a "two-centre decomposition" of molecular states into one-centre components could be made, it would be possible to define switching functions from the properties of the bound states alone. For H_2^+, Thorson, Kimura, Choi, and Knudson(33) have shown that it is possible to achieve an analytical decomposition of the "angular" wavefunctions (in prolate spheroidal coordinates) which leads to switching functions of the form

$$f_\mu = \tanh[\beta_\mu(R) R\eta] \qquad \text{III-6'}$$

The parameters $\beta_\mu(R)$ may be calculated by a uniquely defined analytical formula.

For asymmetric systems like HeH^{2+}, the same ideas may be extended in an approximate fashion to obtain the form (III-6) as a result. A discussion of the detailed analysis of TKCK(33) is outside the scope of my work; however, the extremely close agreement found between the parameters obtained by the "optimization" calculations I describe below, and the analytical values for H_2^+, confirms that the ideas are correct.

C. OPTIMIZATION CALCULATIONS

1. Overview

The principles and methods used in my calculations are basically the same as those employed by Rankin(29).

We use a switching function f of the form (III-6), with variable parameters $\beta_n(R)$, $\eta_n^\circ(R)$ to be determined at each R. For a transition n ⟶ n' (where the final state n' may be either a discrete state or a continuum state), we may define a "reduction parameter" $\rho_{n'n}$,

$$\rho_{n'n} = |1 + A_{n'n}/P_{n'n}|^2 \qquad \text{III-9}$$

where $\underline{P}_{n'n}$ and $\underline{A}_{n'n}$ are radial or angular nonadiabatic coupling matrix elements defined previously (Eqs.(II-22b,c)). The basic hypothesis of the optimization scheme is that many of the uncorrected PSS couplings $P_{n'n}$ are spuriously large due to "displacement" terms; we therefore look for a particular choice of the parameters β_n (R), η_n°(R) which achieves large simultaneous reductions in as many of the $\rho_{n'n}$ as possible. This hypothesis cannot be rigorously derived from formal variational principles; it is justified by its empirical success, i.e., such parameters can be found with well-defined values.

Rankin's study was confined to continuum final states n'. For a given continuum energy, ϵ' , and a particular type of coupling (radial: $\Delta|m|=0$; angular: $\Delta|m|=+1$ or $\Delta|m|=-1$) he defined sums of reduction parameters,

$$S^c = \sum_{n'} \rho_{n'n} \qquad \text{III-10}$$

the sum being performed over the continuum partial waves. The parameters β_n, η_n^0 were then varied to minimize S^c .

However, Rankin did not include all partial waves in these sums. He found that the first one or two partial waves have matrix elements which are relatively insensitive to changes in β_n and η_n^0 (see Section C.2 below); since these couplings are also large, if they are included in the sum their presence tends to mask the effects of parameter variations on the couplings to higher partial waves. After making these exclusions, Rankin found that precisely determined values for β_n, η_n^0 can be located which very greatly reduce $\rho_{n'n}$ for all terms in the sums (III-10) at once. In some cases (for higher partial waves) $\rho_{n'n}$ may be reduced by several orders of magnitude. The values of the parameters obtained are independent of the continuum state energy ϵ' and of the type of coupling considered. By restricting attention to higher partial waves in the sums (III-10), Rankin was able in favorable cases to determine β_n to nearly three significant figures, and η_n^0 to somewhat lower precision (about two significant figures).

After study of couplings to discrete states, I found that some of these couplings are also quite sensitive to the switching function parameters. I also found that the precisely determined parameters of Rankin do not always give an "optimum" reduction of these discrete state couplings; nearby, but slightly different, parameter values are indicated. As was found for the lower continuum partial waves, some groups of discrete state couplings appear insensitive to the switching function parameters.

As a result of these investigations, summarized in more detail below, I have reported "optimum" values for the parameters β_n, η_n which differ somewhat from those given by Rankin; they also have a larger uncertainty (about 10 % in worst cases). (In one case (the 3dσ_g state for H_2^+) I have determined a quite different value from that reported by Rankin; he seems to have found a secondary minimum in that case).

From the standpoint of overall method, there is no question that couplings to continuum states are the most sensitive to the switching function parameters, and provide the most definite general indication what values the "optimum" parameters should have. (I found that couplings to Rydberg states with $\Delta\ell \neq 0$ show the same behavior, and agree with continuum state couplings for determining the region of "optimum" values). However, after establishing a range (±8 %) for the "optimum" values from the continuum and

Rydberg state couplings, study of the discrete state couplings (as well as continuum couplings to lower partial waves) suggests a choice for parameters which can deviate slightly from the precise values found by Rankin, who considered only the higher continuum partial wave reductions. The new choices still make large reductions in the continuum couplings, but also make a significant reduction of discrete state couplings.

The symmetric case of H_2^+ (η_n^{0} =0) is much simpler, and the parameters β_n may be located somewhat more precisely, than for the asymmetric case (HeH^{2+}) studied. Therefore for clarity and convenience I have presented the two cases separately, with H_2^+ first.

2. β_n -Determination in H_2^+ Couplings

For most (but not all) coupling matrix elements n → n', it is possible to select parameters for the switching function f which cause the corrected coupling matrix element ($\underline{P}_{n'n} + \underline{A}_{n'n}$) to vanish exactly. Some of these zeroes occur at isolated values of the parameter for the specific couplings (they could be related to nodal structure in the coupling), but others are systematic in the sense that many different matrix elements have zeroes at or near the same parameter value. This is the situation in the continuum couplings, which Rankin used. Of course, we are not looking for such zeroes exactly, but if a large number of them for different couplings are clustered in a narrow range of the parameter, it is reasonable to conclude that somewhere within that range there is an "optimum" choice which will greatly reduce the magnitudes of all of the couplings which have nearby zeroes, and that such a choice has physical meaning for "displacement" corrections in the state n. I have found that when discrete as well as continuum couplings are considered, such a clustering of zeroes is also found, but that the range is a little bit broader and the "best" choice appears to be a little different than in continuum cases alone.

For both discrete and continuum coupling matrix elements in H_2^+, the general pattern found is as follows (let l be the united-atom orbital angular momentum quantum number):

a. For couplings l'=l, the matrix elements have non-zero values for all β_n values, do not have a minimum for any reasonable β_n-value (0.0 to 1.0) and are relatively insensitive to β_n (see Figure(III-1a))

b. Couplings with l'=l+2 have two zeroes vs. β_n in the reasonable range (Figure(III-1b)

c. Couplings with l'=l+4 have three zeroes vs. β_n in the reasonable range (Figure(III-1c); for $\Delta \ell \geq 5$ we can expect this behavior to continue.

d. A fairly narrow range of β_n-values, associated

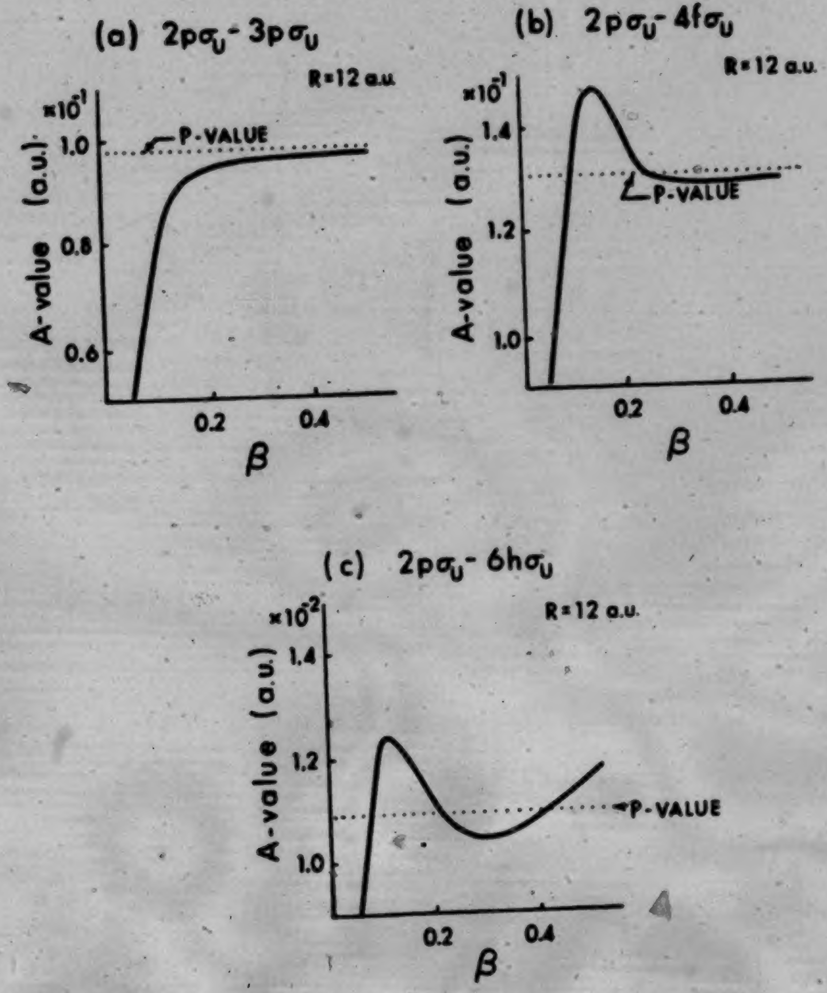

Figure(III-1) A-values vs. β for (a) $2p\sigma_u$ - $3p\sigma_u$ $(l'=l)$ coupling (b) $2p\sigma_u$ - $4f\sigma_u$ $(l'=l+2)$ coupling, (c) $2p\sigma_u$ - $6h\sigma_u$ $(l'=l+3)$ coupling at R=12 a.u.. The corresponding P-values at R=12 a.u. are also shown with dot.

with one particular set of zeroes in each group of sensitive couplings, can be defined, in which a common "optimum" value can be found for both discrete and continuum transitions (see procedure below)

e. These features are independent of principal quantum number n' or continuum energy ϵ' .

f. They are also independent of the type of coupling considered (radial or angular).

g. In general, the effects are sharper and more definite at larger R-values (≥8.0 a.u.), and the total reduction in couplings is also greater. This is to be expected from the theory of "displacement" effects.

Using these facts we have developed the procedure to choose optimum β_n's for H_2^+ states as follows:

1) Perform a systematic calculation minimizing sums (III-10) for continuum states only, repeating for different continuum energies and different types of couplings. Omit the first two or three partial waves to obtain a "best" continuum β_n^c (Rankin's procedure).

2) Define from this an "allowed range" for further search, at most ± 8 % around β_n^c . (In this range, continuum couplings will still be greatly

reduced, but not absolutely minimized.)

3) Considering discrete-state couplings for as many transitions with $|\Delta l| \geq 2$ as possible (both radial and angular), locate a range of "best" discrete parameter, β_n^D .
4) The two ranges will lie within one another or at least overlap each other. Choose the optimum β_n from within the overlapped region. The uncertainty in the value corresponds to width of the overlap region.

Values for at the resulting parameters are listed in Table(III-1), for 16 states of H_2^+ at R=2,4,6,8,10,and 12 a.u. . (See discussion of Results, C.3 below). (A similar procedure can be used to locate β_n for HeH^{2+} states, after the determination of η_n^0).

3. Determination of Parameters for HeH^{2+}

In the asymmetric case HeH^{2+} , behavior of couplings between molecular states is strongly influenced by their asymptotic connection to atomic states of He^+ or H, except perhaps at small R values. The parameter η_n^0 gives clear indication of the limiting atomic character of a state, since it is the "crossover point" for which the switching function changes sign: for example, if the He nucleus is the

Table III.1 H_2^+ Switching Function Parameters

H_2^+ Switching Function Parameters β_n (u-state)

$f_n(r,R) = \tanh[\beta_n R\eta]$

State	R (a.u.)					
	2.0	4.0	6.0	8.0	10.0	12.0
$2p\sigma_u$	0.260	0.270	0.270	0.270	0.271	0.272
$3p\sigma_u$	0.160	0.158	0.154	0.151	0.148	0.146
$4p\sigma_u$	0.116	0.115	0.112	0.110	0.107	0.106
$5p\sigma_u$	0.093	0.092	0.088	0.087	0.086	0.085
$4f\sigma_u$	0.084	0.085	0.090	0.097	0.104	0.109
$5f\sigma_u$	0.067	0.068	0.071	0.075	0.077	0.078
$6f\sigma_u$	0.055	0.057	0.058	0.061	0.062	0.062
$2p\pi_u$	0.209	0.195	0.185	0.180	0.179	0.180
$3p\pi_u$	0.143	0.134	0.129	0.125	0.123	0.122
$4p\pi_u$	0.108	0.106	0.101	0.097	0.095	0.095
$5p\pi_u$	0.088	0.084	0.082	0.080	0.078	0.077
$6p\pi_u$	0.078	0.073	0.070	0.069	0.068	0.067

Table III.2 H_2^+ Switching Function Parameters

State	R (a.u.)					
	2.0	4.0	6.0	8.0	10.0	12.0
$4f\pi_u$	0.082	0.082	0.085	0.086	0.088	0.090
$5f\pi_u$	0.065	0.065	0.066	0.067	0.068	0.068
$6f\pi_u$	0.051	0.052	0.053	0.054	0.054	0.055
$4f\delta_u$	0.080	0.079	0.081	0.082	0.084	0.085
$5f\delta_u$	0.061	0.061	0.063	0.064	0.065	0.066

Table III.3 H_2^+ Switching Function Parameters

H_2^+ Switching Function Parameters β_n (g-state)

$f_n(r,R) = \tanh[\beta_n R\eta]$

State	R (a.u.)					
	2.0	4.0	6.0	8.0	10.0	12.0
$1s\sigma_g$	0.448	0.421	0.422	0.435	0.447	0.457
$2s\sigma_g$	0.248	0.230	0.224	0.221	0.224	0.228
$3s\sigma_g$	0.172	0.163	0.156	0.156	0.156	0.157
$4s\sigma_g$	0.133	0.126	0.123	0.121	0.120	0.120
$5s\sigma_g$	0.108	0.104	0.101	0.099	0.098	0.098
$3d\sigma_g$	0.130	0.144	0.152	0.151	0.150	0.149
$4d\sigma_g$	0.096	0.101	0.104	0.105	0.104	0.103
$5d\sigma_g$	0.077	0.081	0.082	0.082	0.081	0.080
$3d\pi_g$	0.126	0.129	0.129	0.129	0.128	0.128
$4d\pi_g$	0.095	0.095	0.095	0.095	0.094	0.093
$5d\pi_g$	0.076	0.076	0.076	0.076	0.075	0.075

A nucleus (η =-1), then a state for which η^*_n ≥0 (or even ≥+1) is evidently a "He^+-like" state. The 1sσ and 2pπ states of HeH^{2+} are clear cases of such states. At large enough distances R, some HeH^{2+} states also can be found with $\eta^*_n \leq 0$, corresponding to "H-atom" states; the 2pσ state is a good example. However, as a rule the "H-atom" states become really molecular states at smaller R-values and have two-centre character; some "He^+" states (e.g.3dσ) have some mixing and two-centre character,but it is usually less important.

a. For a completely atomic (one-centre) state, we know that Bates-McCarroll ETF's are correct. This means, for such a state, $f_n = -1$ (He^+), or $f_n = +1$ (H) everywhere, which would correspond to $\eta^*_n \gg +1$ or $\eta^*_n \ll -1$, respectively. For such a case, we should then find that couplings to other discrete states should be quite insensitive to the parameters of the switching function β_n, η^*_n . Any choice of these parameters which gives f= -1 (or =+1) everywhere will give good behavior of the matrix elements for most transitions. This is what we find, especially at larger R-values, for the "He^+" type states like 1sσ ,2sσ ,2pπ ,etc. For "H" states (like 2pσ) this behavior is found only at very large R values.

b. For the same reason, even at smaller R-values, coupling matrix elements from such an "atomic" He^+ state to other tightly bound discrete states are not very sensitive to parameters β_n, η_n° of the switching function, because the switching function is close to -1 everywhere in the region of overlap of the wave functions. As a rule, we find that for states where $\eta_n^\circ \geq +0.2$, couplings to discrete states are not very sensitive for this reason. For such states most information about the optimum parameters is found from the continuum couplings (and also Rydberg state couplings) because their wavefunctions can have overlap in regions where f is different from -1.

c. On the other hand, for the "molecular" type of states, both the continuum and discrete state couplings are sensitive to the switching function parameters, and determination of optimum values can be made using both types of data.

d. For those couplings which are sensitive to switching function parameters, qualitative features similar to those described in items (a)-(g) for H_2^+ (C.2 above) are found, but most consistently for couplings to continuum and Rydberg states. To some extent, the location of "clustering" zeroes vs. β_n can be affected by the value taken for η_n° and it is therefore important to locate the correct η_n° value before fixing β_n more carefully.

The procedure used to find parameters for HeH^{2+} is as follows:

1) Perform systematic calculations minimizing sums (III-10) for continuum states only, repeating for different ϵ' and coupling types. Omit the first two or three partial waves in such sums, to obtain "best" continuum parameters (Rankin's procedure).
2) From these calculations an "allowed range" for further search may be defined (±8 % about β_n^c ±15 % about η_n^c). Within this range, continuum couplings are greatly reduced, though not absolutely minimized.
3) The range of acceptable η_n° may be reduced to ±10 % by consideration of couplings to Rydberg states. The range of β_n, η_n° obtained by the above steps is narrow enough to identify "atomic" and "molecular" type states by their parameter values, and for "atomic He" states like $1s\sigma$ or $2p\pi$, the switching functions are adequately defined at this stage.
4) For "molecular" type states, couplings to discrete states are next examined to determine which couplings are sensitive to switching function parameters--within the ranges indicated by the continuum coupling study. (Because of the complications introduced by atomic character and

the asymmetry of the system, the couplings among the tightly-bound discrete states do not fall into a simple classification scheme like that found for H_2^+). For as many discrete couplings as possible, the locations of clustering zeroes vs. β_n^D and $\dot{\eta}_n^D$ are determined, and the final "optimum" values for these parameters are obtained from the region of overlap between the discrete and continuum parameter ranges.

Values for the resulting parameters are listed in Table(III-2), for 12 states of HeH^{2+} at the same R-values as for H_2^+. In general the uncertainties in these values are larger than those for H^+_2 .

4. Behavior of Optimum Parameters (H_2^+ and HeH^{2+})

a. H_2^+

Table(III-1) shows β_n values vs. R for a number of H_2^+ states. The values reported for $1s\sigma_g$,$2p\sigma_u$, $2p\pi_u$, and $2s\sigma_g$ are 5 % to 10 % larger than those previously reported by Rankin, and the estimated uncertainties are larger. For the $3d\sigma_g$ state, a quite different set of β_n values is found. This value corresponds to a different minimum in the continuum couplings than that selected by Rankin, and its correctness is confirmed by the behavior of

Table III.4 HeH^{2+} Switching Function Parameters

HeH^{2+} Switching Function Parameters β_n, η_n^o

$$f_n(\vec{r},R) = \tanh[\beta_n R(\eta-\eta_n^o)]$$

State	Param.	R (a.u.)					
		2.0	4.0	6.0	8.0	10.0	12.0
1sσ	β	0.844	0.918	0.948	0.964	0.973	0.975
	η^o	0.952	0.885	0.894	0.896	0.906	1.02
2sσ	β	0.554	0.548	0.541	0.539	0.537	0.533
	η^o	1.84	1.46	1.33	1.25	1.19	1.17
2pσ	β	0.411	0.361	0.341	0.328	0.322	0.325
	η^o	0.732	0.278	0.076	-0.145	-0.226	-0.332
2pπ	β	0.364	0.371	0.392	0.423	0.437	0.448
	η^o	1.37	0.970	0.878	0.798	0.828	0.837
3dσ	β	0.232	0.257	0.266	0.274	0.282	0.286
	η^o	1.83	0.724	0.513	0.484	0.485	0.506

Table III.5 HeH^{2+} Switching Function Parameters

3d π	β	0.229	0.226	0.221	0.220	0.224	0.238
	η^0	2.00	1.03	0.726	0.590	0.545	0.539
3p σ	β	0.271	0.267	0.260	0.256	0.251	0.247
	η^0	2.09	1.30	1.12	0.952	0.906	0.861
3p π	β	0.297	0.296	0.306	0.317	0.321	0.329
	η^0	2.27	1.53	1.26	1.14	1.10	1.04
4f σ	β	0.166	0.163	0.168	0.178	0.181	0.182
	η^0	2.96	1.53	0.871	0.586	0.466	0.411
4f π	β	0.164	0.160	0.161	0.161	0.161	0.158
	η^0	3.04	1.58	1.04	0.763	0.592	0.475
4d σ	β	0.162	0.171	0.176	0.177	0.179	0.180
	η^0	2.77	1.41	0.940	0.668	0.296	0.073
5g σ	β	0.142	0.136	0.134	0.134	0.133	0.133
	η^0	3.81	2.08	1.46	1.04	0.807	0.614

the discrete couplings, which do not have clustering zeroes near Rankin's value for $\beta_{3d\sigma_g}$. Confirmation for the values I have obtained here is obtained by their extraordinarily close agreement with the parameters β_n determined by Thorson et al using analytical decomposition of the angular wave functions (see Figure(III-2)).

An interesting regular behavior pattern is observed in the ratios of β_n for successively increasing principal quantum number:$(n \geq l+2)$

$$\beta_{3lm}/\beta_{2lm} = 0.70 \pm 0.05 \qquad \text{III-11a}$$

$$\beta_{4lm}/\beta_{3lm} = 0.75 \pm 0.05 \qquad \text{III-11b}$$

$$\beta_{5lm}/\beta_{4lm} = 0.81 \pm 0.02 \qquad \text{III-11c}$$

irrespective of the value of R and of (l,m). These and certain other regularities in the behavior of the parameters β_{lm} are confirmed and explained, by the analysis of TKCK. According to this analysis, the quantities $b_{nlm} = \beta_{nlm} R$ can depend only on (l,m) and the energy parameter c, $C^2 = -\epsilon_{nlm} R^2/2$.

Hence

$$(\beta_{n+1\ lm}/\beta_{nlm}) = (\epsilon_{n+1\ lm}/\epsilon_{nlm})^{1/2} \approx n/(n+1) \qquad \text{III-12}$$

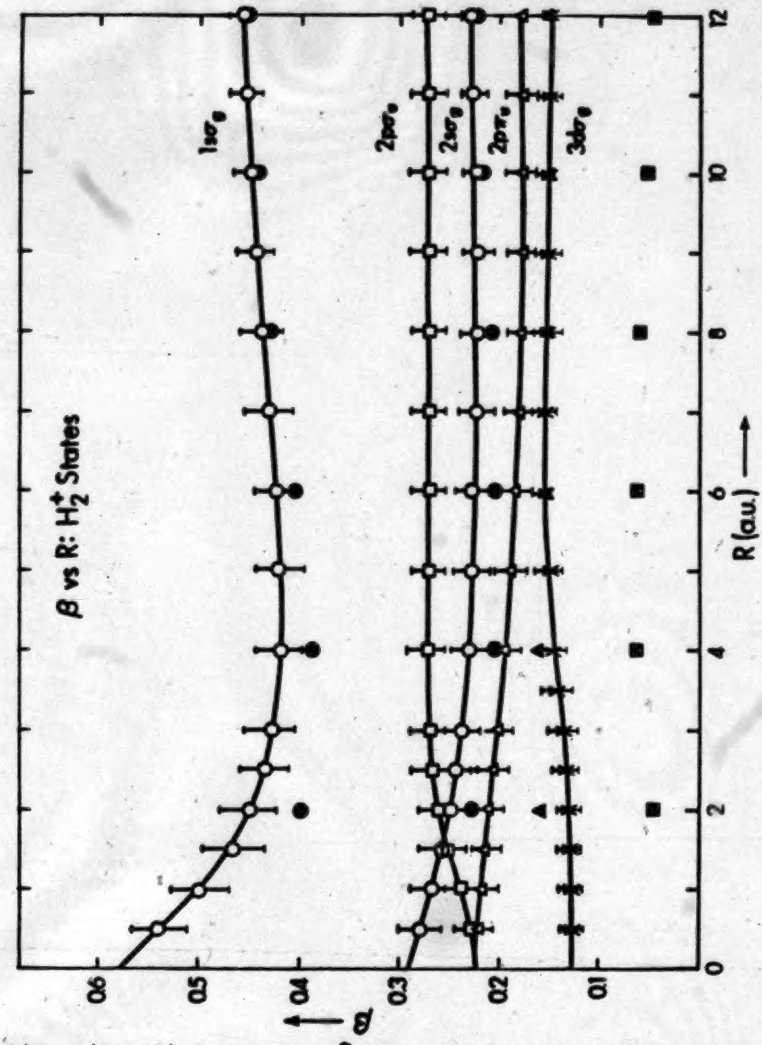

Figure(III-2) Parameter β vs. R for H_2^+ states. Solid curves show analytical results. All data points are values from "optimization" calculations. (●,●,▲,⊠ , values of Rankin and Thorson(29) for 1sσg ,2sσg ,2pπu , 3dσg ; ○,□,○,△,‡ as modified by inclusion of discrete-state coupling effects). Error bars indicate uncertainties in the latter.

For the lower lying states (e.g. $\beta_{2s\sigma_g}/\beta_{1s\sigma_g}$,etc) the ratios deviate from the rule (n/n+1) because the electronic energies deviate from the Bohr formula $-(1/n^2)$ due to bonding effects; however, the first equality in (III-11) still holds. Other regularities in the H_2^+ parameters may also be deduced from the analytical theory.

b. HeH^{2+}

Table(III-2) gives the parameters β_m. η_m° vs. R for HeH^{2+} states.

In his study, Rankin proposed a scaling law relating β_m for HeH^{2+} to β_m values for H^+_2,

$$\beta_n(HeH^{2+}) = \frac{3}{2}\beta_n(H_2^+)$$

and he argued on the basis of continuum matrix element behavior that this relation was confirmed. Comparison of the results in Tables (III-1, and III-2) shows that this rule is not very accurate when the discrete state couplings and a more complete study of continuum couplings is made.

Further studies on this subject should be pursued to understand the characteristic features of the detailed switching function in the different states in the different systems.

The analysis presented in TKCK(33) for H_2^+ may be extended only in an approximate way to asymmetric systems like HeH^{2+} . For the more "molecular" types of states, estimates of the parameters β_m, η_m^0 based on decomposition of the angular wave functions have been made. These agree fairly well with the values I have obtained here (see Figure(III-3,4)).

If empirical regularities of the type found for H_2^+ could be found here also, they could be useful to predict β_m values for upper states without performing optimization calculations. Some regularities of this kind are observed, but only between states which belong to the same nucleus as $R \rightarrow \infty$ and also large $R(\geq 8$ a.u.) only.

D. COUPLING MATRIX ELEMENTS

Figures(III-5) to (III-15) show nonadiabatic couplings calculated using switching functions determined by the above procedures for the H_2^+ and HeH^{2+} systems. For practical applications in the collision studies done here, I have used linear approximations to describe the R-dependence of the parameters β_m , η_m^0 for each state. Such an approximation appears quite drastic in some cases (especially for the behaviour of η_m^0 at small R) but in fact it has only a small effect on the coupling matrix elements and no effect on computed cross sections.

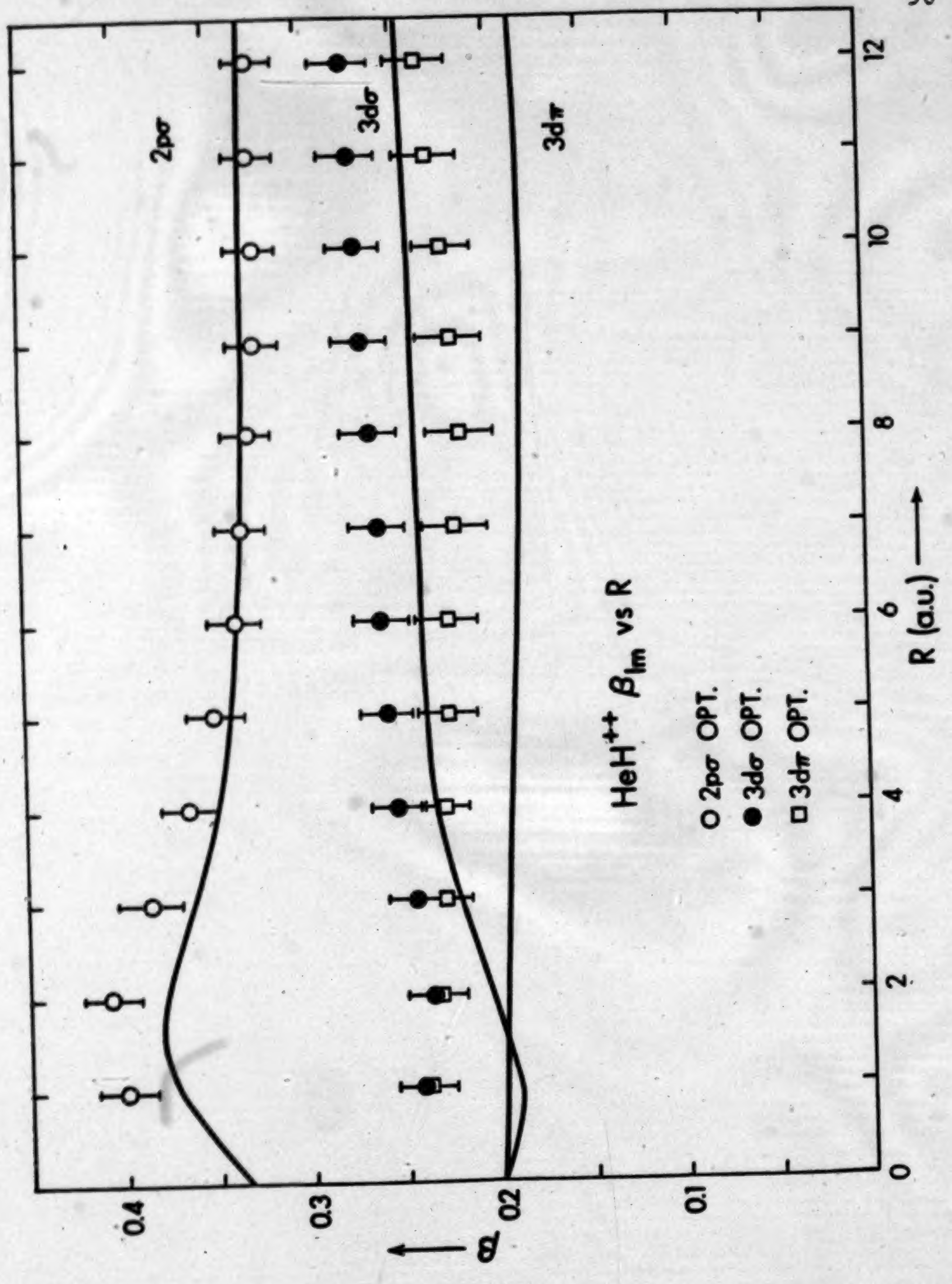

Figure(III-3) Parameters β vs. R for three states of HeH^{2+}; data points show "optimization" values for comparison.

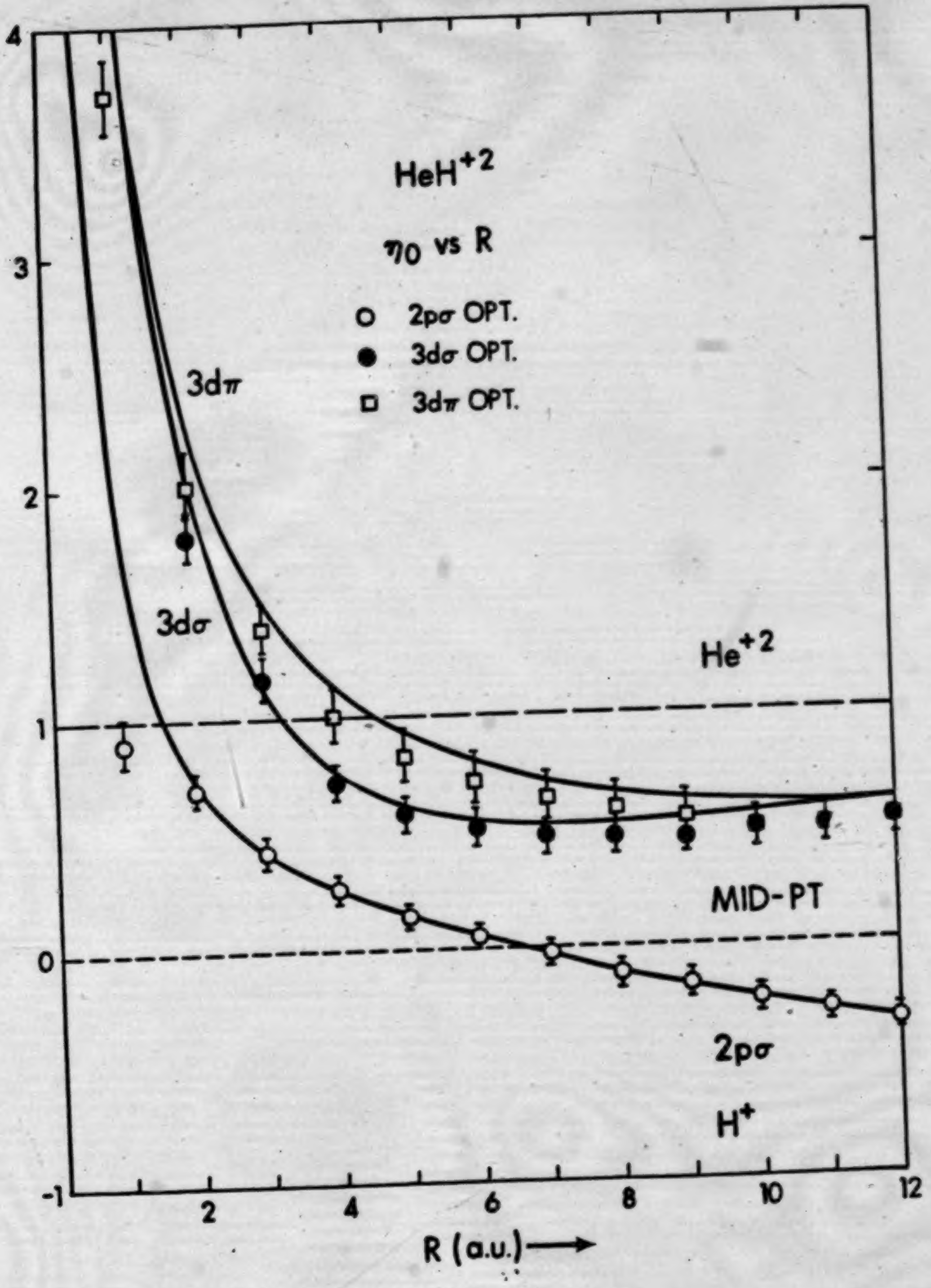

Figure(III-4) Parameters η^0 vs. R for three states of HeH²⁺; data points show "optimized" values for comparison.

More than 240 corrected nonadiabatic coupling matrix elements have been computed for the H_2^+ system, and more than 130 matrix elements for HeH^{2+} (this does not include the couplings to continuum states which were studied in the optimizing process). Figures(III-5) to (III-15) give only a representative sample of these matrix elements, but include especially the couplings which are most important in the collision processes studied in this work. I shall not discuss individual couplings and excitation processes in detail here (see Chapter V). However, a rough classification of the different types of couplings shown in the figures is helpful to understand where ETF correction effects are most likely to be important:

1. Classification of Couplings

The efficiency of coupling between two states in quantum mechanics is affected not only by the size and range of the coupling matrix element which connects them but also by the energy spacing between them. In particular, for low and even intermediate energy collisions the most efficient excitation processes always involve a resonance or near-resonance of two or more levels, that is, a "mediating degeneracy" which makes efficient coupling possible; such a degeneracy may be associated with the asymptotic limit $R \rightarrow \infty$, with the united-atom limit $R \rightarrow 0$, or with an isolated crossing or avoided crossing of levels at some finite R-value. For the one-electron systems studied here, crossings and avoided crossings do occur, but they play only a minor part in excitations. Couplings associated with orbital degeneracy of united atom levels are the most important excitation mechanisms in these systems (for example, the strong rotational $2p\sigma_u - 2p\pi_u$ coupling), but there are also some important couplings at very long range connected with degeneracy as $R \longrightarrow \infty$.

Below collision energies of ~1 KeV/amu, degeneracy-mediated couplings are really the only effective ones for excitation but in the intermediate range 1-10 KeV/amu this simple picture (based on the "Massey adiabatic criterion"(2)) is complicated by increased efficiency of excitation processes which are not so clearly connected with a mediating degeneracy. This is what makes collision processes in this energy region so much more interesting, and harder to predict without actual calculations. As the energy increases still more, above 10-15 KeV/amu, so many "non-resonant" excitation processes play a part that the idea of mediating degeneracy loses its significance. However for the intermediate energy region it is still very important and so energy gaps as well as coupling matrix elements must be considered to understand excitation processes.

Looking at coupling matrix elements themselves, it is useful to group them into two main categories, those which involve short-range coupling and those which involve couplings with very long range. [In a few cases a coupling may show both characteristics-for example, the $3d\sigma_g$ -$3d\pi_g$ coupling in H_2^+, Fig.(III-4), but this is not usual].

For the systems studied here the short range couplings mainly occur at distances $R \leq 12$ a.u.. They are associated with "quasimolecule" formation or even with united-atom behaviour. It is useful to divide them into subsets; first, the rotational couplings connected with orbital degeneracy of the united atom (for example, $2p\sigma$ -$2p\pi$,$3d\sigma$ -$3d\pi$,$3p\sigma$ -$3p\pi$,etc), and secondly, the many short-range radial couplings. The primary excitation steps in the H_2^+ and HeH^{2+} collision systems all involve these short-range couplings.

Long-range couplings may involve significant effects out to distances as large as 100 a.u. or more in some cases. They can be understood as perturbations of atomic states by the collision partner, which is an ion in these cases and causes Coulomb field perturbations. Here also we can distinguish two classes of long-range couplings relevant to the present case; first, asymptotic couplings within a degenerate atomic level (both Coriolis and radial couplings), and secondly, some long-range radial couplings between non-degenerate levels caused by polarization in the ion field (for example, π - π couplings in H_2^+). The long-range couplings play an important secondary part in producing further excitations following the primary (short-range) excitation steps.

The distinction between long-range and short-range couplings is important when considering ETF corrections to coupling matrix elements. As pointed out in the discussion on PSS theory, the most obvious defects of PSS theory are connected with its failure to describe asymptotic ($R \rightarrow \infty$) behaviour correctly; many couplings which actually have short-range character appear to have long-range behaviour due to the spurious displacement terms. However, these defects are also the easiest ones to remove, using almost any type of ETF description, because the states are almost atomic states (or linear combinations of them). At large R-values, therefore (say, $R \geq 12$ a.u.), there is no significant difference between corrected couplings computed using our switching functions and those computed with (say) appropriately constructed Bates-McCarroll-type ETF's, or with some other switching function. Therefore although the effects of long-range couplings are interesting by themselves, they do not provide any test of switching functions in comparison to other ETF descriptions.

On the other hand, the detailed form of the short-range couplings, which depend on molecular state behaviour, can be very sensitive to the choice used for ETF description.

Therefore we can expect the most significant effects resulting from differences in ETF descriptions to be seen in the intermediate energy region 1-10 KeV, where short-range non-resonant radial or degeneracy-mediated angular couplings can play an important part in excitation. As I shall show in Chapter V and VI, this turns out to be the case for both of the collision systems I have studied.

In comparing the behaviour of radial and angular coupling matrix elements shown in the Figures, it should be remembered that the radial coupling matrix elements must be multiplied by the radial velocity R, but angular coupling matrix elements by $\dot{\theta} = v_0 \rho / R^2$, to obtain the actual couplings; this moderates the apparently long range of many angular coupling matrix elements shown in the Figures.

2. Examples of Coupling Matrix Elements

(a) H_2^+ couplings

Figures(III-5) to (III-9) show all the coupling matrix elements used in the H^+-H(1s) collision calculations, for the 5 u-states and 5 g-states basis sets listed in Table(V-1). Examples of most of the types of couplings discussed above appear in these figures.

H_2^+ u-state

$2p\sigma_u$ coupling

Radial Coupling

Angular Coupling

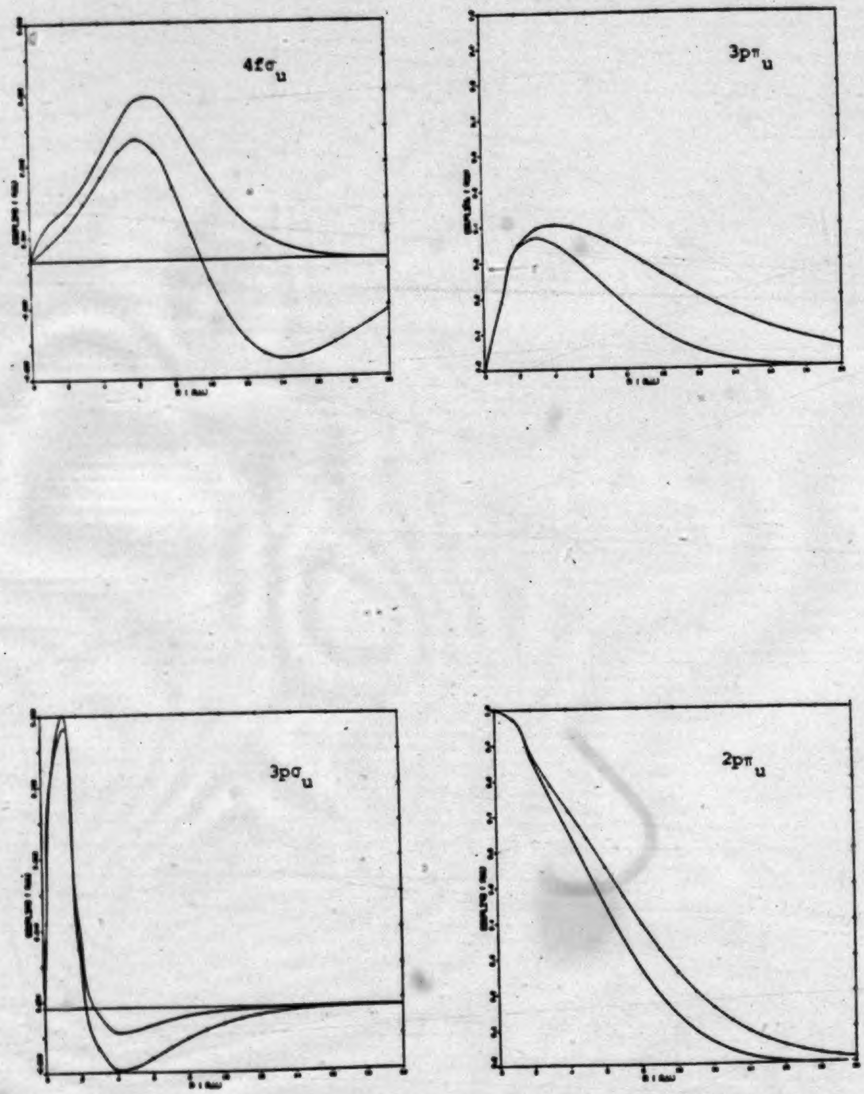

Figures(III-5 through 9) ETF-corrected nonadiabatic coupling matrix elements for H_2^+ system ——— , n ⟶ n' coupling and ●——● , n' ⟶ n coupling (e.g., n=$2p\sigma_u$ in Fig.(III-5)(shown on the top), and n' are shown in each figure.)

H_2^+ u-state

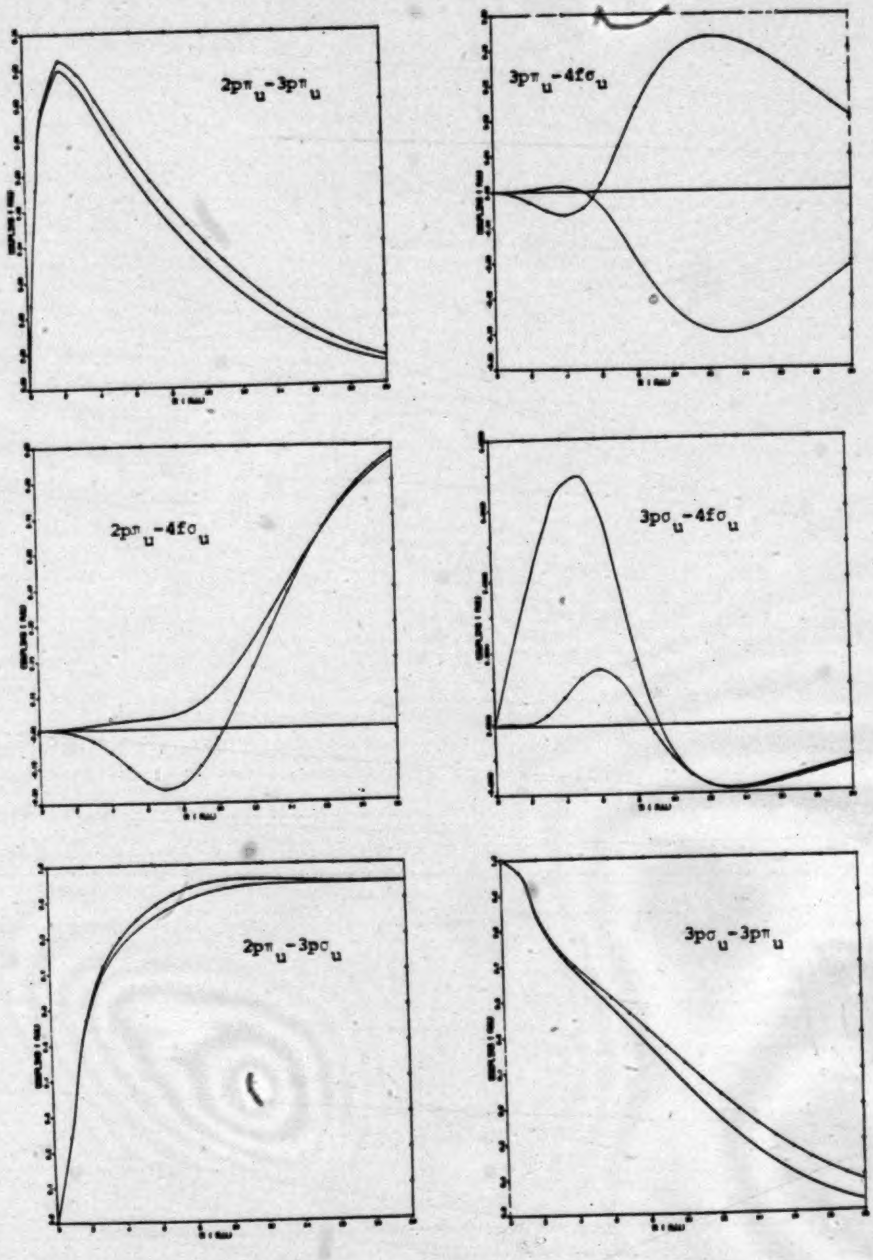

Figure III.6 ETF-corrected nonadiabatic coupling matrix for H_2^+ n corresponds to the state described on the left side in the figure, and n' corresponds to the state described on the right side in the figure.

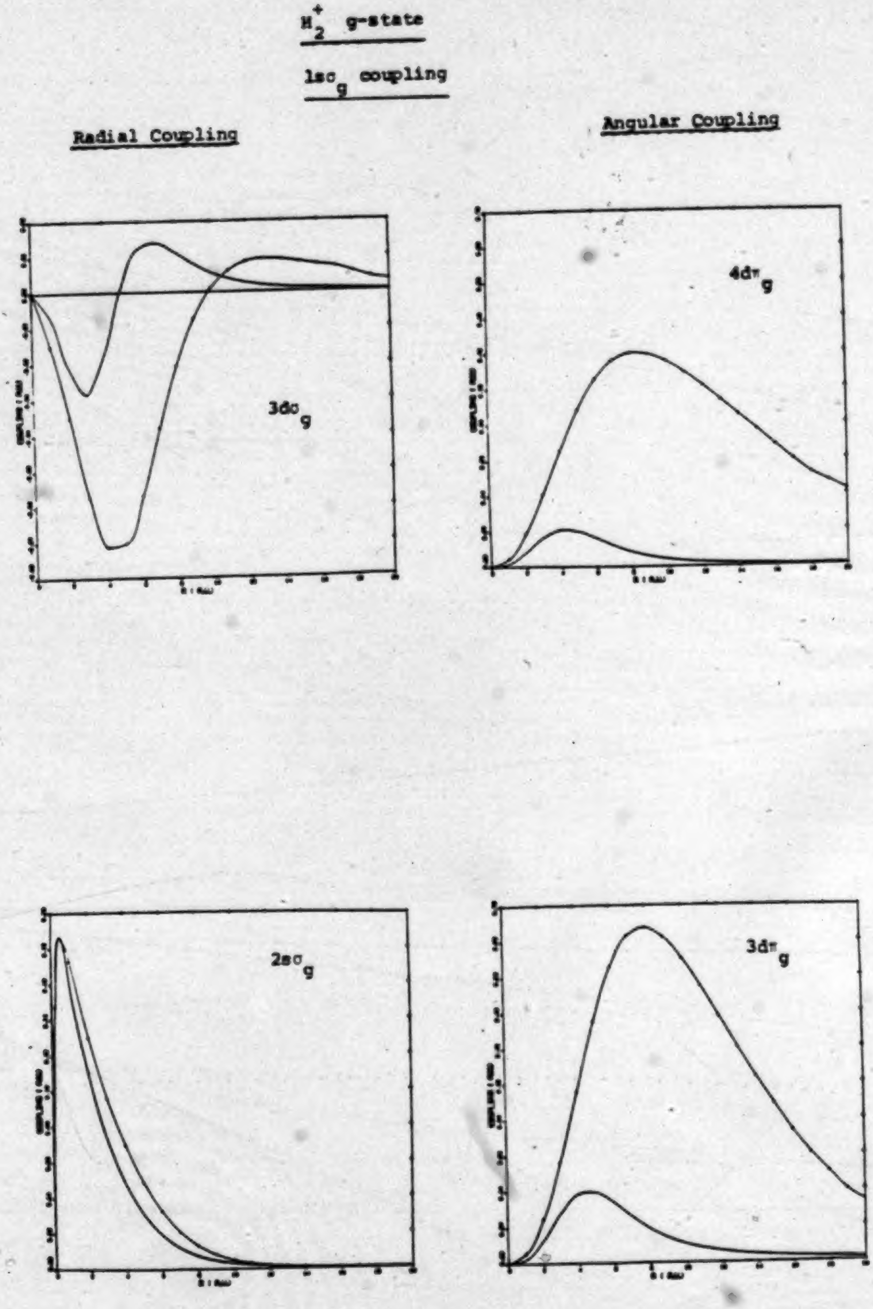

H_2^+ g-state

$1s\sigma_g$ coupling

Radial Coupling

Angular Coupling

Figure III.7 ETF-corrected nonadiabatic coupling matrix for H_2^+

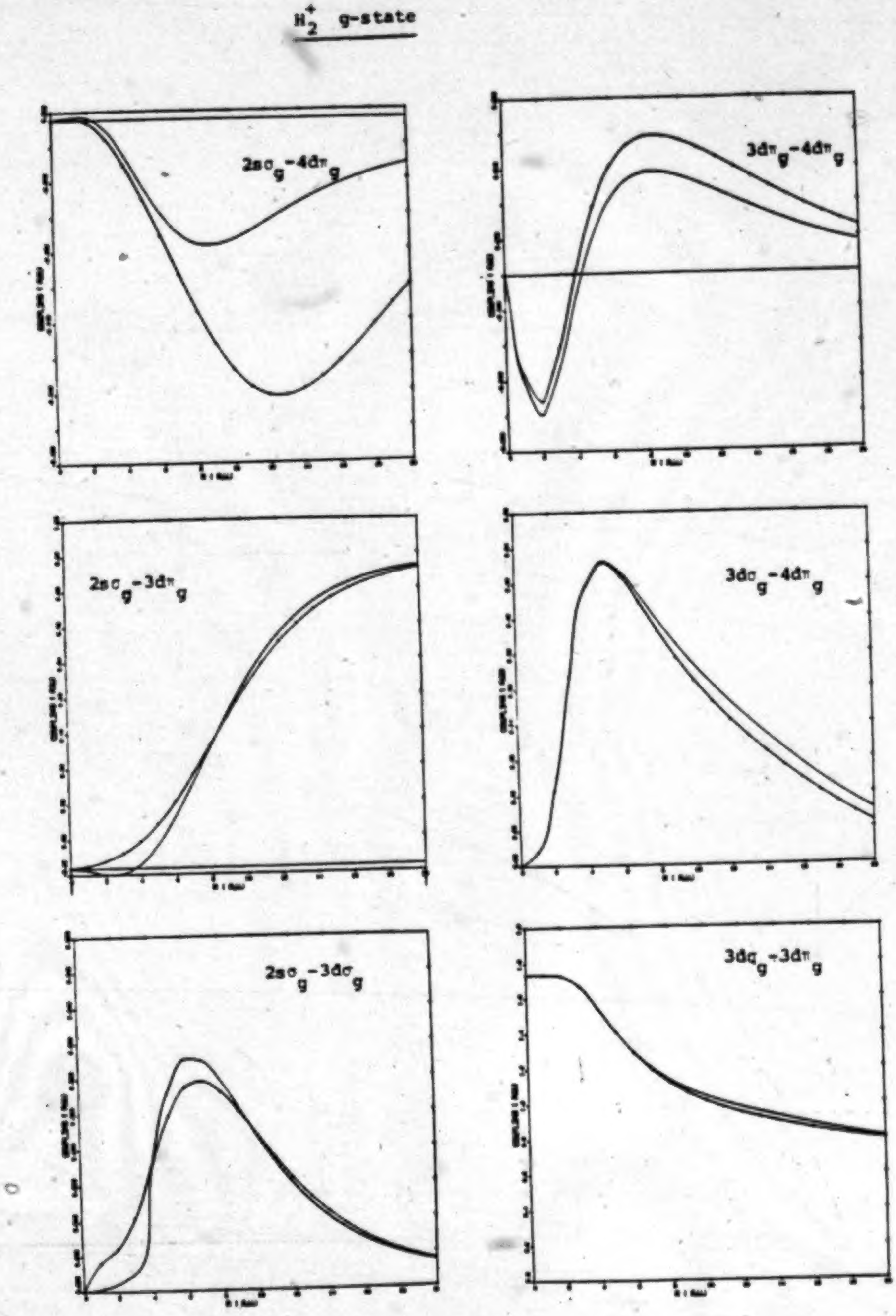

Figure III.8 ETF-corrected nonadiabatic coupling matrix for H_2^+

H_2^+ u-state long range π-π radial coupling

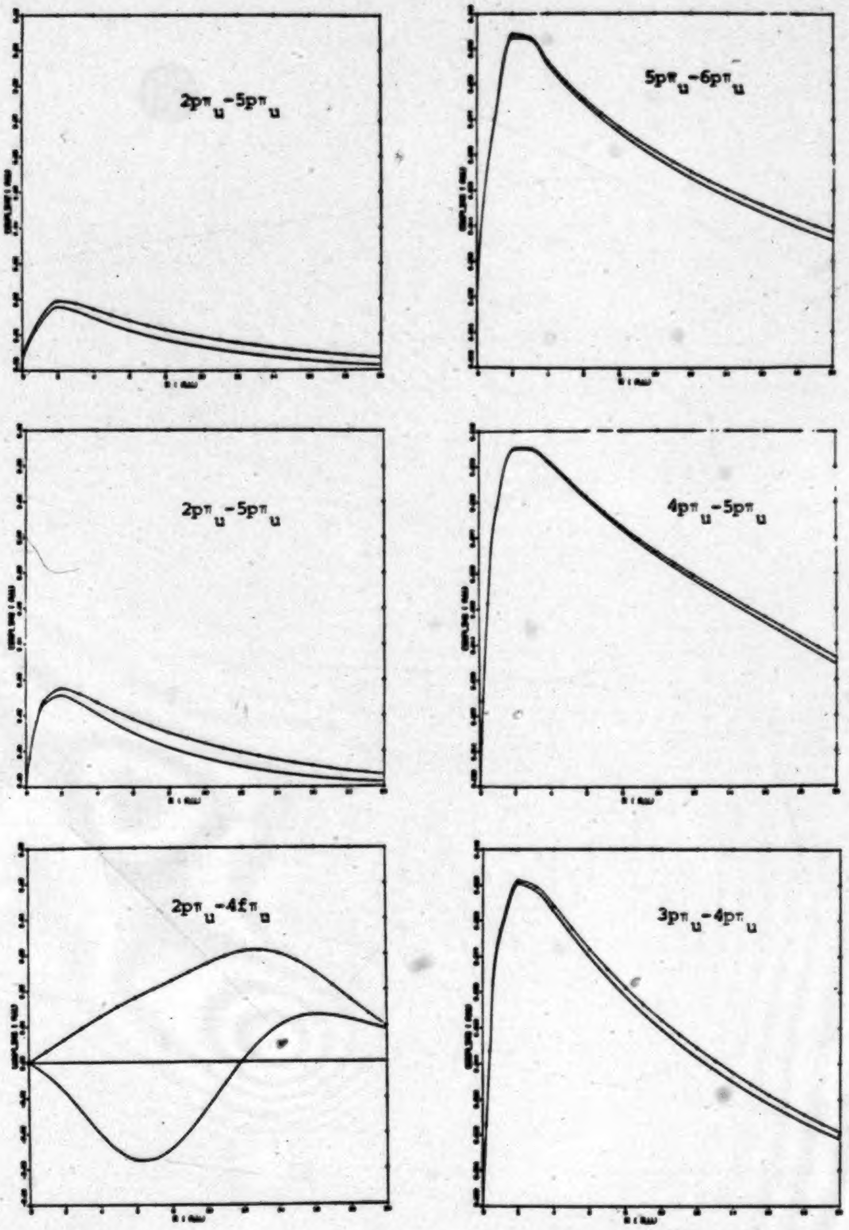

Figure III.9 ETF-corrected nonadiabatic coupling matrix for H_2^+

(b) HeH^{2+} couplings

Figures(III-10) to (III-15) show coupling matrix elements for HeH^{2+}, in particular for couplings linking 2pσ (initial state for He^{2+}-H(1s) collisions) and 1sσ (initial state for H^{+}-He^{+}(1s) collisions) with other states, and for couplings involving other important states in the excitation processes which occur.

(c) Asymptotic couplings in degenerate manifolds

The atomic H(2s),H(2p) levels and He^{+}(2s),He^{+}(2p) levels are degenerate asymptotically. The molecular states involved are (2pπ_u ,3pσ_u ,4fσ_u) and (3dπ_g ,3dσ_g ,2sσ_g) in H_2^{+}, and (2pπ ,3dσ ,2sσ) in HeH^{2+}. In each set of three states the two σ states are correlated asymptotically to sp hybrid (Stark field) orbitals. They are both coupled to the π level by Coriolis coupling [within the atomic level, the matrix element of the atomic orbital angular momentum $\hat{L}_y^T$ between 2p$_1$ and 2p$_0$ is a constant], and they are coupled to each other by a radial coupling which decreases as R^{-2} (the effective Coriolis coupling also decreases as R^{-2} when the angular velocity is included). The splittings within each set of states also decrease to zero as R^{-3} asymptotically, and the result is a long-range coupling problem which we found most convenient to solve separately by a method described in Chapter IV.(Section D).

HeH^{2+}

2pσ Radial Coupling

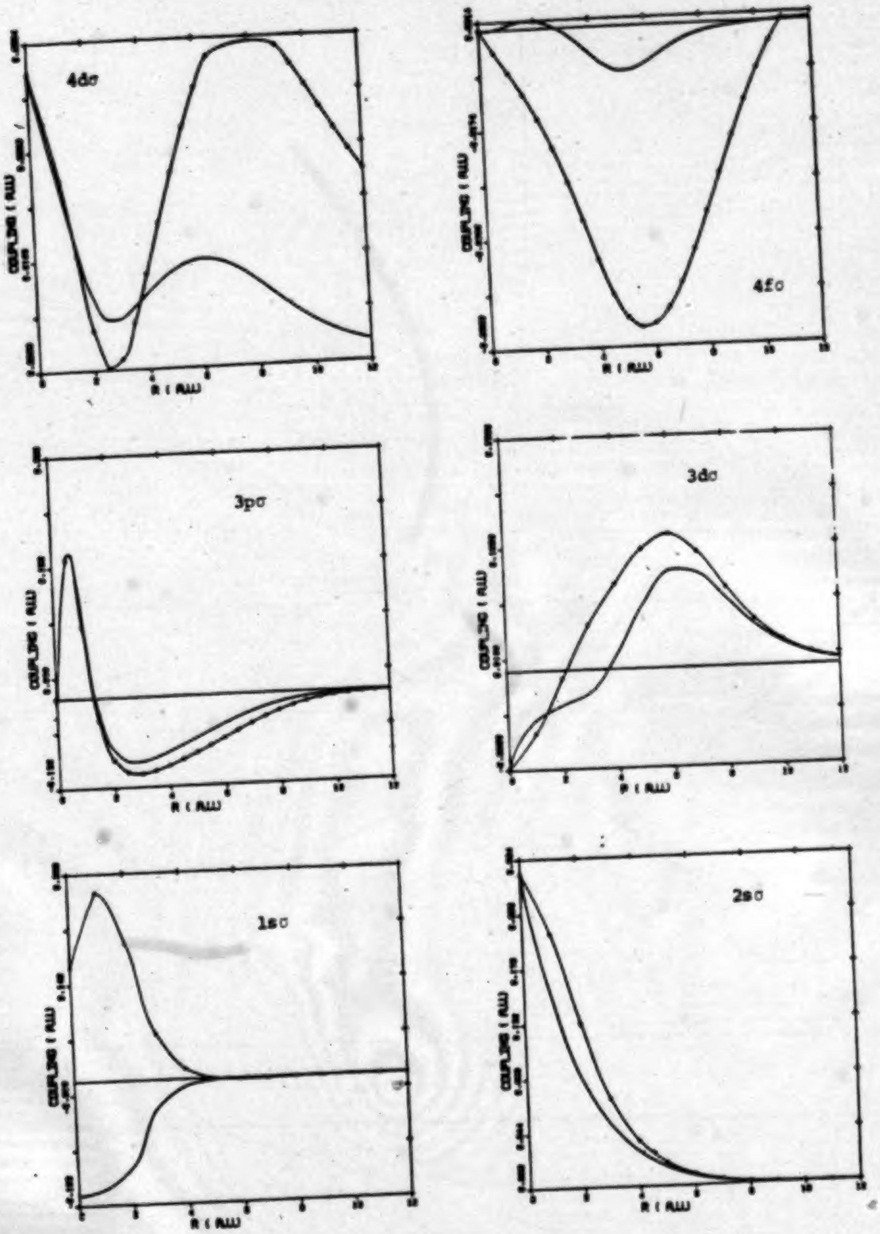

Figures(III-10 through 15) ETF-corrected nonadiabatic coupling matrix elements for HeH^{2+} system ——, n ⟶ n' coupling and ●—●, n' ⟶ n coupling (e.g., n=2pσ in Fig.(III-10) (shown on the top), and n' are shown in each figure.)

HeH^{2+}

2pσ Angular Coupling

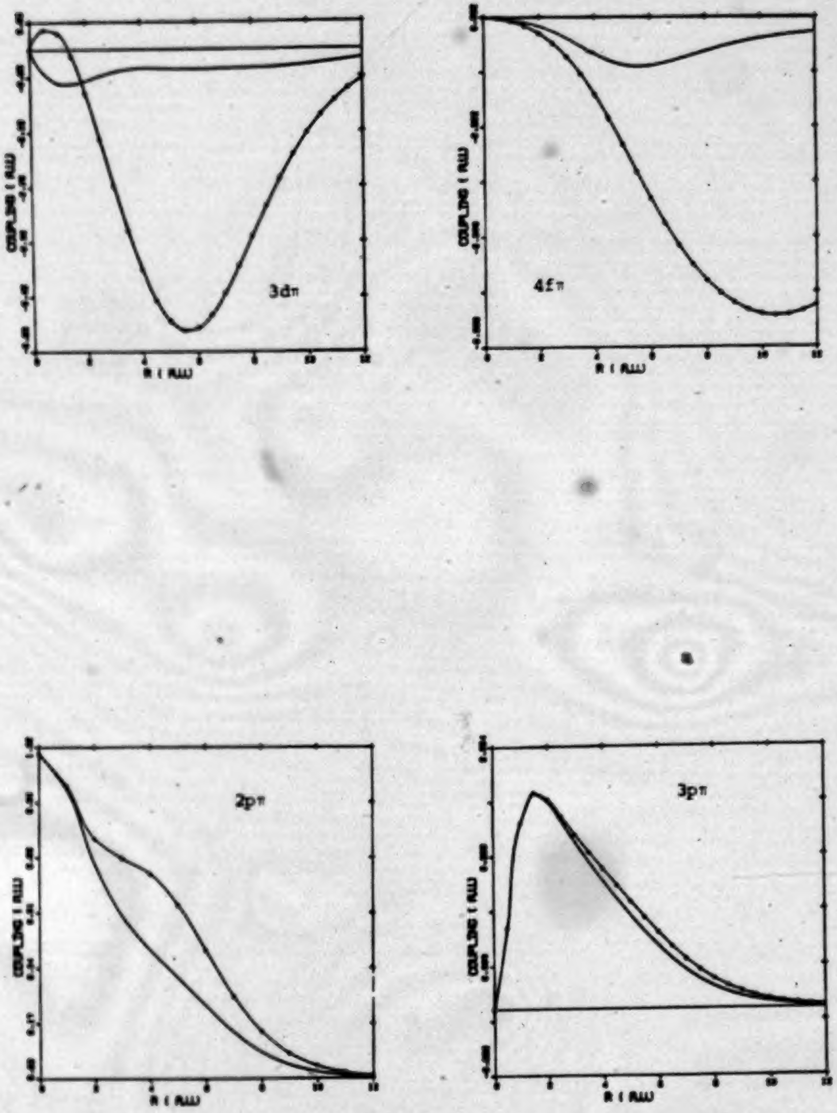

Figure III.11 ETF-corrected nonadiabatic coupling matrix for He^{2+}

HeH^{2+}

3dσ Radial Coupling

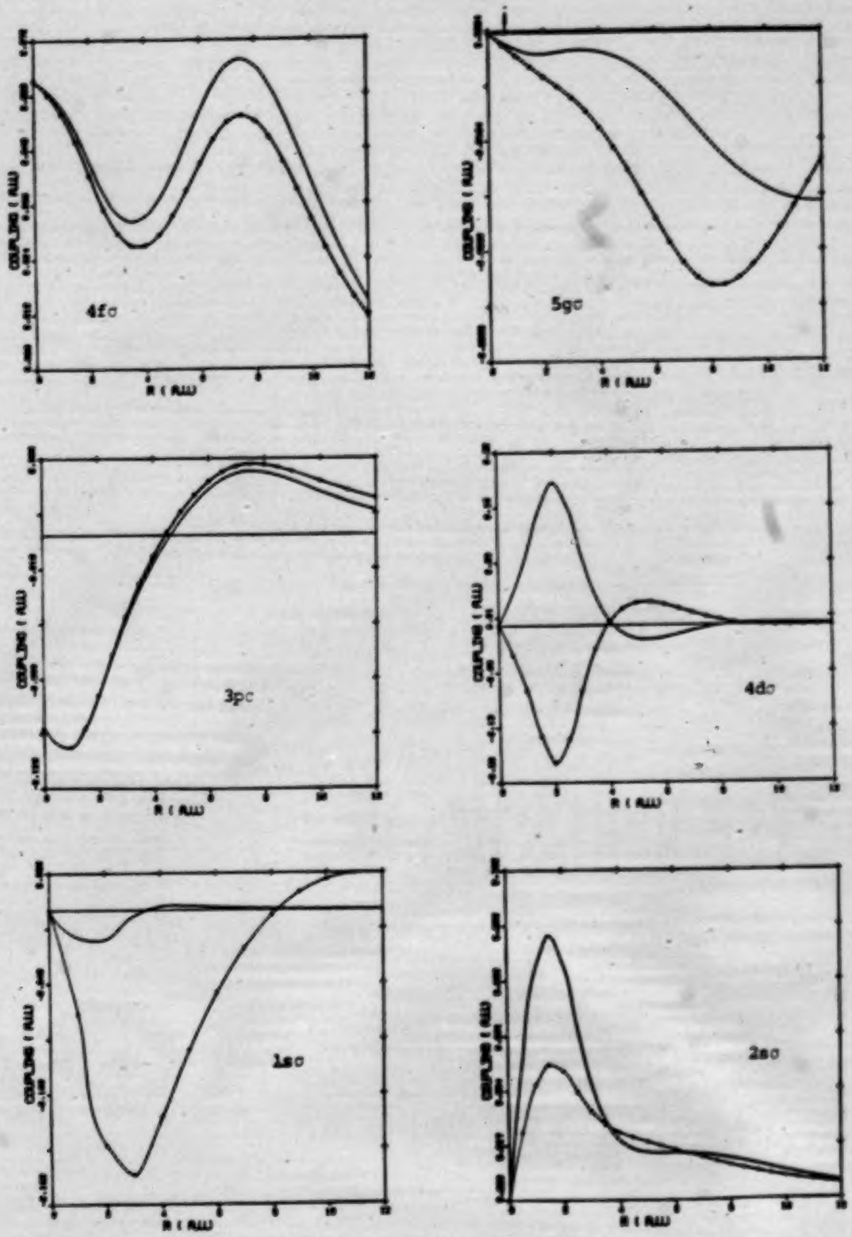

Figure III.12 ETF-corrected nonadiabatic coupling matrix for He^{2+}

HeH^{2+}

3dσ Angular Coupling

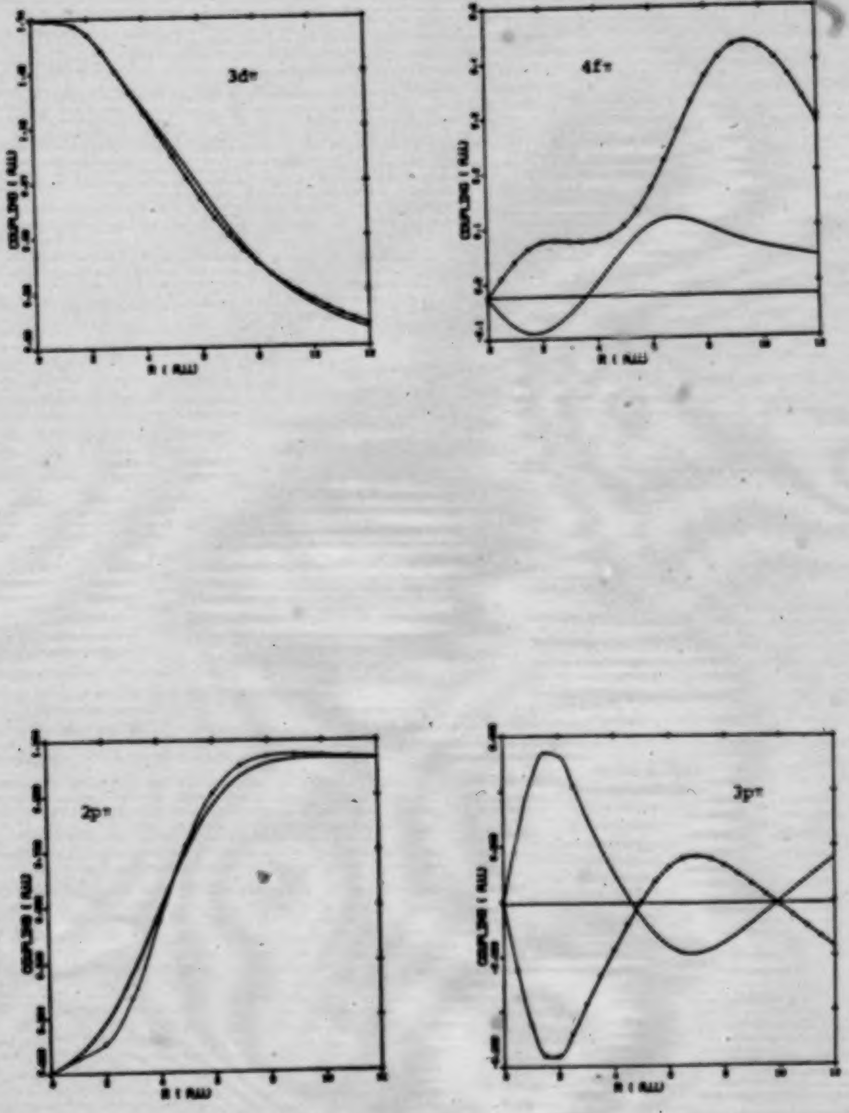

Figure III.13 ETF-corrected nonadiabatic coupling matrix for He^{2+}

HeH^{2+}

2pπ Radial Coupling

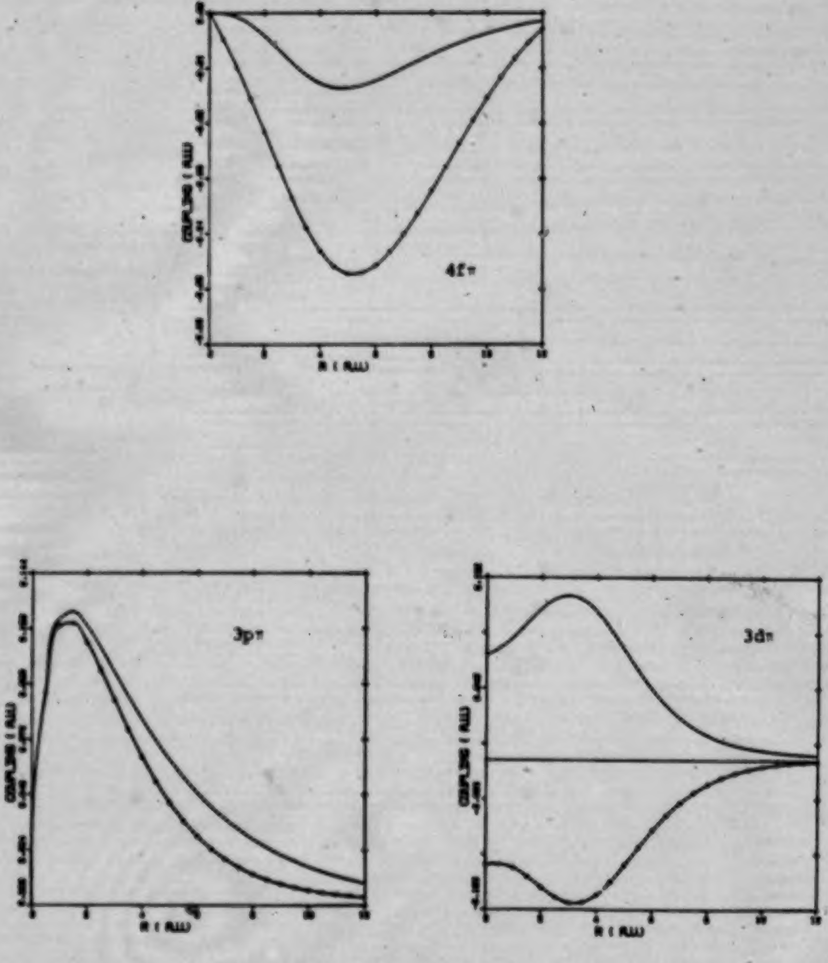

Figure III.14 ETF-corrected nonadiabatic coupling matrix for He^{2+}

HeH^{2+}

2pπ Angular Coupling

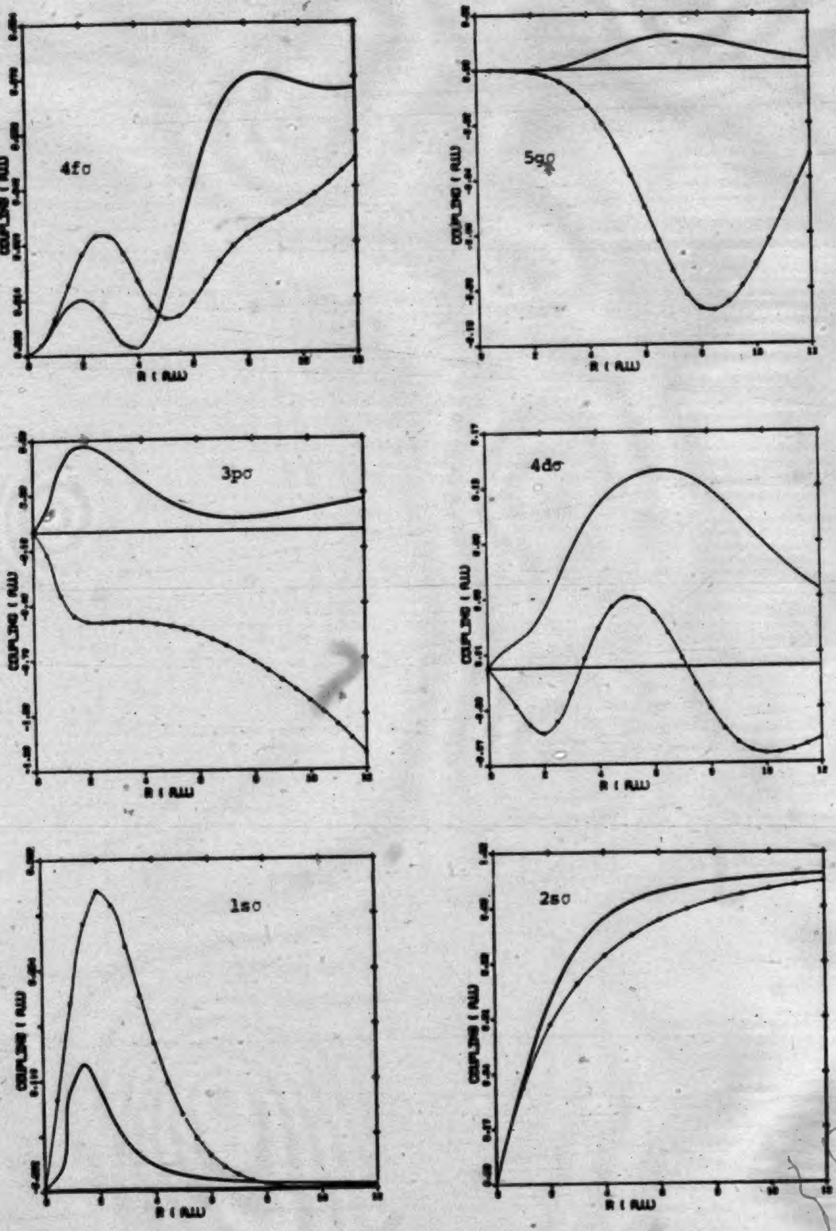

Figure III.15 ETF-corrected nonadiabatic coupling matrix for He^{2+}

Figure(III-16) shows typical examples of these long range Coriolis and radial couplings along with some examples of short range radial and angular couplings in HeH^{2+} system. (Note that the couplings shown in the Figure are not multiplied by the radial and angular velocities, respectively.)

(d) Long-range radial ($\pi - \pi$) couplings in H_2^+

As shown in Figure(III-9), the $2p\pi_u$ -$3p\pi_u$ radial coupling has a long "tail" extending well beyond $R \geq 20$ a.u.. This effect is due to polarization of the diffuse atomic π orbitals by the ion field. The phenomenon is quite general and Figure(III-9) shows a whole series of these $\pi - \pi$ radial couplings for π states of the H_2^+ system. Asymptotically these tails decrease as R^{-2}, a result which can be predicted by considering the field of the distant proton as the R-dependent potential (seen from the atom to which an electron is bound) and using the Hellmann-Feynman theorem to compute the corrected nonadiabatic coupling. The same couplings can be seen among π_g states.

We have found that these couplings play a significant part in H^+-H(1s) collisions, since they provide the mechanism for sequential excitation of higher Rydberg levels by a "ladder climbing" process. A substantial portion of the flux involved may eventually appear as ionization.

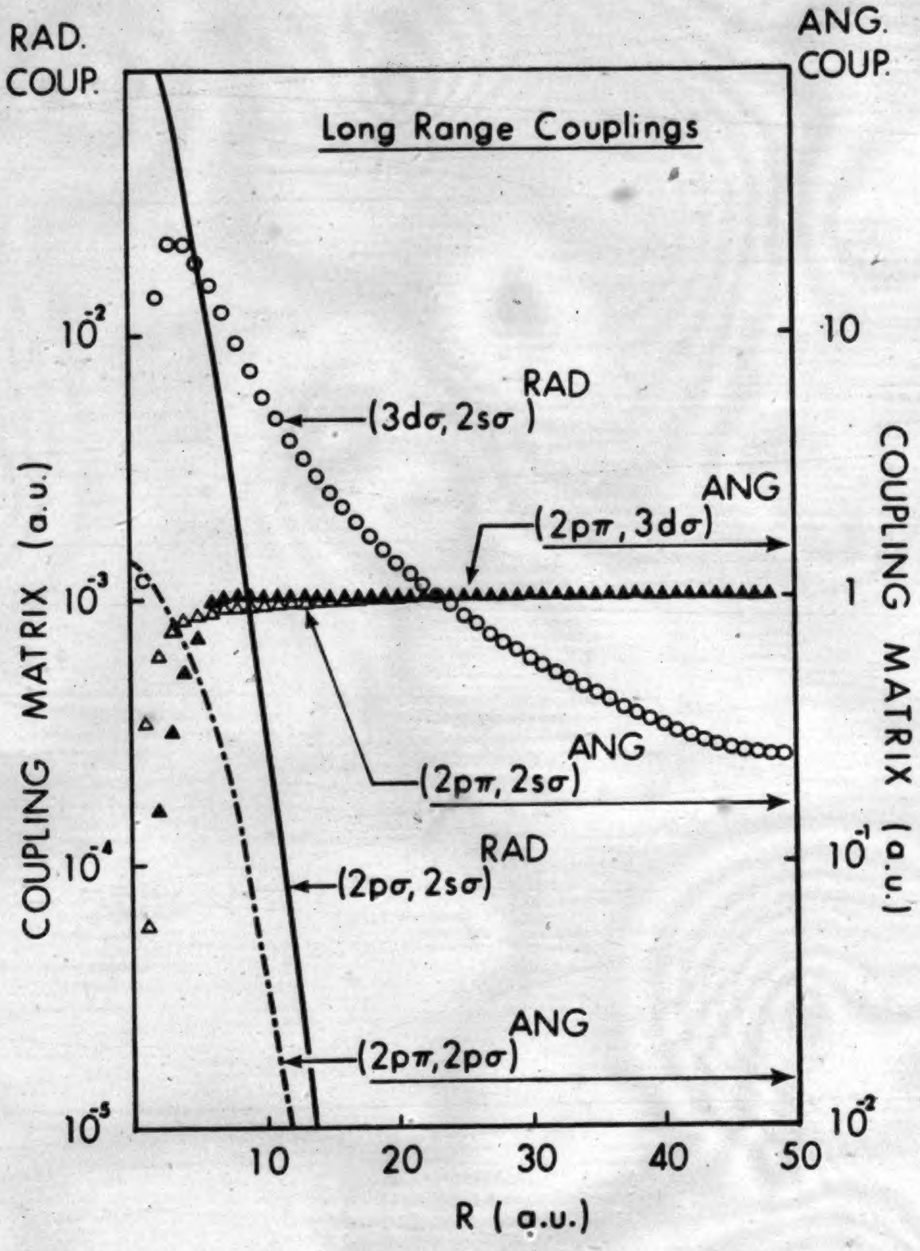

Figure(III-16) long-range coupling matrix elements for both Coriolis and radial couplings along with short range radial and angular couplings in HeH^{2+} system.

IV. METHODS OF COMPUTATION

In this section, we define some mathematical details of the wave functions and coupling matrix elements and discuss briefly the computational methods used in this study. The discussion can be divided into four topics:

A. Calculation of electronic wavefunctions.

B. Calculation of coupling matrix elements.

C. Numerical integration of coupled equations.

D. Long range coupling problem

A. CALCULATION OF ELECTRONIC WAVEFUNCTIONS

The one-electron two-centre problem has well known solutions. The electronic Schroedinger equation for fixed nuclei is

$$[-(\hbar^2/2\mu)\vec{\nabla}_r^2 - (Z_A e^2/r_A + Z_B e^2/r_B) - \varepsilon_\mu(R)]\psi_\mu(\vec{r};\vec{R}) = 0 \qquad \text{IV-1}$$

where $\epsilon_\mu(R)$ is the electronic binding energy. Introduction of prolate spheroidal coordinates

$$\xi = (r_A + r_B)/R , \qquad 1 \leqslant \xi < \infty$$

$$\eta = (r_A - r_B)/R , \qquad -1 \leqslant \eta \leqslant +1 \qquad \text{IV-2}$$

$$\phi = \text{azimuth about } \vec{R}, \qquad 0 \leqslant \phi \leqslant 2\pi$$

leads to separation of the eigenfunctions in the form

$$\psi_\mu(\vec{r};\vec{R}) = F_\mu(\xi)S_\mu(\eta)\Phi_\mu(\phi) \qquad \text{IV-3}$$

The factors obey the eigenvalue equations:

a. Radial equation

$$d/d\xi[(\xi^2-1)dF_\mu/d\xi] + [-c^2\xi^2 + q\xi + A_\mu - m^2/(\xi^2-1)]F_\mu = 0 \qquad \text{IV-4a}$$

b. Angular equation

$$d/d\eta[(1-\eta^2)dS_\mu/d\eta] + [c^2\eta^2 + p\eta - A_\mu - m^2/(1-\eta^2)]S_\mu = 0 \qquad \text{IV-4b}$$

c. Azimuthal equation

$$d^2\Phi_\mu/d\phi^2 + m_\mu^2\Phi_\mu = 0 \qquad \text{IV-4c}$$

In these equations, $q = R(Z_A + Z_B)$, $p = R(Z_A - Z_B)$, and $c^2 = -\varepsilon_\mu R^2/2$, if ϵ_μ is in a.u.. A_μ is the separation constant associated with the angular equation.

We represent the eigenfunctions in the forms

$$F_\mu(\xi) = (\xi^2-1)^{m/2}(\xi+1)^\sigma e^{-c\xi}\sum_{j=0}^{\infty} c_j(\xi-1/\xi+1)^j \qquad \text{IV-5a}$$

$$S_\mu(\eta) = e^{-c\eta}\sum_{k=m}^{\infty} f_k P_k^m(\eta) \qquad \text{IV-5b}$$

$$\Phi_\mu(\phi) = (2\pi)^{-1/2} e^{im\phi} \qquad \text{IV-5c}$$

m is the azimuthal quantum number (=0,+1,+2,etc). In the united atom limit, R → 0, $A_\mu \rightarrow -l(l+1)$, and the states may be labelled at all R by the limiting quantum numbers (nlm).

To compute eigenfunctions and eigenvalues, the main task is the search procedure and calculation of separation constant A_μ and energy parameter C in a self-consistent way. The problem is a well-known one and has been adequately described elsewhere(35-37). We found it most convenient to compute eigenvalues and eigenfunctions by following a state from its known limiting properties at R=0 and continuing outward with a sufficiently small stepsize in R (~0.25 a.u.) to guarantee convergence on the same state. Eigenvalue computation methods are based on that described by Bates and Carson(35) and some parts of the scheme developed by Rankin(29) are also used.

Precision errors in the computed eigenvalues and eigenfunctions are less than 10^{-9} and 10^{-7} respectively.

B. CALCULATION OF COUPLING MATRIX ELEMENTS

In Eqs.(II-20) there are nonadiabatic coupling terms of first- and second-order in the collision velocity. The first-order terms are more important and we discuss their computation in detail. The second-order terms are small enough to be neglected over the whole energy range I studied for the HeH^{2+} collision system, and are non-negligible only at energies $E \geq 5$ KeV for the H_2^+ collision system.

1. Computation of First-Order Coupling Matrix Elements

a. PSS Radial Coupling

$$P^R_{mn} = -i\hbar \langle m|\partial/\partial R|n\rangle \qquad \text{IV-6}$$

A number of computational techniques may be used:

(i) Direct Differentiation

Explicit application of the formula (IV-6) requires the calculation (numerically) of derivatives of parameters and expansion coefficients in Eqs.(IV-6) with respect to R and this is an inefficient procedure.

(ii)Usual Hellmann-Feynman Theorem

Alternatively, we can use Eq.(IV-6)

$$-i\hbar\langle m|(\partial/\partial R)_{\vec{r}}|n\rangle = -i\hbar\langle m|(\partial V/\partial R)_{\vec{r}}|n\rangle/(\varepsilon_m - \varepsilon_n) \qquad \text{IV-7}$$

Unfortunately, the evaluation of the numerator in the RHS of Eq(IV-7) involves integrals with logarithmic singularities which are also tedious and relatively inefficient to compute.

(iii)Modified Hellmann-Feynman Relation

A third alternative involves the best of both of the above methods and requires neither numerical differentiation nor unpleasant integrals. Noting that

$$(\partial/\partial R)_{\vec{r}} = (\partial/\partial R)_{\xi,\eta} - R^{-1}\ \mathrm{X}$$
$$\{1/(\xi^2-\eta^2)[\xi(\xi^2-1)(\partial/\partial\xi)_{R,\eta} + \eta(1-\eta^2)(\partial/\partial\eta)_{R,\xi}]\} \qquad \text{IV-8}$$

it follows that

$$-i\hbar\langle m|(\partial/\partial R)_{\vec{r}}|n\rangle = -i\hbar\{\langle m|(\partial H_{el}/\partial R)_{\xi,\eta}|n\rangle/(\varepsilon_m - \varepsilon_n)$$
$$-R^{-1}[\langle m|\xi(\xi^2-1)/(\xi^2-\eta^2)\partial/\partial\xi|n\rangle + \langle m|\eta(1-\eta^2)/(\xi^2-\eta^2)\partial/\partial\eta|n\rangle]\} \qquad \text{IV-9}$$

Since

$$(\partial\hat{H}_{el}/\partial R)_{\xi,\eta} = -2/R\hat{H}_{el} - (e^2/a_0)\hat{V}/R^2 \qquad \text{IV-10}$$

it follows that the evaluation of all integrals in (IV-9) is completely straightforward. To check numerical accuracy we have compared results obtained by all three of the above techniques, and agreement to five or six significant figures was obtained. In practice we have used the third method as it is about three times faster and much easier to program.

b. PSS Angular Coupling

$$P^{\Theta}_{mn} = -R^{-1}\langle m|\hat{L}_y|n\rangle \qquad \text{IV-11}$$

$\hat{L}_y$ is the electronic orbital angular momentum component on the y-axis (⊥ to R), measured from the geometric centre. In prolate spheroidal coordinates, it is given by

$$\hat{L}_y = -i\{\cos\phi[(\xi^2-1)(1-\eta^2)]^{1/2}/(\xi^2-\eta^2)[\eta\partial/\partial\xi - \xi\partial/\partial\eta]$$

$$-\sin\phi\,\xi\eta/[(\xi^2-1)(1-\eta^2)]^{1/2}\partial/\partial\phi\} \qquad \text{IV-12}$$

The resulting integrals may be done straightforwardly.

c. ETF Correction Matrix Elements A^R_{mn} , A^θ_{mn}

$$A^R_{mn} = (im/2\hbar)(\varepsilon_m - \varepsilon_n)\langle m|zf_n(\vec{r};R)|n\rangle \qquad \text{IV-13}$$

$$A^\Theta_{mn} = (im/2\hbar)(\varepsilon_m - \varepsilon_n)\langle m|xf_n(\vec{r};R)|n\rangle \qquad \text{IV-14}$$

Here

$$z = R/2\xi\eta \qquad\qquad x = R/2[(\xi^2-1)(1-\eta^2)]^{1/2}\cos\phi$$

and $f_m(\vec{r};R)$ (defined in Eq(III-6)) depends only upon η ,R.

It is most convenient in this case to do the integrals over η by Gauss-Legendre quadrature, rather than employ analytical methods. Again evaluation presents no difficulties.

2. Computation of Second-Order Coupling Matrix Elements

The matrix elements which must be evaluated for the second-order couplings are catalogued explicitly in the following equations:

$$(im/\hbar)\{<k|[\vec{V}\cdot(\vec{s}_n-\vec{s}_k)][\vec{V}\cdot(-i\hbar\vec{\nabla}_R + (im/\hbar)[H_{el},\vec{s}_n]))]|n> \qquad \text{IV-15a}$$

$$\sum_j <k|[\vec{V}\cdot(\vec{s}_j-\vec{s}_k)]|j><j|\vec{V}\cdot(-i\hbar\vec{\nabla}_R + (im/\hbar)[H_{el},\vec{s}_n])|n> \qquad \text{IV-15b}$$

$$\begin{aligned}&<k|(m/8)[(f_n^2-1)\vec{V}^2 + (\vec{V}\cdot\vec{r})^2(\vec{\nabla}_r\cdot f_n\vec{r})^2 \\ &+ 2(\vec{V}\cdot\vec{r})(f_n\vec{V}\cdot\vec{\nabla}_r f_n + 2\vec{V}\cdot\vec{\nabla}_R f_n)]|n> \qquad \text{IV-15c}\end{aligned}$$

To evaluate these very messy expressions requires some unavoidable algebra. In the case of terms (III-15a) involving ($\vec{\nabla}_R$) we cannot make use of the Hellmann-Feynman trick and it is necessary to compute derivatives of the wavefunction coefficients numerically. However, all the integrals which appear are completely straightforward to evaluate numerically.

The most important second-order terms are those of Eqs.(IV-15a). The complicated radial-angular cross terms (IV-15) are quite unimportant, since in nearly all couplings either the radial or the angular coupling is the dominant part.

We found it most efficient to evaluate both integrals over ξ and over η by numerical quadrature for all matrix elements, Gauss-Laguerre for ξ, and Gauss-Legendre for η. We tested 10,28,64, and 98 point Gauss-Laguerre and 10,32,80 point Gauss-Legendre quadratures and found that 28 point Gauss-Laguerre and 32-point Gauss-Legendre quadrature give a precision in every case of at least five significant figures.

C. NUMERICAL INTEGRATION OF COUPLED EQUATIONS

The coupled equations (II-19),(II-23) must be solved to determine the final state scattering amplitudes $a_n(+\infty ; \rho)$, given the initial conditions for each collision problem. I integrated the coupled equations numerically using time t (a.u.) as an independent variable. For most calculations, straight-line constant velocity trajectories were used; for cases where Coulombic trajectories were employed, the configuration variables (R, θ) must be related to the time t by the Coulomb trajectory formula.

I used the method of Bulirsch and Stoer(39) which is based on the principle of rational extrapolation, for numerical integration of the coupled equations. This method seems to have found wide acceptance by workers in atomic collision theory. It is faster and more accurate than multistep predictor-corrector methods such as the Adams-Moulton-Bashforth method and requires no special start-up codes as they do. In my calculations, the relative truncation error (controlling the step-size) was automatically maintained between 1×10^{-4} and 1×10^{-6}.

Conservation of probability (cf. Chapter II.) was checked and maintained between 1×10^{-4} and 1×10^{-8}. I found that in much of the integration , surprisingly large step-sizes could be used (3-12 a.u. in time t, depending on the collision energy).

To compute cross sections for individual transitions, it is necessary to combine the coherent amplitudes (II-39) to obtain atomic state amplitudes according to formulas of the type (II-41), and then to integrate the resulting probabilities for individual states over impact parameter, Eq.(II-40). The integral was performed by the trapezoidal method and multipoint Simpson's rules. Precision of this last integration depends on the number of impact parameter grid points used. Depending upon the detailed cross section being evaluated, I always took enough grid points to ensure a numerical precision in all cross sections reported of at least 0.1 %.

D. ANALYTICAL FORMULATION OF COUPLED EQUATIONS FOR ASYMPTOTIC LONG RANGE COUPLINGS

In these ion-atom collision systems, the molecular states which belong asymptotically to the same (degenerate) atomic level are nonadiabatically coupled over a very long range, due to effects of the Coulomb field of the ion on the atom levels. Both the splittings between the coupled states, and the couplings themselves, decay only as R^{-2}, and the effects of these couplings must be taken into account if the transition amplitudes for individual molecular and atomic states are to be calculated correctly. For the H_2^+ system we required to solve this problem for the H(n=2) manifold ($2s, 2p_1, 2p_0$), and similarly for the He^+(n=2) manifold in HeH^{2+}. The molecular states involved are ($3d\sigma$,$2s\sigma$,$2p\pi$) in HeH^{2+}, and in H_2^+, ($3p\sigma_u$,$4f\sigma_u$,$2p\pi_u$) for u-symmetry and ($3d\sigma_g$,$2s\sigma_g$,$3d\pi_g$) for g-symmetry. Beyond some "cutoff" distance R_0, couplings to states outside one of these manifolds are negligible, so (in the cases treated here) we have to solve separately a three-state coupling problem from R_0 to $R \rightarrow \infty$. The effects of this coupling may be represented in terms of a unitary propagator $\underline{U}(\infty : R_0)$ which converts molecular state amplitudes at R_0 to those at $R \rightarrow \infty$

(or vice-versa). In our present problems, the incident channel states do not belong to these degenerate manifolds, hence we really only have to consider these couplings in the outgoing part of the collision trajectory. Because of the long range of the coupling, neither R nor the time t is a suitable progress variable for the integration of coupled equations.

To illustrate the methods used we will consider the HeH^{2+} case in detail; exactly the same principles may be extended to the cases occuring in H_2^+, with at most minor modifications.

The $3d\sigma$ and $2s\sigma$ states of HeH^{2+} correspond asymptotically to the bonding and antibonding sp σ-hybrid atomic orbitals of $He^+(n=2)$. These are coupled to the $2p\pi$ state by long-range Coriolis coupling, and to each other by an equally long-range radial coupling. For $R \geq R_0$, we found that both the couplings of these states and the splittings between them may be accurately described by analytical expressions obtained from atomic perturbation theory.

To obtain these expressions, we use the asymptotic wave functions for the three states,

$$\psi_{3d\sigma} = 1/\sqrt{2}(Z_A^{3/2}/4\sqrt{2\pi})[\rho_A\cos\theta_A-(2-\rho_A)]e^{-\rho_A/2} \qquad \text{IV-16a}$$

$$\psi_{2s\sigma} = -1/\sqrt{2}(Z_A^{3/2}/4\sqrt{2\pi})[\rho_A\cos\theta_A+(2-\rho_A)]e^{-\rho_A/2} \qquad \text{IV-16b}$$

$$\psi_{2p\pi_x} = (Z_A^{3/2}/4\sqrt{2\pi})\rho_A\sin\theta_A\cos\phi e^{-\rho_A/2} \qquad \text{IV-16c}$$

and represent the molecular electronic Hamiltonian as

$$h_e = h_e^A - Z_B/r_B \qquad \text{IV-17}$$

where "A" is the He^{2+} nucleus and B the proton. If the perturbing potential is expressed as a multipole expansion (assuming $r_A \ll R$), then we have

$$-Z_B/r_B = -1/R - r_A\cos\theta_A/R^2 - r_A P_2^0(\cos\theta_A)/R^3 \cdots \qquad \text{IV-18}$$

1. Asymptotic energies for the three states are found by evaluating the diagonal matrix elements of h_e for the three states:

$$\varepsilon_{3d\sigma}^{(1)} = -0.5 - 1/R - 3/2R^2 - 3/2R^3 + \cdots$$

$$\varepsilon_{2s\sigma}^{(1)} = -0.5 - 1/R + 3/2R^2 - 3/2R^3 + \cdots \qquad \text{IV-19}$$

$$\varepsilon_{2p\pi}^{(1)} = -0.5 - 1/R \qquad + 3/2R^3 + \cdots$$

2. Asymptotic couplings. The Coriolis couplings between the $2p\pi$ state and $2s\sigma$, $3d\sigma$ are evaluated using the operator

$$\hat{L}_y^A = i[-\cos\phi\,\partial/\partial\theta_A + \cot\theta_A \sin\phi\,\partial/\partial\phi] \qquad \text{IV-20}$$

the radial couplings between $3d\sigma$ and $2s\sigma$ are evaluated using the Hellman-Feynman theorem,

$$\langle 2s\sigma|(\partial/\partial R)_{\vec{r}_A}|3d\sigma\rangle = \langle 2s\sigma|[\partial(-Z_B/r_B)/\partial R]_{\vec{r}_A}|3d\sigma\rangle/(\epsilon_{3d\sigma} - \epsilon_{2s\sigma}) \qquad \text{IV-21}$$

and expanding the perturbation via (IV-18) (in both cases, the reference origin for the electron is thus taken to be the He^{2+} nucleus). The resulting couplings are

$$V_{3d\sigma,2s\sigma} = -i\dot{R}[-1/2R^2 - 1/R^3 + 1/2R^4] = V^*_{2s\sigma,3d\sigma}$$

$$V_{2p\pi,3d\sigma} = i\rho V_0/\sqrt{2}R^2[1 + 1/2R + C/R^2\cdots] = V^*_{3d\sigma,2p\pi} \qquad \text{IV-22}$$

$$V_{2p\pi,2s\sigma} = -i\rho V_0/\sqrt{2}R^2[1 - 1/2R + C/R^2 \quad] = V^*_{2s\sigma,2p\pi}$$

where ρ is impact parameter, V_0 the asymptotic collision velocity and the radial velocity $\dot{R}$ is

$$\dot{R} = (\pm)V_0[1 - \rho^2/R^2]^{1/2} \qquad \text{IV-23}$$

for straight-line trajectories. For both HeH^{2+} and H$_2^+$, keeping terms up through order R^{-3} in Eqs.(IV-19) and

(IV-22) gives splittings and couplings accurate to three significant figures for $R \geq 15\text{-}16$ a.u. and "cutoff" distances R, of this size were used.

3. Coupled equations to be solved have the form

$$i\dot{a}_k = \sum_{n\neq k} V_{kn} a_n \exp[-i\Delta_{nk}] \qquad \text{IV-24a}$$

where

$$\Delta_{nk} = \omega_{nk}\, dt'/\hbar \qquad \text{IV-24b}$$

The splittings $\omega_{nk} = \epsilon_n - \epsilon_k$ are

$$\omega_{2s\sigma,3d\sigma} = 3/R^2$$

$$\omega_{2s\sigma,2p\pi} = 3/2R^2 - 3/R^3 \qquad \text{IV-25}$$

$$\omega_{2p\pi,3d\sigma} = 3/2R^2 + 3/R^3$$

and V_{nk} are given by Eqs.(IV-22).

4. Progress variable Considering explicitly the outgoing trajectory case, we set $u = \rho/R$ (taking positive sign in (IV-23)), and define a progress variable

$$\delta = - (\rho V_o/R^2)dt' = \rho dR/R^2(1-u^2)^{1/2} = \sin^{-1}u \qquad \text{IV-26}$$

so δ ranges from 0 to $\pi/2$ as R goes from ∞ to ρ . The coupled equations are now expressed in terms of δ as independent variable,

$$i(da_k/d\delta) = \sum_n V_{kn} a_n \exp[-i\Delta_{nk}] \qquad \text{IV-24c}$$

with

$$\Delta_{2s\sigma,3d\sigma} = -2\alpha\delta$$

$$\Delta_{2s\sigma,2p\pi} = -\alpha[\delta + 4/\rho^2 \sin^2\delta/2] \qquad \text{IV-27}$$

$$\Delta_{2p\pi,3d\sigma} = -\alpha[\delta - 4/\rho^2 \sin^2\delta/2]$$

where $\alpha = 3/2\rho V_0$, while

$$V_{3d\sigma,2s\sigma} = -\ 1/2 \cos\delta[1 + 2/\rho\sin\delta - 1/\rho^2\sin^2\delta]$$

$$V_{2p\pi,3d\sigma} = 1/\sqrt{2}[1 + 1/2\rho\sin\delta + C/\rho^2\sin^2\delta] \qquad \text{IV-28}$$

$$V_{2p\pi,2s\sigma} = -\ 1/\sqrt{2}[1 - 1/2\rho\sin\delta + C/\rho^2\sin^2\delta]$$

For the collisions of interest, $R_0 \gg \rho$ and δ_0 thus corresponds to values $\ll \pi/2$. The coupled equations are easily and efficiently solved by the numerical method of Bulirsh and Stoer described in SectionIII.C., and the unitary propagator $\underline{U}(0; \delta_0)$ is constructed as the required connection between outgoing amplitudes at R_0 and those as $R \rightarrow \infty$.

V. H^+-H(1s) COLLISIONS

In this chapter we present and discuss our calculated results for direct excitation,

$$H^+ + H(1s) \longrightarrow H^+ + H(nl)$$

and charge exchange,

$$H^+ + H(1s) \longrightarrow H(nl) + H^+$$

in proton-hydrogen atom collisions at projectile energies 1-7 KeV. Switching functions obtained by the methods described in Chapter III were used to construct ETF's and compute ETF corrections (n.b: for H_2^+, switching functions found by the "optimization" scheme are in quantitative agreement with the analytical results of TKCK(33)). Basis sets with up to 10 molecular states have been used in systematic cross section calculations, and good convergence of cross section values is found for excitation to all atomic states with $n \leq 2$.

Our results can be compared with those of other molecular calculations, especially the recent study by Crothers and Hughes (48), and with a variety of experimental measurements of detailed atomic state excitation cross sections, polarization of Lyman-α radiation excited by collision, and total and differential charge exchange cross sections. Special emphasis is placed on the excitation cross sections for atomic H(2s) and H(2p) states, for which there is at present a very chaotic situation both experimentally and theoretically. Later in the chapter, we present results of extended-basis-set calculations which bear on excitation to higher levels and a new mechanism for ionization in H^+-H(1s) collisions.

Early molecular state studies of H^+-H(1s) collisions were mostly concerned with resonant charge transfer oscillations or the efficient Ly-α excitation process (see Knudson and Thorson), and employed bases of two or at most three states ($1s\sigma_g$;$2p\sigma_u$,$2p\pi_u$). Later calculations using larger bases were done by Rosenthal(45), Chidichimo-Frank and Piacentini(46), Schinke and Krüger(47) and most recently and completely, by Crothers and Hughes(1979) (work published after the present study was undertaken). With the exception of the work by Crothers and Hughes, these later calculations all employed uncorrected PSS theory and completely neglected ETF corrections. The calculations by Chidichimo-Frank and Piacentini and by Schinke and Krüger also entirely neglected radial couplings.

When compared with the PSS calculations, our results, in agreement with the findings of Crothers and Hughes, show that both ETF corrections and radial couplings have significant effects and must be taken into account to obtain a correct description of excitations in this system.

Comparison between our results and those reported by Crothers and Hughes is also interesting, because their ETF description and resulting coupling matrix elements are quite different at some points from ours. In a few cases there are substantial disagreements between their cross sections for individual atomic state excitations and those we have obtained. Discrepancies in the total H(2p) excitation cross section and in the $2p_0/2p_1$ sublevel distribution are in fact traceable to the differences in ETF's used; however, an even more marked disagreement on the cross sections for charge exchange and direct H(2s) excitation does not seem to arise from this, and its origin is so far not explained.

In all cases there is good agreement between our results and recent experimental measurements, where these are available. In particular, in those cases where our results disagree with those of Crothers and Hughes, our values are in much better agreement with the most recent experiments.

Finally, we have also carried out selected studies with larger basis sets (up to 16 ungerade states) to examine the behavior and convergence of cross sections for excitation to atomic levels with $n \geq 3$. These studies strongly suggest that a "ladder-climbing" sequence of excitations via these upper levels may be the dominant mechanism for ionization in H^+-H(1s) collisions at these energies.

A. COUPLINGS AND EXCITATION PATHS

1. Basis States

We used sets of 4,8 and 10 molecular states for systematic calculations, as listed in Table(V-1). These contain equal numbers of *gerade* and *ungerade* basis states, but as we shall see most of the excitation occurs in the *u*-manifold. Table(V-2) lists the basis sets of up to 16 *u*-states which we used for selected studies of convergence and excitation to upper levels. States were chosen for inclusion in these sets if preliminary study showed that they are significantly linked to relevant lower levels; the high preponderance of π states, for example, is explained on this basis, because strong $\pi - \pi$ couplings have an important role in higher excitations.

Figures(V-1) and (V-2) show electronic binding energy curves vs. R for the 10-state basis of Table(V-1) and for the 16 *u*-state basis of Table(V-2), respectively.

2. Couplings and Excitation Paths

Figures(V-3) and (V-4) show some of the more prominent couplings linking lower levels and associated energy gaps. For H^{+}-H(1s) collisions in the energy range considered, the strong $2p\sigma_u$-$2p\pi_u$ rotational coupling associated with united atom orbital degeneracy is the main source of excitation and excitations from the entire *g*-manifold , or from $2p\sigma_u$ via radial couplings, are less important. Thus for example, a good qualitative picture for the $3p\sigma_u$ excitation is the two step process $2p\sigma_u$ -$2p\pi_u$ -$3p\sigma_u$. However the radial $2p\sigma_u$ -$3p\sigma_u$

Table V.1 4,8,10 Molecular basis sets

Molecular Basis Sets for systematic close-coupling calculations			
# of states	gerade basis states	ungerade basis states	Limiting atomic states
4	$\|1s\sigma_g>$ $\|3d\pi_g>$	$\|2p\sigma_u>$ $\|2p\pi_u>$	1s $2p_1$
8	2 above, plus $\|3d\sigma_g>$ $\|4d\pi_g>$	2 above, plus $\|3p\sigma_u>$ $\|3p\pi_u>$	$2s + 2p_0$ $3p_1$
10	4 above, plus $\|2s\sigma_g>$	4 above, plus $\|4f\sigma_u>$	$2s + 2p_0$

Table V.2 16 u-state basis sets

Molecular Basis Sets (u-states only) for upper state excitation/convergence studies		
# of u states	**Basis States**	**Atomic principal quantum #**
8	$|2p\sigma_u\rangle$;	**1**
	$|2p\pi_u\rangle$, $|3p\sigma_u\rangle$, $|4f\sigma_u\rangle$;	**2**
	$|3p\pi_u\rangle$, $|4f\pi_u\rangle$, $|4p\sigma_u\rangle$;	**3**
	$|4p\pi_u\rangle$;	**4**
14	**8 above, plus**	**-**
	$|4f\delta_u\rangle$, $|5f\sigma_u\rangle$	**3**
	$|5f\pi_u\rangle$, $|5p\sigma_u\rangle$, $|5f\delta_u\rangle$	**4**
	$|5p\pi_u\rangle$	**5**
16	**14 above, plus**	**-**
	$|6f\pi_u\rangle$	**5**
	$|6p\pi_u\rangle$	**6**

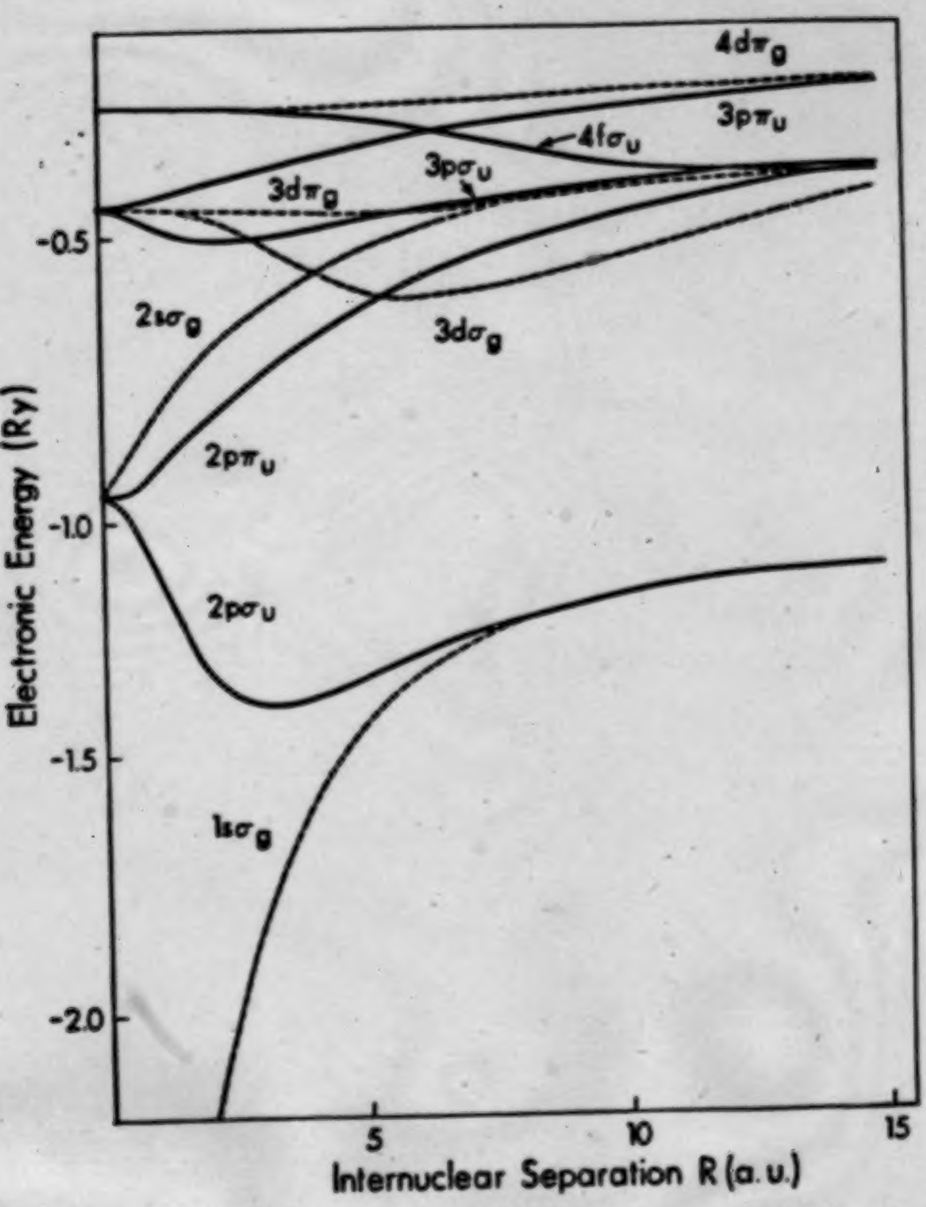

Figure(V-1) Electronic potential energy curves, $\epsilon(R)$ vs. R, for 10 states of H_2^+.

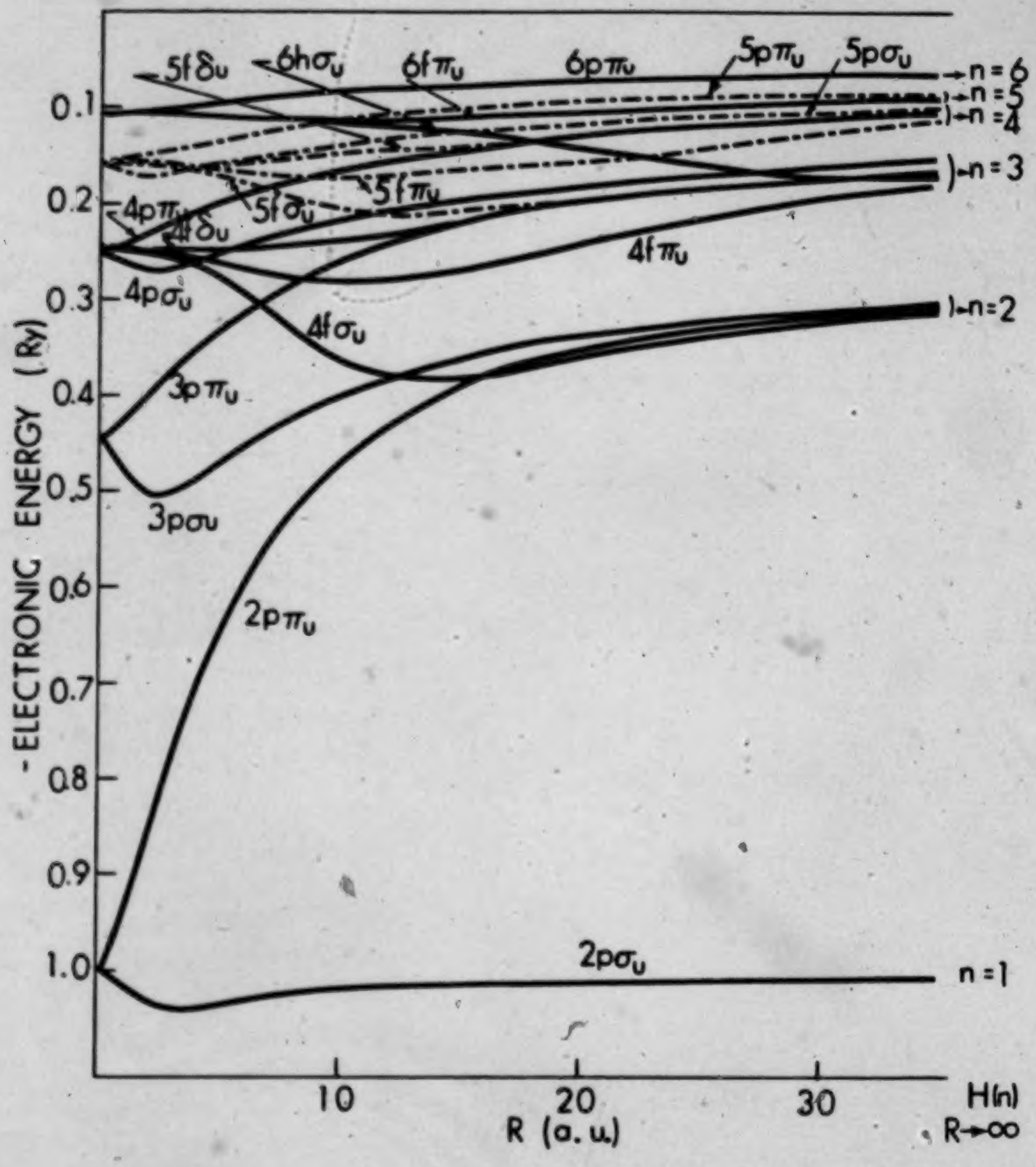

Figure(V-2) Electronic potential energy curves, $\epsilon(R)$ vs. R, for 16 states of H_2^+.

coupling is not negligible and at higher energies it plays an important secondary part in the $3p\sigma_u$ excitation and resulting atomic $(2s,2p_0)$ cross sections.

In the g-manifold, the most significant couplings from $1s\sigma_g$ are radial $1s\sigma_g$ $-3d\sigma_g$ and angular $1s\sigma_g$ $-3d\pi_g$, but due to the large energy gaps, neither is very effective except at the higher energies studied. At small impact parameters, radial $1s\sigma_g$ $-2s\sigma_g$ coupling plays some part, but it is unimportant at the intermediate and larger impact parameters which make most contribution to the cross sections. Which initial process is more important in the g-manifold depends sensitively on both energy and impact parameter, but in any case the strong rotational $3d\sigma_g$ $-3d\pi_g$ coupling populates both states in a second step. Because the contribution of the g-manifold to overall excitation is small, most of our discussion (and study) focusses on the u-components.

Figure(V-5) depicts in a qualitative way the main pathways for excitation of the 5 lowest molecular states of each symmetry: thicknesses of the arrows indicate the effective coupling strengths. Note that both angular and radial couplings to $4f\sigma_u$ are comparable and relatively weak (a different result than is found by Crothers and Hughes who have a stronger $2p\sigma_u$ $-4f\sigma_u$ coupling). In the g-manifold we can see that couplings among excited levels (e.g., $3d\sigma_g$ $-3d\pi_g$) are as strong as those in the u-manifold, but the difference which makes g-manifold excitation unimportant is the very weak initial links from $1s\sigma_g$.

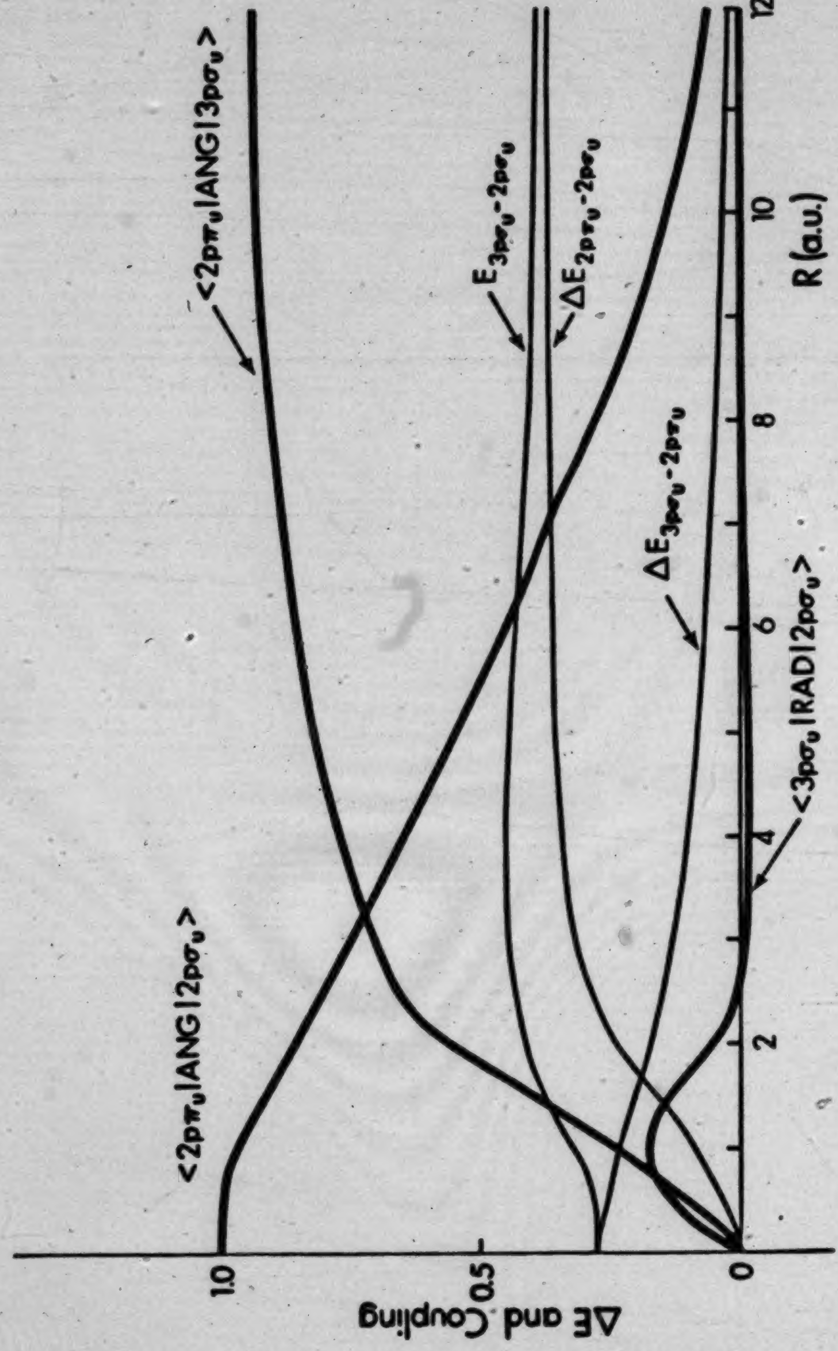

Figure(V-3) Prominent radial and angular coupling matrix elements and corresponding energy separations, vs. R for u-manifold.

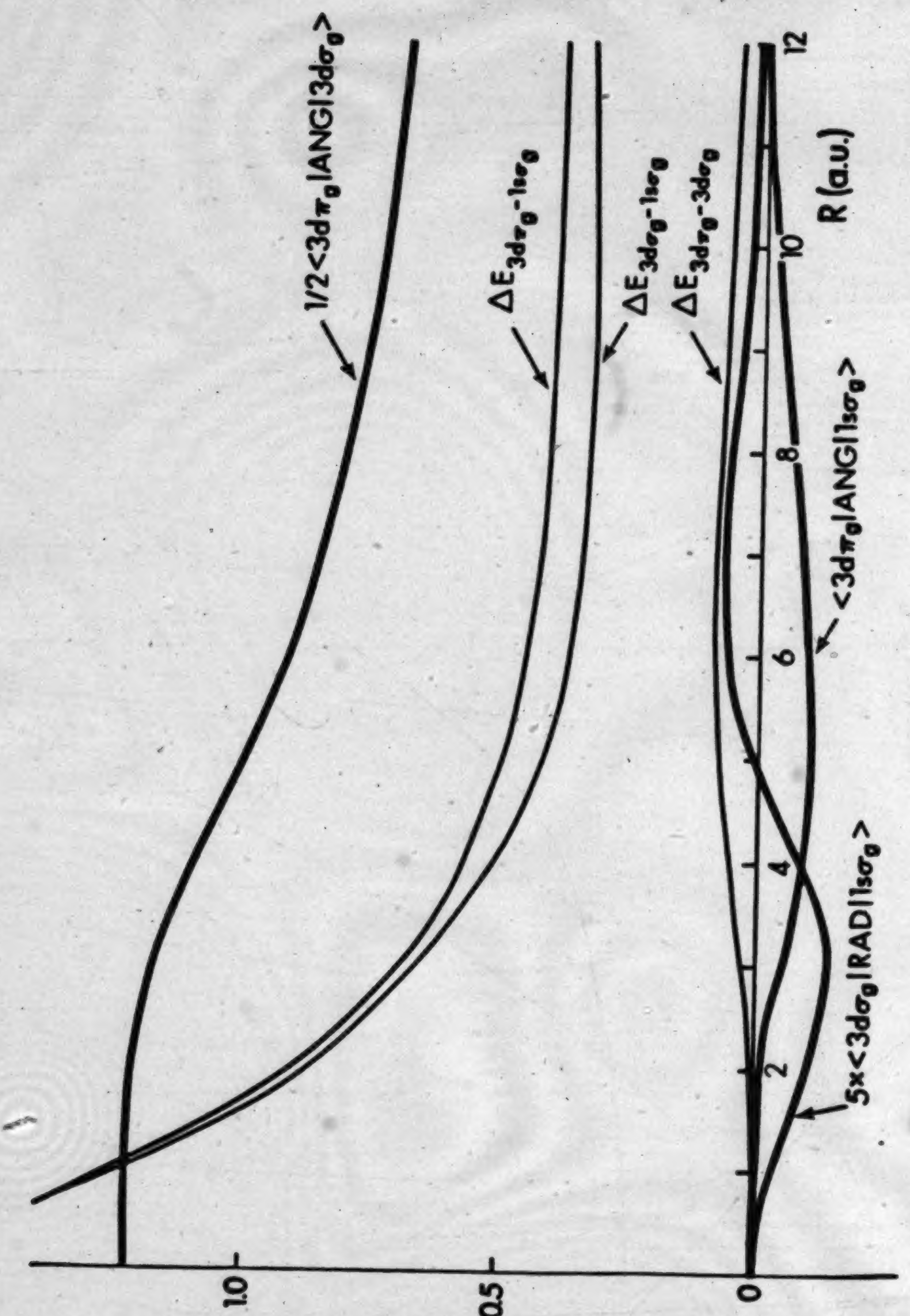

Figure(V-4) Prominent radial and angular coupling matrix elements and corresponding energy separations, vs. R for g-manifold.

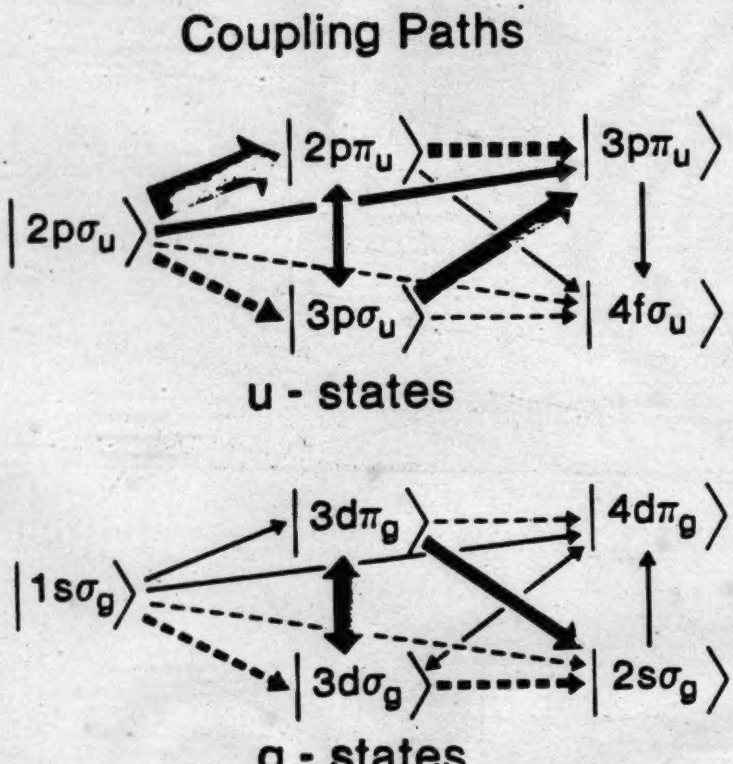

Figure(V-5) Effective couplings and excitation paths for u- and g-manifolds in H$^+$-H(1s) collisions (1-7 KeV). ⟶ , angular coupling; - - - -→ ,radial coupling; thickness of connecting arrow indicates qualitative importance.

As noted in Chapter III, there are many strong couplings among the more highly excited levels; the states involved are diffuse and easily polarized, so that couplings have quite long range, as in the radial $\pi - \pi$ couplings shown in Figures(III-9). Our study of upper (ungerade) state excitation paths has not been as systematic as for the lower states, but Figure(V-6) indicates in an approximate way some of the important flux pathways leading to upper-state excitation in the *u*-manifold. The $\pi - \pi$ couplings lead to upper-state excitation through the sequential neighbouring npπ_u -(n+1)pπ_u radial coupling. Some flux is promoted to the npσ_u states from the initial 2pσ_u state through the radial coupling, but the strong npσ_u -npπ_u angular couplings populate the flux back into π_u states. The role of nf π_u states through radial and angular couplings is relatively weak and hence no significant contributions have been observed for upper-state excitations by this route.

It may be of interest to point out again that the upper-state *g*-manifold couplings (e.g.,3dσ_g -3dσ_g ,etc.) are just as strong as those for the *u*-states, but play no important role only because of the weak initial step from 1s σ_g .

3. Asymptotic Couplings within the H(n=2) manifold

Within the asymptotically degenerate (2s,2p) manifold, long-range radial and Coriolis couplings have a significant

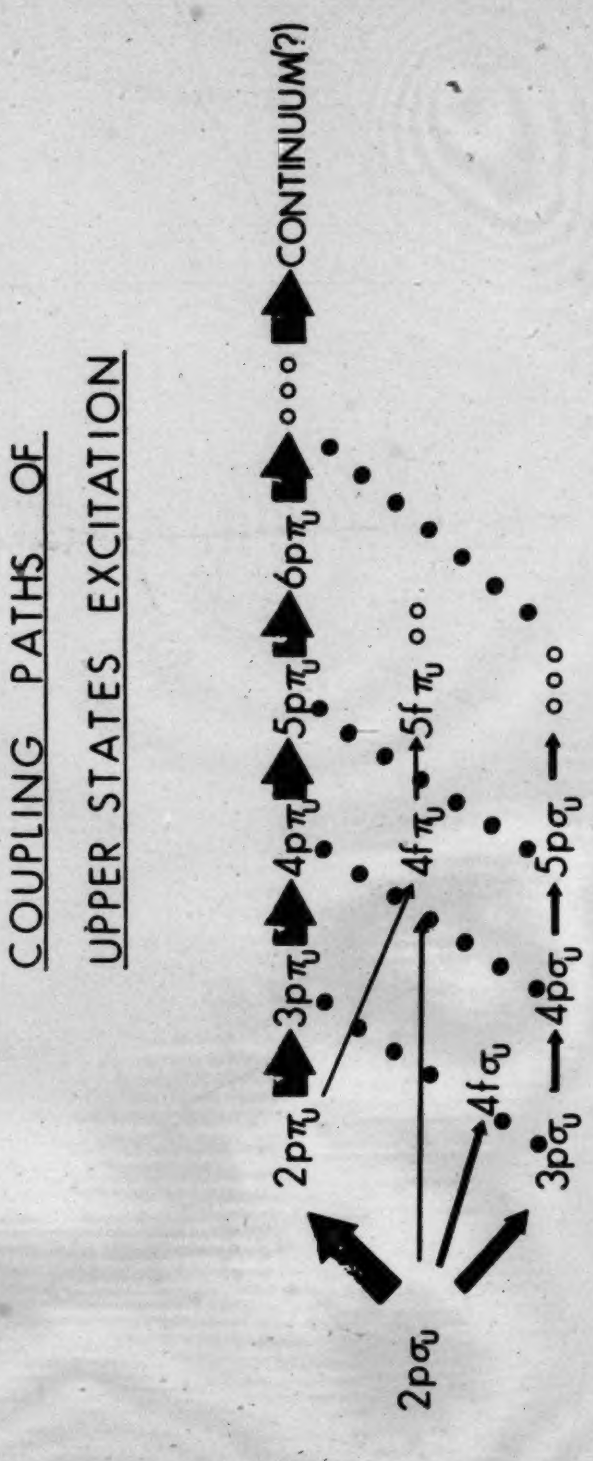

Figure(V-6) Important flux pathways leading to upper-state excitation in the u-manifold; thickness of connecting arrow indicates qualitative importance and dot-line indicates weak couplings.

effect on the detailed atomic state populations. Both the couplings and the splittings between coupled levels decrease as R^{-2}. Beyond $R \geq 20$ a.u., however, the n=2 sublevels are effectively decoupled from levels not degenerate with them, and for each symmetry there is therefore a three-state asymptotic coupling problem, which we have found convenient to treat separately. The three states involved for the u-manifold are ($3p\sigma_u$,$2p\pi_u$,$4f\sigma_u$), and for the g-manifold ($3d\sigma_g$,$3d\pi_g$,$2s\sigma_g$). In each case the two σ -states are sp-hybrid atomic states and are linked to the π -state by Coriolis coupling and to each other by radial coupling. For $R \geq$ 15-16 a.u. we found we can describe both couplings and splittings accurately by analytical models using atomic-state perturbation theory. By introducing an appropriate action variable as a progress variable (instead of R, or time t), the resulting asymptotic coupling problem can be solved efficiently. In effect, its solution may be represented as a three-state propagator $U(\infty;R\ )$ which converts molecular state amplitudes at R_0 to those at $R \to \infty$: This is attached to the output from the integration over the interior "real collisions" region. We used this device to generate amplitudes for all three final molecular states, even in those cases where the basis used in the interior did not span all those states (e.g. in the 8-state basis $4f\sigma_u$ and $2s\sigma_g$ do not appear in the close-coupling problem, but amplitudes for these states at $R \to \infty$ are fed from amplitudes in the other components ($2p\pi_u$,$3p\sigma_u$) and ($3d\pi_g$,$3d\sigma_g$) at

$R=R_0$). Effects of the asymptotic coupling are small (≤ 10 % changes) but are certainly not negligible. This should be taken into account to give predictions of atomic 2s,$2p_0$ and $2p_1$ excitation probabilities.

Section D. in Chapter IV gives a detailed account of our procedures for treating this asymptotic coupling.

4. ETF Effects on the Couplings

In this section we compare our coupling matrix elements (with ETF corrections based on switching functions, as described in Chapter III) with those employed by Crothers and Hughes who used a different treatment of ETF's. (Comparison with uncorrected PSS matrix elements is not considered here since it is now generally well known that there are very substantial corrections in most cases; the papers by Crothers and Hughes give specific examples of such comparisons with their corrected couplings for this system). As pointed out in ChapterIII(see also TKCK(33)) the ETF description used by Crothers and Hughes is equivalent, to lowest order in the collision velocity, to the use of a particular type of switching function. For the $1s\sigma_g$ state, their effective switching function closely resembles the one used here ($R\geq 2.0$ a.u.), but for the $2p\sigma_u$ state it is qualitatively very different (see TKCK(33)) and leads to quite different coupling matrix elements.

As relevant examples, Figures(V-7,8 & 9) show our coupling matrix elements for $2p\sigma_u$ $-2p\pi_u$, $2p\sigma_u$ $-4f\sigma_u$,$2p\pi_u$ $-4f\sigma_u$, and $1s\sigma_g$ $-3d\sigma_g$, in comparison with those employed by Crothers and Hughes (Hermitian averages). The asymptotic behavior of the couplings is the same, but in most cases there are substantial differences at finite internuclear separations($\leq$10-12 a.u.).

As we have found by actual calculations (see Section V.C below) these differences in coupling matrix elements can lead to significant differences in excitation probabilities and cross sections. For the $2p\sigma_u$ $-2p\pi_u$ coupling, the node and steeper slope in the matrix elements of Crothers and Hughes leads to a considerable increase in the $2p\pi_u$ excitation cross section (to first order in velocity), relative to our values. The much larger $2p\sigma_u$ $-4f\sigma_u$ radial coupling of Crothers and Hughes is mainly responsible for discrepancies between our results and theirs on the detailed magnitudes of $2p_0$ and $2p_1$ cross sections, the resulting polarization of Lyman-α radiation, and (to a smaller extent) the total 2p excitation cross section (see Section C.2. below). Similar effects might be expected to result from differences in the $1s\sigma_g$ $-3d\sigma_g$ couplings, but of course these are much less important because of the much smaller g-manifold excitation cross sections.

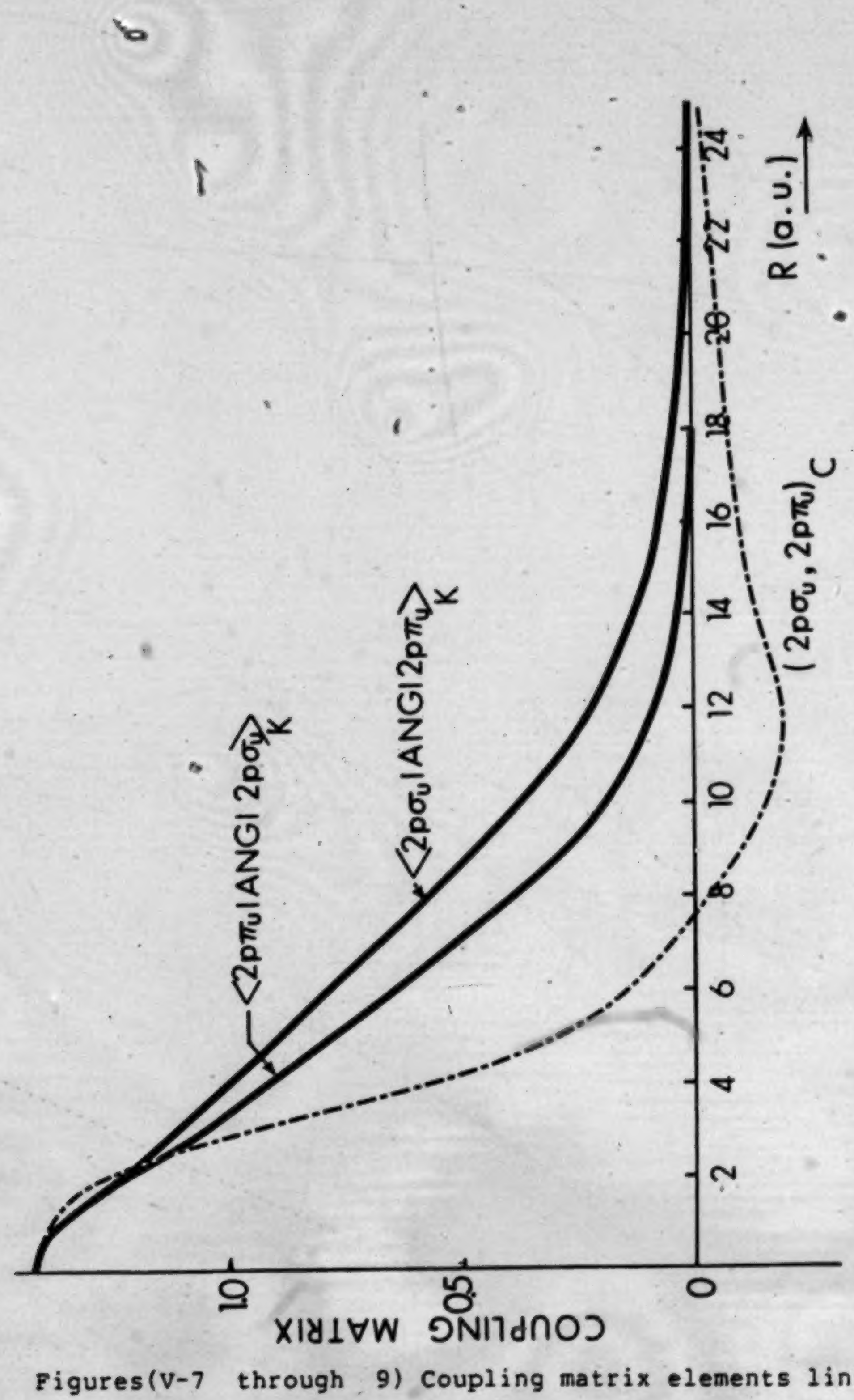

Figures(V-7 through 9) Coupling matrix elements linking 2p σ_u ,2pπ_u 4fσ_u states, and 1sσ_g ,3dσ_g states, as computed with analytically determined switching functions (solid curves--note non-Hermitian character), and as computed by Crothers and Hughes(48) (dashed curves--Hermitian average).

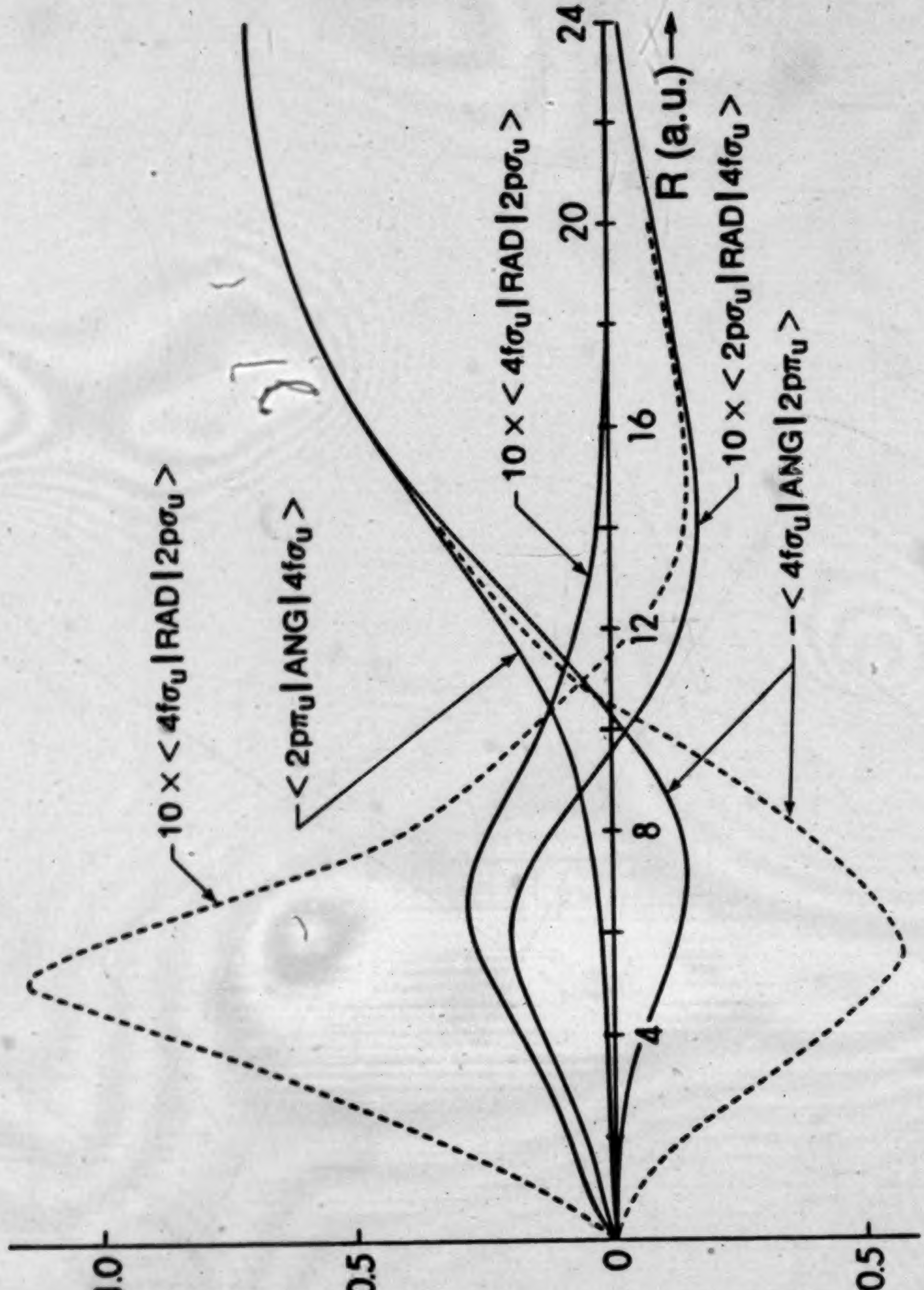

Figure V.8 Coupling matrix

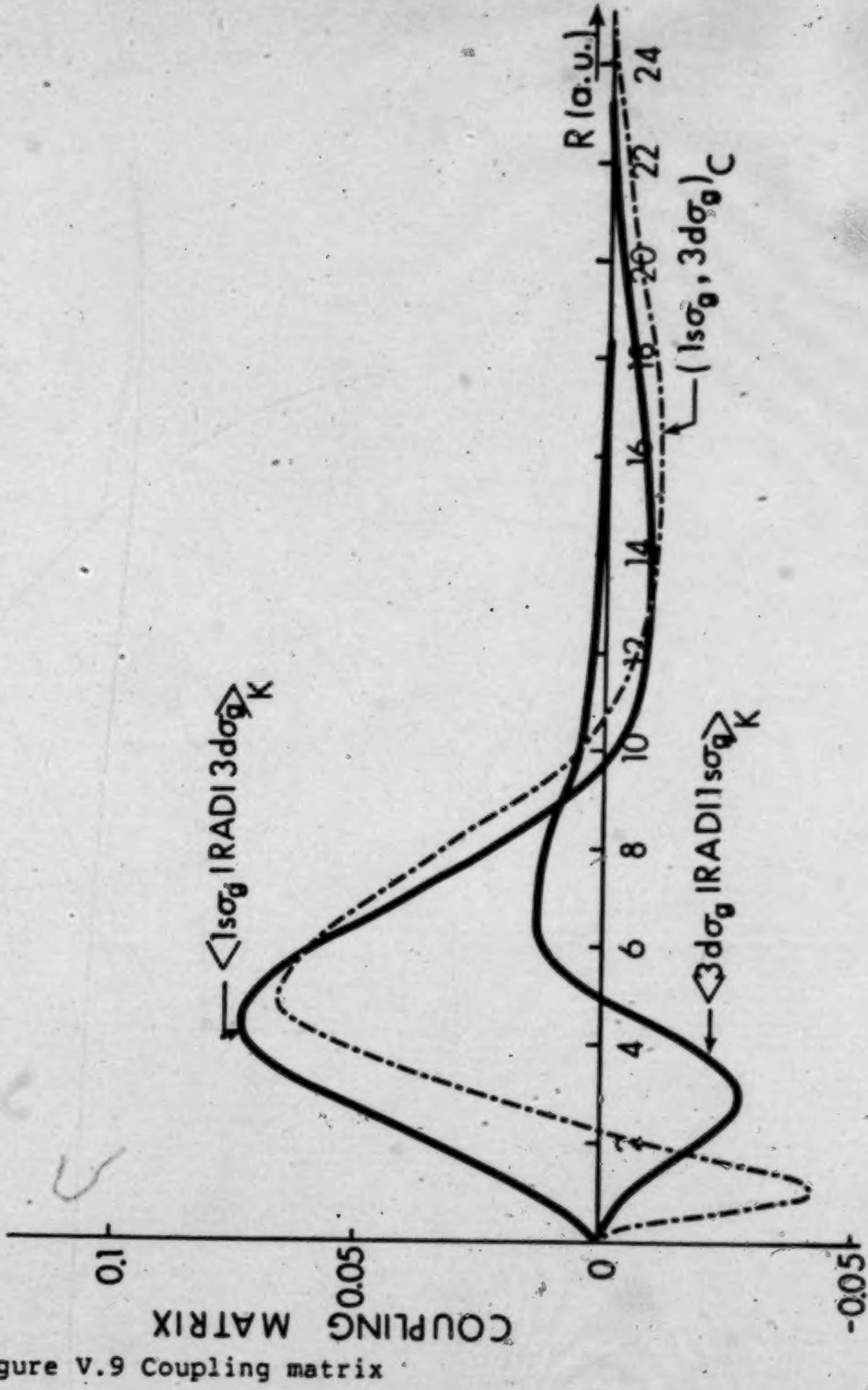

Figure V.9 Coupling matrix

B. EXCITATION PROBABILITIES

1. Collision Histories

Figures(V-10 & 11) show two typical "histories" of collisions (molecular state probability vs. time t) for the 5 u-state basis at E=5 KeV and impact parameters ρ =0.5 and 5.0 a.u., respectively. Early in the collisions some effects of the long range tail in the $2p\sigma_u$ -$4f\sigma_u$ coupling can be seen, followed by $2p\sigma_u$ -$3p\sigma_u$ radial coupling and (at small impact parameters) the dominant $2p\sigma_u$ -$2p\pi_u$ coupling. Later excitation of $3p\pi_u$ via rotational coupling from $3p\sigma_u$ can also be seen at smaller R. Finally during the outgoing part of the collisions there are effects of $3p\pi_u$ -$4f\sigma_u$ and $3p\pi_u$ -$2p\pi_u$ couplings. The sudden dip of $4f\sigma_u$ probability around t=0 for ρ =5 a.u. is probably connected with the $3p\pi_u$ -$4f\sigma_u$ curve crossing at R=6.5 a.u. and a smaller effect at both earlier and later times may be similarly related to the $3p\sigma_u$ -$4f\sigma_u$ crossing at 13 a.u..

2. Excitation Probabilities vs. Impact Parameter

Figure(V-12) shows molecular state excitation probabilities vs. impact parameter at 5 KeV for the 5 u-state basis. The importance of radial couplings is illustrated clearly by comparison with Figure(V-13), which shows the same data when only angular couplings are retained. The most obvious effect of radial coupling is the

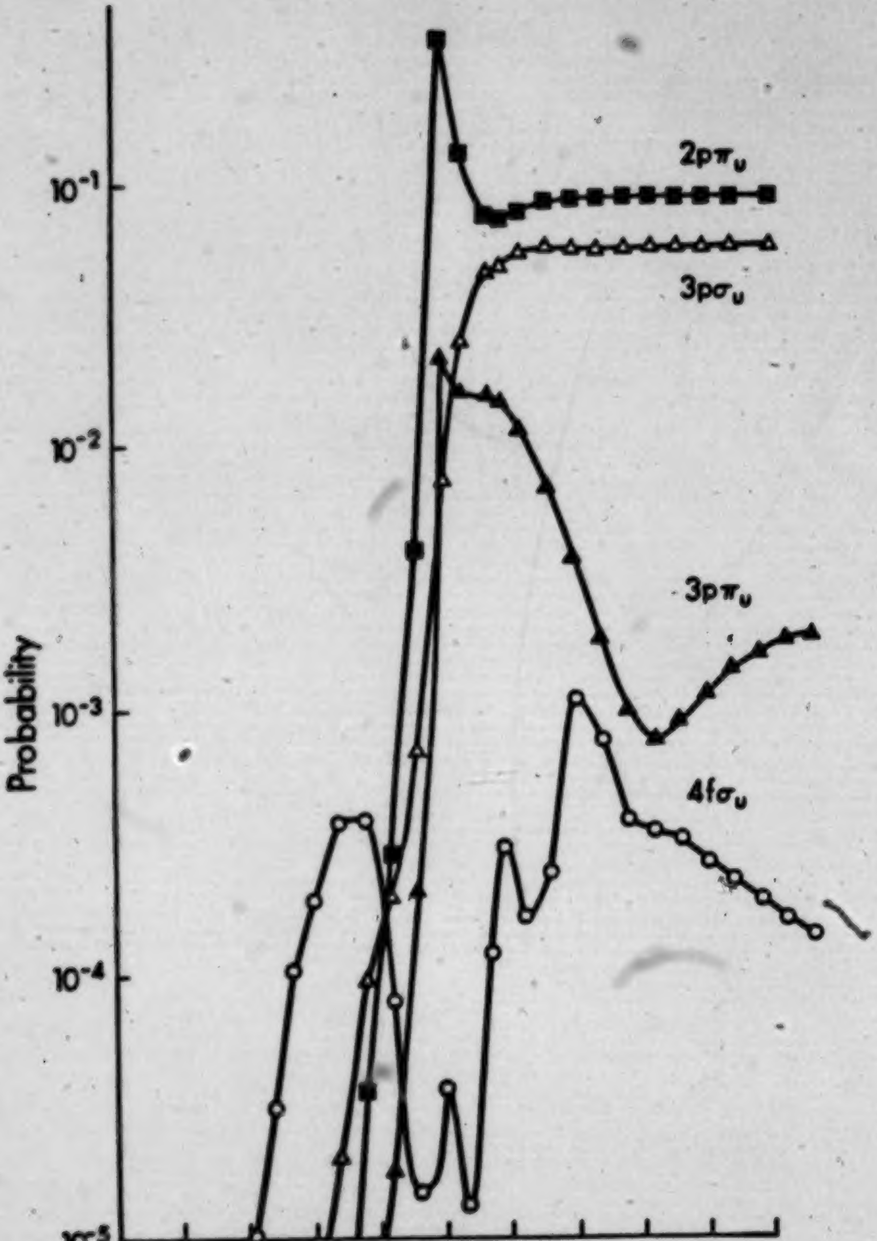

Figure(V-10) Collision "history" (molecular state probabilities vs. time (a.u.)) for E=5 KeV, impact parameter 0.5 a.u..

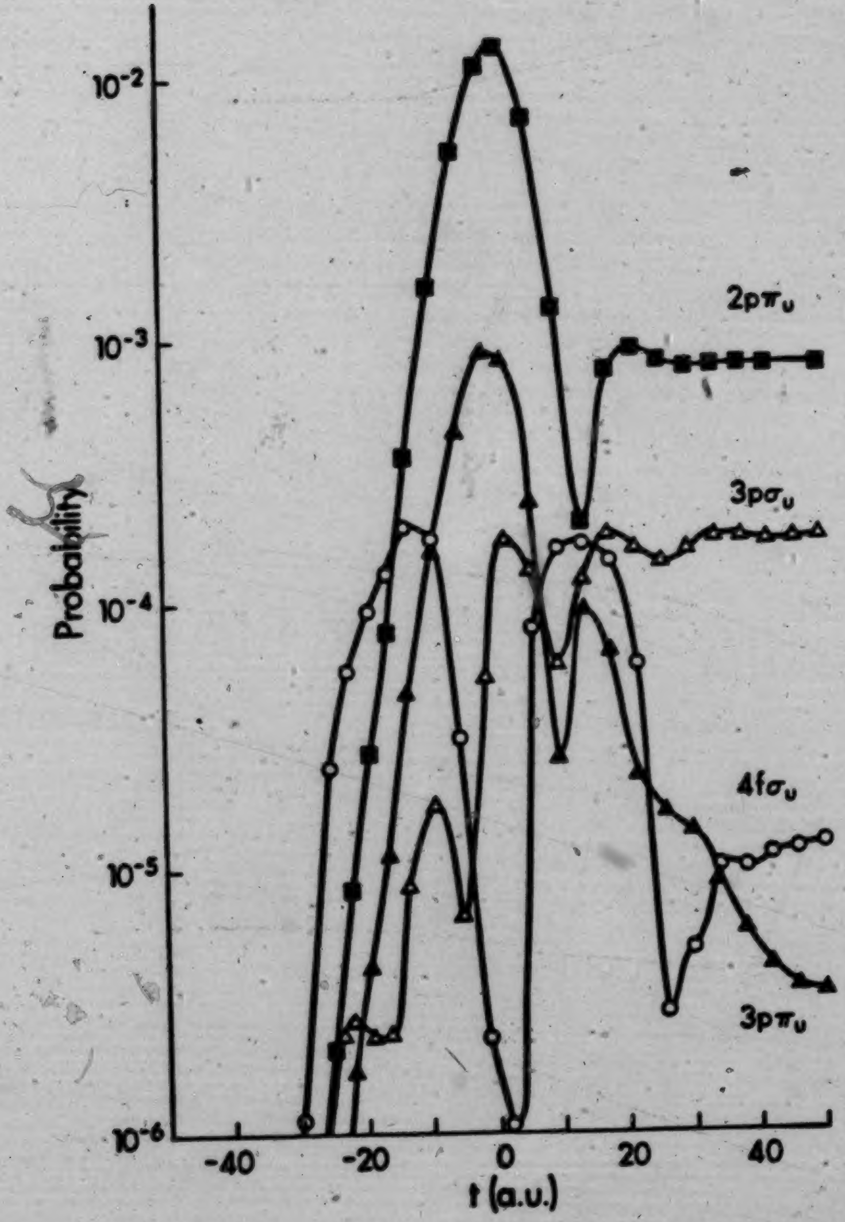

Figure(V-11) Same as Fig.(V-10), but impact parameter 5.0 a.u..

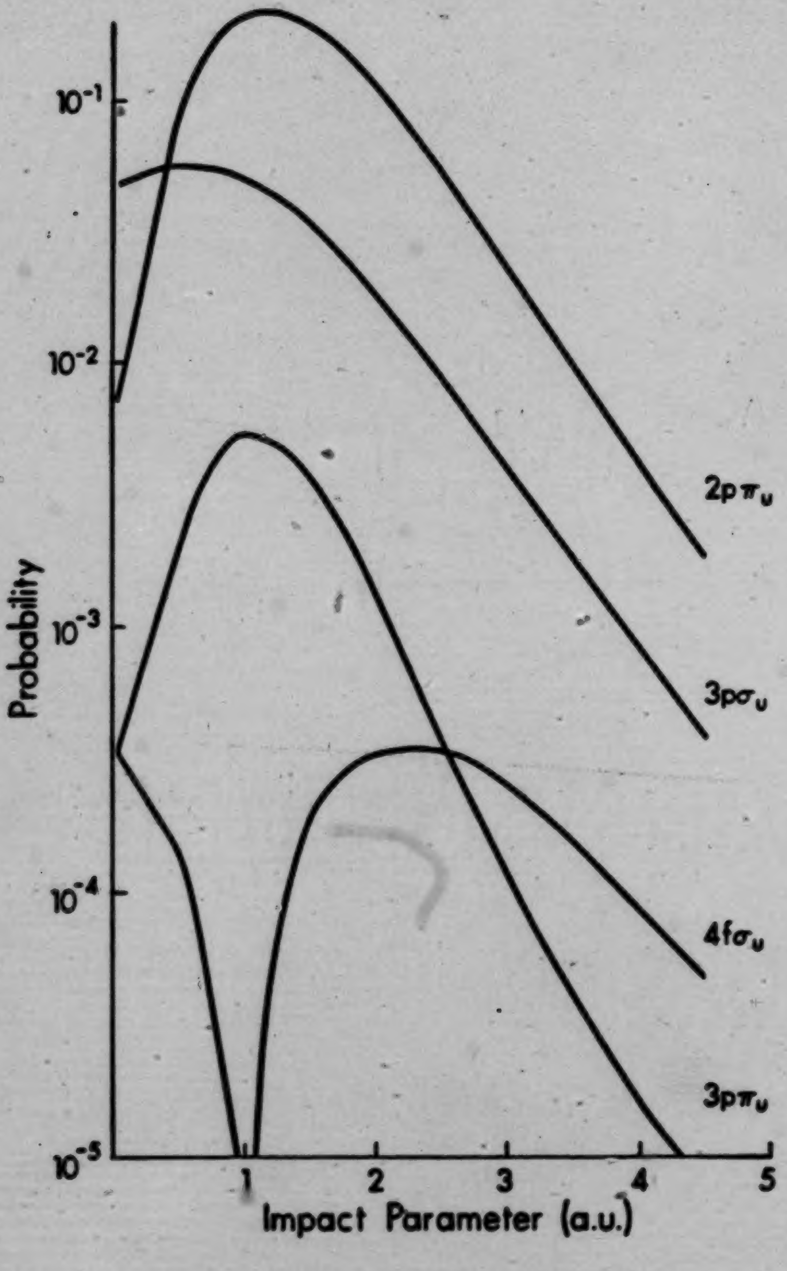

Figure(V-12) Probabilities for excitation of molecular states vs. impact parameter at 5 KeV. Angular and radial couplings included.

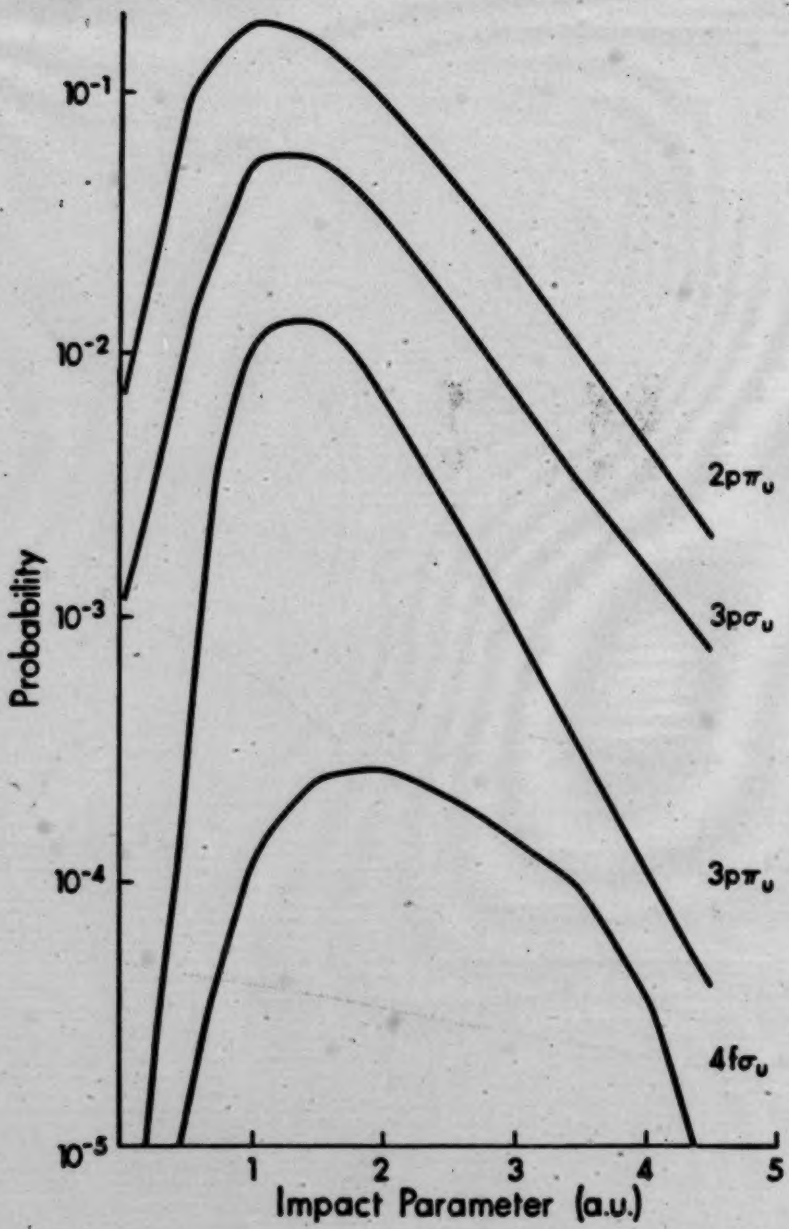

Figure(V-13) Same as Fig.(V-12), but only angular couplings included.

change in the $3p\sigma_u$ excitation probability, especially at small impact parameters, arising from direct excitation $2p\sigma_u - 3p\sigma_u$. A secondary effect is the 5-fold decrease in the $3p\pi_u$ probability which occurs when radial coupling is included: $3p\pi_u$ amplitude, produced at small R by angular coupling, returns to $2p\pi_u$ late in the collision due to the long-range $\pi - \pi$ radial coupling. The effect of the direct radial $2p\sigma_u - 4f\sigma_u$ coupling on the $4f\sigma_u$ probability can also be seen, though this is much smaller and mainly influences the shape rather than magnitude of the $4f\sigma_u$ curve.

The effects of radial coupling are also very evident in Figure(V-14), which compares atomic state excitation probabilities vs. impact parameter at 1 KeV for the states $2p_1$, $2s+2p_0$, and $3p_{\pm1}$, with the results of Schinke and Krüger who neglected radial couplings (and also ETF corrections). The dominant $2p_1$ ($2p\pi_u$) probability is not much affected and hardly even changes its shape when radial coupling is included, but the ($2s+2p_0$) probability is very different, due to our inclusion of the $2p\sigma_u - 3p\sigma_u$ direct coupling. Also, our $3p\pi_u$ probability is significantly increased at larger ρ, relative to that found by Schinke and Krüger, (though the absolute magnitude is in any case much smaller). From these comparisons, we can see that there is no theoretical justification for neglecting the radial couplings; although their matrix elements are smaller, they act effectively over a wider range of impact parameters and become particularly important for increasing collision energies.

C. CROSS SECTIONS

1. Total and Differential Charge Exchange Cross Sections

Charge exchange in H^+-H(1s) collisions at these energies is dominated by the resonant charge transfer process. Figure(V-15) shows the H(1s) charge transfer cross section vs. energy together with the H(2p) and H(2s) charge transfer cross sections; the contribution from H(n=2) charge exchange is only 3.5 % even at the highest energy studied here. Because of this dominance of the resonant process, nearly all theoretical results, both from atomic-state and from molecular-state basis calculations, are in reasonably good agreement with each other and also with the experimental values reported by McClure(63) and by Fite, Smith and Stebbings(80) (below 3 KeV, the results of Fite *et al* are somewhat higher than those of McClure). The flat portion of the cross section slowly increases toward a maximum in the neighburhood of 1 KeV. Uncorrected PSS calculations are quite sufficient to obtain a good account of the total charge transfer cross section in this region, as has been shown by F.J.Smith(41). This is easy to explain, since

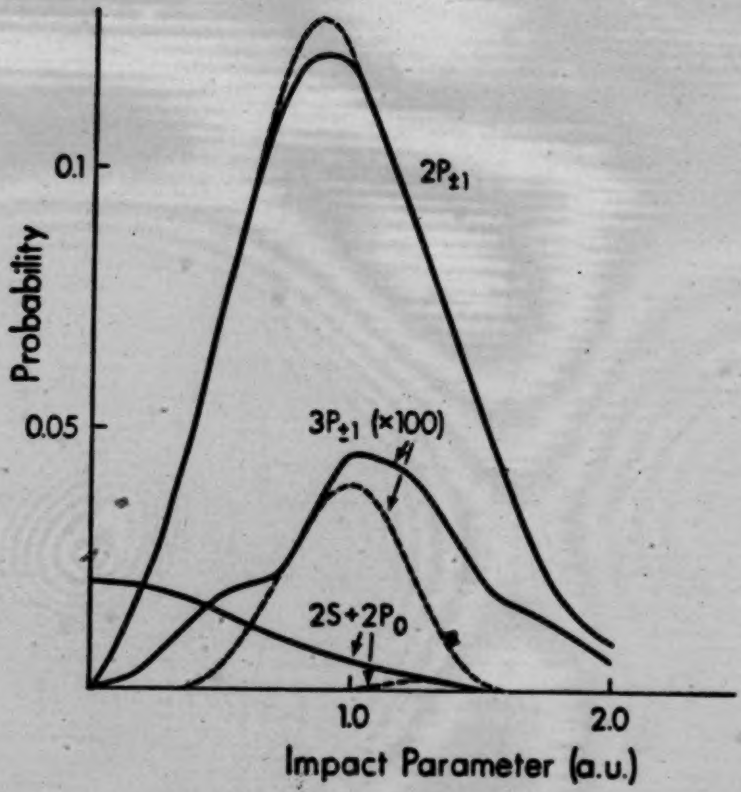

Figure(V-14) Atomic state excitation probabilities vs. impact parameter at E=1 KeV. Solid curves, present work; dashed curves, results of Schinke and Krüger(47-a) (angular couplings only, no ETF corrections).

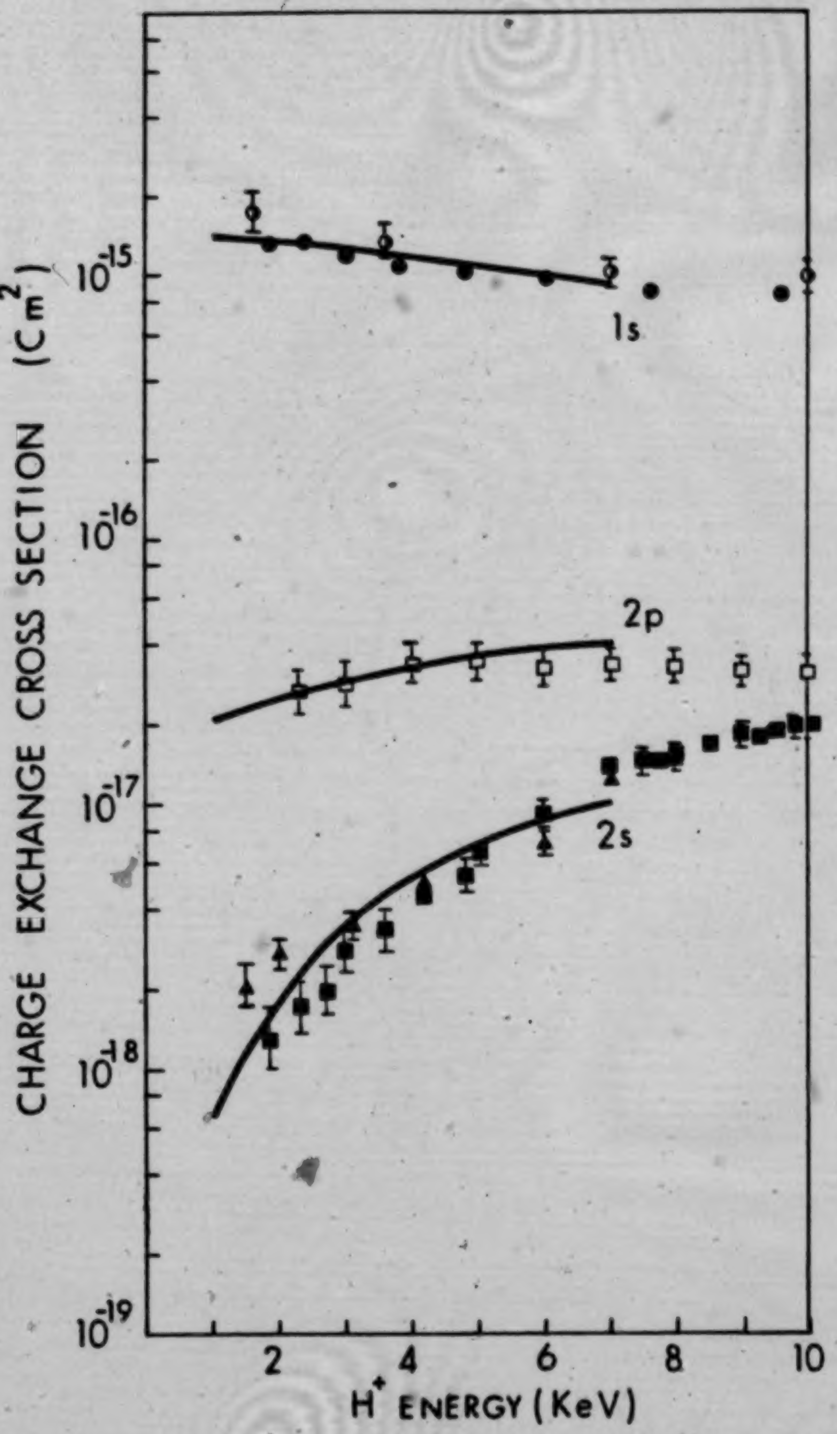

Figure(V-15) Charge exchange cross sections for H(1s),H(2p) and H(2s) vs. E: ——— ,present work. Experimental data: ● ,McClure(63); ◑,Fite et al(80) for H(1s) charge exchange cross section. For H(2p) and H(2s) charge exchange cross sections, data are the same as in Figs.(V-17) & (V-20).

(1) the PSS results are exact within the two-state (1s σ_g ,2pσ_u) approximation where only elastic scattering occurs, and

(2) below 1-2 KeV the dominant excitation occurs via the strong 2pσ_u -2pπ_u rotational coupling, and is not much affected by ETF corrections below 1 KeV.

Our results for the total charge exchange cross section are therefore in good agreement with other molecular state calculations and comparison with these other results is not particularly significant. (All our numerical results for direct and charge exchange cross sections are tabulated in Tables(V-3) and (V-4)).

We have also computed the differential cross section for charge transfer into all states, using the small-angle formula given in Section(II.D) (Eq.II-42). This is shown vs. scattering angle θ for E=1 KeV, in Figure(V-16). Here also the dominance of resonant charge transfer and the 2pσ_u -2p π_u excitation process at low energies means that the calculated results from nearly all molecular state studies should be in good agreement, especially at small angles, and this is confirmed by the very good agreement between our values and those found in the three-state calculation by McCarroll and Piacentini(44), for $\theta \leq 2°$. At larger angles, however, our results show improved agreement with experiments by Helbig and Everhart(60) and by Houver,

Table V.3 Charge exchange cross sections

Atomic Level Charge Exchange Cross Sections
$H^+ + H(1s)$ (10-State Basis) (cm^2)

H^+ Energy (KeV)	$H(2p_{\pm 1})$	$H(2s)$	$H(2p_0)$	$H(1s)$
1	1.98×10^{-17}	0.637×10^{-18}	0.761×10^{-18}	14.0×10^{-16}
2	2.10	1.82	2.83	13.5
3	2.40	3.64	3.85	12.7
4	2.64	5.06	5.84	11.8
5	2.86	7.06	7.88	10.6
7	3.32	10.1	8.51	9.58

Table V.4 Direct excitation cross sections

Atomic Level Direct Excitation Cross Sections $H^+ + H(1s)$ (10-State Basis) (cm^2)			
H^+ Energy (KeV)	$H(2p_{\pm 1})$	$H(2s)$	$H(2p_0)$
1	1.98×10^{-17}	0.589×10^{-18}	0.759×10^{-18}
2	2.12	1.74	2.84
3	2.44	3.31	3.94
4	2.74	4.75	6.23
5	2.98	6.37	8.45
7	3.61	8.21	12.8

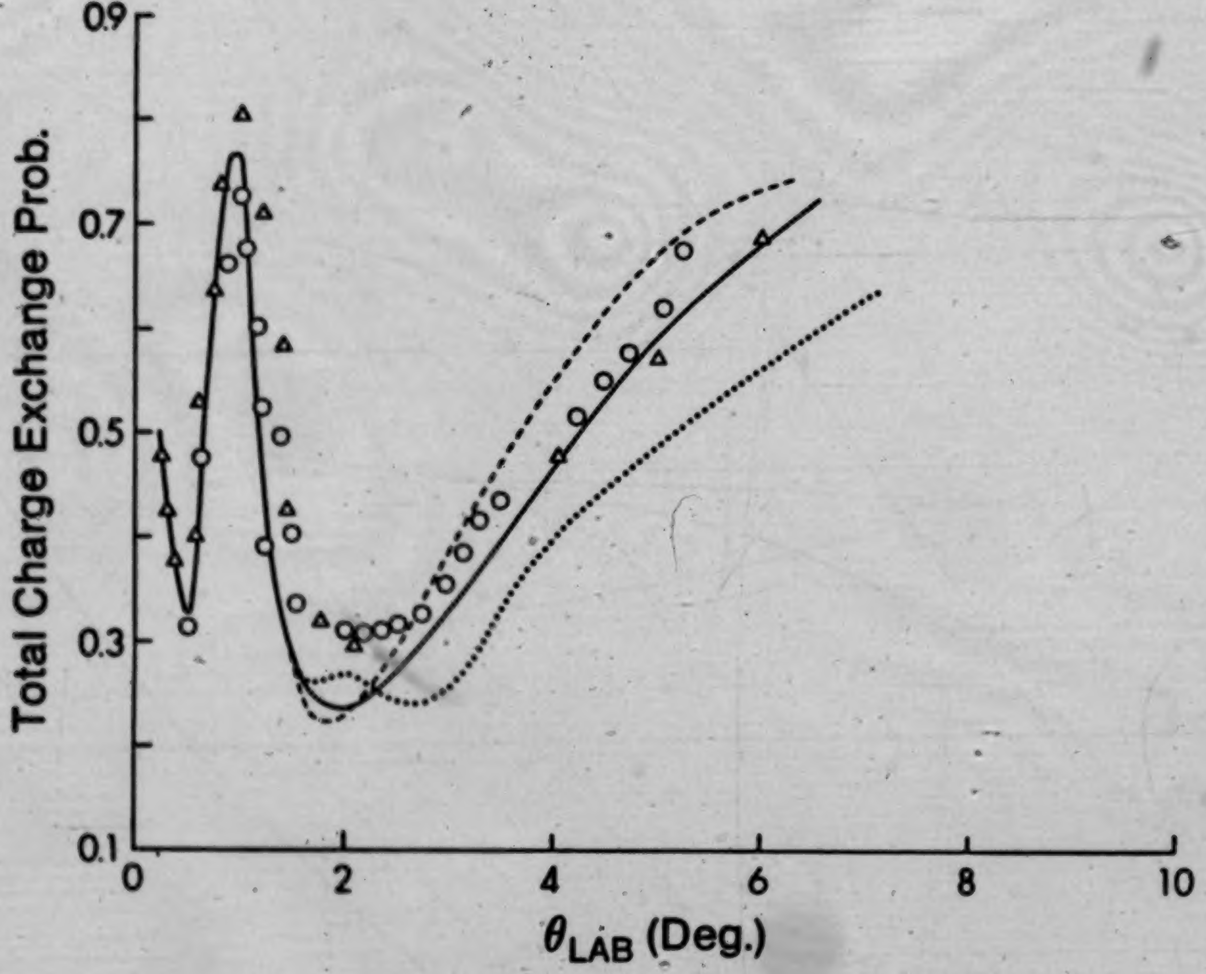

Figure(V-16) Charge exchange differential cross section (all states) vs. lab. scattering angle at E=1 KeV. ——— ,present work; – – – – – Schinke et al(47-a); •••••••• McCarroll et al(44). Results of Crothers et al (48), not shown, nearly coincide with ours. Experimental data: ○ Houver et al(61); △ Everhart et al(60).

Fayeton and Barat(61), relative to the three-state results; this was also found by Crothers and Hughes, whose results (not shown) essentially coincide with ours. The improvement is mainly due to the inclusion of the radial coupling effects (including ETF corrections). For still larger angles, the approximations involved in the small-angle formula (and the use of a straight-line trajectory) are no longer valid and Eq.(II-42) should not be expected to give results in agreement with experiment.

2. H(2p) Cross Sections

In Figure(V-17) our 10-state results for the H(2p) charge exchange cross section ($2p_0+2p_1$) are compared with results of Schinke and Krüger and Crothers and Hughes, and with the experimental values reported by Morgan, Geddes and Gilbody(66) in the energy range 1-7 KeV. For 2p excitation, the contribution of the *g*-manifold is relatively small, hence direct and charge exchange cross sections for H(2p) differ by less than 8 % over the energy range studied. The (included) corrections due to second-order terms in velocity (see Section(V.D) below) are at most 16 %, at the highest energy studied. The agreement of our results with experiment is generally very good, and is somewhat better than that of the other theoretical results, though these also are in general accord with experiment. [The success of molecular state calculations in predicting correctly at least the

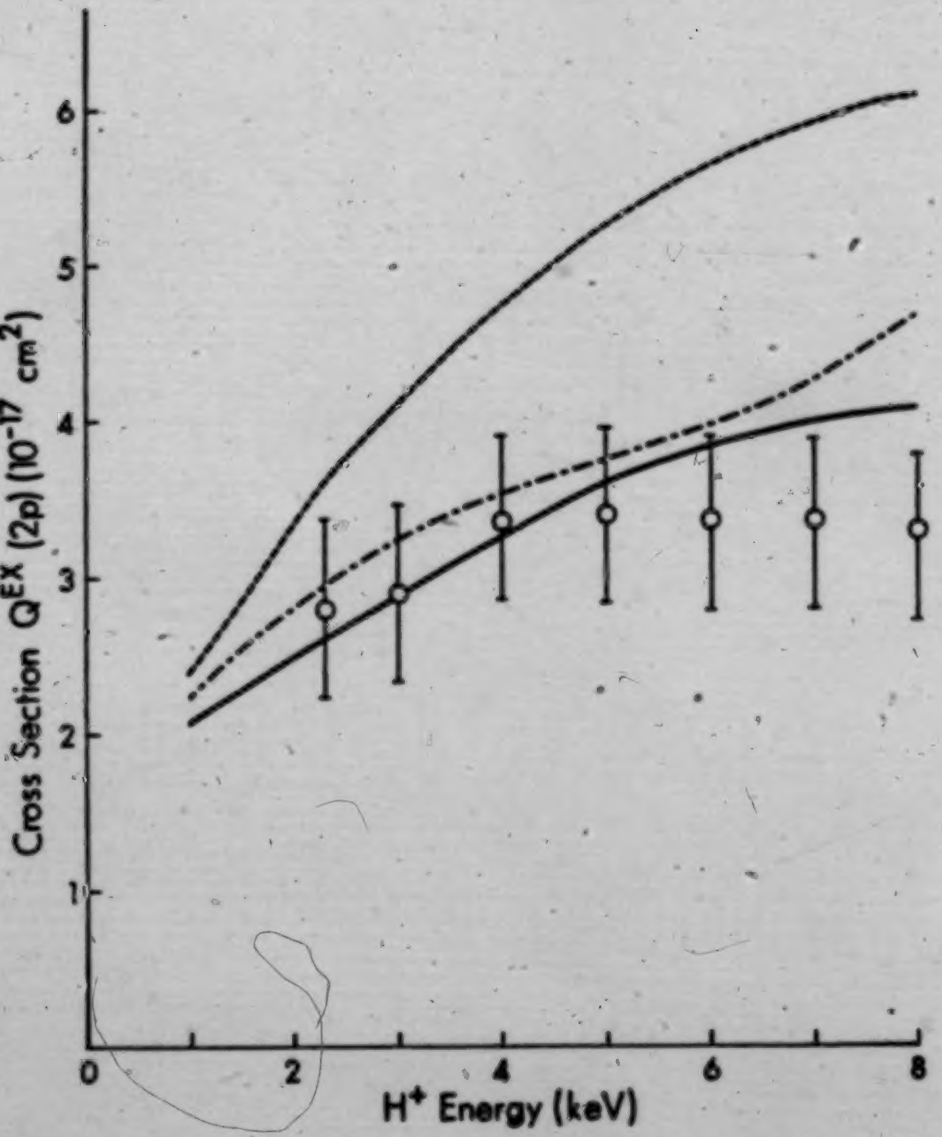

Figure(V-17) Charge exchange cross section for H(2p) (all components), vs. E: ▬▬▬ present work; –·–·–· Crothers et al(48); ------ Schinke et al(47-a). Experimental data: O Morgan et al(66).

qualitative behavior vs. energy for this cross section confirms that they are appropriate at these energies; atomic-state basis calculations (not shown) give much larger (more than a factor of 3) cross sections which vary rapidly at low energies and predict the location of the maximum cross section incorrectly, although the inclusion of pseudostates(Cheshire,Gallaher and Taylor(57)) causes marked improvement in the results].

The discrepancy between our results and those of Schinke and Krüger can be shown to arise mainly from the neglect of ETF corrections, and (to lesser extent) from the neglect of radial couplings. (The curve shown for their results was constructed by addition of their published curves for $2p_1$ and for 2s (equal to $2p_0$, in their calculation)). At 5 KeV, for example, more than 90 % of their total H(2p) cross section arises from the $2p_1$ excitation via angular coupling from the initial $2p\sigma_u$ state. As Crothers and Hughes also point out, the uncorrected PSS $2p\sigma_u$ -$2p\pi_u$ coupling matrix element behaves in a completely incorrect way for $R \geq 3$ a.u., due to the linearly increasing "moment-arm" term in the uncorrected operator $\hat{L}_y$. Calculations made by Dr. V. SethuRaman and Professor Thorson (unpublished) in this laboratory indicate that above 1-2 KeV the resulting spurious coupling leads to significantly larger $2p\pi_u$ excitation probabilities, as were found by Schinke and Krüger.

The results of Crothers and Hughes are in good agreement with ours up to about 6 KeV and then show a rapid increase relative to ours and to the experimental values. Calculations we have made (see sub-Section(D.4(b)) below) indicate that this increase is due to the much larger $4f\sigma_u$ populations they computed on the basis of their ETF description and the resulting coupling matrix elements (Figures(V-7)-(V-9)). Our own calculations (Table(V-3)) show that the $2p_1$ and $2p_0$ charge exchange cross sections are approaching their maximum values near 6-8 KeV and that the $H(2p_0)$ charge exchange contribution is at most 25 % (at the highest energy shown). For the direct excitation cross sections, the $2p_1$ cross section (as noted earlier) is only slightly different from that for charge exchange, with a maximum near 6-8 KeV, while the $2p_0$ direct excitation cross section is still increasing (maximum near 20 KeV ?); at the highest energy studied here, the $2p_0$ contribution to direct H(2p) excitation is still only 35 % of the total. These findings are in contrast with those of Crothers and Hughes who obtained $2p_0$ cross sections larger than those for $2p_1$ at these energies, again directly related to larger $4f\sigma_u$ excitation probabilities.

3. Polarization

The polarization of the Lyman-α radiation emitted by the inelastically scattered atom can be calculated by using the formula derived by Percival and Seaton(49)

$$\Pi = \frac{Q^{D}(2p_{0}) - Q^{D}(2p_{1})}{\alpha Q^{D}(2p_{0}) + \beta Q^{D}(2p_{1})}$$

where α =2.375, β =3.749. Results are shown in Figure(V-18) together with some other theoretical calculations and one set of experimental values (Kauppila *et al*(69)). Since our excitation cross sections for $2p_1$ are much larger than those for $2p_0$ over the entire energy range considered, we obtain consistently negative values. These disagree with those of Crothers & Hughes, which become positive between 4 and 5 KeV. The sign change in their results is directly attributable to the much larger $4f\sigma$ excitation probability they predicted due to their description of ETF effects.

Actually, all sorts of numbers between +1 and -1 have been reported in the various theoretical studies, using many different approximations. Only one set of experimental values is available to test these predictions and unfortunately its reliability is not really adequate even for a qualitative conclusion which might reduce the theoretical chaos. It would clearly be very useful to have more reliable data on the Ly-α polarization in this energy range.

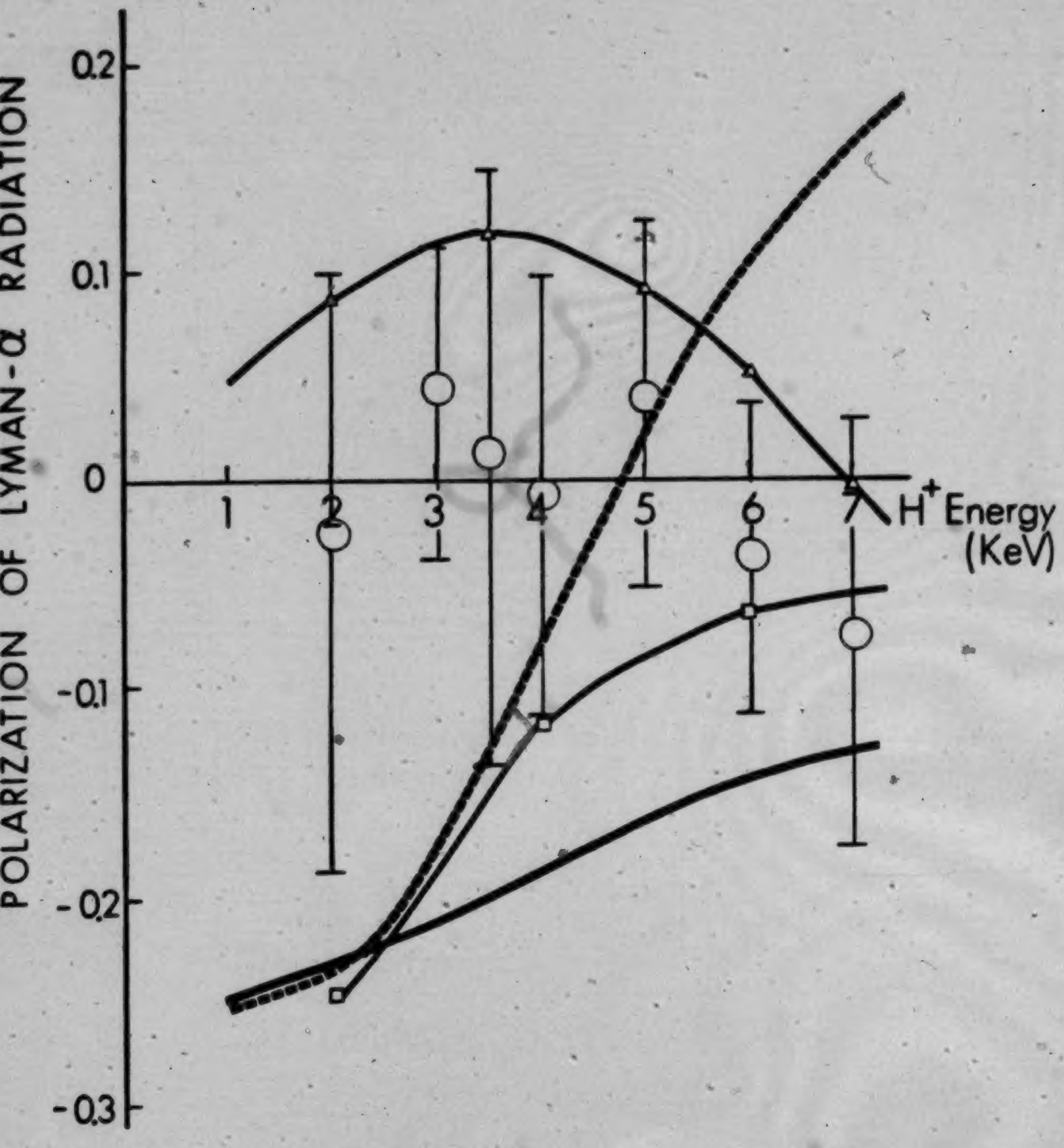

Figure(V-18)Polarization of Lyman- α radiation vs. E: ——— present work; – – – – – –, Crothers et al(48); —□—, Rapp et al(58); —△—, Gallaher et al(57). Experimental data: O, Kaupila et al(69).

4. H(2s) Cross Section

(a) Cross Section

Cross sections for direct and charge exchange excitation to the 2s atomic state are shown in Figures(V-19 & 20). Effects of $1s\sigma_g - 3d\sigma_g$ and other g-manifold couplings play some role at higher energies so we find that Q_{2S}^{EX} and Q_{2S}^{D} are slightly different. For charge exchange, our results agree rather well with the recent data of Morgan, Stone and Mayo(68) and of Hill, Geddes and Gilbody(67) from 1.5 to 6 KeV (though Hill *et al* give somewhat larger values than those of Morgan *et al* below 3 KeV); Our values seem to agree more closely with those of Hill *et al* in this region, and fall somewhat below both experimental values at 7 KeV.

On the other hand our results differ very much from those reported by Crothers and Hughes, which show a pronounced minimum near 3-4 KeV in both direct and charge exchange cross sections. This behavior is similar to results found in some atomic basis set calculations[3] (not shown) and appears to follow closely the older experimental values reported by Bayfield(64).

(b) Calculations using Crothers and Hughes matrix elements

In an effort to determine the origin of this and other discrepancies between our results and those of

---

[3] The atomic calculations (Cheshire, Gallaher and Taylor(57)) show a change of slope, but not such a deep minimum, as that found by Crothers and Hughes,

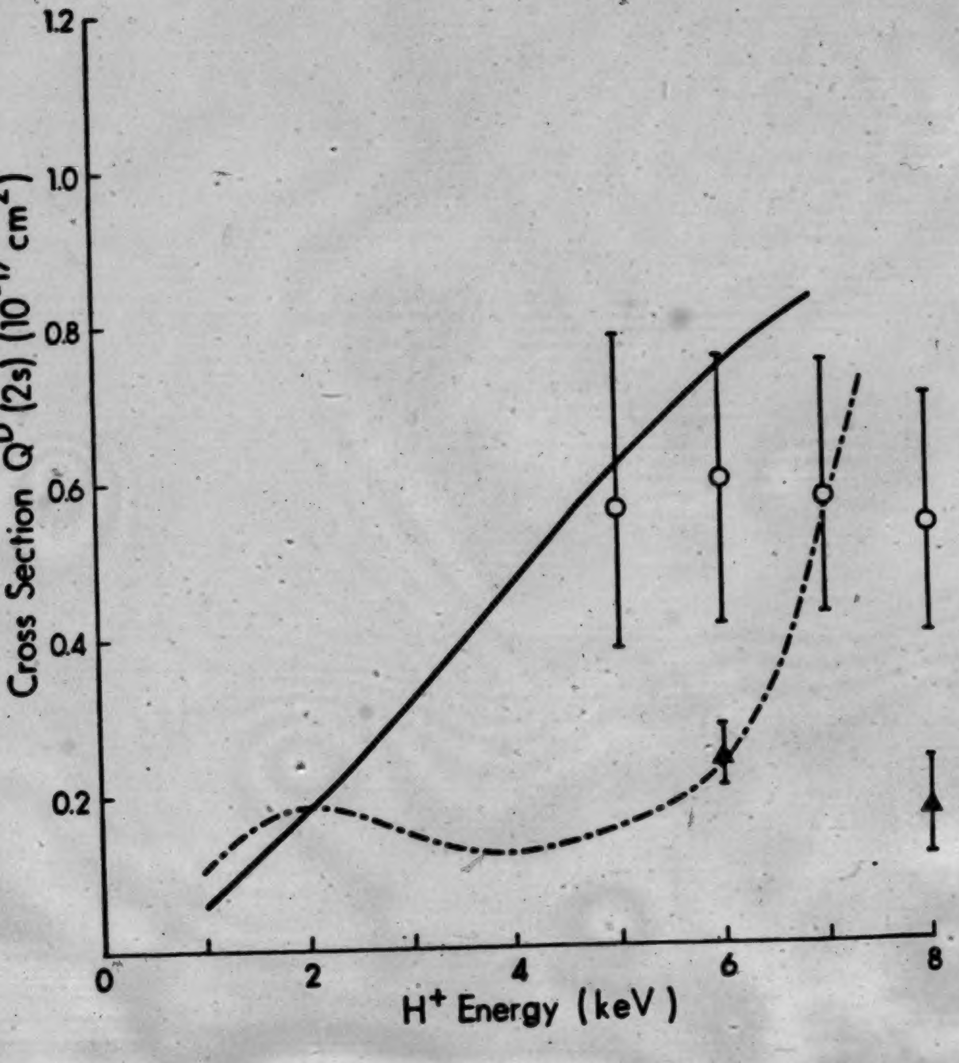

Figure(V-19) Direct excitation cross section for H(2s) vs. E: ——— present work; —·—·— Crothers et al. Experimental data: ○ Morgan et al(66); ▲ Chong et al(65).

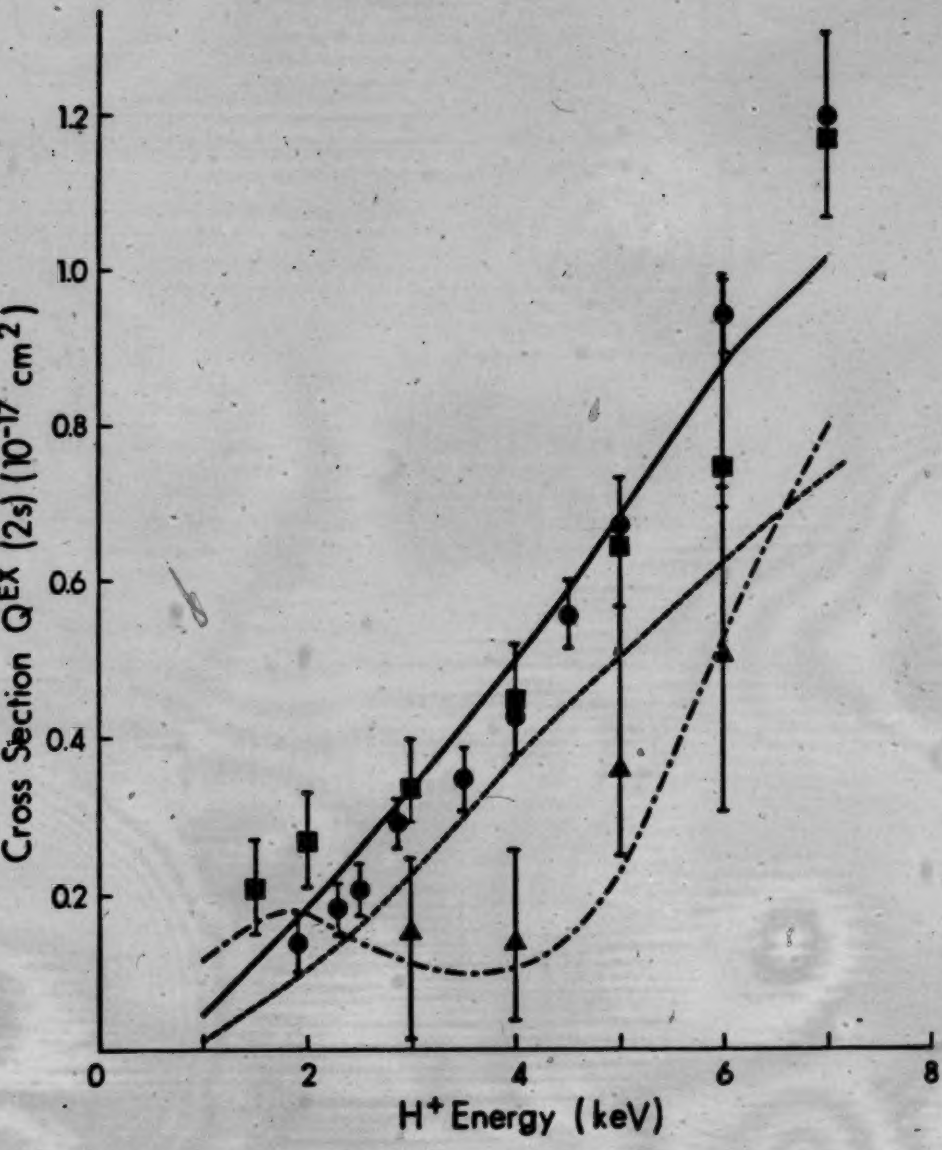

Figure(V-20) Charge exchange cross section for H(2s) vs. E: ———, present work; —— - ——, Crothers et al(48); - - - - Schinke et al(47-a). Experimental data: ●, Morgan et al(68); ■, Hill et al(67); ▲, Bayfield(64).

Crothers and Hughes, we have carried out close-coupling calculations using the same 10-state basis, but employing the matrix elements shown in their papers, for E=2,3,4 and 5 KeV. Straight-line trajectories were used, and we retained only terms of first-order in velocity. The essential features of the results we obtained are shown in Table(V-5). For all except the 2s excitation cross sections, we have obtained reasonable qualitative agreement with their published curves. For example, the 2p excitation cross sections we obtained in these calculations differ from their reported values by at most 20 % (at 5 KeV) and follow the same uniform trend; the discrepancy in this case is probably attributable to the effects of higher-order terms in the velocity, which are included in their reported values, as well as in our own calculations. However, in the case of the 2s cross sections, we have not been able to reproduce Crothers and Hughes' results even qualitatively; the results we obtained from these calculations lie about 30-40 % above our curves in Figure(V-19) and show no sign of any dip or even a marked change in slope. We therefore cannot prove that this large discrepancy necessarily results from the different treatment of ETF effects by Crothers and Hughes.

From remarks made by these authors and comparison with our own experience, (Section(V.E.1) below) it appears that their second-order velocity corrections are

Table V.5 ETF effects on cross sections

ETF Effects on Individual Cross Section

First-Order in V Only (units of cm^2)

	$2p_{\pm1}$		2s		$2p_0$	
E(KeV)	**K & T**	**C & H**	**K & T**	**C & H**	**K & T**	**C & H**
2	2.12×10^{-17}	2.35×10^{-17}	1.84×10^{-18}	2.25×10^{-18}	2.84×10^{-18}	3.56×10^{-18}
3	2.47	2.83	3.72	4.81	3.93	6.90
4	2.78	3.32	5.28	7.57	6.09	10.8
5	3.12	3.72	7.53	11.7	8.07	17.5

rather larger than those found in our approach. As shown in Section(III.A) (see also TKCK(33)), the ETF description employed by Crothers and Hughes is equivalent to the use of switching functions only up to *first*-order terms in V. Therefore it is possible that their second- and higher-order corrections behave quite differently from ours, and we cannot exclude the possibility that such second-order terms are the origin of the 2s cross section discrepancy. In our own case, however, we find that the second-order corrections are much smaller than would be needed to do this, and they are also steadily increasing functions of the energy (cf. Section(V.E.1) below).

(c)Comparison with Charge Exchange Results of Schinke and Krüger

Figure(V-20) also shows the results for the 2s charge exchange cross section reported by Schinke and Krüger; the results found by Chidichimo-Frank and Piacentini (not shown) are very similar. There is a substantial discrepancy between our results and these, which is masked to some extent by the linear plot used for Figure(V-20); at 1 KeV our value is at least 4 or 5 times larger than that of Schinke and Krüger and at 5 KeV it is still about 40 % larger. As is shown by comparison of Figures(V-12) and (V-13) (5 KeV), our larger cross sections result from inclusion of the radial couplings, especially $2p\sigma$ -$3p\sigma$, leading to a higher population of the $3p\sigma$ level at smaller impact parameters. Figure(V-14) (1 KeV) shows that this effect is even larger at lower energies. Given the limits of error on the experimental values reported in Hill et al and Morgan et al, we cannot say that these clearly confirm our results as correct, but they seem to agree somewhat more closely with our predictions than with those made by Schinke and Krüger.

D. VELOCITY AND TRAJECTORY EFFECTS

1. Effects of Second-Order Terms in Velocity

In this study we have included the effects of second-order terms in the collision velocity where these could be shown to have a significant effect on the cross sections. In this section I present data showing the size of these corrections for various cross sections as a function of the collision energy. Table(V-6) shows the comparison of the cross sections calculated using the first-order terms only and by the inclusion of up to second-order terms. The effects of the second-order terms can not be seen clearly below 3 KeV; however, they become significant as energy increases. At the highest energies studied, the second-order contribution rises up to 17 % for some individual cross sections. Therefore in H^{+}-H(1s) collisions, the second-order terms

Table V.6 Effects of second-order terms in velocity

Effects of Second-Order Terms in Velocity on Charge Exchange Cross Sections

(units of cm^2)

E (KeV)	$2p_{\pm1}$		$2s$		$2p_0$	
	v^1	v^2	v^1	v^2	v^1	v^2
1	1.99×10^{-17}	1.98×10^{-17}	0.637×10^{-18}	0.637×10^{-18}	0.761×10^{-18}	0.761×10^{-18}
3	2.47	2.40	3.72	3.64	3.93	3.85
5	3.12	2.86	7.53	7.06	8.07	7.58
7	3.98	3.32	11.6	10.1	9.75	8.51

play an important role, (as I already pointed out the sizes of the matrix elements are relatively larger at large distances than those for the asymmetric case. (see Section(III.D))).

2. Effect of Coulombic vs. Straight-line trajectories

I have also made some studies at low energy of the effects of using a straight-line trajectory, by comparing with calculations made using Coulombic trajectories, and these studies are summarized here. Table(V-7) compares the effect of the two trajectories at 1 KeV. The discrepancy between the two different trajectories employed is at most 4 % in the $H(2p_1)$ cross section, due to the creation of the new peaks at small impact parameter in the Coulombic trajectory calculation, and in H(2s) and $H(2p_0)$, the effect is much smaller, about 2 %. Therefore we can conclude that a straight-line trajectory is adequate to the present purposes.

Table V.7 Trajectory effects on cross sections

Effect of Trajectories on Atomic Level
Charge Exchange Cross Sections
H^+ energy E=1 KeV (units of cm^2)

Trajectory	$2p_{\pm 1}$	$2s$	$2p_0$
Straigh-line	1.98×10^{-17}	0.637×10^{-18}	0.761×10^{-18}
Coulombic	2.06	0.625	0.744

E. CONVERGENCE STUDIES

1. Convergence of n=2 Levels

Tables(V-8) and (V-9) shows excitation cross sections for H(n=2) levels as a function of basis size, for the basis sets of Table(V-1) , and for energies 1,3,5 and 7 KeV. In all cases the $H(2p_1)$cross section appears to have converged; on the other hand, for the H(2s)cross section there is a 15 % change at 7 KeV when the basis is augmented from 8 to 10 states, and similarly a 20 % change in the $H(2p_0)$ cross section, so in these cases the effects of further increases in basis size are worth further study. Unfortunately no data on convergence vs. basis size were provided in the study by Crothers and Hughes or by earlier calculations on this system.

2. Convergence and Flux Loss to Ionization

To explore further the convergence properties of a close-coupling calculation on this system, we increased the size of the u-basis by adding more highly excited molecular-states strongly coupled to those already considered, and performed calculations of molecular state excitation probabilities at selected energies and impact parameters. In addition to the 5-state basis already considered, we used basis with 8,14,16 u-state. Table(V-2)

Table V.8 Convergence of cross sections

Charge Exchange Cross Sections (cm^2)*
showing convergence vs. basis size at E = 1, 3, 5 & 7 KeV

E (KeV)	1			3			5			7		
Atomic States	$2p_{\underline{+}1}$	2s	$2p_0$	$2p_{\underline{+}1}$	2s	$2p_0$	$2p_{\underline{+}1}$	2s	$2p_0$	$2p_{\underline{+}1}$	2s	$2p_0$
4-state Basis	2.00	-----	-----	2.42	-----	-----	2.92	-----	-----	3.47	-----	-----
8-state Basis	1.98	0.653	0.653	2.40	3.70	3.70	2.87	8.23	8.23	3.39	10.9	10.9
10-state Basis	1.98	0.637	0.761	2.39	3.64	3.85	2.87	7.06	7.88	3.32	10.1	8.51

* $2p_{\underline{+}1}$ = X 10^{-17}, 2s, $2p_0$ = X 10^{-18}

Table V.9 Convergence of cross sections

Direct Excitation Cross Sections (cm^2)*

showing convergence vs. basis size at E = 1, 3, 5 & 7 KeV

E(KeV)	1			3			5			7		
Atomic States	$2p_{\pm1}$	2s	$2p_0$	$2p_{\pm1}$	2s	$2p_0$	$2p_{\pm1}$	2s	$2p_0$	$2p_{\pm1}$	2s	$2p_0$
4-state Basis	2.00	-----	-----	2.47	-----	-----	3.02	-----	-----	3.74	-----	-----
8-state Basis	1.98	0.652	0.652	2.45	3.76	3.76	2.99	8.42	8.42	3.68	11.5	11.5
10-state Basis	1.98	0.589	0.759	2.44	3.44	3.94	2.98	6.37	8.45	3.61	8.21	12.8

*$2p_{\pm1}$ = X 10^{-17}, $2s, 2p_0$ = X 10^{-18}

lists these states and the corresponding atomic state manifolds to which they dissociate. As these Rydberg states are very loosely bound and closely spaced in energy, they can hardly be expected to behave even approximately in adiabatic fashion. Moreover the coupling matrix elements linking them, both radial and angular, are of very long range and reflect the very large polarizabilities of these states. Even at the low end of the energy range we considered, it has proved impossible to obtain reasonable convergence of excitation probabilities for atomic levels n=3. Moreover, as the basis size is increased a small but non-negligible portion of the flux persistently moves up to the highest levels accessible; a collision history diagram in Figure(V-21) shows that this is occurring in the outgoing portion of the collision trajectory and is due to the long-range $\pi - \pi$ couplings in particular. Table(V-10) indicates the size of the effects in question for E=0.7 KeV and three impact parameters. It can be seen that a small portion of the flux always escapes to the highest Rydberg states as the basis size increases, while the probability for n=2 levels is relatively stable for all impact parameters. However, as n increases, the probabilities change by more than 30 % for each impact parameters and this is particularly so at large impact parameter when the basis is expanded from 14 to 16 states.

Since close-coupling molecular state calculations, as currently performed, include only bound states which follow

Table V.10 Excitation probabilities for higher n levels

Total Excitation Probabilities for Atomic Level n

(E = 0.7 keV, $|2p\sigma_u>$ initial state (n_0 = 1); impact parameters 1, 2, 3 a.u.)

Impact Parameter	Basis size	n = 2	n = 3	n = 4	n = 5	n = 6
1 a.u.	8	2.406×10^{-1}	2.141×10^{-2}	1.341×10^{-3}	---	---
	14	2.324×10^{-1}	1.762×10^{-2}	3.791×10^{-3}	1.230×10^{-4}	---
	16	2.351×10^{-1}	1.239×10^{-2}	2.237×10^{-3}	1.738×10^{-4}	1.335×10^{-4}
2 a.u.	8	1.588×10^{-2}	8.010×10^{-4}	1.018×10^{-4}	---	---
	14	1.498×10^{-2}	6.732×10^{-4}	1.029×10^{-3}	1.354×10^{-5}	---
	16	1.595×10^{-2}	5.978×10^{-4}	2.903×10^{-4}	2.303×10^{-5}	1.550×10^{-5}
3 a.u.	8	1.175×10^{-4}	5.506×10^{-5}	7.616×10^{-7}	---	---
	14	1.001×10^{-4}	4.176×10^{-5}	6.354×10^{-6}	8.862×10^{-6}	---
	16	1.131×10^{-4}	2.500×10^{-5}	2.103×10^{-6}	1.915×10^{-5}	2.391×10^{-6}

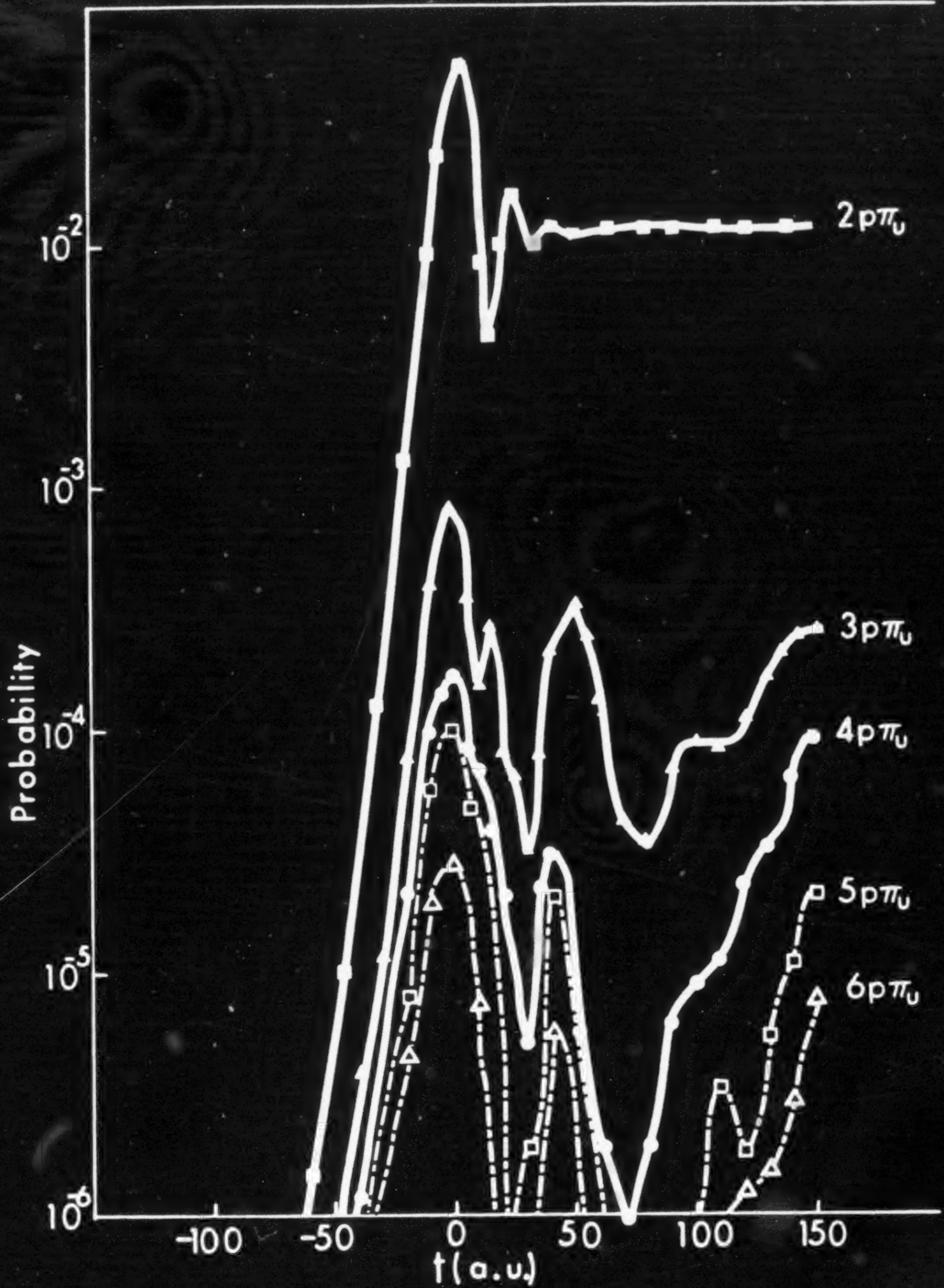

Figure(V-21) Collision "history" (molecular state probability vs. time (a.u.)) for E=0.7 KeV, impact parameter 2.0 a.u. for 16 states.

the nuclei, they make no allowance for flux loss due to ionization. However, as was pointed out by Thorson & Levy(8), it is physically unreasonable to regard a state as "bound" in a collision, if the transport kinetic energy of the electron, relative to the other collision partner, is comparable to or greater than the static binding energy; events corresponding in a tightly bound state to charge exchange will lead in such a case to ionization. At E=0.7 KeV, levels with n≥5 fall in this category. This suggests that a significant portion of the probability listed in Table(V-6) for the high levels corresponds in reality to ionizing events. SethuRaman, Thorson and Lebeda(8) and recently Choi and Thorson(8) have calculated the direct ionization from the close-coupled $1s\sigma_g$,$2p\sigma_u$ and $2p\pi_u$ molecular states of H^+ for projectile energies E= 1 KeV, assuming that ionization dominantly occurs by a single impulsive excitation from a tightly bound level to the continuum. The results obtained show that at 0.7 KeV and ρ =1.0 a.u., the resulting u-state impact ionization probabilities are 50-100 times smaller than the aggregates for n=5 and n=4 listed in Table(V-10) and drop off much more rapidly with increasing impact parameter than those in Table(V-10).

From reasonable extrapolation of the experimental data of Fite, Stebbings, Hummer and Brackman(62) on ionization, the experimental values should be about 50-100 times larger than those theoretical results and give nearly the same order of magnitude as are found here due to the "ladder climbing" process.

In conclusion, we may expect that a small but non-negligible portion of the flux leaving the ground state in H^+-H(1s) collisions, even at energies $\sim$1 KeV or less, will be promoted to higher (Rydberg-type) states by the multistep "ladder-climbing" process seen above, and that a large portion of that will actually be ionized in the end. We may also expect that close-coupling methods which do not include flux loss to the continuum as part of their formulation cannot represent the excitation to upper levels correctly or convergently. Further theoretical study of the "ladder-climbing" ionization mechanism in this prototype system is obviously highly desirable to further understand slow collision processes.

VI. He^{2+}-H(1s) AND H^{+}-He^{+}(1s) COLLISIONS

In this chapter we present and discuss our calculated cross sections for the processes

(a) $He^{2+} + H(1s) \longrightarrow He^{2+} + H(nl)$ (DIRECT)

$\longrightarrow He^{+}(nl) + H^{+}$ (CHARGE TRANSFER)

at He^{2+} projectile energies 1-20 KeV (c.m. energies 0.25-4 KeV), and

(b) $H^{+} + He^{+}(1s) \longrightarrow H^{+} + He^{+}(nl)$ (DIRECT)

$\longrightarrow H(nl) + He^{2+}$ (CHARGE TRANSFER)

at c.m. energies 1.6-8 KeV. Basis sets with up to 12 molecular states (Table(VI-1)) have been used, and good convergence of results as a function of basis size has been found. These collision processes have earlier been studied extensively by Winter and Lane(71), Hatton, Lane and Winter (HLW)(74), Winter and Hatton (WH)(73), and Winter, Hatton and Lane (WHL)(75), using both the uncorrected PSS method and PSS method with Bates-McCarroll ETF corrections. Comparison with their results provides information about the influence of ETF descriptions on cross sections. Our results may also be compared with the available experimental measurements on these processes.

For process (a), our total cross sections for charge transfer are in generally good agreement with those found by WH & HLW using Bates-McCarroll ETF's, except perhaps at the

Table VI.1 Molecular state basis sets

HeH^{2+} Molecular State Basis Sets
for He^{2+}-H(1s) and H^{+}-He^{+}(1s) Collisions

No. of States in Basis	Basis States	Limiting Atomic Levels
3	$2p\sigma$ $2p\pi$, $3d\sigma$	H(1s) + He^{2+} H^{+} + He^{+} (n=2)
4	as above, PLUS $2s\sigma$	 H^{+} + He^{+} (n=2)
5	as above, PLUS $1s\sigma$	 H^{+} + He^{+}(1s)
10	as above, PLUS $3p\sigma$, $3p\pi$, $3d\pi$ $4d\sigma$, $4f\pi$	 H^{+} + He^{+} (n=3) H (n=2) + He^{2+}
12	as above, PLUS $4f\sigma$ $5g\sigma$	 H^{+} + He^{+} (n=3) H (n=2) + He^{2+}

highest energy studied. There is less quantitative but still reasonably good agreement with Winter and Hatton's cross sections for charge transfer to individual states of $He^+(2s,2p_0,2p_1)$. Both our results and those of WH & HLW are in good agreement with experimental measurements of total cross section for charge transfer and the individual state cross section for $He^+(2s)$(Gilbody's group) (see Figure(VI-18)).

For process (b), on the other hand, some discrepancies between our values and those of Winter, Hatton and Lane(WHL) are found, using basis sets of comparable size, for both charge transfer and direct excitation cross sections; the charge transfer cross sections of WHL are 14 % to 32 % larger than ours, and their individual state direct excitation cross sections (He^+ $2s,2p_0,2p_1$) are systematically larger as well, in some cases by as much as a factor of two. These differences appear to be traceable to differences in ETF description used and the resulting coupling matrix elements; given the convergence behavior found in augmenting the basis from 5 to 10 states, it is our view that the "converged" values obtained by the two methods will in fact be significantly different. Comparison of the charge transfer cross sections with measurements by Peart, Grey and Dolder(85) suggests that our values are in slightly better accord with these than the values found by WHL, but a more definite conclusion on this question will probably require further experimental and theoretical investigations.

We will discuss the results for process (a) calculations and then those for process (b). However, we will give first a discussion of the basis sets used, and the coupling matrix elements, since these are common to both calculations.

Figure(VI-1) depicts electronic binding energies vs. internuclear distance R for 22 molecular states of HeH^{2+}; this diagram is useful in understanding coupling and excitation paths in this system.

A. BASIS SETS AND COUPLING MATRIX ELEMENTS

1. Basis Set

The basis sets used were selected as follows:

(a) $2p\sigma$, $2p\pi$, $3d\sigma$ and $2s\sigma$ states form an essential first block of basis states for He^{2+}-H(1s) collisions, and (although it plays a negligible role in process (a)) the $1s\sigma$ state must be added to these for a treatment of H^{+}-He^{+}(1s) collisions, where it is the initial state.

(b) In their calculation, WH included as the next block all remaining states associated with principal quantum number n=3 (united atom), that is, the states $3p\sigma$, $3p\pi$, $3d\pi$, $3d\delta$, and $3s\sigma$. The first three of these states couple strongly with the $3d\sigma$ state. On the other

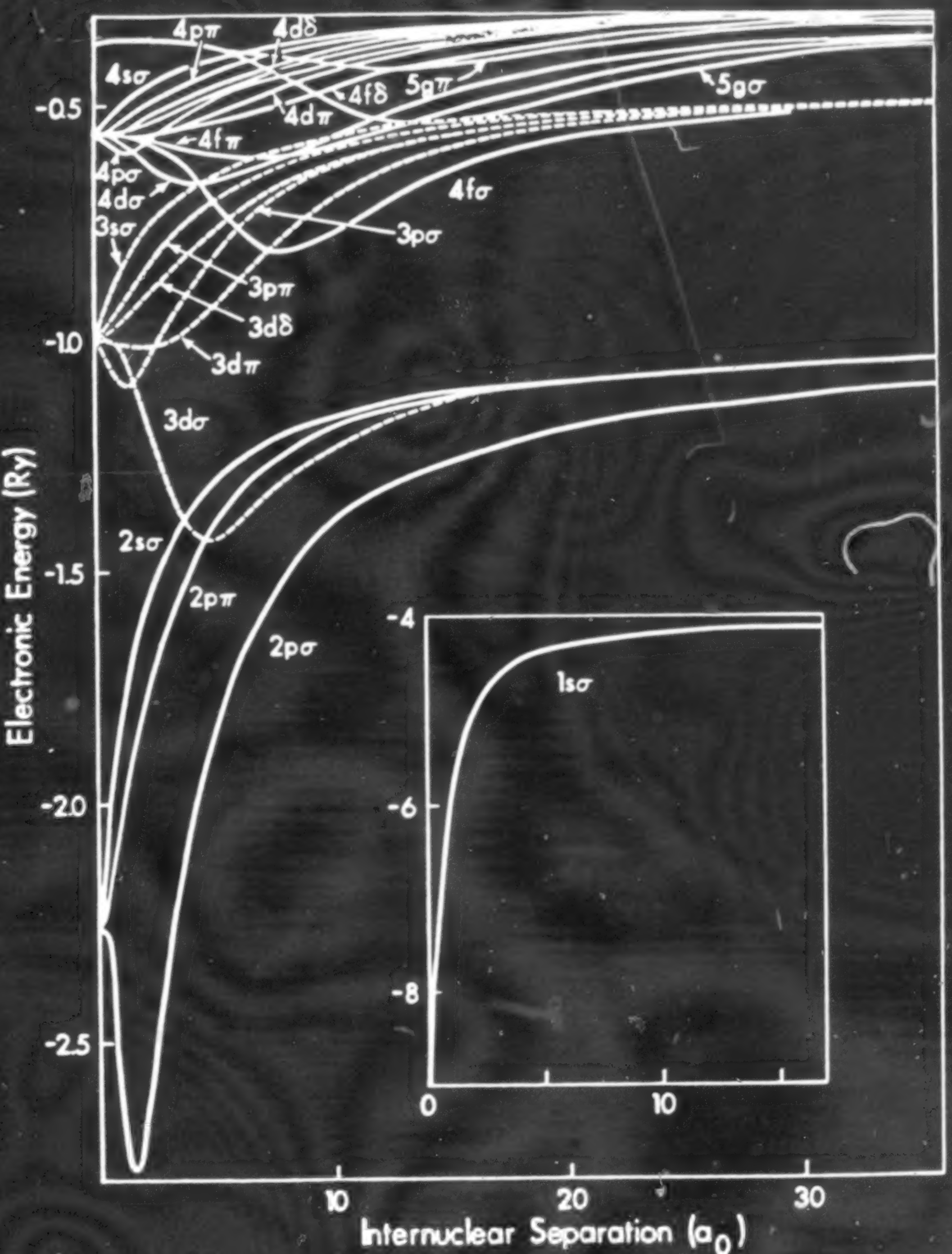

Figure(VI-1) Electronic energy $\in(R)$ (in Ry.) vs. R, for 22 molecular states of HeH^{2+}.

hand, Winter and Hatton found that the 3sσ and 3dδ states make a very small contribution to the total charge transfer cross section in process (a), and I also found after comparing coupling matrix elements computed here that coupling to these states from the first block of states should be quite small. Therefore I excluded these states from the 10-state basis, and added instead the states 4dσ ,4fπ , which correspond asymptotically to He^{2+}+H(n=2) levels. Inclusion of these states gives a rough indication of the role of H(n=2) production in processes (a) and (b).

(c) Selected calculations of molecular state probabilities at various impact parameters and energies have been done using a 12-state basis consisting of the ten states above, plus 4fσ and 5gσ . 4fσ is strongly coupled to states in the 10-state block, and its inclusion amplifies excitation to the 4fπ state (via rotational coupling) by factor of as much as 4 or 5. 5gσ was included because it plays an important role as an intermediate state: when 5gσ is in the basis, there is a significant increase in H(n=2) populations, even though the 5gσ population itself is negligible at the end of the collision. A similar effect or effects was noted by WH & HLW.

2. Dominant Couplings and Excitation Paths

The two factors which determine effective coupling strength, i.e. coupling matrix elements and the associated energy gaps, are shown for the dominant couplings linking 2p σ (the initial channel for process (a)), 2pπ and 3dσ states, in Figure(VI-2). As for H^+-H(1s) collisions, there is very strong rotational coupling between 2pσ and 2pπ states in the united atom limit due to their orbital degeneracy and this coupling is the primary one for process (a). A second important link is the radial 2pσ -3dσ coupling which is strong around R=6-7 a.u. because there is a fairly small energy gap between these states at larger R, and this connection may be expected to be a dominant one at larger impact parameters. Also given in the Figure is the 3d σ -2pπ angular coupling matrix element, showing the typical long-range Coriolis coupling associated with orbital degeneracy of the separated atom; the problem of asymptotic couplings is most conveniently handled separately (see Section(IV.D)). The molecular state 2sσ is not coupled strongly to the above three states at small R values, but it must be considered in the asymptotic coupling problem. Coupling to 1sσ is very weak due to the large energy gap to all other states, hence charge transfer to He^+(1s) is almost negligible in process (a) and the total cross sections for process (b) charge transfer are also very small in comparison to those for process (a).

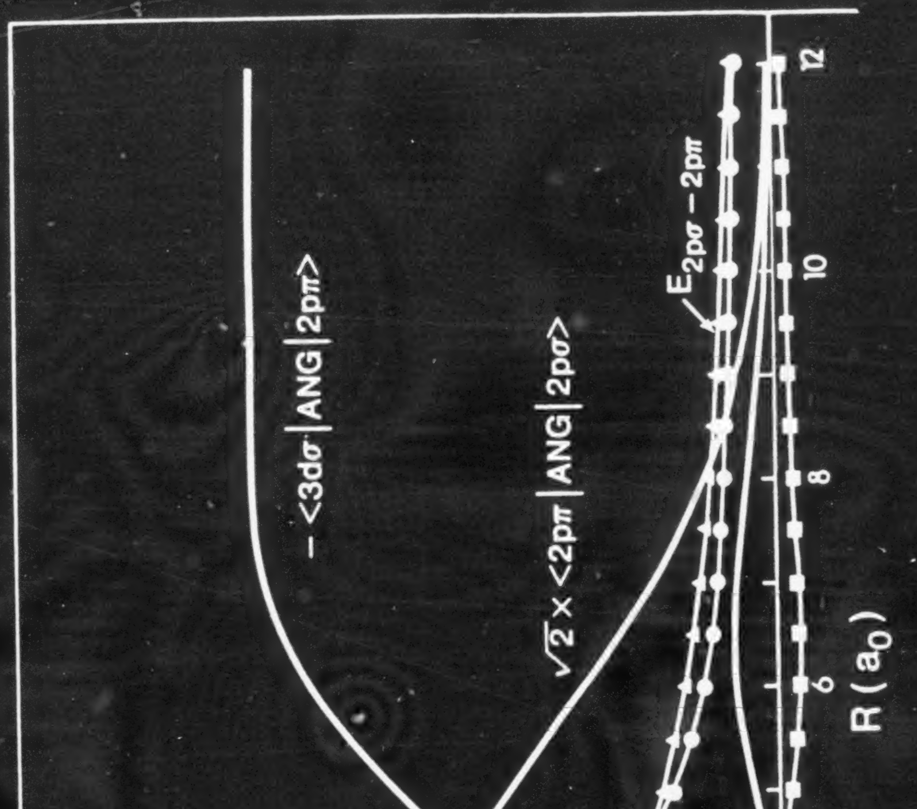

Figure(VI-2) Dominant coupling matrix elements for He^{2+}-H(1s) collisions, with associated energy gaps, vs. R.

In process (b), the most important coupling out of $1s\sigma$ is the $1s\sigma - 2p\sigma$ coupling, secondarily the $1s\sigma - 2p\pi$ angular coupling, and (much less important) $1s\sigma - 2s\sigma$ coupling (see Figures(III-10-15)). After these weak first steps, the strong $2p\sigma - 2p\pi$, $2p\sigma - 3d\sigma$, $2p\pi - 3d\sigma$ couplings play an important role in determining the further path of excitation, similar to their role for process (a), and most of the important transitions in process (b) involve two-step mechanisms in which $2p\sigma$ is the intermediate or "gateway" state. Figure(VI-3) depicts in a qualitative way the main coupling pathway for excitation in both processes (a) and (b); thickness of the arrows indicates qualitatively the coupling strength.

For excitations beyond these five molecular states, the $3d\sigma$ state plays a most important role as a "gateway", since it is correlated with united atom manifold n=3 and is strongly linked to $3d\pi$, $3p\sigma$, and $3p\pi$ (these states are of course also coupled strongly among themselves). As was found by Winter and Hatton, $3d\delta$ is less important (it can only be reached through $3d\pi$ or $3p\pi$) and $3s\sigma$ still less important.

As one goes still further up in energy, the smaller energy gaps and greater number of states leads to a very rapid increase in the number of couplings which can play a (minor) part.

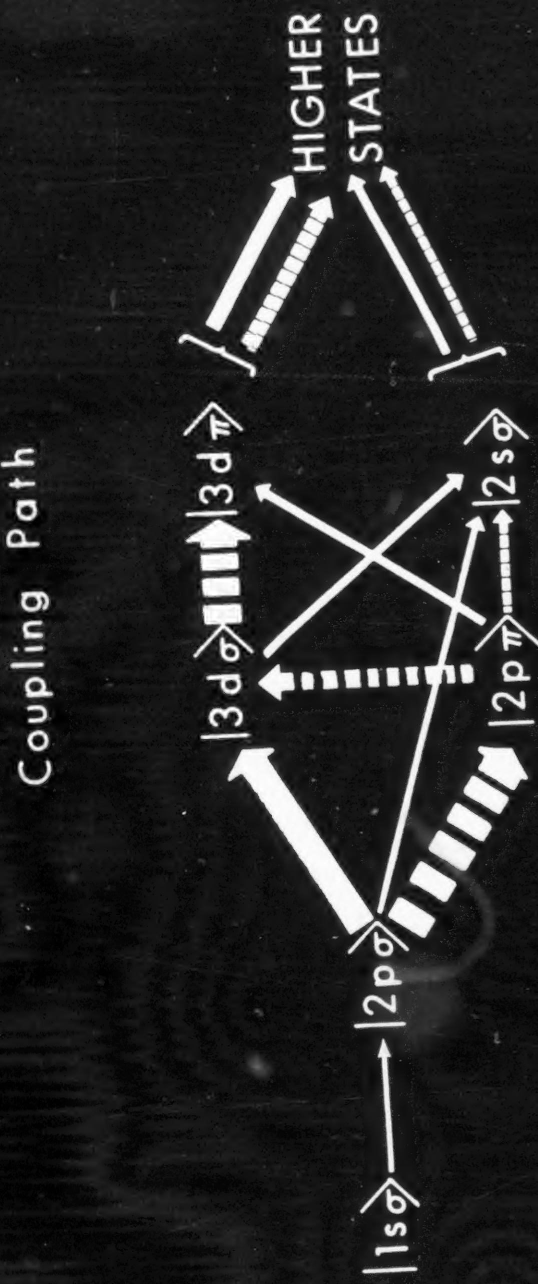

Figure(VI-3) Effective couplings and excitation paths for He^{2+}-H(1s) collsions. ⟶ radial coupling; - - - -→ angular coupling; thichness of connecting arrow indicates qualitative importance.

3. Asymptotic Coupling

Within an asymptotically degenerate atomic manifold---- such as the $He^{+}(n=2)$ manifold of $2s\sigma$, $3d\sigma$ and $2p\pi$ states---- a long range coupling problem arises which we found convenient to treat separately since these states are completely decoupled from other states for $R\geq15$ a.u.. The two hybrid $(sp)\sigma$ states are linked to $2p\pi$ by Corioli couplings and to each other by long range radial coupling, and both couplings and splittings decrease only as R^{-2}. For $R\geq16$ a.u., both couplings and splittings can be accurately modelled by an analytical perturbation expression and, using a new progress variable, the numerical problem may be solved very efficiently. The effects of this coupling are significant; for example, at 8 KeV, the probabilities for $He^{+}(2s)$ excitation as computed by this procedure differ by about 25 % from those found by direct numerical integration of Eq.(II-20) even as far as $R = 25$ a.u.. The details of the method are given in Sec.D. of Chap.IV..

4. ETF Effects on Couplings

In this section I compare effects of different ETF descriptions on the resulting coupling matrix elements for the HeH^{2+} system (comparison with uncorrected PSS couplings is not so much of interest, since the work of WH & HLW shows that ETF corrections of some kind are necessary). We compare our coupling matrix elements (based on switching functions "optimized" for each molecular state) with those of WH & HLW who used the simpler Bates-McCarroll (atomic state) ETF's, and with some matrix elements we have computed using Taulbjerg and Vaaben's(28) "universal" switching function (the same for all states). The couplings shown are for the dominant couplings in processes (a) and (b) (or for the primary excitation steps even though the coupling is weak, as in (b)). Even more pronounced effects of different ETF descriptions may be seen in couplings of secondary or more highly excited states, but these are not so significant for the collision processes considered.

Figures(VI-4) & (VI-5) show coupling matrix elements linking $2p\sigma$ with $2p\pi$ and $3d\sigma$; these are the dominant, primary couplings in process (a) and are also important in process (b).

For the strong $2p\sigma$ -$2p\pi$ couplings (Figure(VI-4)) our matrix elements and those of WH & HLW, or Taulbjerg and Vaaben, are different mainly at distances between 2 and 10 a.u.. This coupling is strong because of the united atom orbital degeneracy of $2p\sigma$ and $2p\pi$; the differences between the coupling matrix elements beyond $R=2$ a.u. should therefore have little effect, except at higher energies, and this is the main reason why the total charge transfer cross section for process (a) is relatively insensitive to the ETF used, especially at lower energies.

For the radial $2p\sigma$ -$3d\sigma$ coupling (Figure(VI-5)) our matrix elements are generally quite different from those of WH & HLW, especially for $R \leq 8$ a.u.. These couplings play

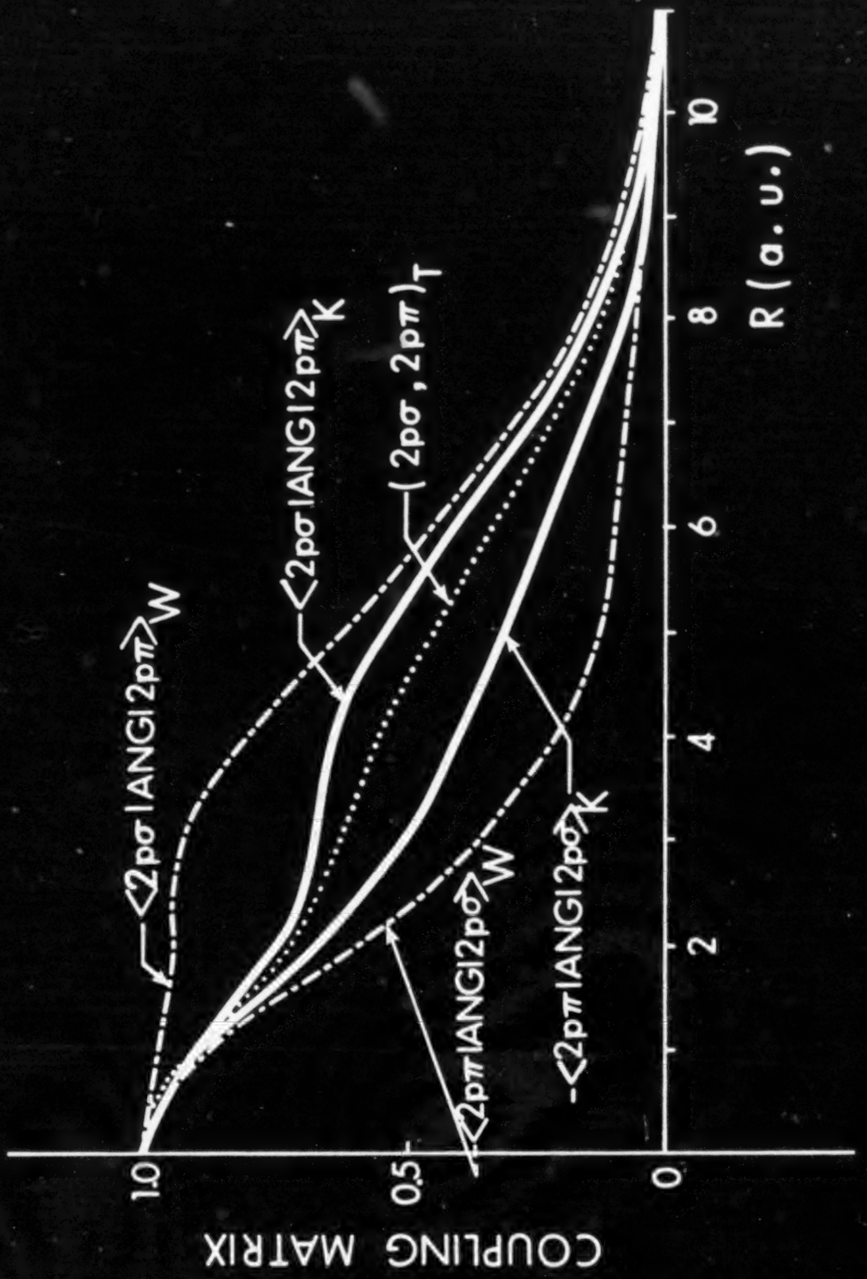

Figures(VI-4) & (VI-5) Coupling matrix elements for $2p\sigma$ -$2p\pi$ angular coupling and $2p\sigma$ -$3d\sigma$ radial coupling, respectively. Solid curves, matrix elements used in the present work, based on the different switching functions for each molucular state; dashed curves, matrix elements used by Winter et al, based on Bates-McCarroll ETF's; dot curves, used by Taulbjerg et al, based on the common switching function for each molecular state.

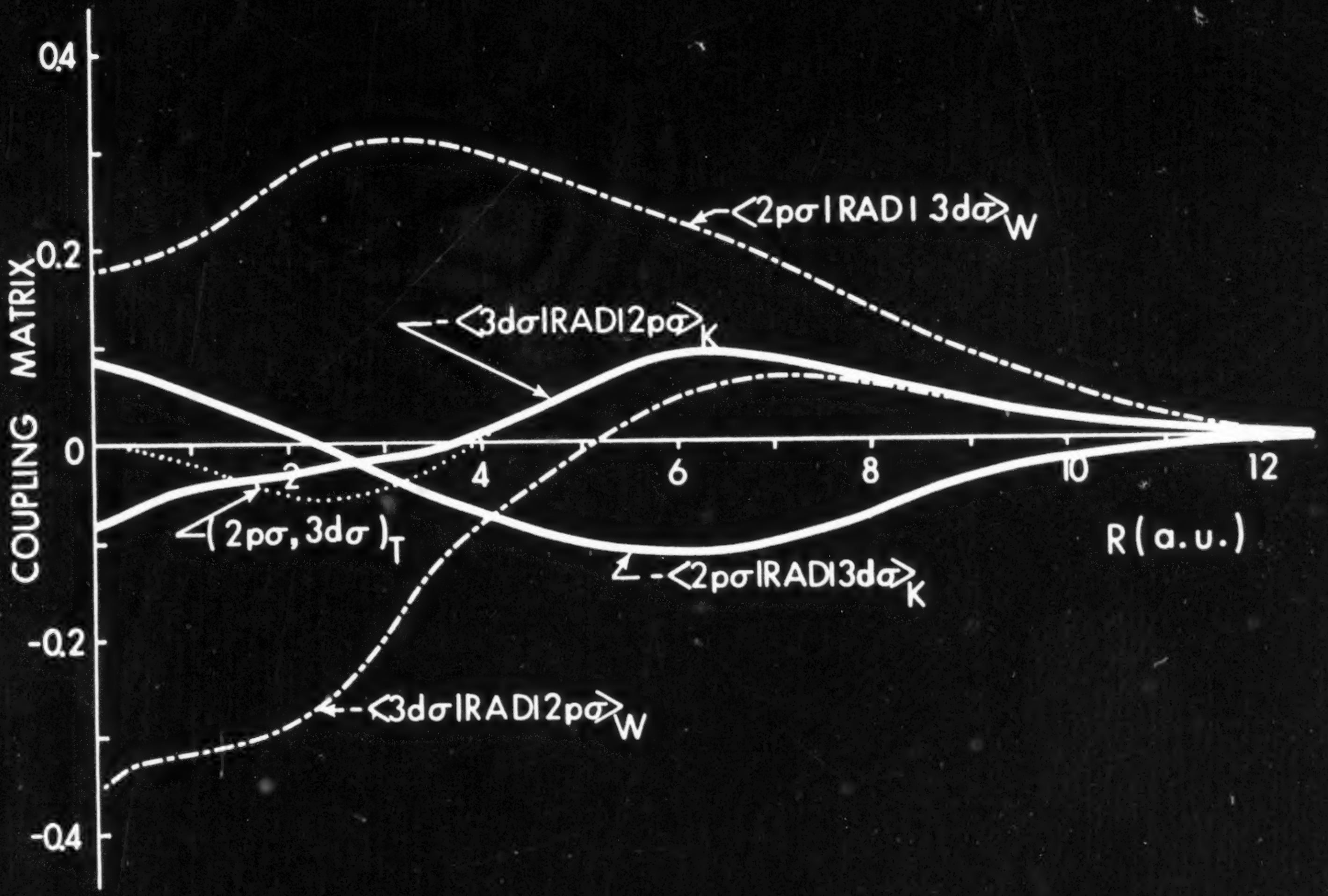
COUPLING MATRIX
0.4
0.2
0
-0.2
-0.4
2
4
6
8
10
12
R(a.u.)
<2pσ|RAD|3dσ>W
<3dσ|RAD|2pσ>K
(2pσ, 3dσ)T
<2pσ|RAD|3dσ>K
<3dσ|RAD|2pσ>W

the important role at larger impact parameters and can be expected to have some effect on detailed excitation probabilities. Our couplings are generally smaller than those found using Bates-McCarroll ETF's, but the gross differences found at smaller R-values really have less importance than may appear because of the dominance of $2p\sigma$ $-2p\pi$ coupling at small R.

Figures(VI-6) & (VI-7) show the primary excitation couplings for process (b), linking $1s\sigma$ with $2p\sigma$,$2p\pi$, and $2s\sigma$ states; although these couplings are much weaker than those for process (a) (because of large energy gaps), they have a controlling influence on all excitations in this collision process.

The $1s\sigma$,$2s\sigma$,and $2p\pi$ states are all "He^+"-like states; for this reason, the couplings found using Bates-McCarroll ETF's are Hermitian (non-Hermitian couplings only occur for states with different ETF's), and also the couplings linking them are relatively insensitive to ETF description (i.e., our "optimized" ETF's are nearly the same as the Bates-McCarroll ones in the region of wavefunction overlaps). For the $1s\sigma$ $-2p\pi$ couplings our matrix elements have maxima at a somewhat larger distance than that of WH & HLW but the shapes are generally similar.

For the $1s\sigma$ $-2p\sigma$ couplings the situation is quite different. $2p\sigma$ is a truly "molecular" state for $R \leq 4$ a.u., with substantial two-centre character, and the $2p\sigma$ switching function used in our calculations reflects this

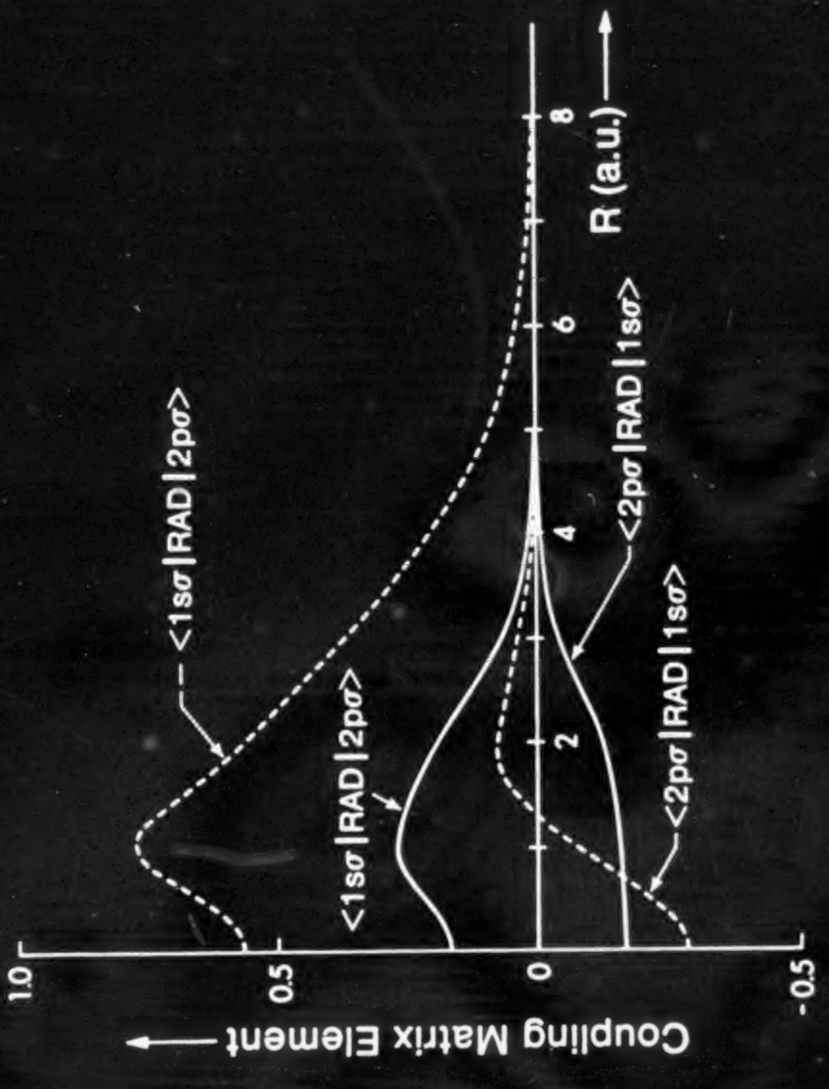

Figure(VI-6) Coupling matrix elements linking 1sσ and 2pσ HeH^{2+} states. Solid curves, matrix elements used in present work, based on switching functions; dashed curves, matrix elements of Winter et al, based on Bates-McCarroll ETF's.

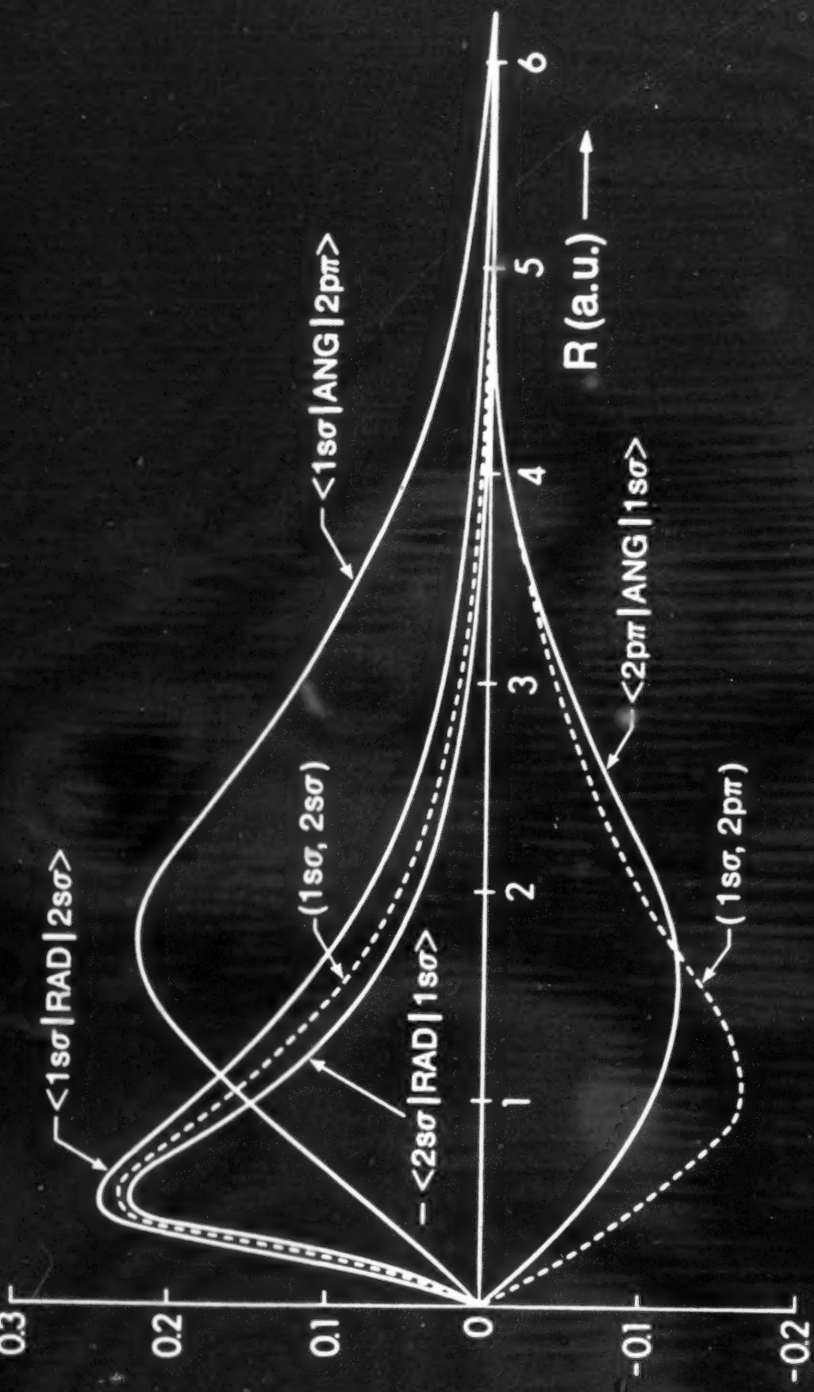

Figure(VI-7) Other coupling matrix elements linking 1sσ to excited states in HeH^{2+}. Solid curves, present work;dashed curves, matrix elements based on Bates-McCarroll ETF's.

fact; the Bates-McCarroll ETF corresponds to setting $f_{2p\sigma}=+1$ everywhere. As a result, our matrix element for $\langle 1s\sigma |RAD| 2p\sigma \rangle$ ($2p\sigma \rightarrow 1s\sigma$) is much smaller than that calculated by WH & HLW. Even more important however is the complete difference in shape and character of the element $\langle 2p\sigma |RAD| 1s\sigma \rangle$ ($1s\sigma \rightarrow 2p\sigma$) resulting from the use of switching functions. As can be seen from the parameters given in Table(III-2), our $1s\sigma$ switching function differs significantly from the Bates-McCarroll value $f_{1s\sigma}=-1$ at small R values, even for this "He^{+}-like" state, and this is especially true in regions of important overlap with the $2p\sigma$ state.

It appears that the difference between our couplings and those of WH & HLW for $1s\sigma \leftrightarrow 2p\sigma$ (especially $1s\sigma \longrightarrow 2p\sigma$) is the main reason for differences in computed cross sections for process (b). This is at first surprising since the sizes of the two matrix elements are similar; however, we have found in the course of studies on couplings in H^{+}-H(1s) collisions that shape has an effect which is as important, or more important, than integrated area, especially for non-resonant couplings: steeper slopes, or the occurrence of sign changes, have a tendency to increase transition amplitudes. (Such an effect can be understood from a Fourier analysis point of view: the more efficient couplings are those with components at frequencies closer to the frequency difference of the nonresonant coupled states).

B. α - PARTICLE - H(1s) COLLISIONS (PROCESS(a))

1. Excitation Paths

Typical collision histories are shown in Figures(VI-8) through (VI-11) for process (a): probabilities $P(\rho:E)$ for molecular states (in a four-state basis calculation) are shown vs. time t, at impact parameters , ρ, 0.5 and 5.0, and 0.3 and 3.0 a.u. and energies 8, 3 KeV, respectively. For all impact parameters the effect of 2pσ -3dσ radial coupling is evident during the early part of the collision, but for small impact parameters this is later dominated by the strong 2pσ -2pπ rotational coupling at small internuclear distances (Figures(VI-8) & (VI-10)). For large ρ , on the other hand, the effects of the 2pσ -3dσ coupling are dominant; for example, here even the 2pπ excitation results in most part from the two-step process 2pσ -3dσ -2pπ . (The curve crossing of 2pπ and 3dσ at 4.5 a.u. may be important for the efficiency of this mechanism). The small 2sσ probability for both large and small impact parameters is attributable to the processes 2pσ -3dσ -2sσ and 2pσ -2pπ -2sσ , rather than direct 2pσ -2sσ excitation.

2. Probabilities vs. Impact Parameter

a. Molecular states

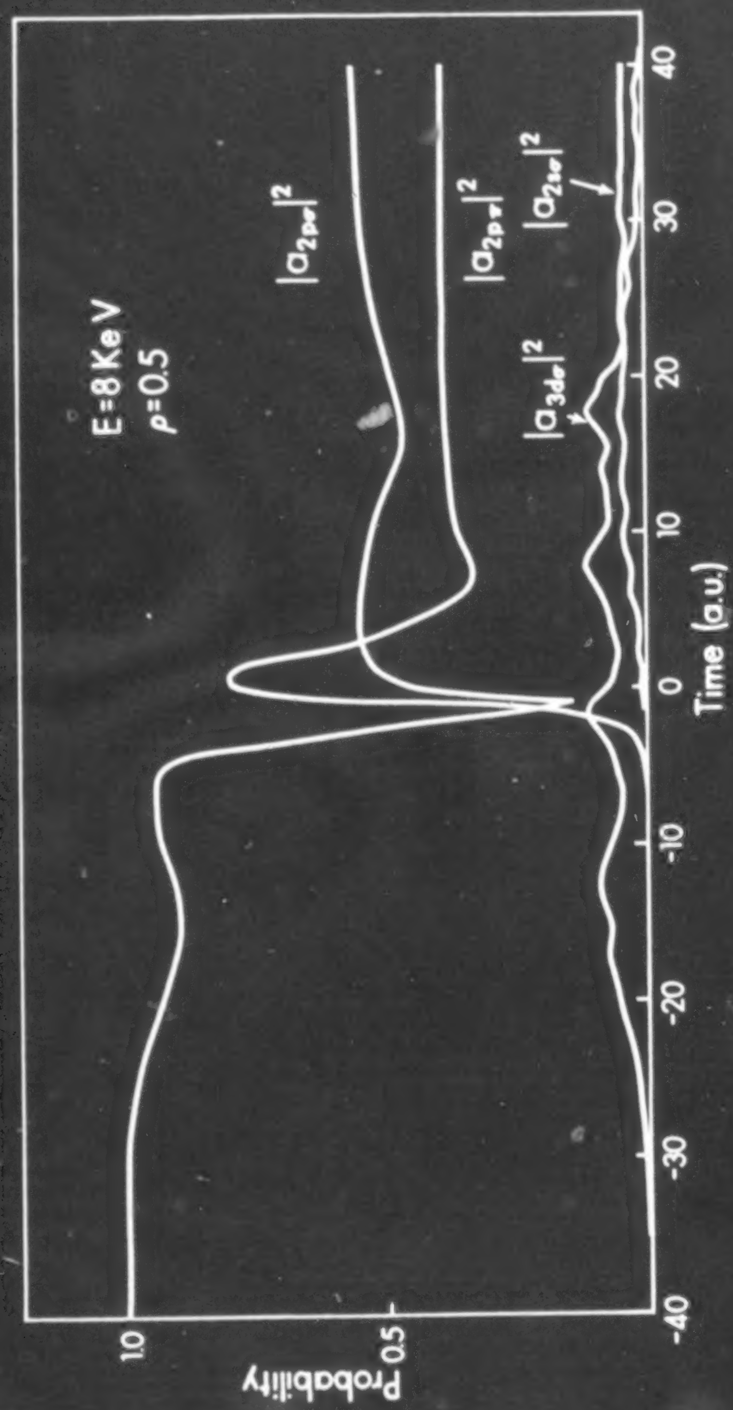

Figure(VI-8) Collision "history" (molecular state probabilities vs. time (a.u.)) for E=8 KeV at impact parameter 0.5 a.u. .

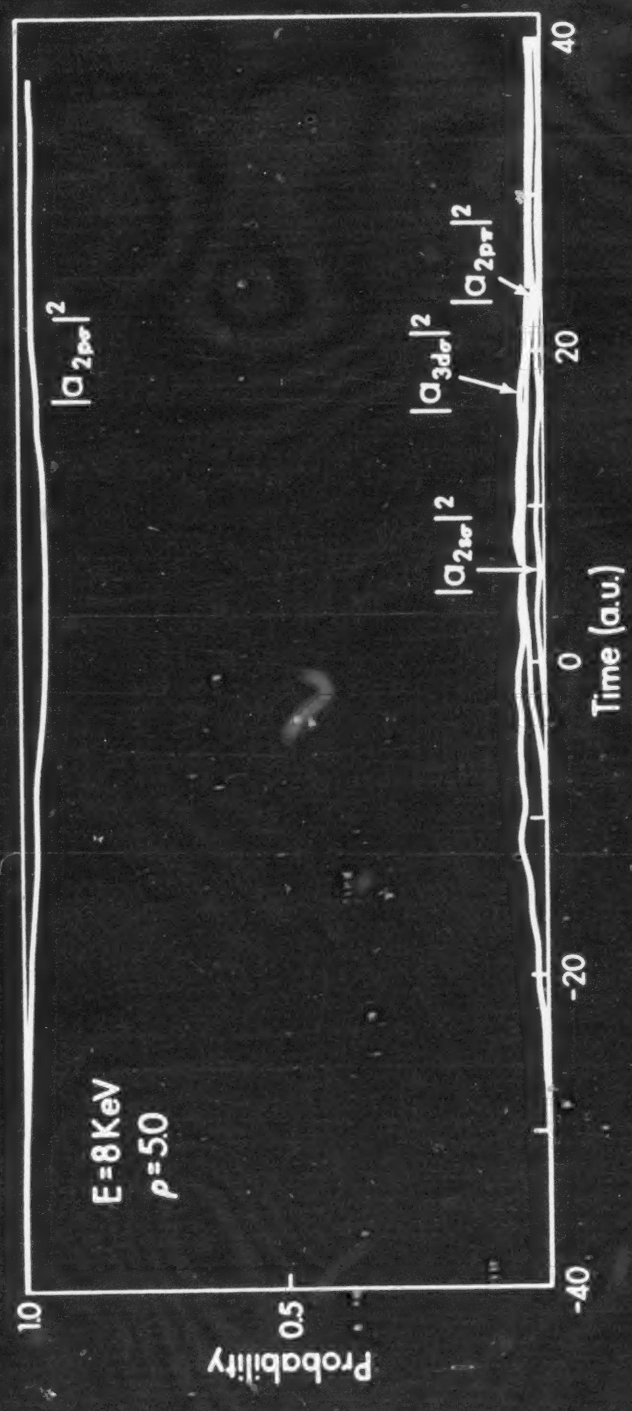

Figure(VI-9) Collision "history" (molecular state probabilities vs. time (a.u.)) for E=8 KeV at impact parameter 5.0 a.u..

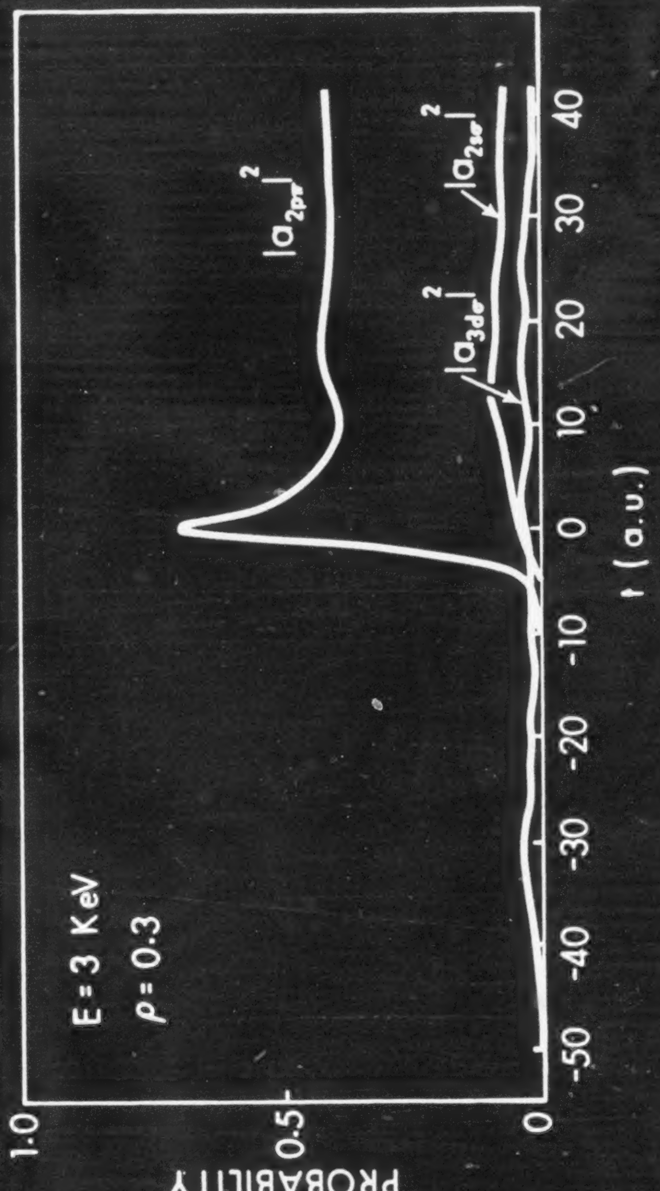

Figure(VI-10) The same data as Figs.(VI-8) & (VI-9), but for E=3 KeV at impact parameter 0.3 a.u..

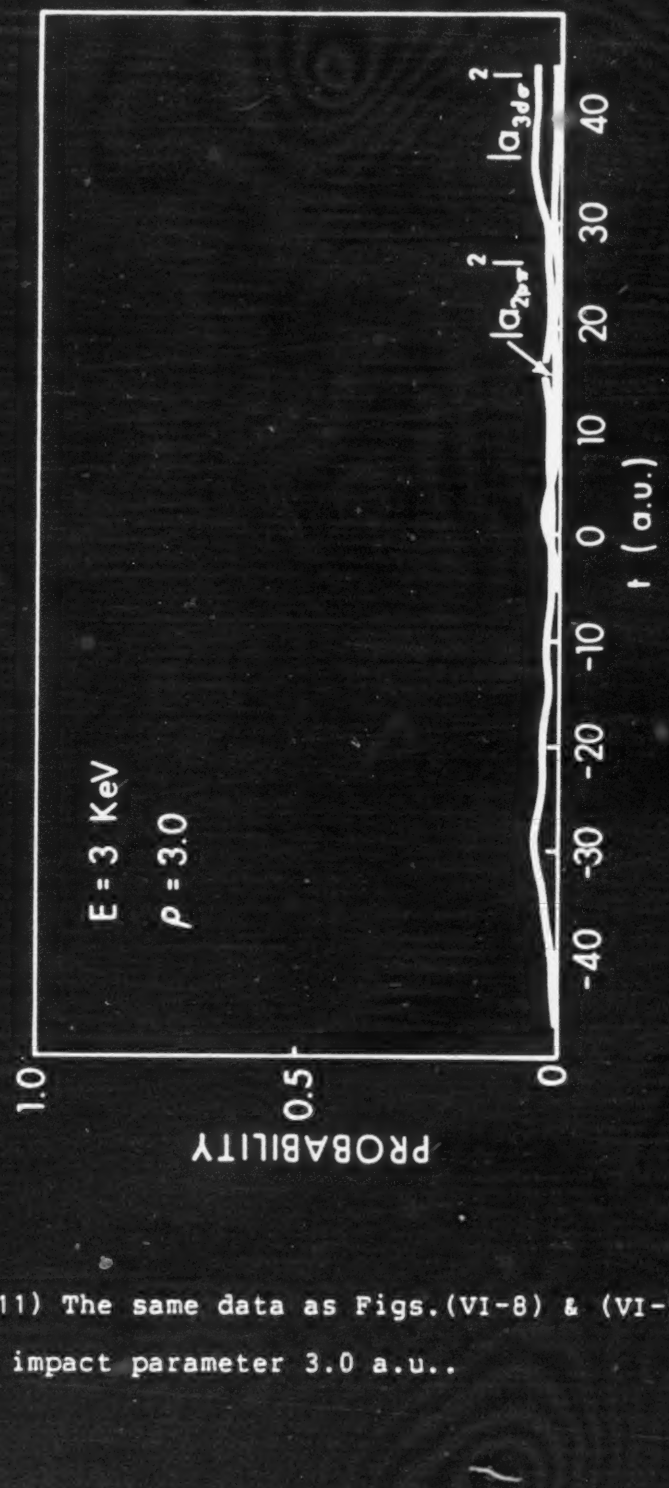

Figure(VI-11) The same data as Figs.(VI-8) & (VI-9), but for E=3 KeV at impact parameter 3.0 a.u..

Excitation probability vs. impact parameter at E=8 KeV is shown in Figure(VI-12). The large peaks at small impact parameter is due to 2pσ -2p π angular coupling . The 3dσ probability shows Rosen-Zener-Demkov oscillatory peak structure at larger impact parameters resulting from coherence between the 2pσ and 3dσ states in the extended region over which they are coupled. There are secondary 2pπ peaks in phase with these, which are due to the two-step process 2pσ -3dσ -2pπ . The small 2sσ probability shows its two-step origin in the same way. There is no coherent interference between the amplitudes produced by 2pσ -2pπ and 2p σ -3dσ couplings, as was also noted by WH & HLW.

b. Total charge transfer probability

The total transfer probabilities times impact parameter have been plotted versus ρ in Figures(VI-13) through (VI-15) for 1,8 and 20 KeV, respectively, and for both 4-state and 10-state basis sets. These figures may be directly compared with figures of the paper by Winter and Hatton(73). For 20 KeV (Figure(VI-15)) we have included Winter and Hatton's 10-state results for direct comparison; at lower energies, the agreement between their 10-state results (not shown) and ours is even better than at 20 KeV.

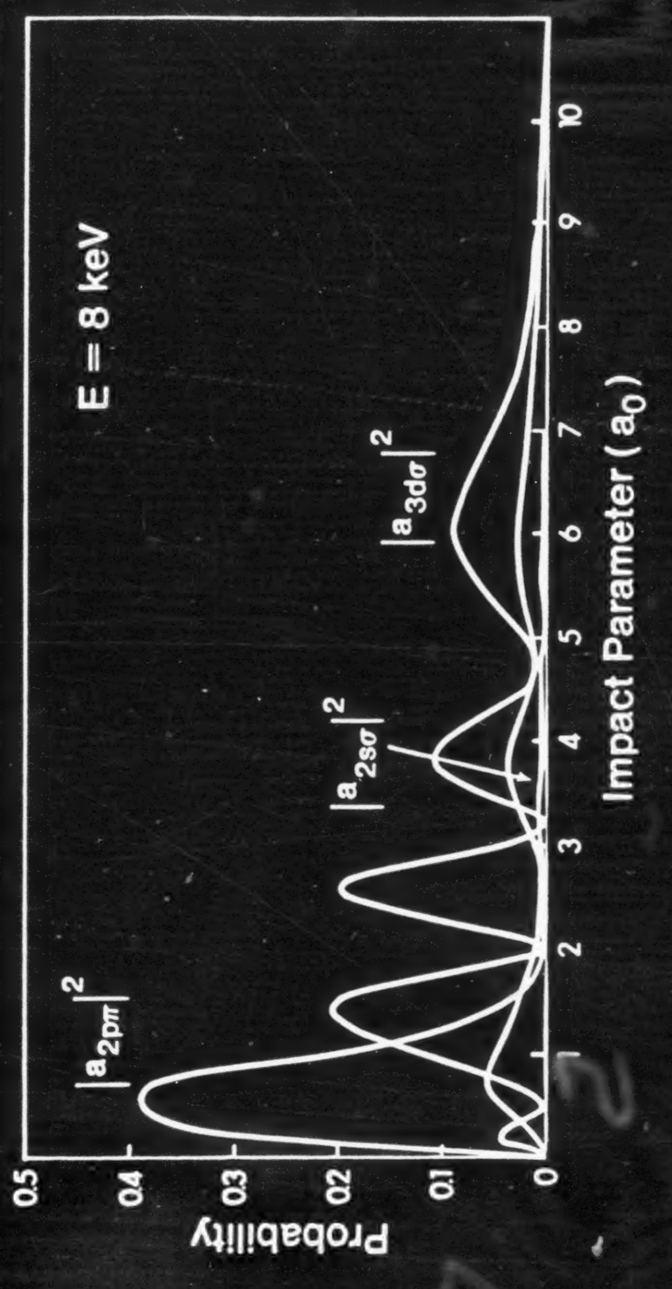

Figure(VI-12) Molecular state excitation probabilities vs. impact parameter for He^{++}-H(1s) collisions at 8 KeV.

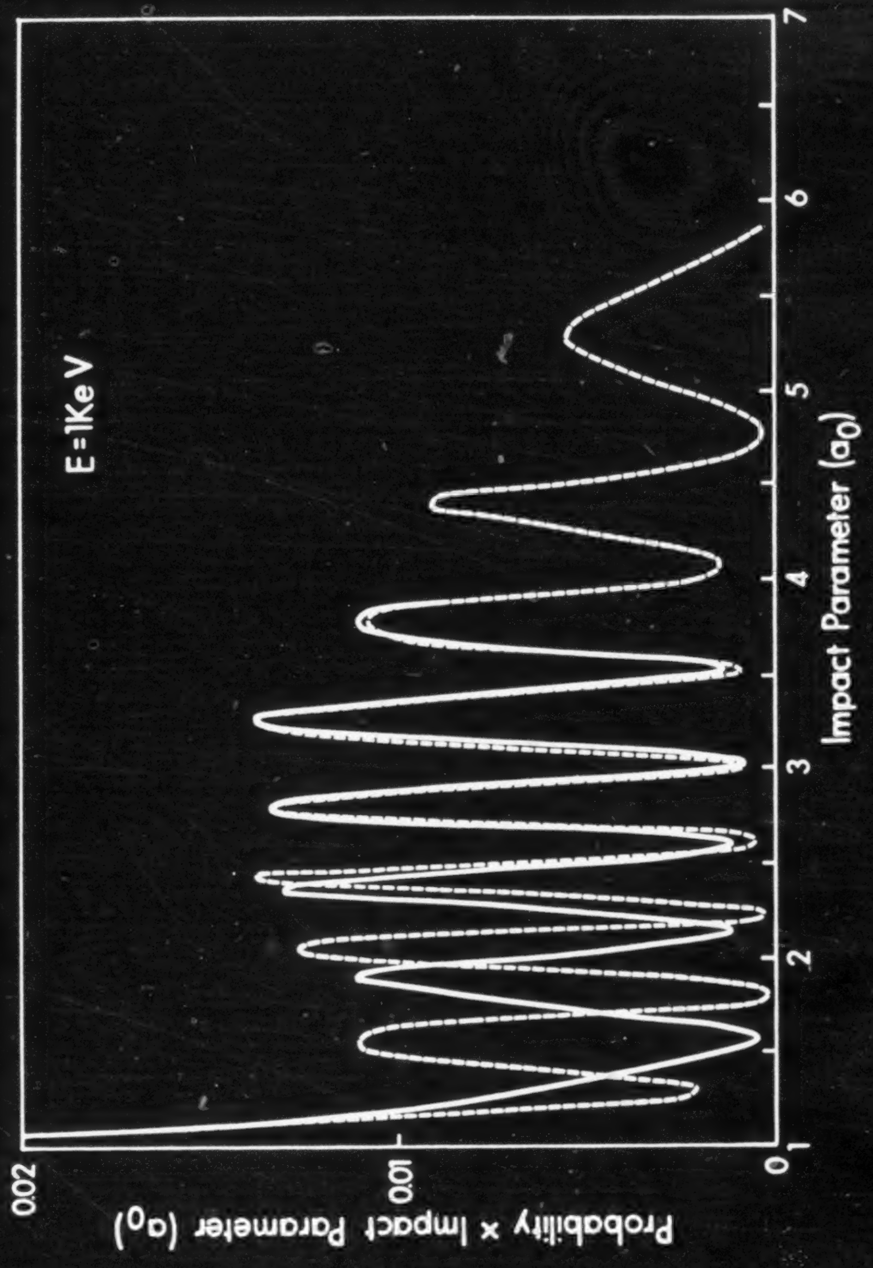

Figures(VI-13 through 15) Probability times impact parameter vs. impact parameter at 1, 8, and 20 KeV, respectively. ———, 10-state basis, ----,4-state basis; ······Winter et al(74).

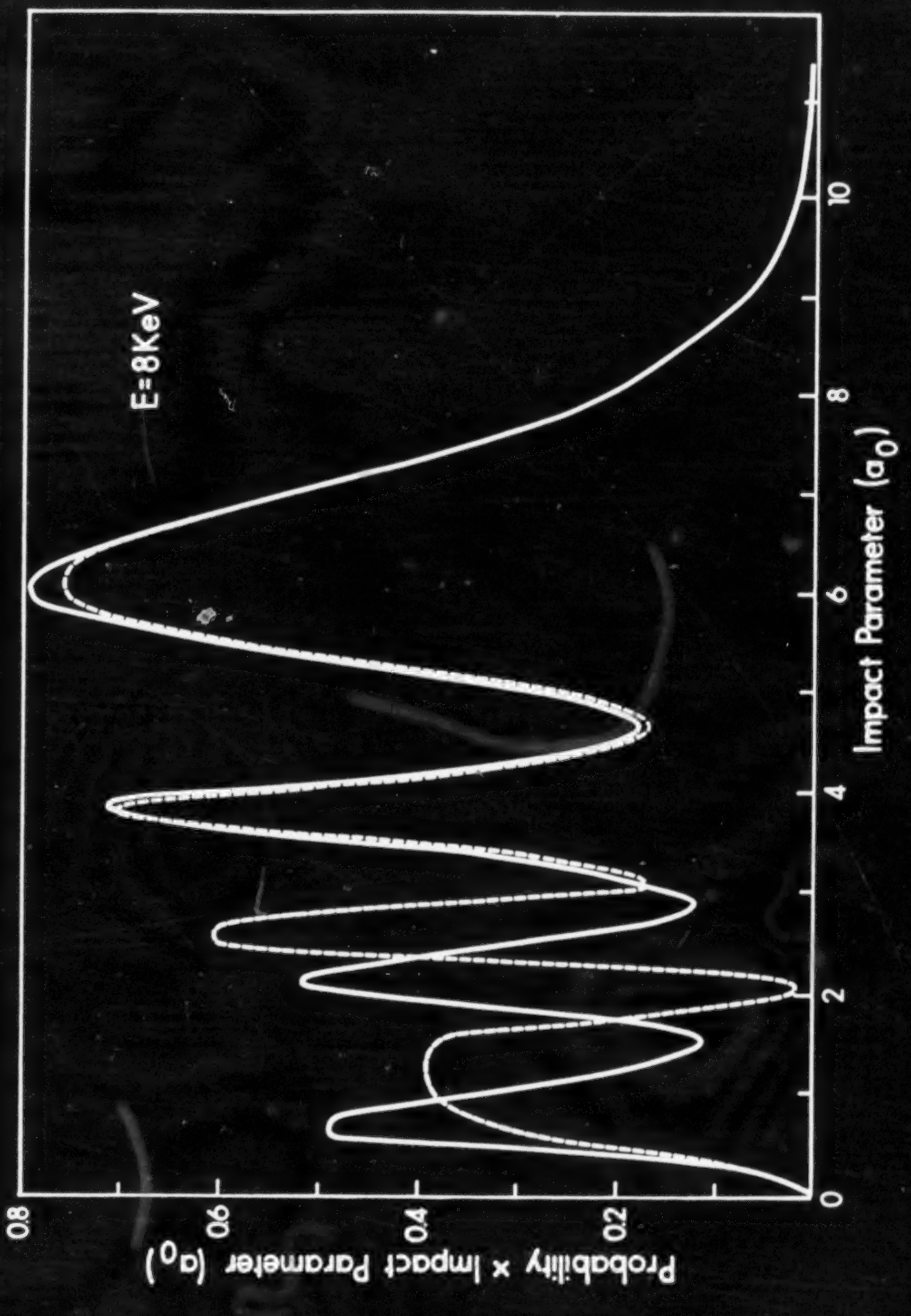

Figure VI.14 Probability X impact parameter vs. impact parameter

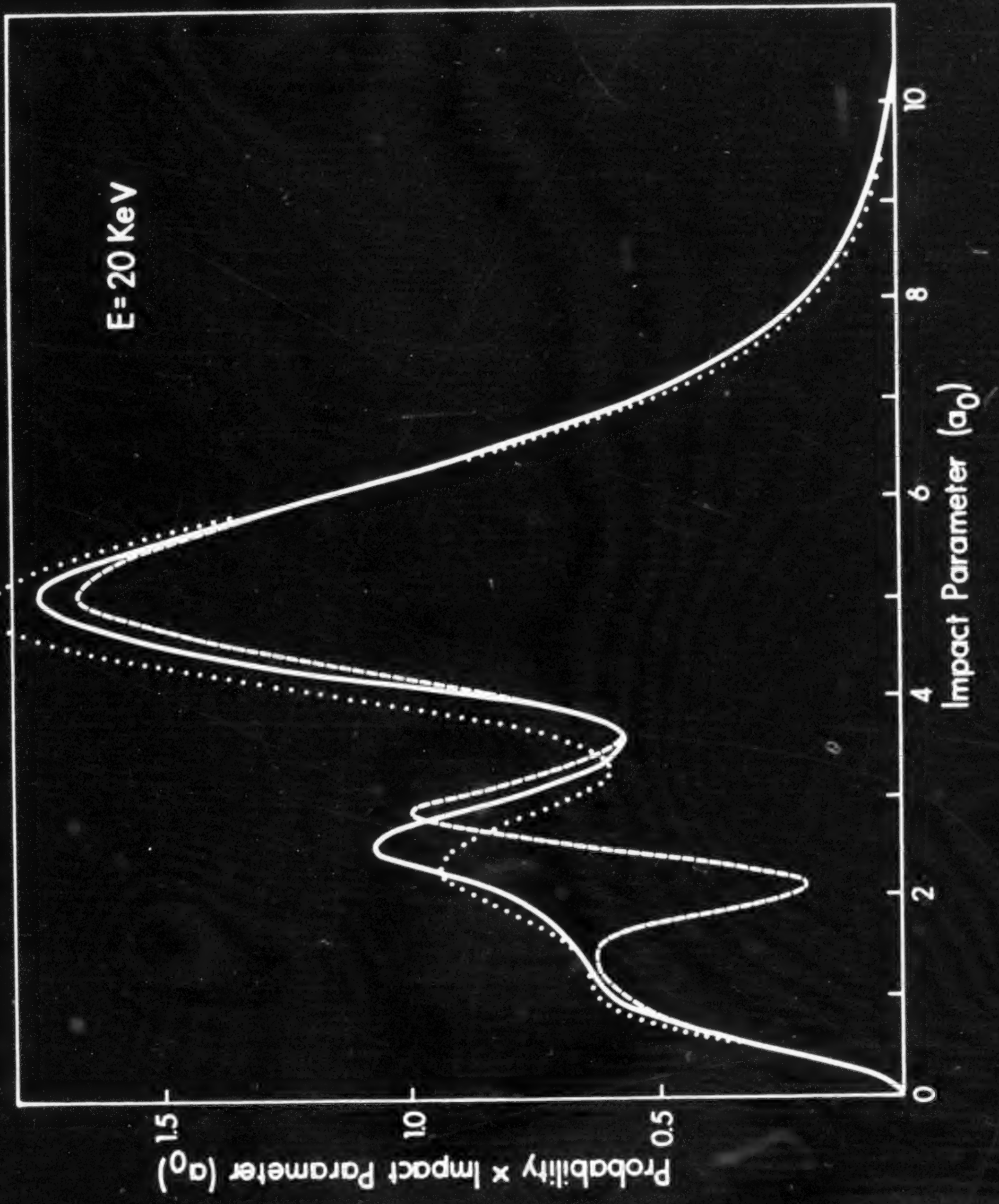

Figure VI.15 Probability X impact parameter vs. impact parameter

Some general trends may be seen in the Figures:

(i) $\rho \times P(\rho : E)$ for the 4-state and 10-state results agree closely at low energy and disagree at higher energy, showing that excitation to higher levels becomes more important at higher energies. However, even at 20 KeV the disagreement of 4-state and 10-state results is only 12 % at the highest peak maximum.

(ii) As noted in (i), above, the peak at small impact parameter ($\rho \approx 2$ a.u.) is primarily due to angular coupling of $2p\sigma$ -$2p\pi$ states.

(iii) The larger impact parameter peaks (ρ ≥ 2 a.u.) are primarily due to radial coupling of $2p\sigma$ -$3d\sigma$ states. and show typical Rosen-Zener-Demkov oscillations associated with coherence of the $2p\sigma$ and $3d\sigma$ states which have an almost constant energy gap over an extended region.

(iv) These two different peaks caused by angular and radial couplings do not interfere coherently. The two major couplings occur in different regions and the $2p\sigma$ -$3d\sigma$ coupling is weak at the smaller R-values where rotational $2p\sigma$ -$2p\pi$ coupling plays a part.

(v) The phase difference in the oscillatory peaks at smaller ρ between the 4-state and 10-state basis results is mainly the result of strong coupling from $3d\sigma$ to the upper levels $3p\sigma$,$3p\pi$,$3d\pi$; $3d\sigma$ is a "gateway" to these higher states, and as a result of this coupling the effective phase of the peak amplitude is shifted. As was noted some years ago by Knudson and Thorson(42), the influence of couplings to other states is often detectable most easily in their effects on phases, rather than the magnitudes of excitation probabilities.

3. Cross Sections

In this section, we present our results for the total as well as the individual (n,l) cross sections calculated by using 3,4,10,12 states as in Table(VI-1). Emphasis is placed on the comparisons of the cross sections and the convergence of the cross sections in terms of the basis sets with other theoretical results particularly those of HLW & WH and Taulbjerg *et al*(72).

(a)Total Cross Section

Table(VI-2) shows our total charge transfer cross sections for 3-, 4-, and 10-state basis, together with results of previous calculations. There is generally good agreement at most energies between our results and those of HLW; like them we find that convergence of the results as function of basis size is much improved (relative to the PSS results of Winter and Lane), when ETF effects are included. Setting aside for the moment the results reported by Vaaben and Taulbjerg, it also appears that the convergence *limits* of the ETF-corrected calculations are significantly different from those of the uncorrected calculations, at least at the higher energies. At 8 and 20 KeV the convergence of our total cross sections is somewhat faster than that of WH & HLW (changes from 4-state to 10-state basis cross sections are 64 % of those of WH & HLW in both cases); however, the comparison is not clear cut, since the 10-state bases differ slightly. Additional information about convergence is provided by results of calculations using 12 basis states at 8-10 values of impact parameter (1-12 a.u.), for both energies. Table(VI-3) shows a comparison of molecular state excitation probabilities for the 12-state and 10-state basis. It can be seen that in every case the total charge transfer probability has changed by less than 1 %, relative to the 10-state result.

At 20 KeV, it appears that the convergence limits for total charge transfer cross section resulting from the differnt ETF treatments by ourselves and by WH & HLW may be diverging slightly also. As shown in Figures(VI-13) through (VI-15), the main differences result from collisions at small impact parameter and are probably associated with 2pσ-2pπ coupling. However, calculations using still larger basis sets would be needed to settle the question clearly.

The results reported by Vaaben and Taulbjerg(72), using a common switching function for all molecular states, are in marked disagreement with our values and those of Hatton,Lane and Winter, especially at the lowest energies, where the effects of ETF corrections appear to be least significant for this system and where all other calculations reported in

Table VI.2 Total charge transfer cross section

Total Charge Transfer Cross Sections:

He^{2+}+H(1s) → He^{+}+H^{+} (units 10^{-16} cm^{2})

Calculation	Basis Size	He^{2+} Energy, keV			
		1	3	8	20
Piacentini and Salin (1977)	3	0.238	0.985	3.27	5.36
Winter and Lane (1978)	3	0.238	0.994	3.27	5.34
	10	0.247	1.03	3.80	7.20
	20	---	1.22	4.66	9.37
Vaaben and Taulbjerg (1979)	3	0.134	1.25	5.40	10.36
	10	0.135	1.26	5.19	9.63
Hatton, Winter and Lane (1980)	3	0.247	1.45	5.93	10.1
	4	0.264	1.49	6.07	10.8
	10	0.265	1.49	6.30	12.2
Kimura and Thorson (1981)	3	0.258	1.40	5.90	9.85
	4	0.260	1.43	6.01	10.40
	10	0.260	1.43	6.15	11.23

Table VI.3 Convergence of excitation probabilities

Convergence of Excitation Probabilities for the
10- and 12-State Basis.
He^{2+} energy E=20 KeV

Impact Parameter (a.u.)	1.0	2.0	3.0	4.0	5.0	6.0	7.0
10-state	0.572	0.765	0.801	0.799	1.73	1.21	0.549
12-state	0.573	0.768	0.806	0.805	1.75	1.22	0.553

Table(VI-2) agree most closely. These results were sufficiently disturbing that we performed a calculation at 1 KeV using their switching function. For the 3-state basis at 1 KeV we find the value 0.247 X 10^{-16} cm^2, in general agreement with other values in Table(VI-2). Our result was obtained using straight-line trajectories, while Vaaben and Taulbjerg used the HeH^{2+} $2p\sigma$ potential curve to determine trajectories.[3] However, the extensive studies by Winter and Lane on the effects of Coulombic vs. straight-line trajectories, show that these are relatively small, and we think it unlikely that the discrepancy is a trajectory effect.

Figure(VI-16) compares our 10-state results and those of HLW with experimental measurements of the total charge exchange cross section. Except at the lowest energies (≤4 KeV), there is good agreement of the theoretical results with the values reported by Shah and Gilbody(83) and by Nutt, McCullough ,Shah and Gilbody(84). The measurements of Bayfield and Khayrallah(82) lie above the other experimental values as well as above our result and those of HLW & WH, for energies above 10 KeV. At lower energies, the older data of Fite Smith and Stebbings(80) lie considerably above the values given by Gilbody et al, who have attributed the discrepancy in part to the nonnegligible formation of molecular species, not taken into account by Fite et al.

---

[3] Dr.J. Vaaben (private communication) has confirmed that a result close to the above value is also obtained by him using straight-line trajectories.

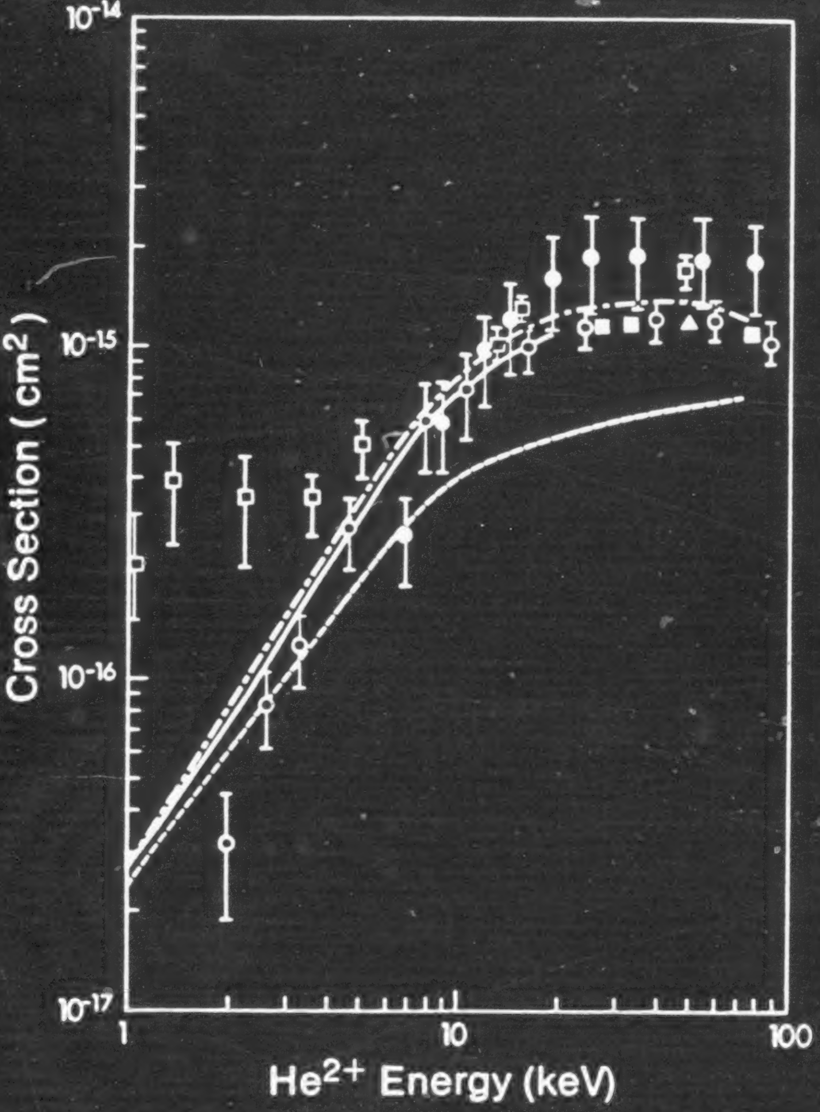

Figure(VI-16) Total charge transfer cross section for He^{2+}-H(1s) collisions, vs. projectile energy E. Theoretical results: ——— ,present work; -·-·-·- ,Winter et al(73,74); – – – – , Piacentini et al(70). Experimental data: □ ,Fite et al(80); ● ,Bayfield et al(82); ○, Gilbody et al(83,84); ■ ,Olson et al(81).

The success of molecular state calculations in accounting for the marked decrease in charge transfer cross section seen experimentally below 10-20 KeV confirms their appropriateness for collisions at low energies. Atomic state basis calculationss by Rapp *et al* and by Gallaher *et al* (not depicted in Figure(VI-16)) show reasonably good agreement with experiment above 15 KeV, but below this energy give much larger cross sections (about one order of magnitude at 1 KeV), agreeing only with the older data of Fite *et al*. Our results practically coincide with the measured values reported by Gilbody and coworkers in the region 5-20 KeV.

Below ~4 KeV, the experimental values given by Gilbody *et al* fall off still more rapidly than the theoretical values both of ourselves and of Hatton,Lane and Winter, while the two theoretical results are in excellent agreement at lower energies. Given the difficulties of experimental measurements at such low energies, we believe the theoretical results are more reliable in this region.

As was pointed out by Winter and Hatton, when ETF effects are taken into account the four states $2p\sigma$; $2p\pi$,$3d\sigma$,$2s\sigma$ are almost completely sufficient to study charge exchange and to determine the total cross section quantitatively, since the levels $He^{2+}+H(1s)$ and $He^{+}(n=2)+H^{+}$ are *near-resonant*. Our calculations and those of HLW & WH for total cross sections establish that inclusion of ETF corrections has an important practical effect on convergence, and that uncorrected calculations probably do not converge on the same result as corrected ones (except perhaps at the lowest energies considered, where only $2p\sigma$-$2p\pi$ coupling at small R (insensitive to ETF corrections) has much effect). Moreover, there are small but not negligible differences in the apparent convergence limit values obtained using different ETF descriptions, at least at the higher energies, which suggests that in general a more elaborate description of ETF's for molecular states may be needed than is provided by Bates-McCarroll ETF's.

(b)Detailed Cross Sections

Cross sections for electron transfer to individual levels $He^{+}(n=1)$, $He^{+}(n=2)$, $He^{+}(n=3)$, and direct excitation to $H(n=2)$ are shown for the 10-state basis in Table(VI-4) and Figure(VI-17). By far the largest contribution to charge transfer comes in the $He^{+}(n=2)$ manifold due to the near-resonance with $H(1s)$--99.2 %, 95.6 % and 93.9 % at 1, 8, and 20 KeV, respectively. A secondary contribution is made to $He^{+}(n=3)$, 0.6 %, 2.9 %, and 4.8 %, respectively. Capture into the $He^{+}(1s)$ ground state is unimportant at these energies. Direct excitation of $H(n=2)$ amounts to about 1.5 % of the charge transfer cross section at E=8 and 20 KeV; however, these higher level cross sections may be expected to change significantly if a larger basis set is used. We find, for example, using the 12-state basis set at 8 KeV, that the population of $H(n=2)$ is increased by $\sim$40 %, mainly because the inclusion of $4f\sigma$ greatly increases the

Table VI.4 Atomic level excitation cross sections

Atomic Level Excitation Cross Sections

He^{2+}+H(1s) (units 10^{-16} cm^2) (10-State Basis)

He^{2+} Energy (keV)	He^{+}(1s)	He^{+}(n=2)	He^{+} (n=3)	H (n=2)
1	4.89×10^{-7}	0.258	1.6×10^{-3}	4.1×10^{-4}
8	2.8×10^{-4}	5.88	0.176	0.094
20	2.5×10^{-3}	10.54	0.535	0.155

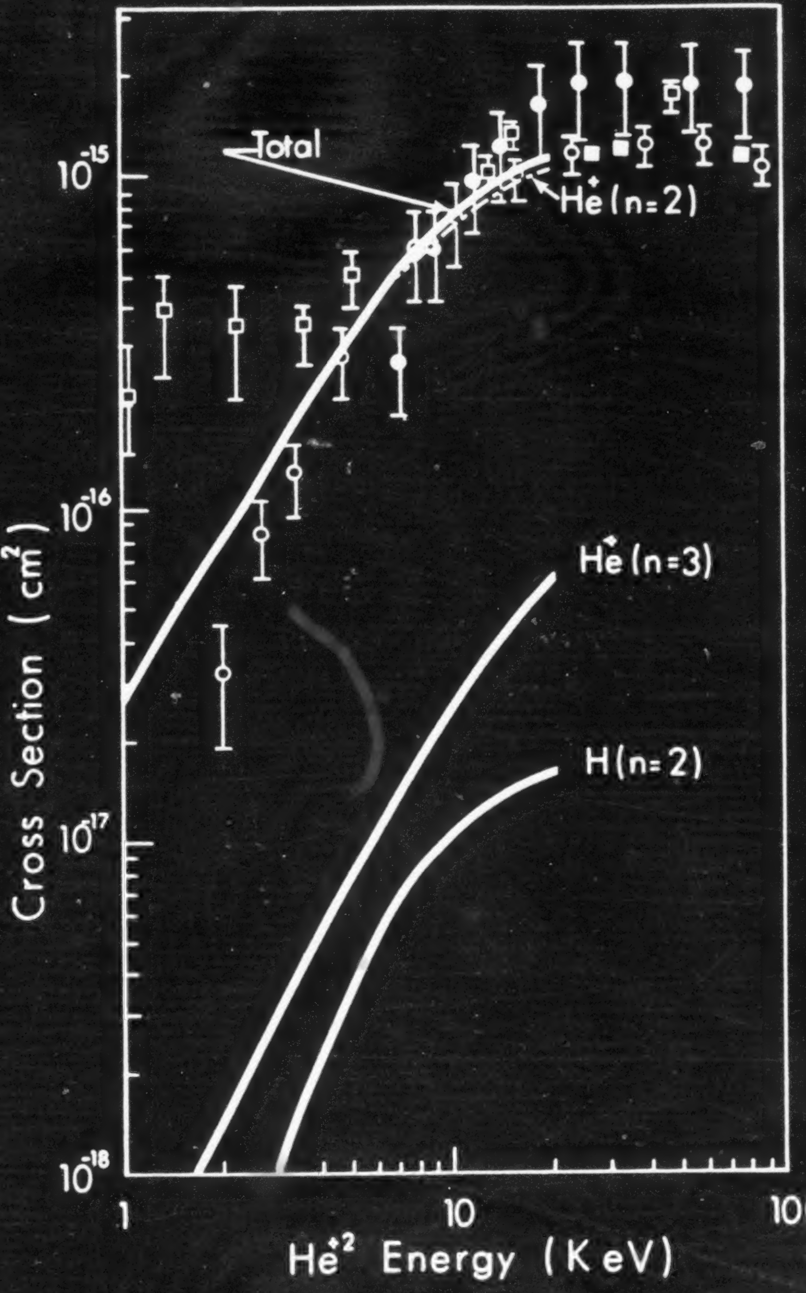

Figure(VI-17) Detailed level cross sections vs. E. ———— ,present work. Experimental data are the same in Fig.(VI-16)

$4f\pi$ population via the rotational coupling between them; a secondary effect is introduced by inclusion of $5g\sigma$, even though the final $5g\sigma$ population is itself negligible. (Similar effects are mentioned by WH & HLW). Expansion of the basis to include such states as $4d\sigma$,$3d\delta$,$4d\pi$, etc would be likely to shift upper level populations back (from H(n=2)) toward He$^+$(n=3,4) levels again. However, these results do confirm that (when ETF effects are included) the 4-state basis is sufficient for a qualitative account of He^{2+}+H(1s) collisions at these energies.

(c)He(n=2) Manifold Cross sections

Table(VI-5) presents an analysis of individual atomic state cross sections within the He$^+$(n=2) level.

At low energies the principal contribution comes from $2p\pi$ excitation associated with the $2p\sigma$ -$2p\pi$ rotational coupling, but as the energy increases this is overshadowed by the radial $2p\sigma$ -$3d\sigma$ coupling and , to a lesser extent, the $2p\sigma$ -$2s\sigma$ coupling, which populate the 2s and $2p_0$ atomic states. He$^+$(2s) and He$^+$($2p_0$) cross sections are sensitive to the basis size and energy since as already discussed $3d\sigma$ state plays the role of a gateway to higher Rydberg states. Increase in the basis from 4- to 10-states affects the $2p_1$ cross section much less than those for 2s and $2p_0$. This happens because a number of higher states (e.g., $3d\pi$) couple strongly with $3d\sigma$ due to its "promotion" in the united atom limit, while the $2s\sigma$ and $2p\pi$

Table VI.5 He^{+}(n=2) atomic state cross sections

He^{+} (n=2) Atomic State Cross Sections

He^{2+}+H(1s) Collisions (units 10^{-16} cm^2)

He^{2+} Energy (keV)	Basis Size	2s	$^2P_0$	$^2P_{\pm1}$
1	4	0.040	0.026	0.194
	10	0.038	0.024	0.195
8	4	1.40	2.66	1.95
	10	1.21	2.65	2.02
20	4	2.65	3.97	3.78
	10	2.18	4.66	3.70

states are relatively isolated from the higher levels (cf. Figure(VI-1)).

Figure(VI-18) shows a comparison of our and other theoretical results for the $He^+(2s)$ cross section with experimental values obtained by Bayfield and Khayrallah, and Shah and Gilbody. Our results and those of Winter and Hatton are in good agreement with the experiments, especially those of Gilbody *et al* above 5 KeV, although our values are somewhat larger than the experimental value: as already noted by Winter and Hatton, however, the energy dependence at low energies is in better accord with the trend of Bayfield et al's measurements. The 3-molecular state results by Piacentini and Salin(70) are also shown. Also as noted by WH ,the better agreement of their values with the experiment results should be considered fortuitous, since their total capture cross section does not agree with the experimental values and they did not test the convergence of the cross section as a function of basis set.

Figure(VI-19) shows the individual $2s, 2p_0, 2p_1$ cross sections along with $He^+(2s)$ excitation cross sections measurements.

(d)Effect of Higher Order Terms in Collision Velocity

In the study of He^{2+}-H(1s) collisions and H^+-He^+(1s) collisions, we used the coupled equations(Eq.(II-20)), which are accurate to first-order in V. As discussed in

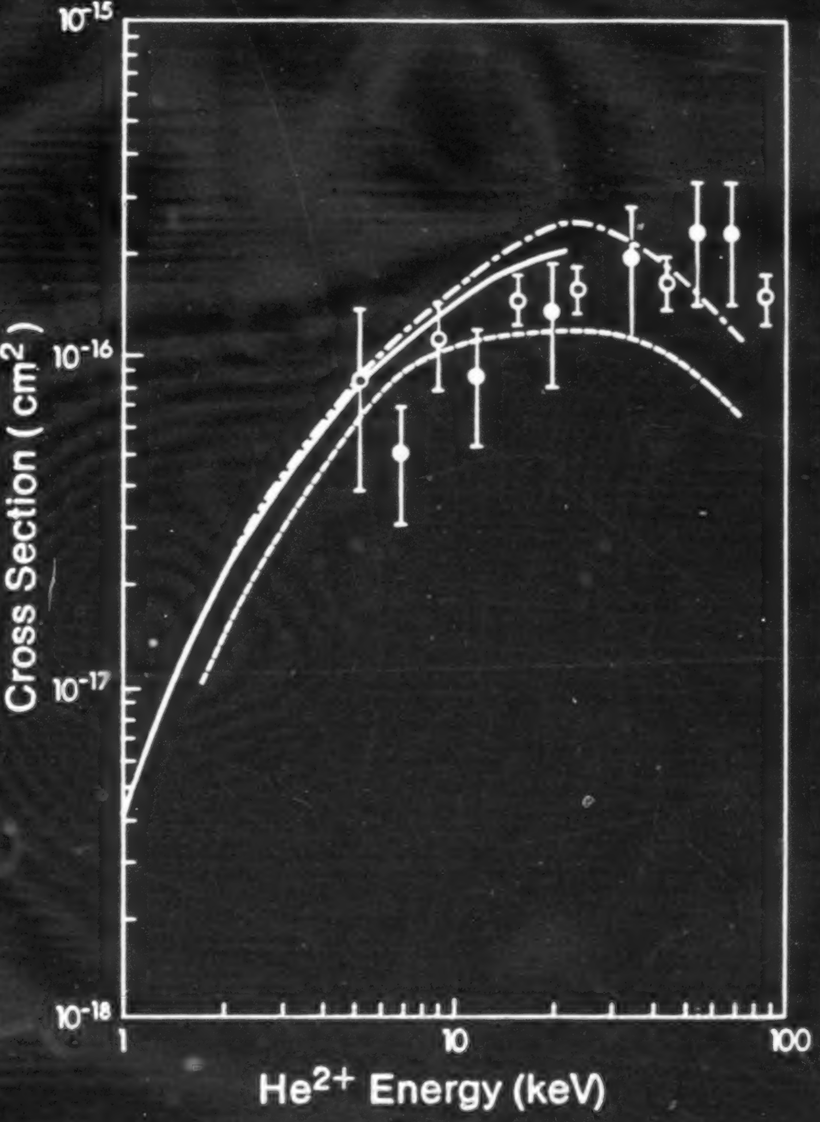

Figure(VI-18) $He^+(2s)$ capture cross section vs. E for He^{2+}-H(1s) collisions. Theoretical results: ——— ,present work; —·—·—·—,Winter et al(73); - - - - - ,Piacentini et al(70). Experimental values: ●,Bayfield et al(82); ○,Gilbody et al(83,84).

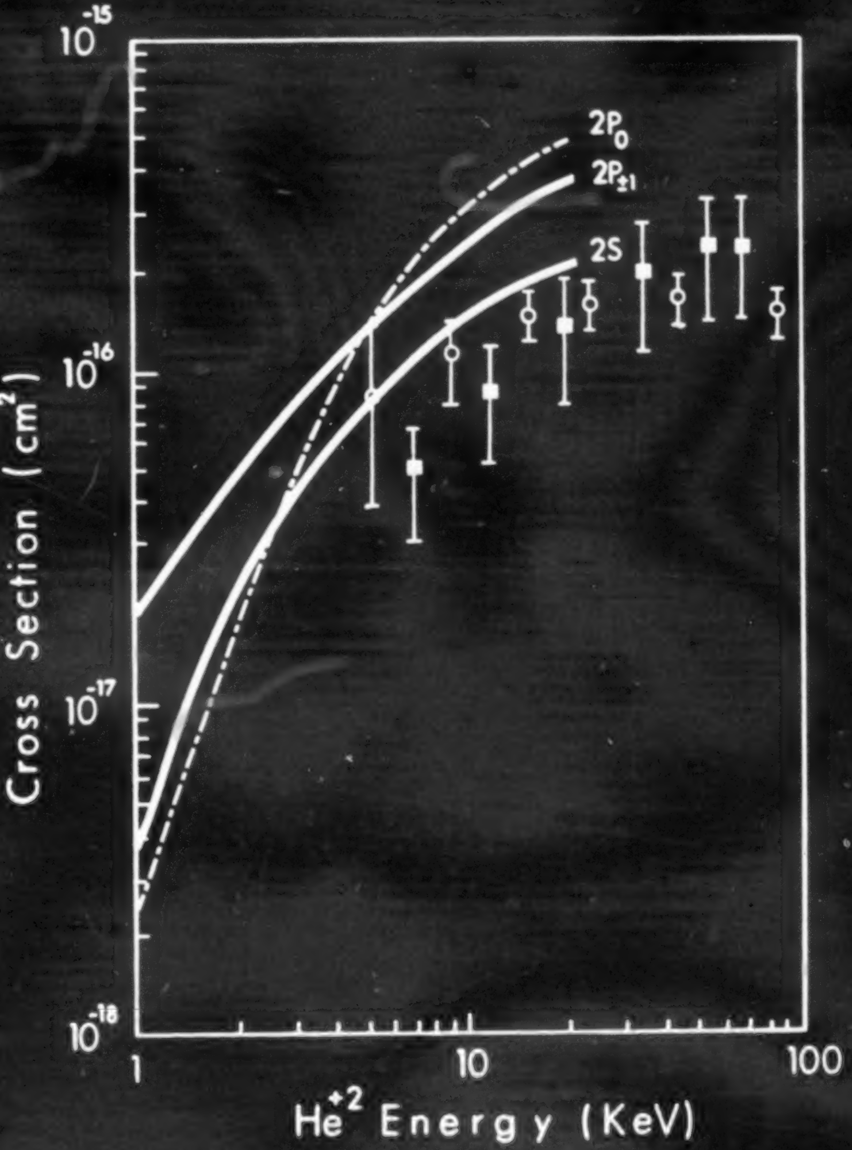

Figure(VI-19) Detailed He$^+$(n=2) level capture cross sections vs. E. Experimental data are the same in Fig.(VI-18).

Section(II.C.1b), the effect of second-order and higher terms in V is much less important for the HeH^{2+} collision system than it is for the H_2^+ system, primarily because of the shorter range of couplings between states correlating to the size of the higher-order terms. We did some calculations of molecular state probabilities vs. impact parameter at 20 KeV (4 KeV in c.m. frame), with the 4-state basis, using coupled equations accurate to second-order in V. The results are tabulated in Table(VI-6) along with the 4-state basis calculated values which include only the first-order in V term only for eight different impact parameters.

It can be seen from Table(VI-6) that in all cases the individual state probabilities change by at most 1 %.

We have not made tests for process (b) at the higher energy of 8 KeV (c.m. frame); however, since our studies in H_2^+ suggested that second-order effects increase in roughly linear fashion with increasing energy (see Section(V.D.1)), we believe that errors of about 2 % (at most) in individual state probabilities in process (b) might result due to neglect of second-order terms at 8 KeV (c.m. frame).

Table VI.6 Effects of second-order terms in velocity

Effects of Second-Order Terms in Velocity on
Total Electron Transfer Probability (4-state basis set)*

He^{2+} energy E=20 KeV

Impact Parameter (a.u.)	0.5	1.0	1.5	2.0	2.5	3.0	4.0	5.0
V^1 Term	0.261	0.556	0.625	0.281	0.571	0.928	0.742	1.65
V^2 Term	0.261	0.555	0.625	0.279	0.570	0.927	0.742	1.64

*The four states $2p\sigma$, $2p\pi$, $3d\sigma$, $2s\sigma$.

C. He$^+$(1s)-PROTON COLLISIONS (PROCESS(b))

Since He$^+$(1s) formation plays a negligible part in He^{2+}-H(1s) collisions, it is not surprising that the total charge transfer and direct excitation cross sections for H$^+$-He$^+$(1s) collisions are very much smaller than those for process (a) --- as has already been shown by Winter, Hatton and Lane(WHL)(75). The main reason for this is the highly nonresonant energy transfer required to go from 1sσ (the incident channel) to all upper states. Moreover, the couplings responsible for such excitation (primarily 1sσ-2pσ and to a secondary extent, 1sσ-2pπ) are effective at relatively small internuclear separations ($\leq$ 5 a.u.), and one might expect molecular state ETF's to give some different effects than a Bates-McCarroll description does. In fact, we find in this case that the treatment given to ETF corrections has a more significant effect on the values found for both charge transfer and direct excitation cross sections, than is the case for process (a). Our 5-state basis and that of WHL are identical; as noted previously, the two 10-state basis sets differ slightly, but they do so only in respect to states which are relatively weakly and indirectly linked to the more important lower levels. In both cases we find that the cross sections computed by WHL (using Bates-McCarroll ETF's) are all systematically larger than those obtained here.

We have already described the coupling matrix elements linking 1sσ to the manifold (2pσ, 2pπ, 2sσ, 3dσ) and shown that the different ETF description resulting from our molecular state switching functions leads to markedly different coupling matrix elements from those of WHL (see Section VI.A.4). Furthermore, the most important differences appear for the $1s\sigma$ -$2p\sigma$ coupling, which is the primary mechanism for excitation in these collisions.

1. Excitation Paths

Figures(VI-20) & (VI-21) show collision histories (molecular state probability vs. time (a.u.)), using the 5-state basis, at E=4 KeV (c.m. system) and impact parameters 0.5 and 2.0 a.u., respectively. Dominant interactions occur for $|t| \leq 12$ a.u. (or $R \leq 4.7$ a.u.), since the couplings (Figures(VI-6)) have short ranges. While some very small $3d\sigma$ and $2s\sigma$ amplitudes can be seen early in the collision due to direct coupling from $1s\sigma$, both are eclipsed by the primary excitation process $1s\sigma$ -$2p\sigma$. At higher energy (8 KeV), direct $1s\sigma$ -$2p\pi$ excitation plays some part but (for example) the peak in $2p\pi$ probability in Figure(VI-20) (0.5 a.u.) results mainly from the two-step process $1s\sigma$ -$2p\sigma$ -$2p\pi$ rather than a direct coupling. Similarly, population of $3d\sigma$, and the (small) $2s\sigma$ population, come from two-step processes (e.g., $1s\sigma$ -$2p\sigma$, followed by $2p\sigma$ -$3d\sigma$ radial coupling later in the collision). Thus a large portion of the flux which eventually appears in $He^{+}(n=2)$ levels passes through the "gateway" of the $2p\sigma$ (charge exchange) state as an

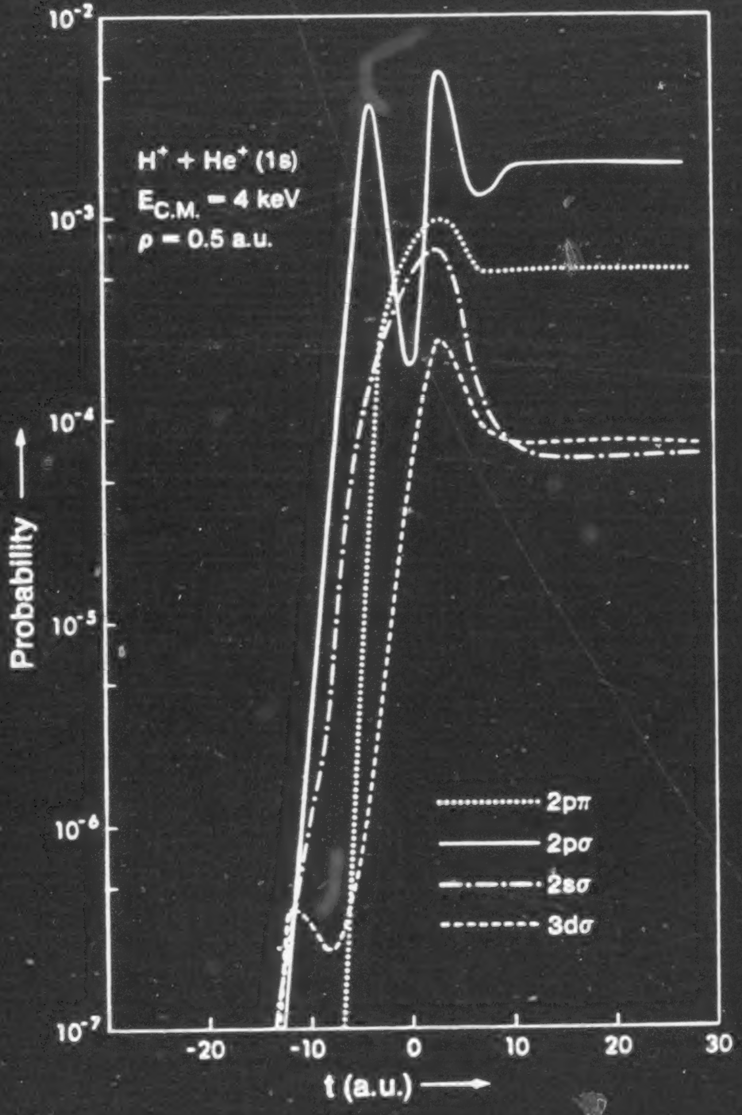

Figures(VI-20) Collision "history" (probability vs. time) for 5-state basis, H⁺-He⁺(1s) collision at c.m. energy 4 KeV and impact parameter 0.5 a.u. .

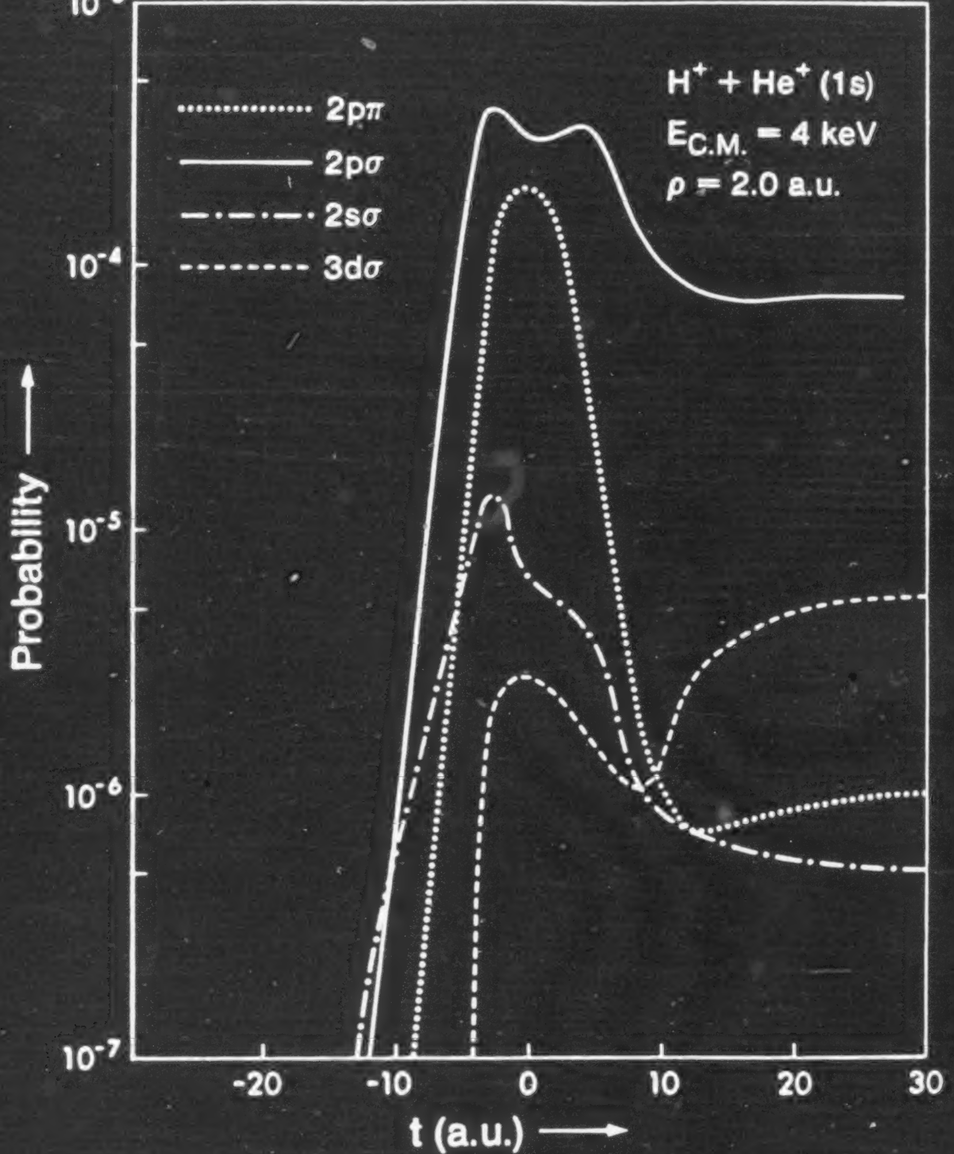

Figures(VI-21) Collision "history" (probability vs. time) for 5-state basis, H^+-He^+(1s) collision at c.m. energy 4 KeV and impact parameter 2.0 a.u. .

intermediate; in this sense, the term "direct excitation", though it is the correct technical name for the excitation processes leading to $He^+(n=2)$, is perhaps a little misleading. This picture is not changed by increasing the basis to ten states, and it explains why both the charge transfer and "direct excitation" cross sections in process (b) are sensitive to the $1s\sigma - 2p\sigma$ coupling.

Figure(VI-22) shows impact parameter times probability of charge transfer to H(1s) ($2p\sigma$ state) vs. impact parameter, at $E_{c.m.}=4$ KeV, for both 5-state and 10-state basis. All the transitions occur for $\rho \leq 3$ a.u., which demonstrates the short range of the primary coupling, and no significant range of the primary coupling, and no significant change occurs when the basis is increased. Thus the five states ($1s\sigma$;$2p\sigma$,$2p\pi$,$3d\sigma$,$2s\sigma$) are sufficient both qualitatively and quantitatively to evaluate the cross section for charge transfer (to H(1s)).

Probabilities for excitation to $He^+(n=3)$ and charge transfer to H(n=2) (found using our 10-state basis) are relatively small (less than 10 % of the total excitation probability in all cases). These more highly excited levels are accessed mainly via the $3d\sigma$ state as "gateway", just as in process (a), while the $2s\sigma$,$2p\pi$ levels are relatively "isolated" from these upper states.

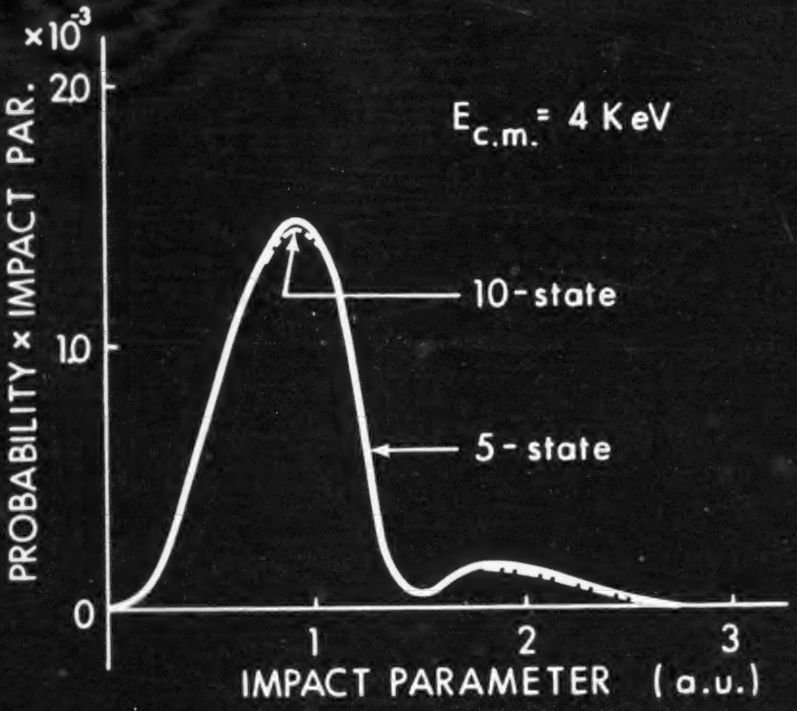

Figure(VI-22) Probability times impact parameter vs. impact parameter at c.m. energy 4 KeV.

2. Cross Sections

Table(VI-7) presents our calculated charge transfer and "direct excitation" cross sections for the 5-state (KT-5) and 10-state (KT-10) basis. Also shown for comparison are the values reported for their 5-state and 10-state basis by WHL (WHL-5,WHL-10). Note that for WHL-10 no basis state correlating to H(n=2) occurs, and also that cross sections for $He^+(n=3)$ were not reported in their paper.

a. Convergence

For the H(1s) charge transfer cross section, the largest change we find on augmenting the basis from five to ten states is -4.3 % (8 KeV), compared to -7.9 % (4 KeV) for WHL. For excitation of $He^+(n=2)$ levels, the stability of the individual $2s, 2p_0$, and $2p_1$ cross sections is much poorer, particularly at 8 KeV (changes of +14 %, -26 %, -12 %, respectively, compared to +13 %, -55 %, -19 % for WHL). The reason for this instability of course is the substantial redistribution of flux into $He^+(n=3)$ and H(n=2) levels due to coupling from $3d\sigma$ to $3d\pi$, $3p\sigma$, $3p\pi$ (and $4d\sigma$ in our case), when these states are included; that it is $3d\sigma$ which serves as the connection is reflected in the somewhat better stability of $2p\pi$ cross sections. A more significant measure of "overall convergence" is given by the changes of -1 %, +2 %, and +10 % (at 1.6, 4, and 8 KeV, respectively) in the total cross section for

Table VI.7 Atomic level excitation cross sections

Atomic Level Excitation Cross Sections for H^+-$He^+(1s)$ Collisions

(units 10^{-16} cm^2) [Present Results: KT5, KT10; Results of Ref. 75: WHL5, WHL10]

$E_{C.M.}$ (keV)	Basis & Calc.	H(1s)	$He^+(2s)$	$He^+(2p_0)$	$He^+(2p_{\pm1})$	H(n=2)	$He^+(n=3)$
1.6	KT5	2.88×10^{-5}	3.68×10^{-6}	3.21×10^{-6}	7.10×10^{-6}	---	---
	KT10	2.82×10^{-5}	3.62×10^{-6}	2.88×10^{-6}	6.92×10^{-6}	2.15×10^{-7}	4.75×10^{-7}
	WHL5	3.41×10^{-5}	6.51×10^{-6}	5.62×10^{-6}	7.95×10^{-6}	---	---
	WHL10	3.23×10^{-5}	6.40×10^{-6}	4.71×10^{-6}	7.40×10^{-6}		
4	KT5	1.98×10^{-3}	2.56×10^{-4}	2.38×10^{-4}	3.56×10^{-4}	---	---
	KT10	1.94×10^{-3}	2.64×10^{-4}	1.87×10^{-4}	3.47×10^{-4}	4.98×10^{-5}	9.72×10^{-5}
	WHL5	2.46×10^{-3}	3.08×10^{-4}	4.06×10^{-4}	4.20×10^{-4}	---	---
	WHL10	2.28×10^{-3}	3.30×10^{-4}	2.66×10^{-4}	4.01×10^{-4}		
8	KT5	9.27×10^{-3}	2.31×10^{-3}	1.37×10^{-3}	2.84×10^{-3}	---	---
	KT10	8.89×10^{-3}	2.67×10^{-3}	1.09×10^{-3}	2.54×10^{-3}	9.62×10^{-4}	1.55×10^{-3}
	WHL5	12.2×10^{-3}	4.70×10^{-3}	2.78×10^{-3}	3.64×10^{-3}	---	---
	WHL10	12.4×10^{-3}	5.39×10^{-3}	1.79×10^{-3}	3.05×10^{-3}		

both charge transfer plus excitations of all kinds; these values make it clear that augmentation of the basis from 5 to 10-states has not caused massive changes in the flux drained from 1sσ . Unfortunately the corresponding data is not available from WHL.

While it appears that the convergence of our results is slightly faster than that of WHL, a comparison is weakened by the differences in the two ten-state bases. In both cases, further augmentations of the basis may be expected to cause significant changes in the $He^+(n=2)$ individual state cross sections. On the other hand it may be reasonable to expect that the charge transfer to H(1s), and especially the total flux loss from 1sσ, will be much more stable (≤ 10 % change at 8 KeV?).

b. Cross Section Values

In our opinion, a more significant difference is found in comparisons of the cross section magnitudes found here with those reported in WHL (see Table(VI-7)), and comparisons of both 5-state and 10-state results are relevant for this purpose. In every case, the cross section values reported by WHL are appreciably larger than those we obtain for the comparable basis. For the more stable H(1s) charge transfer cross section, the cross sections of WHL are 18 % to 32 % larger than ours for the five-state basis, and 14 % to 26 % larger than ours for the 10-state basis. These differences are at least twice as large as changes occurring due to basis augmentation in WHL, and at least four times as large as those due to augmentation in our results. While it is conceivable that further, large augmentation of the basis (discrete states only) might lead to reconciliation of these differences, it is our opinion that this will not occur. In principle, there is no reason to expect that such convergence on a common value must occur, unless completeness of the two basis sets is explicitly ensured by inclusion of both continuum and discrete states in each.

An alternative explanation of these differences, i.e., that they result from effects of higher order terms in the velocity, (we retained only first-order terms in our calculation), seems improbable to us because (a) the differences are 18 %-14 % even at 1.6 KeV, (b) as stated previously, we studied effects of the second-order terms for process (a) at $E_{c.m.}$=4 KeV (20 KeV projectile energy) and found them less than 1 % for individual state probabilities, and (c) the sign of these second-order corrections is always negative-- which would increase the observed discrepancies.

Similarly large or even larger discrepancies (as much as a factor of 2 for 2s and $2p_0$, and 17 % to 22 % for $2p_1$) occur for the individual direct excitation cross sections. Given the poorer convergence in both sets of calculations for these detailed cross sections, it is not so clear that the values would converge on different limits; however, the consistency of the discrepancies found suggests this is a reasonable conclusion.

Cumulative level cross sections for $He^+(n=3)$ and $H(n=2)$ are also computed in Table(VI-7) for the 10-state calculations. We do not attribute firm significance to these numbers, as they may be expected to change appreciably when additional states belonging to the same manifold are included in the basis. Our estimates of the contribution of $H(n=2)$ are probably a little high; we have included $H(n=2)$ states, but not the comparable $He^+(n=3,4)$ states which are their competitors for coupling to $3d\sigma$ as excitation source, and inclusion of these states might be expected to shift flux back toward He^+ formation. We do agree with the conclusion of WHL (based on PSS studies) that the $H(n=2)$ cross section is "small" (4 %-10 % of $H(1s)$ at 8 KeV).

In summary, the comparisons made suggest that the different treatments of ETF corrections made by ourselves and by WHL may lead, for process (b), to significantly different cross sections both for charge transfer and for direct excitations, and it is our opinion that this is in fact the case. (It should be possible to test this by calculations using a basis perhaps twice as large as those employed here.)

c. Comparison with Experiment

Experimental values for the total charge transfer cross section, as reported by Peart,Grey and Dolder(85) are shown in Figure(VI-23) together with our 10-state results (including H(n=2)), and those of WHL. The experimental values have been determined from the measured He^{2+} formation; hence they include both charge transfer and ionization events, though it may be reasonable to assume that the contribution of ionization is less than 1 %. In spite of differences between them, both our results and those of WHL appear to be in good agreement with the experiments. Our lower values at 4 and 8 KeV do lie slightly closer to the data values given by Peart *et al* than do those of WHL. The same data for total charge transfer cross section for both theoretical and experimental values are plotted on a linear graph in Figure(VI-24). It clearly shows that discrepancies between ours and WHL are significant, especially at 8 KeV. A conservative opinion on the error limits for the experimental data does not

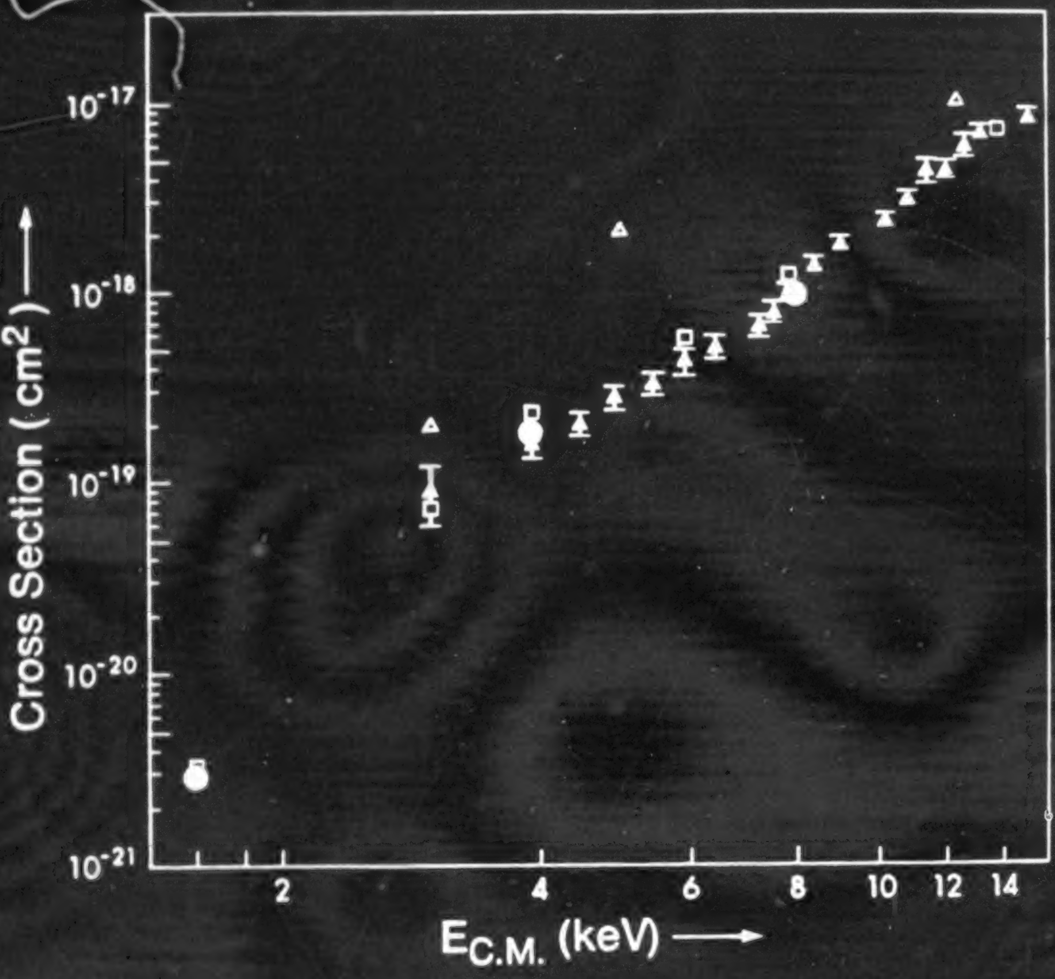

Figure(VI-23) Total charge transfer cross section for H$^+$-He$^+$(1s) collisions, vs. c.m. energy E. Theoretical results: ●,present work; □,Winter et al(75); △ Rapp et al(76): Experimental result: ▲ Peart et al(85).

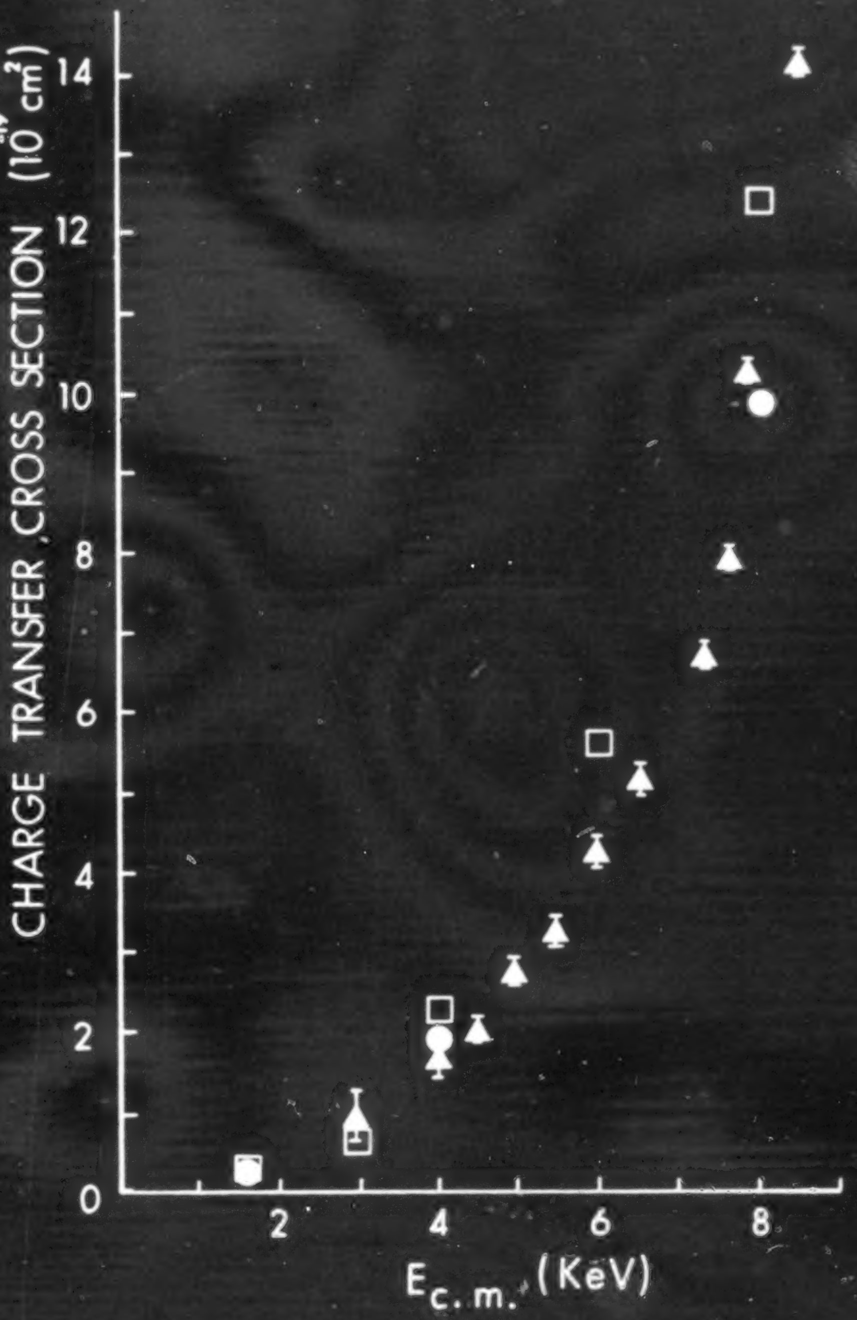

Figure(VI-24) The same data as Fig.(VI-23), but in linear scale.

permit a strong conclusion as to which set of results is more accurate.

More accurate measurements of this cross section, or accurate measurements of the direct excitation cross sections, would be of considerable interest for the questions discussed here.

BIBLIOGRAPHY

1. Born M. and Oppenheimer J.R. Ann. Phys. 84 457 (1927)

2. Mott N.F. Proc. Camb. Phil. Soc. 27 553 (1933)

   Mott N.F. and Massey H.S.W. *The Theory of Atomic Collisions (Oxford Univ Press)*

3. Bates D.R. , Massey H.S.W. and Stewart A.L. Proc. Roy Soc. A216 437 (1953)

4. (a)Bates D.R. and McCarroll R. Proc.Roy.Soc.. A245 175 (1958);

   (b)Bates D.R. and McCarroll R. Adv. Phys. 11 39 (1962)

5. McCarroll R. Proc. Roy. Soc. London A264 547 (1961)

6. Mittleman M.H. Phys. Rev. 122 499 (1961)

7. Thorson W.R. J. Chem. Phys. 42 3878 (1965)

8. (a)Thorson W.R. and Levy II H. Phys. Rev. 181 232, (1969)

   (b)Levy II H. and Thorson W.R. Phys. Rev. 181 244,252 (1969)

   (c)Lebeda C.F., Thorson W.R. and Levy II H. Phys. Rev. A4 900 (1971)

   (d) SethuRaman V., Thorson W.R. and Lebeda C.F. Phys. Rev. A8 1316 (1973)

   (e) Choi J.H. and Thorson W.R. private communication (1980)

9. Schneiderman S.B. and Russek A. Phys. Rev. 181 311 (1969)

10. (a)Chen J.C.Y., Ponce V.H. and Watson K.M. J. Phys.B6 965 (1973)

(b)Hatton G.J., Chen J.C.Y., Ishihara T. and Watson K.M. Phys. Rev. A12 1281 (1975)

11. Thorson W.R. and Delos J.B. Phys. Rev. A18 117,135 (1978)

12. Delos J.B. and Thorson W.R. J. Chem. Phys. 70 1774 (1979)

13. Green T.A. Phys. Rev. A23 519,532,546 (1981)

14. Green T.A. Proc. Phys. Soc. London 86 1017 (1965)

15. Smith F. T. Phys. Rev. 179 111 (1969)

16. Kronig R. de. *Band Spectra and Molecular Structure (Cambridge Univ.Press)*

17. Bates. D.R. and Crothers D.S.F. Proc. Roy. Soc. A315 465 (1970)

Bates D.R. and Holt R. *ibid* A292 168 (1966)

18. Delos J.B. and Thorson W.R. Phys. Rev. A6 709 (1972); *ibid* A6 720 (1972)

19. Riley M. E. Phys. Rev. A7 626 (1973)

20. McCarroll R. and Salin A. J. Phys.B1 163 (1968)

21. (a)Morse P.M. and Feshbach H. *Methods of Theoretical Physics (McGraw-Hill,1953)*

(b)Riley M.E. and Green T.A. Phys. Rev. A4 619 (1971)

22. Mittleman M.H. and Tai H. Phys. Rev. A8 1880 (1973)

23. Melius C.F. and Goddard III W.A. Phys. Rev. A10 1541 (1974)

24. Taulbjerg K., Vaaben J. and Fastrup B. Phys. Rev. A12 2325 (1975)

25. Taulbjerg K. and Briggs J.S. J.Phys.B8 1895,1909 (1975)

26. Matveenko A.V. J.Phys.B9 1419 (1976)

27. (a)Schmidt G.B. Phys. Rev. A15 1459 (1977); (to be published in J. Phys.B (1981))

28. Taulbjerg K. and Vaaben J. (to be published)

29. (a)Rankin J. and Thorson W.R. Phys. Rev. A18 1990 (1978)

(b)Rankin J. Ph.D Thesis Univ. of Alberta (1978)

30. Crothers D.S.F. and Hughes J.G. Proc. Phys. Soc. London A359 345 (1978)

31. Ponce V.H. J. Phys.B12 3731 (1979)

32. (a) Green T.A. private communication.

(b) Green T.A. Phys. Rev. A23 519,532,546 (1981); we would like to thank Dr. Green for showing us his results two years before their publication.

33. Thorson W.R. ,Kimura M. , Choi J.H. and Knudson S.K. (to be published, Phys. Rev. A (1981))

34. Riera A. and Salin A. J.Phys.B9 2877 (1976)

35. Bates D.R., Ledsham K. and Stewart A.L. Phil. Trans. R. Soc. London A246 215 (1953)

Bates D.R. and Carson T.R. Roc. Roy. Soc. London A234 207 (1956)

36. Powers J.D. Phil. Trans. Roy. Soc. London 274 663 (1973)

37. Teller E. and Sahlin H. L. in *"Physical Chemistry", edited by H.Eyring, D.Henderson, and W.Jost (Academic Press. 1970), Vol.V, p.35.*

38. Schinke R. and Kruger H. J. Chem. Phys. 64 2450 (1976)

39. Bulirsch R. and Stoer J. Num. Math.8 1 (1966)

40. Bates D.R. and Williams D.A. Proc. Phys. Soc. 83 425 (1964)

41. Smith F.J. Proc. Phys. Soc. London 92 866 (1966)

42. Knudson S.K. and Thorson W.R. Can. J. Phys. 48 313 (1970)

43. Bates D.R. and Sprevak D. J. Phys.B3 1483 (1970)

44. McCarroll R. and Piacentini R.D. J. Phys.B3 1336 (1970)

45. Rosenthal H. Phys. Rev. Lett. 27 635 (1971)

46. Chidichimo-Frank U.C. and Piacentini R.D. J. Phys.B7 548 (1974)

47. (a)Schinke R. and Krüger H. J.Phys.B9 2469 (1976)

(b)Schinke R. J. Chem. Phys. 65 4849 (1976)

48. Crothers D.S.F. and Hughes J.G. Phil. Trans. Roy. Soc. 292 56 (1979)

49. Percival I.C. and Seaton M.J. Phil. Trans. R. Soc. A251 113 (1958)

50. Many papers have been published on this method; see for example, Bates D.R. Proc. Phys. Soc. 77 59 (1961)

51. Ghosh A.S. and Sil N.C. J. Phys. B4 836 (1971)

52. Franco V. and Thomas B.K. Phys. Rev. A4 945 (1971)

53. Coleman J.P. and McDowell M.R.C. Proc. Phys. Soc. 85 1097 (1965)

54. Chen J.C.Y. and Watson K. M. Phys. Rev. 174 152 (1968); *ibid* 188 235 (1969)

55. Chen J.C.Y. and Hambro L. J. Phys. B4 191 (1971)

Chen J.C.Y. and Kramer P. J. Phys. Rev. A5 1207 (1972)

Sil N. C. , Chaudhuri J. and Ghosh A. S. Phys. Rev. A7 1544 (1973) , *ibid* A12 785 (1975)

56. Wilets L. and Gallaher D.F. Phys. Rev. 147 13 (1966)

57. Cheshire I.M. ,Gallaher D.F. and Taylor A.J. J. Phys. B3 813 (1970)

58. Rapp D. and Dinwiddie J. Chem. Phys. 57 4919 (1972)

Rapp D., Dinwiddie D., Storm D. and Sharp T.E. Phys. Rev. A5 1290 (1972)

59. Theodosiou C.E. Phys. Rev. A22 2556 (1980) References of the most recent theoretical works cited therein.

60. Helbig H.F. and Everhart E. Phys. Rev. 140 1715 (1965)

61. Houver J.C., Fayeton J. and Barat M. J. Phys. B7 1358 (1974)

62. Fite W.L., Stebbings R.F., Hummer D.G. and Brackman R.T.

Phys. Rev. 119 663 (1960)

63. McClure G.W. Phys. Rev. 148 47 (1966)

64. Bayfield J.E. Phys. Rev. 185 105 (1969)

65. Chong Y.P. and Fite W.L. Phys. Rev. A16 933 (1977)

66. Morgan T.J., Geddes J. and Gilbody H.B. J. Phys.B6 2118 (1973)

67. Hill J., Geddes J. and Gilbody H.B. J. Phys.B12 L341 (1979)

68. Morgan T.J., Stone J. and Mayo R. Phys. Rev. A22 1460 (1980)

69. Kauppila W.E., Teubner P.J.O., Fite W.L. and Girnius R.J. Phys. Rev. A2 1759 (1970)

70. Piacentini R.D. and Salin A. J. Phys.B7 1666 (1974)
J. Phys.B10 1515 (1977)

71. Winter T.G. and Lane N.F. Phys. Rev. A17 66 (1978)

72. Vaaben J. and Taulbjerg K. XI.ICPEAC kyoto, Japan P566 (1979)

73. Winter T.G. and Hatton G.J. Phys. Rev. A21 793 (1980)

74. Hatton G.J., Lane N.F. and winter T.G. J. Phys.B12 L571 (1979)

75. Winter T.G., Hatton G.J. and Lane N.F. Phys. Rev. A22 930 (1980)

76. Rapp D. J. Chem. Phys. 61 3777 (1974)

77. Msezane A. and Gallaher D.F. J. Phys.B6 2334 (1973)

78. Bransden B.H., Newby C.W. and Noble C.J. J. Phys.B13 4245 (1980)

79. Ryufuku H. and Watanabe T. Phys. Rev. A18 2005 (1978)

80. Fite W.L., Smith A.C.H. and Stebbings R.F. Proc. Roy. Soc. London A268 527 (1962)

81. Olson R.E., Salop A., Phaneuf R.A. and Meyer F.W. Phys. Rev. A16 1867 (1977)

82. Bayfield J.E. and Khayrallah G.A. Phys. Rev. A12 869 (1975)

83. Shah M.B. and Gilbody H.B. J. Phys.B11 121 (1978)

84. Nutt W.L., McCullough R.W., Brady K., Shah M.B. and Gilbody H.B. J. Phys.B11 1457 (1978)

85. Peart B., Grey R. and Dolder K.T. J. Phys.B10 2675 (1977)

86. Angel G.C., Sewell E.C. Dunn K.F. and Gilbody H.B. J. Phys.B11 L297 (1978)

87. Mitchell J.B.A., Dunn K.F., Angel G.C., Browning R. and Gilbody H.B. J. Phys.B10 1897 (1977)